DEVELOPMENT AND IMPLEMENTATION

OF NOVEL OPTOGENETIC TOOLS IN THE NEMATODE

CAENORHABDITIS ELEGANS

Dissertation
zur Erlangung des Doktorgrades
der Naturwissenschaften

vorgelegt beim Fachbereich 14
der Johann Wolfgang Goethe-Universität
in Frankfurt am Main

von
Jatin Nagpal
aus Delhi, India

Frankfurt 2016

Vom Fachbereich 14 der

Johann Wolfgang Goethe-Universität als Dissertation angenommen.

Dekan: Prof. Dr. Michael Karas

Gutachter: Prof. Dr. Alexander Gottschalk; Prof. Dr. Martin Grininger

Datum der Disputation:

ZUSAMMENFASSUNG

Obwohl die Optogenetik ein nur zehn Jahre altes Forschungsgebiet ist, hat sie die Forschung in der Neurobiologie revolutioniert. Sie umfasst Methoden, die die Kontrolle neuronaler Aktivität durch Licht in einer minimal-invasiven, räumlich und zeitlich präzisen, und genetisch gezielten Weise ermöglichen. Die optogenetischen Aktoren, auch als genetisch codierte, lichtempfindliche Elemente zu beschreiben, ermöglichen, durch Licht angetrieben, die Manipulation von Membranpotentialen, von intrazellulären Signalwegen, sowie von neuronalen Netzwerkaktivitäten und Verhalten (Fenno et al. 2011; Dugué et al. 2012). Diese Techniken haben sich als besonders nützlich für die Sektion von neuronalen Schaltkreisen und des Verhaltens in der Nematode *Caenorhabditis elegans* erwiesen; einem transparenten und genetisch zugänglichen Modellsystem (Husson et al. 2013; Fang-yen et al. 2015).

Tatsächlich ist *C. elegans* der erste Organismus, in dem auf mikrobiellem Rhodopsin basierende optogenetische Werkzeuge (Channelrhodopsin-2 oder ChR2 und Halorhodopsin oder NpHR) erfolgreich implementiert wurden und so auch eine bimodale ferngesteuerter Kontrolle des Verhaltens erreicht wurde (Nagel et al. 2005; Zhang et al. 2007). Seitdem ist der Nematode ein hervorragendes Modell für die Entwicklung und Anwendung von neuartigen optogenetischen Werkzeugen und Techniken, vor allem in seinem Nervensystem, welches aus 302 Neuronen besteht und in einer hierarchischen Weise organisiert ist. Stimuli aus der Umgebung werden von den sensorischen Neuronen erkannt, führen zu einer Weiterleitung der Informationen durch die stromabwärts liegenden Interneuronen zu den Motorneuronen, welche synaptisch mit den Muskeln verbunden sind und dort eine bewegungsbasierte Reaktion erwirken. Mikrobielle Rhodopsine wie ChR2 und NpHR vermitteln jeweils Licht angetriebene Depolarisation und Hyperpolarisation, wodurch sie neuronale Aktivität induzieren oder unterdrücken. Sie erlauben jedoch keine lokale Kontrolle des Membranpotentials, da sie überall in der Plasmamembran der Zellen exprimieren und deswegen nicht auf bestimmte Domänen beschränkt sind, wie beispielsweise in den Synapsen. Zudem überschreiten sie die intrinsische Aktivität der Zelle und umgehen so auch die Signaltransduktionsprozesse innerhalb der Zelle. Somit muss, um die intrazellulären Signalwege zu studieren und um die Fragen über die endogene Rolle von Rezeptoren und Kanälen in einem in vivo

Kontext zu beantworten, die Sammlung optogenetischer Werkzeuge erweitert werden.

Das Ziel dieser Arbeit ist die Entwicklung und Umsetzung neuartiger optogenetischer Werkzeuge in *C. elegans*, welche die Kontrolle der subzellulären Signalsteuerung sowie die von endogenen Rezeptoren ermöglichen. Diese sind: zwei Licht-aktivierte Guanylylzyklasen (bPGC und BeCyclOp), um die durch zyklisches Guanosinmonophosphat (cGMP) vermittelten Signalwege in den sensorischen Neuronen zu modifizieren, sowie Versuche die endogenen *C. elegans* Rezeptoren - Glutamatrezeptor (GLR-3/-6), Acetylcholin - Rezeptor (ACR-16) und Glutamat gesteuerter Chlorid - Kanal (GLC-1) lichtschaltbar zu machen und ihre biologische Funktion in vivo zu verstehen.

Organismen reagieren auf sensorische Signale durch die Aktivierung eines primären Rezeptors, gefolgt von der Übertragung der Information stromabwärts durch sekundäre Signalisierungsmoleküle zum Wirkungsort. cGMP ist ein weit verbreiteter sekundärer Botenstoff in der zellulären Signaltransduktion, der über Proteinkinase G oder zyklische Nukleotid gesteuerte (CNG) Kanäle wirkt. In sensorischen Neuronen ermöglicht cGMP vor einer Depolarisation eine Modulation und Verstärkung des Signals. Die Chemo-, Thermo- und Sauerstoff-Erkennung in *C. elegans* involviert die sensorischen Neuronen, welche hauptsächlich cGMP als sekundären Botenstoff benutzen. Zum Beispiel reguliert das Pheromon erkennende ASJ Neuron die Larvenentwicklung, reagiert das chemosensorische Neuron AWC auf flüchtige Gerüche und BAG detektiert Sauerstoff und Kohlendioxid in der Umgebung. In diesen Neuronen wirkt cGMP stromabwärts der GPCRs und aktiviert die kationischen TAX-2/-4 CNG - Kanäle, wodurch die sensorischen Neuronen depolarisiert werden. Die Manipulation der cGMP Niveaus ist erforderlich um auf die Signale zwischen Reizerkennung und Depolarisation von sensorischen Neuronen zuzugreifen und Einblick in die Signalkodierung zu erlangen. Dies erreichen wir durch das Implementieren zweier photoaktivierbarer Guanylylzyclasen - 1) einer mutierten Version der Beggiatoa sp bakteriellen, lichtaktivierten Adenylatzyklase, mit Spezifität für GTP (Ryu et al. 2010), die BlgC oder bPGC genannt wird (*Beggiatoa* photoaktivierte Guanylylzyklase) und 2) einem Guanylatzyklase-Rhodopsin (Avelar et al. 2014) von *Blastocladiella emersonii* (BeCyclOp).

bPGC ist eine BLUF (blue light sensing using flavin) Zyklase enthaltende Domäne, die FAD als Co-Faktor verwendet und die Synthese von cGMP aus GTP bei Aktivierung durch blaues Licht katalysiert. Vor der Implementierung in sensorischen Neuronen, wurde ein einfacheres heterologes System mit Koexpression der TAX-2/-4 CNG - Kanäle in *C. elegans* Körperwandmuskeln (BWM) verwendet. Das cGMP, welches durch lichtaktivierte Zyklasen erzeugt wird, aktiviert den CNG Kanal, was zur Muskeldepolarisation führt. Dadurch lassen sich leicht Veränderungen in der Körperlänge erzielen.

Die Lichtaktivierung von bPGC in Muskelzellen, das mit TAX-2 und TAX-4 koexprimiert wurde, führte zu einer langsameren und geringeren Kontraktion (3% Spitzenkontraktion erreicht ~ 10 s nach dem Beginn der bPGC Belichtung/Aktivierung) verglichen mit einer 10%igen Kontraktion bei ChR2 – Aktivierung, die innerhalb einer Sekunde nach Belichtung eintritt (Nagel et al. 2005; Liewald et al. 2008; AzimiHashemi et al. 2014). Durch die Verwendung von zellspezifischen Promotoren wurde bPGC in einer Vielzahl sensorischer Neuronen (ASJ, AWC, BAG) exprimiert, die cGMP als sekundären Botenstoff verwenden. Ziel war es cGMP - vermittelte Signaltransduktion in diesen sensorischen Neuronen durch die optogenetische Aktivierung von bPGC zu rekapitulieren. Die sensorischen ASJ Neuronen steuern die Bildung und Rückbildung des Dauerstadiums durch eine rezeptorähnliche Guanylylzyklase DAF-11. Daf-11(m84) Mutanten zeigen einen konstitutiven Dauer-Phänotyp, was bedeutet, dass die meisten Larven selbst unter günstigen Umgebungsbedingungen ein Dauerstadium annehmen (Vowels and Thomas 1994). In einem solchen konstitutiven Dauer-Phänotyp Hintergrund, führte die optogenetische Aktivierung von bPGC in ASJ Neuronen zu einer teilweisen Repression des Dauer Phänotyps. Für die Photoaktivierung von bPGC in den Neuronen AWC und BAG wurde jedoch kein robuster Verhaltensphänotyp beobachtet.

Kürzlich wurde ein neues Fusionskonstrukt (BeGC1) zwischen der N-terminalen Domäne des mikrobiellen Rhodopsins und der C-terminalen katalytischen Domäne der Guanylylzyclase in dem akuatischen Pilz Blastocladiella emersonii untersucht (Avelar et al. 2014), wobei das entsprechende Protein für die Phototaxis in den Pilzsporen nötig ist. BeGC1 wurde von uns in BeCyclOp (Blastocladiella emersonii

Guanylyl Zyklase Opsin) umbenannt und als ein optogenetisches Werkzeug in *C. elegans* implementiert. Koexprimiert mit TAX-2/-4 CNG Kanälen in den Körperwandmuskel, induzierte BeCyclOp Photoaktivierung eine schnelle lichtgetriebene Depolarisation und Kontraktion der Muskelzellen (~ 10% Spitzenkontraktion, die nach ~ 350 ms erreicht wurde). Die Photoaktivierung zeigte bei grünem Licht eine stärkere Ausprägung und hielt länger an als bei blauem Licht, was sich in den Anregungsmaxima für BeCyclOp wiederspiegelt. Durch die Nutzung von Rohextrakten aus ganzen Tieren, die BeCyclOp in Körperwandmuskeln exprimieren, konnte festgestellt werden, dass BeCyclOp für cGMP spezifischer zu sein scheint als für cAMP.

In den *C. elegans* BAG O_2/CO_2 sensorischen Neuronen löste die BeCyclOp Aktivierung eine schnelle Verlangsamung der Fortbewegung aus, was mit der vorherigen BAG Aktivierung von ChR2 übereinstimmt (Zimmer et al. 2009). Interessanterweise wurde eine schnelle "Erholung" dieser Verlangsamung, trotz der laufenden Photostimulation, sowohl in ChR2 und BeCyclOp Stimulationen beobachtet, was dafür spricht dass diese scheinbare Desensibilisierung weder auf der Ebene des cGMP noch des CNG - Kanals vermittelt wird, sondern an den „output“ Synapsen oder in Netzwerken stromabwärts.

Die Effizienz von bPGC und BeCyclOp als Licht aktivierte cGMP – Generatoren, wurde durch den genetisch kodierten, fluoreszierenden cGMP Indikator WincG2 ausgewertet und verglichen. WincG2 (Worm Indicator of cGMP) basiert auf FlincG3, einem zirkulären permutierten EGFP, welches mit der cGMP Bindungsdomäne von PKG fusioniert ist (Bhargava et al. 2013). Die beiden optogenetischen Aktoren und Sensoren wurden in Muskelzellen exprimiert, was ein großes Areal für die Signalmessung bereitstellt. Wir fanden heraus, dass WincG2 schnelle und langsame Erhöhungen von cGMP detektieren kann, ohne zu bleichen. Die WincG2 Fluoreszenzerhöhung bewegte sich im Minutenbereich im Fall von bPGC, während sich die Steigerung bei BeCyclOp, stärker (dreifach) ausgeprägt zeigte und extrem schnell (im Millisekundenbereich) erfolgte. Die Kinetik und die Größe der Fluoreszenzänderungen in WincG2 reflektieren so die zugrunde liegenden cGMP Dynamiken, die durch zwei verschiedene Guanylylzyklasen erzeugt werden, wobei BeCyclOp viel schneller und effizienter in der cGMP Bildung ist als bPGC.

Um die in vivo Funktion endogener *C. elegans* - Rezeptoren (ACR-16, GLC-1) zu verstehen und um einen lichtaktivierten Glutamatrezeptor in *C. elegans* (GLR-3/6) zu implementieren, haben wir einen optochemisch genetischen Ansatz verwendet (Fehrentz et al. 2011; Kramer et al. 2013; Broichhagen and Trauner 2014). Um diese "blinden" Rezeptoren lichtempfindlich zu machen, wurden photoschaltbare, kovalent bindende Liganden (PTL) entwickelt, die selektiv an Rezeptoren und Kanäle konjugiert sind, welche einen genetisch gezielt eingefügten Cysteinrest zur Bindung des Maleimid enthaltenden PTL haben. Der PTL enthält eine Azobenzeneinheit, die als optischer Schalter funktioniert. Durch Photo-Isomerisierung des Azobenzen Linkers wird der Ligand der Bindestelle in einer vorhersehbaren Weise zur Verfügung gestellt oder entzogen, was in dem für Azobenzen-Photoisomerisierung charakteristischen schnellen Zeitbereich geschieht.

Bewegungssteuernde Interneuronen integrieren Informationen höchstwahrscheinlich durch glutamaterge Innervation, womit die Expression eines LiGluR in diesen Zellen ein besseres Verständnis der sensorischen Transduktion ermöglichen würde. Wir führten in die putativen *C. elegans* Kainat (KA) –Rezeptoren, gebildet aus GLR-3/GLR-6 Heteromeren, Cysteine ein, die sich in analogen Positionen zu jenen die ursprünglich in den LiGluR verwendet wurden (d.h. rat iGluR6), in der Clamshell - Ligandenbindungsdomänen (Volgraf et al. 2006), befanden. Der PTL Maleimid-Azobenzen-glutamat (MAG) ist kovalent an diese Cysteine gebunden, so dass der Rezeptor photogeschaltet werden kann. KA-Rezeptor - Cystein - Mutanten wurden in BWMs exprimiert, wo sie einen funktionellen Glutamatrezeptor bildeten, was aus elektrophysiologischen Aufzeichnungen an der neuromuskulären Verbindungsstelle (NMJ) der Würmer nachgewiesen werden konnte. MAG-1 Inkubation und anschließende Photoschaltung erzeugte eine kleine Strömungsreaktion, die dem "Ein" -Zustand (cis Zustand des MAG-1) entspricht, was suggeriert dass LiGluR funktionell in *C. elegans* wiederhergestellt werden konnte. In Verhaltensexperimenten wurden die LiGluR exprimierenden Tieren mit MAGs mit verschiedenen Linkerlängen inkubiert. Jedoch konnte keine Kontraktion beim Umschalten des MAGs auf den "Ein" -Zustand durch UV - Licht beobachtet werden. Somit könnte erforderlich werden, ein Cystein - Scanning für die GLR-3 und GLR-6 Untereinheiten durchzuführen, um mehr geeignete Stellen für die MAG Konjugation zu erhalten.

Nematoden exprimieren Glutamat-gesteuerte Chloridkanäle (GluCls), die für eine schnelle hemmende Übertragung in normalerweise erregenden glutamatergen Neuronen verwendet werden. Sie sind in verschiedenen Teilen des Nervensystems involviert, ihre Funktionen sind aber nur teilweise verstanden. GluCl ist ein hoch leitfähiger Kanal, dessen Struktur in *C. elegans* gelöst wurde (Hibbs and Gouaux 2011). Somit bietet er die idealen Voraussetzungen um ihn zu einem lichtaktivierten Kanal zu modifizieren. Auf der Basis von molekularen Docking - Studien von GLC-1 und seinem PTL, D-MAG, identifizierten wir Stellen zur Cysteineinführung. Von diesen Kandidaten wurden drei Cysteinstellen (L96C, Q230C, K232C) in HEK 293 - Zellen exprimiert und mit Patch - Clamp Elektrophysiologie überprüft. Die L96C und Q230C Mutanten ergaben keine Reaktion der Ströme auf Glutamat Applikation, was darauf hinwies, dass diese Mutationen die Funktionalität von GLC-1 dramatisch beeinträchtigen. Die K232C Mutation ergab eine robuste Glutamat Reaktion, was auf einen funktionalen GLC-1 hindeutet. Mit D-MAG-0 zeigten sich jedoch keine Photoströme, was darauf hinwies, dass das kovalent gebundene MAG bei K232C die Ligandenbindetasche nicht erreichen konnte, um den Rezeptor zu öffnen, was die Notwendigkeit den PTL zu rekonstruieren suggeriert.

Die *in vivo* Funktion des homomeren nAChR (Acetylcholin Rezeptor), bestehend aus ACR-16 Untereiheiten, ist wenig bekannt. Die Deletion von acr-16 verursacht eine starke Verminderung der Strömungen im neuromuskulären Spalt (neuromuscular junction; NMJ) als Antwort auf Ach (Acetylcholin); in acr-16 Mutanten jedoch sind keine Verhaltensdefekte offensichtlich (Touroutine et al. 2005). Daher wäre LiAChR ein nützliches Werkzeug für die *in vivo* Analyse der NMJ-Funktion. Die PTL für LiAChR basierte auf dem cholinergen Agonist Carbachol. Es wurde gezeigt, dass Carbachol fähig ist, das ACR-16 zu aktivieren ohne von den Acetylcholinesterasen im synaptischen Spalt hydrolysiert zu werden. Danach wurde der PTL Maleimid-Azobenzen-Carbachol (MAC) entworfen und synthetisiert. Wir erzeugten mehrere Cystein - Mutanten auf Basis von Sequenzvergleichen und Modellierung von ACR-16 auf die Struktur des ACh - Bindungsproteins. Die Funktionalität der Cystein - Mutanten wurde durch die Verwendung von lokomotorischen Tests wie Schwimmen und Elektrophysiologie bewertet. Unter den verschiedenen Cystein - Mutanten die erzeugt wurden, zeigte ACR-16 (T78C) in patch clamp Experimenten in der NMJ von *C. elegans* unter Verwendung der PTL MAC bei UV - Beleuchtung

Einwärtsströmungen. Dies zeigte, dass der Rezeptor in der Tat fotogeschaltet werden konnte. In den Schwimmtests jedoch zeigten ACR-16 (T78C) exprimierende Würmer keine funktionelle Wiederherstellung der ACR-16 Funktion, weshalb diese Tiere nicht verwendet werden konnten um die *in vivo* - Rolle von ACR-16 aufzuklären. Die Identifizierung von funktionellen Cystein - Mutanten würde die Implementierung von LiAChR ermöglichen, um die Rolle von ACR-16 im Verhalten von *C. elegans* zu studieren.

Neben den PTLs, konnte für zwei nicht kovalent gebundene, auf Azobenzol basierende Photoschalter, ebenfalls eine lichtabhängige Verhaltensänderung in C. elegans gezeigt werden. Es wurde gezeigt, dass Azocholin, ein photochromer Ligand für α7 nAChRs, eine lichtabhängige Störung des Schwimmverhaltens in *C. elegans* vermutlich über nAChRs evoziert. Der vermeintliche Zielrezeptor, der in *C. elegans* durch Azocholin aktiviert wird, muss jedoch noch identifiziert werden. Erhöhte Mengen des sekundären Botenstoffes Lipid Diacylglycerol (DAG) induzieren Signalereignisse stromabwärts, die die Translokation von C1 - Domänen enthaltenden Proteine zur Plasmamembran mit einschließen, Es wurde gezeigt, dass photoaktivierte DAGs (PhoDAG) in *C. elegans* eine lichtabhängige Überempfindlichkeit zu Aldicarb, einem Azetylcholinesterase - Hemmer, hervorrufen. Die beobachtete Überempfindlichkeit zu Aldicarb, in Gegenwart von aktiviertem PhoDAG, kann einer erhöhten Acetylcholin - Freisetzung in den cholinergen Neuronen zugeschrieben werden. Ein Effekt, der möglicherweise durch die erhöhte Aktivierung von UNC-13, einem präsynaptischen Diacylglycerin-bindenden Protein und Vermittler von synaptischem Vesikel-priming (Lackner et al. 1999), verursacht wird.

SUMMARY

Optogenetics, though still only a decade old field, has revolutionized research in neurobiology. It comprises of methods that allow control of neural activity by light in a minimally-invasive, spatio-temporally precise and genetically targeted manner. The optogenetic actuators or the genetically encoded light sensitive elements mediate light driven manipulation of membrane potential, intracellular signalling, neuronal

network activity and behaviour (Fenno et al. 2011; Dugué et al. 2012). These techniques have been particularly useful for dissecting neural circuits and behaviour in the transparent and genetically amenable nematode model system *Caenorhabditis elegans* (Husson et al. 2013; Fang-yen et al. 2015).

In fact, *C. elegans* was the first living organism in which microbial rhodopsin based optogenetic tools (Channelrhodopsin-2 or ChR2, and Halorhodopsin or NpHR) were successfully implemented and bimodal 'remote' control of behaviour was achieved (Nagel et al. 2005; Zhang et al. 2007). Since then it has been a prominent model for the development and application of novel optogenetic tools and techniques, especially in the nervous system which comprises of 302 neurons and is organised in a hierarchical organization. The environmental stimuli are sensed by the sensory neurons, leading to the processing of information by the downstream interneurons, that relay to motor neurons which in-turn synapse onto muscles that drive the movement-based responses.

The microbial rhodopsins like ChR2 and NpHR mediate light driven depolarization and hyperpolarization, respectively and thereby activate or inhibit neural activity. However, they do not allow local control of membrane potential as they are expressed all over the plasma membrane of the cell rather than being restricted to specific domains, for example synaptic sites. Moreover, they completely over-ride the intrinsic activity of the cell, completely bypassing the signal transduction processes inside the cell. Thus, in order to study intracellular signalling and to answer questions pertaining to the endogenous role of receptors and channels in an *in-vivo* context, the optogenetic tool-kit needs to be expanded.

This thesis aimed at developing and implementing novel optogenetic tools in *C. elegans* that allow for sub-cellular signalling control as well as endogenous receptor control. These are: two light activated guanylyl cyclases (bPGC and BeCyclOp) to modify cyclic guanosine monophosphate (cGMP) mediated signalling in the sensory neurons, as well as attempts towards rendering endogenous *C. elegans* receptors - glutamate receptor (GLR-3/-6), acetylcholine receptor (ACR-16), glutamate gated chloride channel (GLC-1) light switchable and to understand their biological function *in-vivo*.

Organisms respond to sensory cues by activation of a primary receptor followed by relay of information downstream to effector targets by secondary signalling

molecules. cGMP is a widely used 2nd messenger in cellular signaling, acting *via* protein kinase G or cyclic nucleotide gated (CNG) channels. In sensory neurons, cGMP allows for signal modulation and amplification, before depolarization. Chemo-, thermo-, and oxygen-sensation in *C. elegans* involve sensory neurons that use cGMP as the main 2nd messenger. For example, ASJ is the pheromone sensing neuron regulating larval development, AWC is the chemosensory neuron responding to volatile odours and BAG senses oxygen and carbon dioxide in the environment. In these neurons, cGMP acts downstream of the GPCRs and functions by activating cationic TAX-2/-4 CNG channels, thereby depolarising the sensory neuron. Manipulating cGMP levels is required to access signalling between sensation and sensory neuron depolarization, thereby provide insights into signal encoding. We achieve this by implementing two photo-activatable guanylyl cyclases - 1) a mutated version of *Beggiatoa sp.* bacterial light-activated adenylyl cyclase, with specificity for GTP (Ryu et al. 2010), termed BlgC or bPGC (*Beggiatoa* photoactivated guanylyl cyclase) and 2) guanylyl cyclase rhodopsin (Avelar et al. 2014) from *Blastocladiella emersonii* (BeCyclOp).

bPGC is a BLUF (blue light sensing using flavin) domain containing cyclase which uses FAD as the co-factor and catalyses the synthesis of cGMP from GTP upon activation by blue light. Prior to implementation in sensory neurons, a simpler heterologous system with co-expression of the TAX-2/-4 CNG channel in *C. elegans* body wall muscle (BWM) was used. The cGMP generated by the light activated cyclases activates the CNG channel leading to the muscle depolarization, thereby causing changes in body length which can be easily scored.

Light activation of bPGC expressed in muscle cells along with TAX-2 and TAX-4 caused a slow and small contraction (3% peak contraction achieved ~10 s after the onset of illumination for bPGC) as compared to 10% contraction achieved within a second after the onset of ChR2 activation (Nagel et al. 2005; Liewald et al. 2008; AzimiHashemi et al. 2014). Using cell specific promoters, bPGC was expressed in a variety of *C. elegans* sensory neurons (ASJ, AWC, BAG) that use cGMP as the second messenger. It was aimed to recapitulate cGMP mediated signal transduction in these sensory neurons using optogenetic activation of bPGC. ASJ sensory neurons govern dauer formation and recovery through a receptor-like guanylyl cyclase DAF-11. *daf-11(m84)* mutants display a constitutive dauer-phenotype i.e.

most larvae become dauers even under favourable environmental conditions (Vowels and Thomas 1994). In such a constitutive dauer-phenotype background, optogenetic activation of bPGC in ASJ neurons led to partial repression of the dauer phenotype. However, for AWC and BAG neurons, no robust behavioural phenotype was observed upon photo-activation of bPGC.

Recently, a novel gene fusion (BeGC1) of N-terminal microbial rhodopsin domain and C-terminal catalytic guanylyl cyclase domain was reported in the aquatic fungus *Blastocladiella emersonii* (Avelar et al. 2014) where the corresponding protein is required by the fungal zoospores to phototax. We renamed it as BeCyclOp (*Blastocladiella emersonii* Guanylyl Cyclase Opsin) and implemented it as an optogenetic tool in *C. elegans. Via* co-expression of the TAX-2/-4 CNG channel in the body wall muscle, BeCyclOp photoactivation induced rapid light-driven depolarization and contraction of muscle cells (~ 10% peak contraction with the contraction on rate of ~350 ms). The photo-activation was more pronounced and long lasting with the green light as compared to the blue light, highlighting the excitation maxima for BeCyclOp. Using crude extracts derived from whole animals expressing BeCyclOp in BWMs, BeCyclOp was found to be significantly more specific for cGMP as compared to cAMP.

In *C. elegans* O_2/CO_2 sensory BAG neurons, BeCyclOp activation rapidly triggered slowing of locomotion, consistent with the normal sensory function of BAG, and in agreement with previous BAG activation by ChR2 (Zimmer et al. 2009). Interestingly, a quick 'recovery' of the slowing response was observed both in ChR2 and BeCyclOp stimulation, despite ongoing photostimulation, arguing that this apparent desensitization is neither mediated at the level of cGMP nor the CNG channel, but at the output synapses or in downstream networks.

The efficiency of bPGC and BeCyclOp as light activated cGMP generators was also evaluated and compared using a genetically encoded fluorescent cGMP indicator, WincG2. WincG2 (or worm indicator of cGMP) is based on FlincG3, a circularly permutated EGFP fused to cGMP binding domain of PKG (Bhargava et al. 2013). The optogenetic actuator and sensor were expressed in muscle cells which provide a large area for signal measurement. We found that WincG2 can detect fast and slow rises in cGMP without bleaching. The WincG2 fluorescence increased over minutes time scale in case of bPGC as compared to BeCyclOp where the rise was

more pronounced (three-fold) and was extremely fast (in milli-second time range). The kinetics and magnitude of fluorescence changes of WincG2 thus aptly reflect the underlying cGMP dynamics brought about by two different guanylyl cyclases - BeCyclOp being much more rapid and efficient in cGMP generation as compared to bPGC.

To understand the *in-vivo* function of endogenous *C. elegans* receptors (ACR-16, GLC-1) and to implement a light activated glutamate receptor in *C. elegans* (GLR-3/6), we employed an opto-chemical genetic approach (Fehrentz et al. 2011; Kramer et al. 2013; Broichhagen and Trauner 2014). To render these 'blind' receptors light-sensitive, photo-switchable tethered ligands (PTL) were designed that are selectively conjugated to genetically targeted receptors and channels that have an introduced cysteine residue for attachment of the maleimide-containing PTL. The PTL further comprises of an azobenzene moiety, which functions as the optical switch. Photo-isomerization of the azobenzene linker presents or withdraws the ligand from the binding site in a predictable manner and on the fast timescale characteristic of azobenzene photo-isomerization.

Locomotion command interneurons integrate sensory information likely by glutamatergic innervation, thus a LiGluR expressed in these cells would enable to better understand sensory transduction. We introduced cysteines in putative *C. elegans* kainate (KA-) receptors formed by GLR-3/GLR-6 heteromer, in positions analogous to those used in the original LiGluR (i.e. rat iGluR6), in the clamshell ligand binding domain (Volgraf et al. 2006). The PTL maleimide-azobenzene-glutamate (MAG) is covalently linked to these cysteines, allowing the receptor to be photoswitched. KA-receptor cysteine mutants were expressed in BWMs where they formed a functional glutamate receptor as could be demonstrated from electrophysiological recordings at the neuro-muscular junction (NMJ) of worms. Importantly, MAG-1 incubation and subsequent photoswitching produced a small current response corresponding to the 'on' state (cis state of MAG-1) suggesting that LiGluR could be functionally re-constituted in *C. elegans*. In behavior experiments, the animals expressing LiGluR in muscles were incubated with MAGs differing in their linker lengths. However, no contraction could be observed upon switching the MAGs to the 'on' state by UV light. Thus, it may be required to perform a cysteine

scanning for the GLR-3 and GLR-6 subunits to obtain more suitable sites for MAG conjugation.

Nematodes express glutamate-gated chloride channels (GluCls), used for fast inhibitory transmission from otherwise excitatory, glutamatergic neurons. They are involved in several parts of the nervous system, but their functions are only partially understood. GluCl is a high conductance channel, and the structure of *C. elegans* GLC-1 has been solved (Hibbs and Gouaux 2011). Thus, this provides ideal prerequisites to turn it into a light-activated channel. We identified cysteine introduction sites based on molecular docking studies of GLC-1 with its PTL, D-MAG. Among these candidate cysteine sites, three (L96C, Q230C, K232C) were expressed in HEK 293 cells and checked with patch clamp electrophysiology. The L96C and Q230C mutants did not yield a current response upon glutamate application indicating the mutations dramatically impaired the functionality of GLC-1. The K232C mutation gave a robust glutamate response suggesting a functional GLC-1. However, it did not give any photo-currents with D-MAG-0 which indicates that the covalently attached MAG at K232C could not access the ligand binding pocket so as to gate the receptor, suggesting the need to re-engineer the PTL.

The in *vivo* function of the homomeric nAChR consisting of ACR-16 subunits is poorly understood. Deletion of *acr-16* causes strong reduction of NMJ currents in response to ACh, however no behavioral defects are apparent in *acr-16* mutants (Touroutine et al. 2005). Hence for analyzing NMJ function in vivo, LiAChR would be a useful tool. The PTL for LiAChR was based on the cholinergic agonist, carbachol. It was shown that carbachol is capable of activating *ACR-16* without being hydrolysed by the acetylcholinesterases in the synaptic cleft. Thereafter, the PTL - maleimide-azobenzene-carbachol (MAC) was designed and synthesized. We generated several cysteine mutants based on sequence alignments and modelling of ACR-16 onto the structure of ACh binding protein. The functionality of the cysteine mutants was assessed using locomotory assays like swimming and electrophysiology. Among the various cysteine mutants generated, ACR-16(T78C) showed inward currents with the PTL MAC upon UV illumination in the patch clamp experiment done on *C. elegans* NMJ. This showed that the receptor could indeed be photoswitched. However, in swimming assays, the transgenic worms expressing ACR-16(T78C) did not show a functional rescue of ACR-16, hence these animals

could not be used to elucidate the in-*vivo* role of ACR-16. Identification of functional cysteine mutant would enable the implementation of LiAChR to study the role of ACR-16 in *C. elegans* behavior.

Apart from the PTLs, two non-tethered photoswitches based on azobenzenes were also shown to evoke light-dependent behavioral changes in *C. elegans.* Azocholine, a photochromic ligand for α7 nAChRs, was shown to evoke light-dependent perturbation of swimming behavior in *C. elegans* likely affected via nAChRs. However, the putative target receptor activated by AzoCholine in *C. elegans* remains to be identified. Elevated levels of the second messenger lipid diacylglycerol (DAG) induce downstream signaling events which include the translocation of C1 domain-containing proteins toward the plasma membrane. Photoactivated DAGs (PhoDAG) was shown to evoke light-dependent hypersensitivity to Aldicarb, an acetylcholinesterase inhibitor in *C. elegans.* The hypersensitivity to aldicarb observed in the presence of activated PhoDAG can be attributed to increased acetylcholine release from the cholinergic neurons, an effect possibly caused due to the increased activation of UNC-13, a diacylglycerol-binding pre-synaptic protein and mediator of synaptic vesicle priming (Lackner et al. 1999).

1. INTRODUCTION

1.1 Optogenetics: A historical perspective and general overview

One of the grand challenges of the 21st century science is to understand how circuits of neurons through their electrical and chemical interplay give rise to processes by which we feel, act, learn, and remember and thus try to explore the biological basis of consciousness. And to unravel those mysteries and to understand how neuronal circuits process the incoming sensory information and compute a behaviourally relevant output, it is imperative, a) to identify the distinct neuron types involved and their connectivity, b) to have the means to manipulate the activity of the select neurons in the circuit and finally, c) to have the means to record the activity of the neurons in the circuit while monitoring behaviour.

Santiago Ramón y Cajal at the advent of 20th century laid down the foundations of modern neuroscience by providing first detailed descriptions of the morphology and connectivity in most regions of the central nervous system (Ramón Y Cajal 1894; DeFelipe 2002). These advances in histology and anatomy were paralleled by advances in the realm of neurophysiology where electrical perturbation was then the method of choice to investigate neural function. As early as in 1979, post the era of discovery of DNA structure and genetic code, Francis Crick, co-discoverer of the double helical DNA structure, clearly engrossed with the next frontier of science penned an article entitled “Thinking about the brain”. Therein he stressed on the need for “a method by which all neurons of just one type could be inactivated, leaving the others more or less unaltered” (Crick 1979). This aptly reflected the major limitation of electrical perturbation since spatiotemporally precise, minimally invasive and cell-specific stimulation was not possible with it. Twenty years later in another insightful article discussing the impact of molecular biology in neuroscience and the possible future directions, Crick pointed out the requirement of "to be able to turn the firing of one or more types of neuron on and off in the alert animal in a rapid manner. The ideal signal would be light, probably at an infrared wavelength to allow the light to penetrate far enough. This seems rather far-fetched but it is conceivable that molecular biologists could engineer a particular cell type to be sensitive to light in this way"(Crick 1999). Extraordinarily, in the next decade, Crick's vision did come true and 'optogenetics' since then has revolutionized neuro-scientific research.

Optogenetics is a branch of biotechnology that encompasses tools and approaches from optics, genetics and bioengineering to observe and control the function of genetically targeted groups of cells with light (Miesenböck 2009; Miesenböck 2011). Although the term 'optogenetics' was first used in 2006 (Deisseroth et al. 2006), light responsive sensors to monitor neuronal activity had already emerged in the late nineties (Miesenböck and Rothman 1997; Miyawaki et al. 1997; Siegel and Isacoff 1997; Miesenböck et al. 1998).

The first use of light to control neural activity came in the form of caged compounds such as secondary messenger molecules, ions, and neurotransmitters which were developed initially inert, but became active upon light illumination (Kaplan and Somlyo 1989; Nerbonne 1996; Ellis-Davies 2007). However these photochemical approaches did not provide ways to control specific cell types apart from uncaging being an irreversible process.

Cell-type specific activation of neurons was first achieved in a series of pioneering work by the Miesenböck group when they employed the components of the *Drosophila* photoreceptor signalling cascade to activate cultured hippocampal neurons (Zemelman et al. 2002). Later, they light-activated heterologously expressed ligand-gated ionotropic receptors ($P2X_2$ or TRPV1) by photo-uncaging orthogonal ligands (ATP or Capsaicin, respectively) to trigger escape behavior in *Drosophila* (Zemelman et al. 2003; Lima and Miesenböck 2005) providing the first instance of an optically “remote-controlled” animal.

The process of photoactivation of chemically modified ligands can be made more efficient and specific by covalently linking the ligand to the protein and obtaining a 'photoswitchable tethered ligand' (PTL), a technique used successfully to control muscular nicotinic acetylcholine receptors (Bartels et al. 1971), ionotropic glutamate receptors (Volgraf et al. 2006), potassium channels (Banghart et al. 2004; Chambers et al. 2006; Fortin et al. 2011), a chimeric potassium-selective glutamate receptor called HyLighter (Janovjak et al. 2010), neuronal nicotinic acetylcholine receptors (Tochitsky et al. 2012), metabotropic glutamate receptors (Levitz et al. 2013), P2X receptors (Lemoine et al. 2013), GABA receptors (Lin et al. 2014; Lin et al. 2015) and recently NMDA receptors (Berlin et al. 2016). Although they enable receptor sub-type specific control, one major drawback of photochemical approaches is the

necessity of either delivering the ligand or conjugating the PTL to the target protein in the organism in an *in-vivo* context, which can be difficult to accomplish.

Around the time the photochemical approaches to control neural activity were taking flight, microbial rhodopsins- Channelrhodopsin-1(ChR1) and Channelrhodopsin-2 (ChR2) that operate as single component light-gated ion channels were discovered (Sineshchekov et al. 2002; Nagel et al. 2002; Nagel et al. 2003). Remarkably, Channelrhodopsin-2 (ChR2) - the blue light sensitive cation channel and the first member of the microbial rhodopsin based optogenetic tool family, could be heterologously expressed in mammalian neurons and in live *C. elegans* to optically trigger action potentials with millisecond timescale precision (Boyden et al. 2005; Nagel et al. 2005). The chromphore *all-trans* retinal (ATR) which is the necessary co-factor for the rhodopsins, is naturally produced in nearly all mammalian cell types and can be easily provided to *C.elegans* (Blomhoff and Blomhoff 2006; Zhang et al. 2006). In summary, in the last decade or so, a revolution has started wherein a large number of native and engineered natural photoreceptor as well as synthetic photo-switch based optogenetic tools have been successfully implemented in a wide variety of model organisms to achieve a precise, exogenous and non-invasive control of membrane potential, intracellular signaling, network activity or behavior (Miesenböck 2011; Zhang et al. 2011; Fenno et al. 2011; Boyden 2011; Dugué et al. 2012).

1.2 Natural Photoreceptors

Light is used by organisms to drive diverse processes such as plant development, photosynthesis, circadian behaviour, phototaxis and vision. The response to light is mediated by a variety of light-responsive proteins or photoreceptors possessing distinct structures, chromophores, biophysical mechanisms of operation and physiological roles. Chromophores are the site of photon absorption and comprise of a conjugated π system allowing electron delocalization. The larger the size of conjugated π system, the greater is the extent of electron delocalization and the longer is the wavelength of light at which the chromophore will absorb. The effect of photon absorption is then relayed onto the protein, which responds with a conformational change and initiates the downstream biological reaction. Based on the structure and photochemistry of the associated chromophore, photoreceptor

proteins can be broadly classified into 6 major groups: rhodopsins, phototropins, BLUF proteins (blue-light sensors utilizing flavin adenine dinucleotide), cryptochromes, phytochromes, and photoactive yellow proteins (or xanthopsins) (Van Der Horst and Hellingwerf 2004; Hegemann 2008; Möglich et al. 2010; Zoltowski and Gardner 2011) (**Figure I-1**). The photoreceptor families and the use of the natural photoreceptors as optogenetic tools are described in detail in the following subsections.

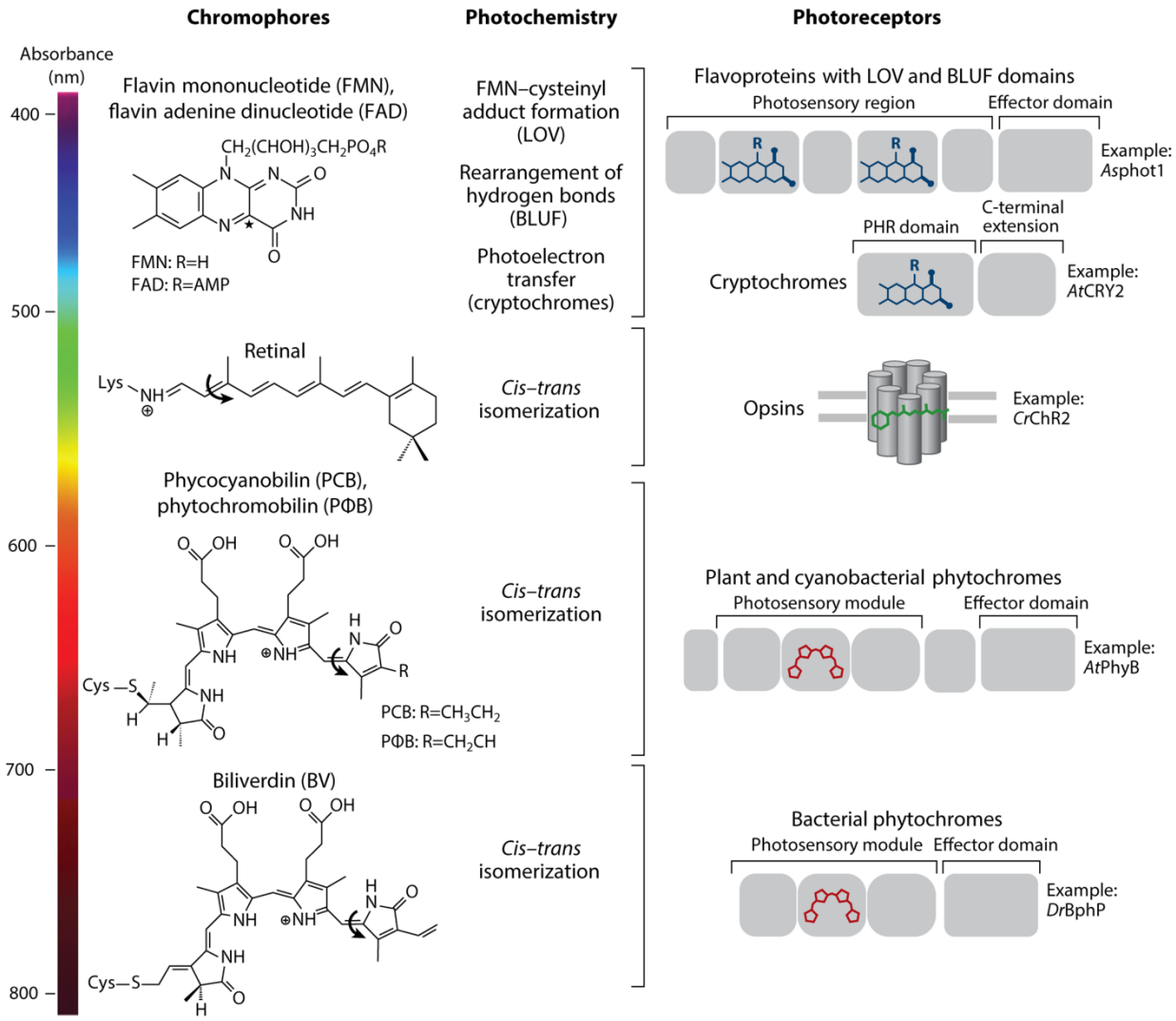

FIGURE I-1: The different classes of photoreceptors and their chromophores utilized as templates to engineer optogenetic tools.(left) Chemical structures of the chromophores and a color-scale bar representing their peak absorption wavelength along with primary photochemistry is indicated. (*Right*) schematic domain structure of one example receptor for each type of photoreceptor is presented. Abbreviations: *As*phot1, *Avena sativa* phototropin 1; *At*CRY2, *Arabidopsis thaliana* cryptochrome 2; *At*PhyB, *A. thaliana* phytochrome B; BLUF, blue-light-utilizing flavin adenine dinucleotide; *Cr*ChR2, *Chlamydomonas reinhardtii* channelrhodopsin-2; *Dr*BphP, *Deinococcus radiodurans* bacterial phytochrome; LOV, light-oxygen-voltage-sensing. (From Shcherbakova et al. 2015)

1.2.1 Rhodopsins

Rhodopsins are integral membrane photoreceptor proteins found in organisms of all domains of life - *Eukaryotes, Bacteria*, and *Archaea*, enabling them to sense and respond to light. Rhodopsins consist of opsin apoproteins and a covalently linked retinal (the aldehyde of vitamin A) chromophore that isomerizes after photon absorption, leading to a structural change that is transmitted to the opsin, causing initiation of intracellular signalling.

Rhodopsins can be broadly classified into two receptor families - type 1 (microbial) and type 2 (animal or G protein coupled) rhodopsins (Spudich et al. 2000). Although the microbial and animal rhodopsins do not share any sequence similarity, they do share a common structural architecture - The opsins comprise of seven transmembrane alpha helices with an extracellular N- and intracellular C-terminus. In both types of photoreceptors, the chromophore retinal forms a protonated Schiff base with the ε-amino group of a conserved lysine residue located in the seventh transmembrane domain (Spudich et al. 2000; Palczewski 2006; Ernst et al. 2014). The changes in the protonation state are crucial to the signal transduction of rhodopsins. While microbial rhodopsins contain all-*trans* retinal in the dark state, which photoisomerizes to 13-*cis* retinal; most animal rhodopsins contain 11-*cis* retinal in the dark state, which photoisomerizes to all-*trans* retinal (ATR).

Microbial rhodopsins comprise of light-driven ion pumps, light-gated ion channels, and light sensors which couple to transducer proteins. The archaeal rhodopsins from *Halobacterium salinarum* (historically referred to as *Halobacterium halobium*) - bacteriorhodopsin (Oesterhelt and Stoeckenius 1971) and halorhodopsin (Matsuno-Yagi and Mukohata 1977; Schobert and Lanyi 1982) act as light-driven outward proton pump and inward chloride pump, respectively. The other two rhodopsins from *H. salinarum* - sensory rhodopsin I and II (Spudich and Bogomolni 1984), act as positive and negative sensors of phototaxis, respectively. Sensory rhodopsin II activates a cytoplasmic signal cascade through a transmembrane transducer protein that binds to the rhodopsin by means of two transmembrane helices (Gordeliy et al. 2002). Another sensory rhodopsin found in *Eubacteria* - *Anabena* sensory rhodopsin - is a sensor that activates a soluble transducer (Jung et al. 2003). Channelrhodopsins (ChRs), another sub-family of microbial rhodopsins, were found in green algae *Chlamydomonas reinhardtii* where they function as light gated cation

channels in the algal eyespot to depolarize the membrane upon light absorption resulting in the relay of signal to the flagella leading to the phototactic response from the algae (Nagel et al. 2002; Nagel et al. 2003).

Despite differences in their photocycle intermediates and kinetics, the photochemical event which is highly conserved among all the microbial rhodopsins, is the increase in the propensity of the protonated Schiff base to donate a proton after the absorption of photon by the chromophore retinal (Spudich et al. 2000). The effect of increase in the acidity of the Schiff base, however, varies in different rhodopsins. In bacteriorhodopsin, representing the family of light driven proton pumps, the Schiff base loses a proton to the extracellular compartment. The re-protonation happens after a conformational change in the protein that allows the Schiff base to be accessible only from the cytoplasmic side. The net result is the outward transport of one proton per photocycle (Lanyi 1995). In case of halorhodopsin, a chloride pump, there exists an electrostatically bound chloride counterion in place of the extracellular proton acceptor site in bacteriorhodopsin, thereby preventing the deprotonation of the Schiff base. Upon retinal isomerization, the N - H dipole moment vector of the Schiff base points to the intracellular orientation, which in case of halorhodopsin pulls the chloride ion towards the cytoplasmic side along the ion conduction path, resulting in the discharge of one chloride ion inwards per transport cycle (Kolbe et al. 2000). For channelrhodopsin-2, the loss and gain of protons from the Schiff base occurs at opposite sides of the membrane, as in the case of bacteriorhodopsin, resulting in active proton shuttling (Feldbauer et al. 2009). However, following reprotonation, ChR2 remains transiently permeable to cations (e.g. Na^+, K^+, Ca^{2+}) , making ChR2 a passively cation conducting leaky proton pump (Nagel et al. 2003; Feldbauer et al. 2009). The major passive leak conductance in ChR2 is identified with the P520 spectroscopic intermediate of the photocycle formed within a milli-second of the photon absorption by ATR (Bamann et al. 2008; Ritter et al. 2008; Bamann et al. 2010).

Animal rhodopsins, which serve as photoreceptors of vertebrate and invertebrate eyes (Baylor 1996; Hardie and Raghu 2001; Palczewski 2006), belong to the superfamily of G-protein coupled receptors (GPCRs) which detect extracellular signals, typically small ligands like hormones and neurotransmitters (Pierce et al. 2002; Rosenbaum et al. 2009). GPCRs upon ligand binding undergo conformational

change thereby catalyzing GDP/GTP exchange on membrane-bound hetero-trimeric G proteins, thus initiating G-protein mediated signalling cascades (Rosenbaum et al. 2009). GPCRs, upon activation-dependent phosphorylation by a GPCR kinase, can also interact with arrestin to induce G-protein independent signalling and suppression of ligand mediated activation signal (Lefkowitz and Shenoy 2005). The visual rhodopsin in the vertebrate photoreceptor cells is a specialized GPCR capable of detecting single photons (Rieke and Baylor 1998). Upon photon absorption, visual rhodopsins in vertebrates signal via the G protein - transducin, which activates cyclic GMP (cGMP) phosphodiesterase, thereby leading to a drop in cGMP concentration resulting in the closing of cGMP-gated sodium/calcium channels and hyperpolarizing the photoreceptor cell, hence relaying the signal onto the next layer of cells in the visual processing (Baylor 1996; Zhang and Cote 2005). The closure of cGMP gated channels leads to a drop of cytoplasmic calcium concentration in the outer segments of the photoreceptor cells, causing the activation of guanylyl cyclases present in the outer segment by the now calcium free guanylyl cyclase activating proteins (GCAPs) thus restoring cGMP levels (Frins et al. 1996; Yu et al. 1999).

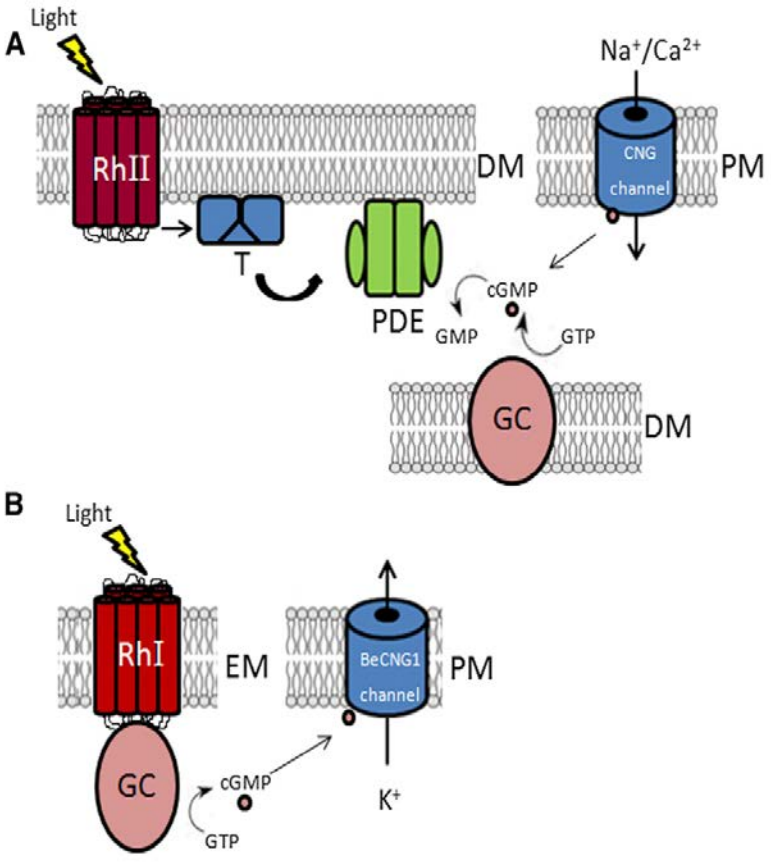

FIGURE I-2 : Schematic representation of signalling in vertebrate rod photoreceptor and *Blastocladiella emersonii* zoospore phototaxis. **A.** Photo-activation of type-2 rhodopsin leads to the downstream GPCR mediated activation of cGMP phospho-diesterase (PDE). **B.** Photoisomerization of rhodopsin in BeGC1 activates guanylyl cyclase activity. Cyclic GMP opens K+-selective BeCNG1 channels, thereby causing hyperpolari-zation of the plasma membrane. (From Avelar et al. 2014)

Invertebrate visual rhodopsins, couple to another G-protein ($G_{q/11}$), which causes the activation of transient receptor potential (TRP) channels and cell depolarization (Hardie and Raghu 2001). Vertebrate rhodopsins lose the chromophore ATR after the light absorption, thereby requiring constant supply of 11-*cis* retinal (Wald 1968). In contrast, the microbial and invertebrate rhodopsins retain the chromophore throughout the photocycle and use another photon at a shifted wavelength to revert back to the dark adapted retinal state (Hardie and Raghu 2001; Bamann et al. 2008).

Recently, a novel gene fusion (BeGC1) of N-terminal microbial rhodopsin domain and C-terminal catalytic guanylyl cyclase domain was reported in the aquatic fungus *Blastocladiella emersonii* (Avelar et al. 2014) (**Figure I-2**).The protein BeGC1 is localized to the eyespot apparatus membrane of the fungal zoospores where upon light reception and retinal isomerization, the rhodopsin-cyclase catalyzes cGMP production which leads to the opening of putative K^+-selective BeCNG1 channels, thereby causing hyperpolarization of the plasma membrane and aiding in the flagellar movement. Using zoospore phototaxis experiments, it was shown that BeGC1 has the peak excitation wavelength in the green range (520-560 nm) of the spectrum. The predicted BeGC1 amino acid sequence (626 amino acids, 68 kDa) has a conserved lysine which forms the Schiff base with amino group of the retinal. BeGC1 possesses an unprecedented domain architecture wherein the light sensing rhodopsin domain and the catalytic cyclase domain are encoded in the same protein molecule, thereby presenting a unique way of light directly triggering the cyclase activity.

1.2.1.1 Application of microbial rhodopsins as optogenetic tools

ChR2 was the first member of the single component optogenetic tool family to be used for neuroscience based applications when it was demonstrated that heterologous expression of ChR2 in cultured neurons conferred them blue light sensitivity and ChR2 could reliably evoke temporally precise action potentials (Boyden et al. 2005) and control animal behaviour (Nagel et al. 2005). In 2007, optical inhibition of neural activity and animal (*C. elegans*) behaviour was made possible using the yellow light activated chloride pump - Halorhodopsin (NpHR) from the archaebacterium *Natronomonas pharaonis* (Zhang et al. 2007). Light gated proton pumps like Archaerhodopsin-3, known as Arch, from *Halorubrum sodomense*, and Mac, from the fungus *Leptosphaeria maculans* were further added onto the list

of optogenetic tools that can act as neuronal inhibitors (Chow et al. 2010) (**Figure I-3**). Recently, two naturally occurring blue and green light-gated chloride conducting channelrhodopsin from the algae *Guillardia theta* have been reported and shown to be the most potent optical inhibitors currently available (Govorunova et al. 2015).

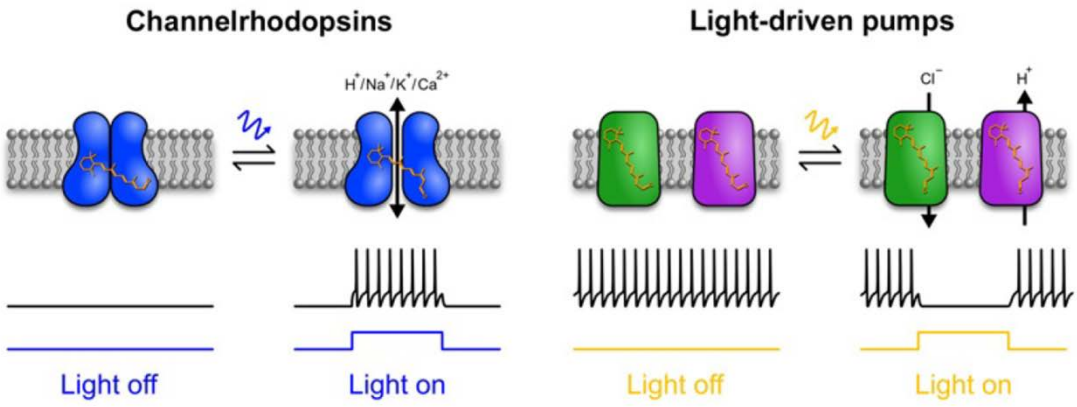

Figure I-3: Microbial rhodopsins as optogenetic tools to control neuronal firing with millisecond precision. Channelrhodopsins with their light-gated cationic conductance can be used to depolarize neurons. Microbial light-driven pumps can produce hyperpolarizing currents by translocating chloride ions into the cell (halorhodopsins) or protons to the outside (archaerhodopsin). (Modified from Dugué et al. 2012)

Over the years, several variants of ChR2 have also been engineered with altered photocycle kinetics, conductance, ion selectivity and optical spectra to allow for specific optogenetic applications (Nagel et al. 2005; Berndt et al. 2009; Lin et al. 2009; Berndt et al. 2011; Lin 2011). Discovery of red-light sensitive Chrimson from *Chlamydomonas noctigama* (Klapoetke et al. 2014) has stretched the excitation spectrum to the red range. Since 2005, microbial rhodopsin based optogenetic tools have been applied in multiple systems and enabled multimodal control of membrane potential and behaviour. Systems include cultured neurons, mammalian brain slices, *C. elegans*, *Drosophila*, zebrafish, chick embryos, live mice and non-human primates and studies include but are not limited to: light-stimulated synaptic plasticity and investigation of synaptic function, functional analysis and mapping of neural circuits, partial restoration of vision in a model of *Retinitis pigmentosa*, insights into mechanisms of depression, anxiety and Parkinson's disease, identification of memory engram cells (Liewald et al. 2008; Stirman et al. 2011; Fenno et al. 2011; Dugué et al. 2012; Husson et al. 2013; Adamantidis et al. 2015; Dejean et al. 2015; Tonegawa et al. 2015; Owald et al. 2015) .

1.2.2 Phototropins, Blue-Light Sensors Utilizing Flavin Adenine Dinucleotide (BLUF Proteins), Cryptochromes, and Phytochromes

Phototropins, BLUF proteins and cryptochromes carry flavin adenine nucleotides as chromophores. While phototropins and cryptochromes are widely distributed across plants, microbes, fungi, animals, BLUF proteins have only been found in bacteria and some lower eukaryotes (Möglich et al. 2010; Zoltowski and Gardner 2011). Phototropins and BLUF proteins have modular structures with distinct light-sensing domains, called LOV (light, oxygen, voltage) and BLUF domains, respectively. These sensor domains are often coupled to enzymatic effector domains, for example a kinase in case of LOV proteins, or an adenylyl/guanylyl cyclase or phosphodiesterase in some BLUF proteins.

The LOV domains of phototropins possess a typical fold of PAS domain family of sensors, of which they are members (Crosson and Moffat 2001). In the dark-adapted state, flavin mononucleotide (FMN) chromophore is held in a non-covalent manner by four α-helices against a scaffold of five β-strands. The scaffold itself is located on top of a fifth, C-terminal helix, which is termed Jα helix. Upon blue light irradiation, LOV domains undergo a reversible photocycle involving the formation of a thiol adduct between the FMN chromophore and a conserved cysteine residue within the protein. This leads to the disruption of the β scaffold, thereby causing the Jα helix to undock from the shelf, resulting in activation (or disinhibition) of enzymatic activity (Crosson and Moffat 2002; Harper et al. 2003). In contrast, the BLUF domain containing photoreceptors bind flavin adenine dinucleotide (FAD) as a chromophore and there is no covalent bond formation involved in a BLUF photocycle. Instead, the blue light illumination causes hydrogen bond network rearrangement within the active site FAD and nearby conserved tyrosine and glutamine residues thus leading to the breaking of a structural anchor between a C-terminal helical cap and a core domain containing the FAD (Gauden et al. 2006; Sadeghian et al. 2008; Wu and Gardner 2009; Zoltowski and Gardner 2011).

The cryptochrome family of flavin-blue light receptors include many photoreceptors in plants and animals, light dependent transcription factors involved in circadian regulation and light-activated DNA repair enzymes (photolyases). The activity of cryptochromes is based on largely disordered C-terminal extensions that are set free

from the light-sensor domain in the illuminated state (Yang et al. 2000; Partch et al. 2005) and expose buried recognition motifs for other proteins.

Phytochromes have two conformational states: a red-sensitive Pr and a far-red-sensitive Pfr (Bae and Choi 2008; Möglich et al. 2010). The photoswitch is controlled by the isomerization of the tetrapyrrole chromophore which lies nested in the three-domain sensory module located at the N-terminus, while the C terminus comprises of a histidine kinase–related domain whose light regulation have been verified in prokaryotes but not in plants. In plants, the Pfr conformer translocates into the nucleus (Yamaguchi et al. 1999; Chen et al. 2005), where it induces the phosphorylation and subsequent destruction of constitutively active transcription factors termed phytochrome-interacting factors (PIFs) (Ni et al. 1999).

1.2.2.1 Application of BLUF proteins, LOV proteins and Phytochromes to Light-activated cyclases and phosophodiesterases

The LOV, BLUF and phytochrome photoreceptors have extensively contributed to the development of fluorescent proteins, biosensors and optogenetic tools (Christie et al. 2012; Shcherbakova et al. 2015). Here I discuss their application as light activated cyclases and phosphodiesterases. BLUF-domain containing blue-light photo-activated adenylyl cyclases - *Euglena gracilis* PAC (euPAC) and *Beggiatoa* PAC (bPAC) have been employed as optogenetic tools to enable fast manipulation of cellular cAMP level by light *in vivo* (Schröder-Lang et al. 2007; Ryu et al. 2010; Stierl et al. 2011). euPAC has been used to control cAMP levels in *Xenopus* oocytes and neurons of *Drosophila* and *C. elegans* (Schröder-Lang et al. 2007; Weissenberger et al. 2011). euPAC photostimulation in cholinergic neurons of *C. elegans* resulted in increased locomotion activity that was coordinated, as opposed to the spastic paralysis observed when photostimulating these neurons via ChR2, emphasizing that PACs permit increased neuronal activity by facilitating transmitter release, thus enhancing intrinsic activity patterns, but not overriding them (Weissenberger et al. 2011). euPAC has some dark activity, and may thus cause constitutively increased [cAMP] when expressed at high levels. bPAC has negligible dark activity, but is extremely light sensitive. bPAC has been used to trigger light induced cAMP production in cultured neurons, neurons of *Drosophila* (Stierl et al. 2011), neurons of *C. elegans* (Flavell et al. 2013) and mouse sperms (Jansen et al. 2015). Based on genome sequence, bPAC encodes a 350-amino acid protein,

consisting of a blue light-sensing BLUF domain linked C-terminally to a Type III adenylyl cyclase with the functional protein likely forming a homodimer with two catalytic sites in between the two cyclase domains (Stierl et al. 2011).

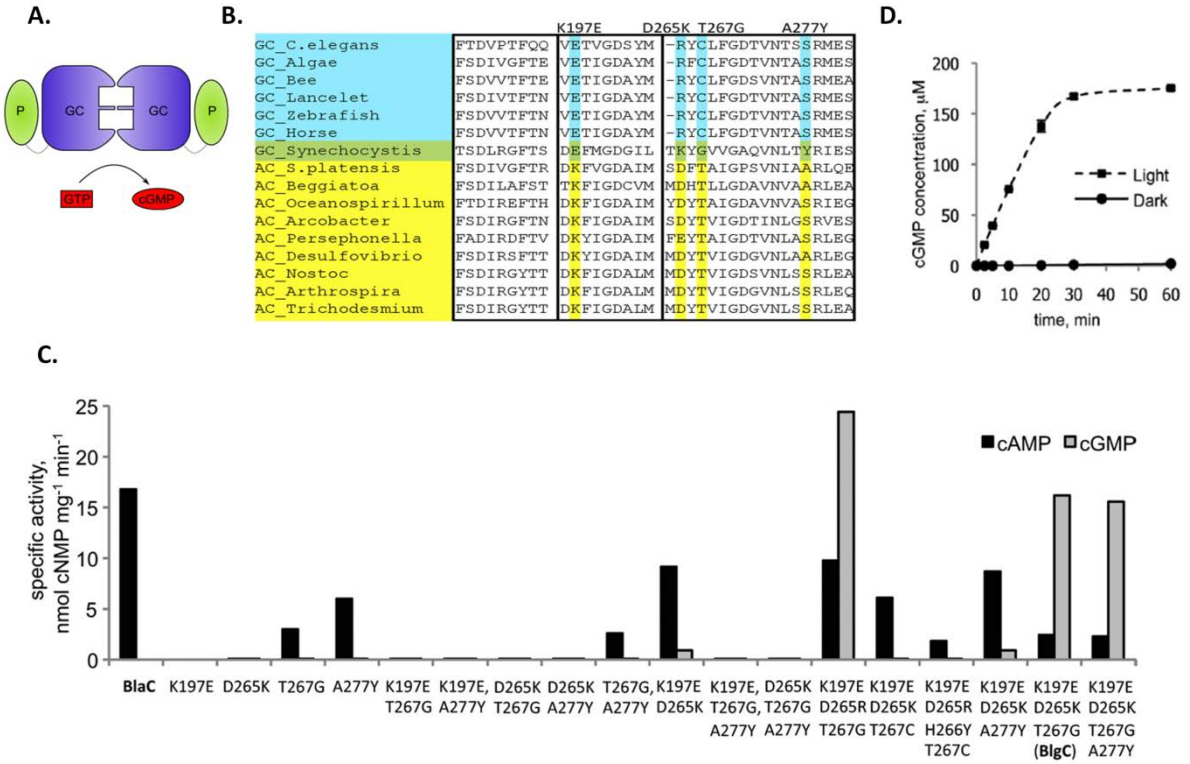

FIGURE I-4: *Beggiatoa* photoactivated guanylyl cyclase (bPGC) **A.** Schematic illustration of the homodimer bPGC consisting of a guanylyl cyclase (GC) and a photoactivated BLUF-domain (P). **B.** Multiple sequence alignment of selected class III nucleotidyl cyclases. **C.** Adenylyl or guanylyl cyclase activities in different bPAC mutants resulting in creation of BlgC or bPGC **D.** Light-dependent guanylyl cyclase activity of bPGC in vitro (adapted from (Ryu et al. 2010)

3 point mutations (K197E/D265K/T267G) in the ATP binding region of bPAC changed its specificity to GTP and resulted in a guanylyl cyclase (GC), named bPGC (for *Beggiatoa* photo-activated guanylyl cyclase) whose GC activity was about 10-fold higher than adenylyl cyclase activity. The point mutations were selected from a bigger screen based on multiple sequence alignment of selected class III nucleotidyl cyclases (Ryu et al. 2010). bPGC shows no dark activity and a 2 orders of magnitude higher activity upon blue-light irradiation (**Figure I-4**).

A blue light activated LOV domain based PAC from cyanobacterium *Microcoleus chthonoplastes* (mPAC) shows higher constitutive activity in the dark, but also when illuminated with blue light as compared to bPAC (Raffelberg et al. 2013). mPAC

partially restored development of an adenylyl cyclase null mutant (aca-) of the eukaryote *Dictyostelium discoideum* (Chen et al. 2014).

A near infra-red light activated adenylyl cyclase has been developed by fusing the photosensory module of the *Rhodobacter sphaeroides* bacteriophytochrome BphG1 and the adenylate cyclase domain from *Nostoc sp*. CyaB1 resulting in a cyclase with a sixfold photodynamic range. When expressed in cholinergic neurons in *Caenorhabditis elegans*, the engineered adenylyl cyclase caused light-dependent manner increase in body bends while moving on solid substrate and swimming frequency (Ryu et al. 2014).

A light-activated phosphodiesterase (LAPD) was engineered by recombining the photosensor module of *Deinococcus radiodurans* bacterial phytochrome with the effector module of human phosphodiesterase 2A (Gasser et al. 2014). Upon red-light illumination, LAPD up-regulates hydrolysis of cAMP and cGMP by up to sixfold, whereas far-red light can be used to down-regulate activity. LAPD was shown to mediate light-dependent cAMP and cGMP hydrolysis in eukaryotic cell cultures and in zebrafish embryos. Both bacteriophytochrome based tools require the biliverdin chromophore for activity.

1.2.2.2 Genetically encoded sensors for cAMP and cGMP

Biochemical methods like radioimmunoassays, enzyme linked immunoassays; indirect electrophysiological readouts using cyclic nucleotide gated ion channels; and FRET and single GFP-linked fluorescent indicators (**Figure I-5**) are some of the strategies which have been used to estimate cAMP and cGMP in living cells and tissues (Sprenger and Nikolaev 2013). The regulatory and catalytic subunits of Protein Kinase A (PKA, major cAMP effector) fused with the FRET pairs like CFP/YFP have been used as genetically encoded cAMP indicators in neonatal and adult rat cardiomyocytes (Zaccolo et al. 2000; Zaccolo and Pozzan 2002; Warrier et al. 2005). Simpler single chain PKA based FRET sensors containing single cAMP binding domain of PKA regulatory subunit IIα have been developed, which provide faster kinetics (Nikolaev et al. 2004). Several Epac (exchange protein directly activated by cAMP)-based, single chain FRET sensors have also been developed and used to measure cAMP dynamics in living cells (Nikolaev et al. 2004; DiPilato et al. 2004; Ponsioen et al. 2004). A further class of FRET-cAMP sensors have a single cAMP binding domain from the murine hyperpolarization activated cyclic nucleotide-

gated potassium channel 2 (HCN2) sandwiched between CFP and YFP (Nikolaev et al. 2006a).

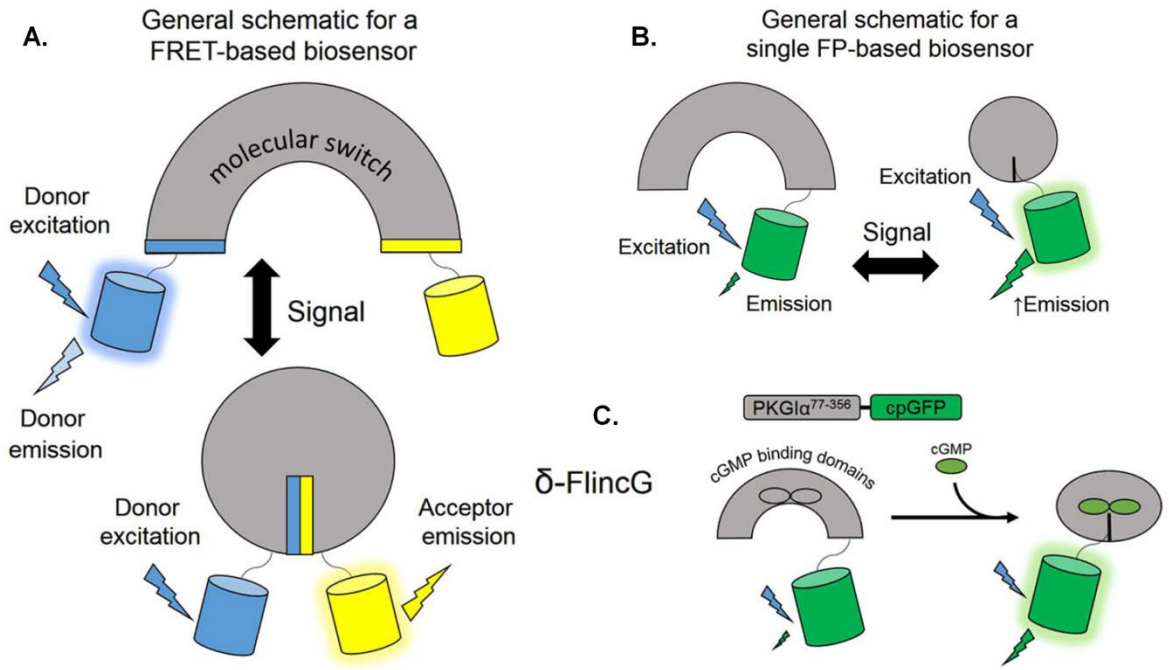

FIGURE I-5: Biosensors for cAMP and cGMP. **A**. and **B.** Schematic illustrations of FRET-based and single fluorescent protein-based biosensors, respectively. **C.** δ-FlincG utilizes a PKG1α$^{77-356}$ truncated domain linked to a single cpGFP reporting unit. Upon binding cGMP, the fluorescence intensity of cpGFP increases (modified from Gorshkov and Zhang 2014).

Many FRET cGMP sensors based on partially truncated Protein kinase G (PKG, major cGMP effector) containing both cGMP domains sandwiched between CFP and YFP have been developed (Sato et al. 2000; Honda et al. 2001; Nikolaev and Lohse 2009). The primary among them being the Cygnet family of cGMP biosensors which have provided novel insights into cGMP dynamics in various cell types (Honda et al. 2005a; Honda et al. 2005b). Development of shorter cGMP sensors containing only single cGMP binding domains has improved the dynamic range and temporal resolution offered by the long PKG-based sensors (Nikolaev et al. 2006b; Russwurm et al. 2007). Single cGMP binding domain B from PKG-I or the GAF domains from PDE2 and PDE5 (PDE, Phosphodieserase) fused to CFP and YFP has resulted in several such fluorescent cGMP sensors (Nikolaev et al. 2006b). The most promising among these was cGES-DE5 (cGMP energy transfer sensor derived from PDE5),

which exhibited the highest cGMP to cAMP selectivity, fast responses to intracellular cGMP signals and good FRET signal amplitudes. Exchange of CFP-YFP with T-Sapphire-Dimer2 as FRET pair increased the cGMP affinity of cGES-DE5 40-fold, making it suitable for detection of low cGMP concentrations (Niino et al. 2009).

Russwurm *et al.* used a systematic approach to design several new cGMP-FRET sensors based on tandem cGMP binding domains from PKG and GAF domains from PDE5 fused to CFP and YFP (Russwurm et al. 2007). Three cGMP indicators (cGi-500, -3000, -6000) with cGMP affinities of 500, 3000, and 6000 nM, respectively displayed high cGMP over cAMP selectivity, fast kinetics, and a greater dynamic range than the cGMP indicators described above. cGi500 was also functionally expressed *in vivo* in *C. elegans* where it was used to analyse cGMP dynamics in oxygen sensing neurons (Couto et al. 2013).

Non-FRET fluorescent indicators of cGMP (FlincGs) containing two in-tandem PKG-1 cGMP binding sites fused to the N-terminus of circularly permuted GFP were subsequently developed (Nausch et al. 2008; Isner and Maathuis 2011). Different truncated PKG-1 variants α, β, δ, which differ in their N-terminal regulatory domain were used leading to α-FlincG, β-FlincG, and δ-FlincG, respectively. cGMP binding to PKG derived sequence leads to conformational changes and an increase in fluorescence from circularly permuted EGFP (**Figure I-5**). Extremely fast dissociation and association kinetics of δ-FlincG (affinity of 170 nM for cGMP and 48 μM for cAMP) allow detection of rapid changes in cGMP concentrations (Nausch et al. 2008). A further engineered version for better expression in mammalian cells and neurons, namely FlincG3 was made by changing the C-terminal tail, introducing a GCaMP (a genetically encoded calcium sensor)-like mutation in the EGFP region and an N-terminal tag (Bhargava et al. 2013). Purified FlincG3 protein showed a lower cGMP affinity (890nM) than reported for the original FlincG (170nM) but nonetheless had fast kinetics and a 230-fold selectivity over cAMP. Like other EGFP-based sensors, it was strongly influenced by pH over the physiological range.

1.3 Artificial Photoreceptors

Apart from the naturally occuring photosensitive proteins and associated chromophores being employed as optogenetic tools, the last few years have also witnessed the growth of 'photopharmacology' - an alternate sub-field within

optogenetics wherein synthetic photo-switches are being used to control biological activity by targeting endogenous ion channels, GPCRs, transporters, enzymes, components of cytoskeleton and lipids, and making them light responsive (Fehrentz et al. 2011; Kramer et al. 2013; Velema et al. 2014; Broichhagen et al. 2015b).

The first synthetic photo-switches used were the caged ligands where the ligand is endowed with a photolabile protecting group that renders it biologically active only upon light induced cleavage of the protecting group (Ellis-Davies 2007). Caged glutamate and ATP have been very successfully used in mapping neural systems (Callaway and Katz 1993; Lutz et al. 2008). However, there are certain functional disadvantages with the caging approach: Uncaging is an irreversible process and also produces by-products which can be toxic. Also some caged compounds have off-target effects, for instance acting as antagonists to other receptors (Canepari et al. 2001). Some of these drawbacks can be overcome by using photoswitchable ligands which toggle between two configurations and can trigger the desired biological effect in a reversible manner. The photo-switches can be tightly bound through non-covalent interactions which are referred to as photochromic ligands (PCL) or can be covalently attached to the suitably modified target called as photo-switchable tethered ligands (PTLs)(Fehrentz et al. 2011). PTLs provide the added advantage of allowing receptor-subtype level control and cell-type specific targeting.

1.3.1 Photo-switchable tethered ligands

PTLs comprise of three structural and functional components: 1) bio-conjugating handle that can latch onto the engineered target molecule by covalent bond formation, 2) a molecular photo-switch and 3) a ligand that can influence the biological activity of the target molecule (Fehrentz et al. 2011; Broichhagen and Trauner 2014). PTL, depending upon the ligand properties and the attachment site, can function as a tethered agonist, antagonist or an allosteric modulator. Maleimide which is a thiol-reactive group has been used to tether onto a strategically positioned cysteine residue introduced on the ligand binding domain of the genetically engineered receptor. Azobenzenes have emerged as the most versatile and reliable choice as far as the photo-switch is concerned for a variety of reasons. Azobenzenes are isomerized to their *cis* form with UV-A or deeply violet light (315-380 nm) and revert back thermally or with another wavelength to the thermodynamically more stable state, usually the *trans* state. *cis* and *trans* forms exhibits large differences in

geometry and dipole moment. They exhibit fast photo-switching in the pico-second time range preventing intersystem-crossing and singlet oxygen formation. Azobenzenes also have high extinction coefficients and quantum yields which means relatively low intensity illumination can be used for photoisomerization. Also, they are highly photostable and can be switched over numerous cycles. While the photostationary *cis*/*trans* ratios can be as high as 9:1 at shorter wavelengths, it is impossible to push the azobenzenes fully into *cis*-state by irradiation. Thus, there is always some background activity of the remaining *trans* isomer (Gorostiza et al. 2007). However, this is not be a drawback when one wants to trigger bi-stable systems, like a neuron below or above the voltage threshold for action potential firing. Maleimide based PTLs possess relative selectivity for the intended cysteines owing to the affinity labelling mechanism - they first interact with the receptor in a non-covalent manner through their ligand head group and then undergo rapid covalent attachment provided the photo-switch is in the right photo-stationary state (Gorostiza et al. 2007). Also, there are very few accessible reduced cysteines available on the surface of cells.

The first system to emerge using this opto-chemical genetic approach was “synthetic photoisomerizable azobenzene-regulated K+ channel” (SPARK). It consists of the PTL MAQ (maleimide/azobenzene/quaternary ammonium) conjugated to a genetically introduced cysteine residue (E422C), chosen on the basis of existing X-ray structures, on an extracellular loop of K_v1-type voltage gated potassium channel (Banghart et al. 2004). It was shown to silence neuronal firing in rat hippocampal neurons upon illumination with UV-A light. In 2006, the approach was expanded to glutamate receptors. Conjugation of the PTL named L-MAG (maleimide/azobenzene/glutamate), which comes in different versions depending on the linker length (L-MAG0/1/2), to the rat kainate receptor GluK2 modified at L439 postion to cysteine yielded light-gated ionotropic glutamate receptor (LiGluR) (Volgraf et al. 2006; Szobota et al. 2007a) (**Figure I-6**). Under 380-nm illumination, the PTL photoisomerizes to the bent *cis* configuration and directs its glutamate end toward the binding site, activating the receptor. With 500-nm light, the agonist is withdrawn and the receptor is deactivated. LiGluR was shown to reliably control spiking in cultured neurons and when expressed in sensory neurons in zebrafish larvae, activation of LiGluR could suppress the escape response to touch in a

reversible manner (Szobota et al. 2007a). It was also used to understand the functional role of so-called Kolmer-Agduhr neurons, whose activity was shown to be essential for forward swimming and thereby aid in dissecting out the neural circuitry underlying locomotion in zebrafish (Wyart et al. 2009). LiGluR has also been implemented in the retinae of blind mice and been able to restore light dependent activity and visually guided behaviour (Caporale et al. 2011).

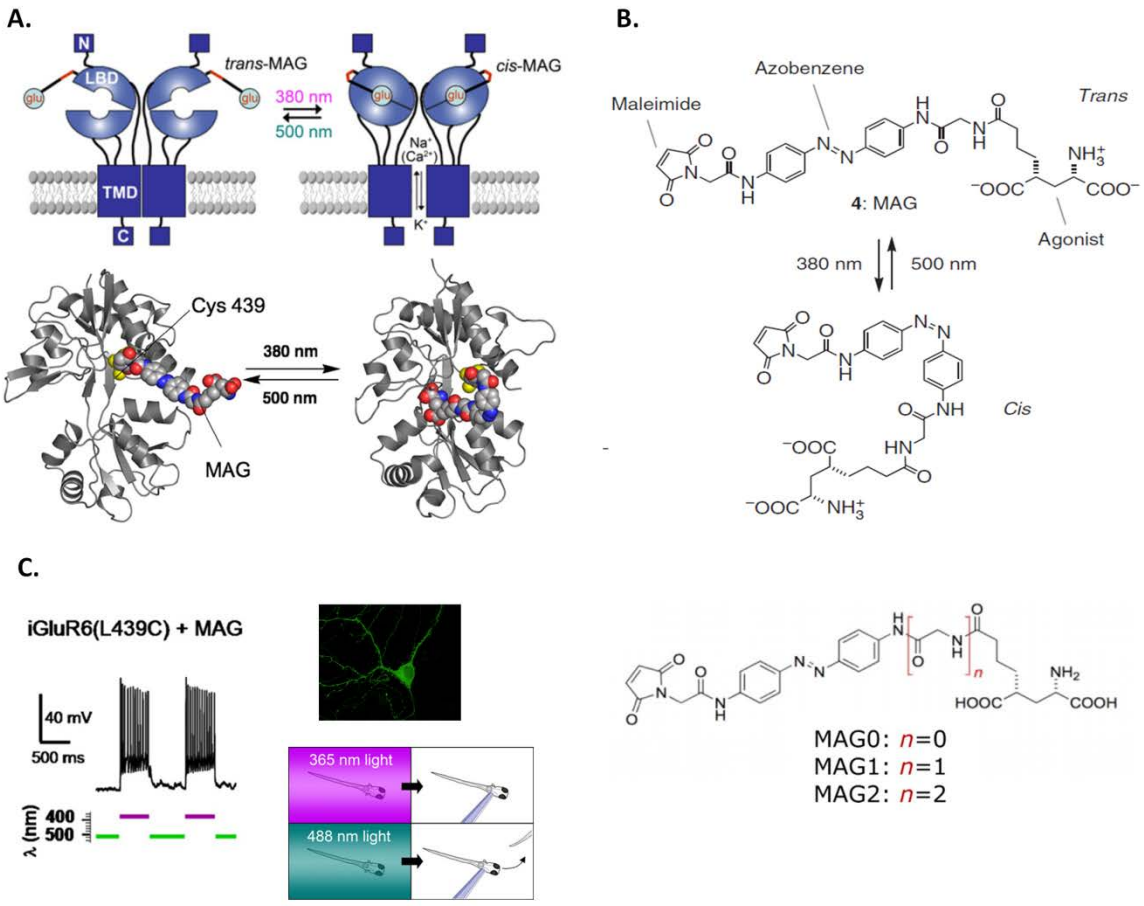

FIGURE I-6: **A.** Schematic of LiGluR with the MAG covalently attached to the L439C of the ligand binding domain of GluK2 and gating the channel in light-dependent fashion. **B.** Maleimide-Azobenzene-Glutamate (MAG) and *cis-trans* isomers. Also shown MAGs with different linker length. **C.** Implementation of LiGluR in cultured neurons can reliably evoke action potentials and alter zebrafish behaviour (Modified from Volgraf et al. 2006; Gorostiza et al. 2007; Szobota et al. 2007; Numano et al. 2009).

The design of LiGluR was based on the X-ray crystal structure of a closed GluK2-Ligand Binding Domain (LBD) containing the agonist (2S,4R)-4-methylglutamate (Mayer 2005). This structure highlighted the existence of an “exit tunnel” from the bound ligand to the surface of the closed LBD arranged in a clamshell-like

arrangement which is highly conserved in glutamate receptors. Due to the exit tunnel, it was proposed that the tethered glutamate with L-stereoisomer conformation could bind to the LBD, trigger the clamshell-closure and activate the receptor as an agonist in a reversible, light dependent fashion. After screening through a number of cysteine mutants of GluK2 as potential LiGluR candidates, L439C resulted in the best position for MAG-1 attachment and light-dependent activation of the receptor (Volgraf et al. 2006; Szobota et al. 2007a).

Several variations to this light driven molecular machine have been implemented. For example, the movement of attachment site to L486C from L439C results in a tethered antagonist instead of an agonist (Numano et al. 2009). Attachment of L-MAG to a channel chimera, made by combining GluK2- derived light sensitive LBD of LiGluR with the potassium selective trans-membrane domain of the prokaryotic glutamate receptor SGluR0, resulted in inhibition instead of activation upon illumination with UV-light (HyLighter) (Janovjak et al. 2010). L-MAG was also used to investigate gating mechanisms in ionotropic glutamate receptor homomers and heteromers. Ultrafast photo-switching yielded a real-time measure of gating and revealed that partially occupied receptors can activate without desensitizing (Reiner and Isacoff 2014). The replacement of an amide moiety by an amine in L-MAG yielded L-MAG460, triggered ionic currents with green light (visible light instead of UV-A), while relaxation and deactivation occurred quickly in the dark (Kienzler et al. 2013). This is desirable when phototoxicity is a concern, e.g. in the restoration of vision. Recently, L-MAG_{2p} and L-$MAGA_{2p}$ were described, which could be switched to the active *cis*-form via two-photon excitation. The latter possesses a naphthalene 'antenna' with a large two-photon cross-section. Attachment of L-$MAG(A)_{2p}$ to the LiGluR permits efficient two-photon activation of neurons and astrocytes with subcellular resolution with near-infrared light (820 nm) (Izquierdo-Serra et al. 2014). The PTL principle has been applied to GPCRs - metabotropic glutamate receptors 2, 3 and 6. Light gated metabotropic glutamate receptors (LimGluRs) were shown to work in rodent brain slices and zebrafish (Levitz et al. 2013).

Pentameric nicotinic acetylcholine receptors have also been rendered photo-switchable with PTLs (Tochitsky et al. 2012). The two different PTL molecules developed, MAACh and MAHoCh are azobenzene based choline derivatives differing in their linker lengths. MAACh was shown to function as a photoswitchable

agonist when tethered to an α3β4 receptor mutant, whereas conjugation of MAHoCh to α4β2 resulted in photo-antagonism. The light-activated nicotinic acetylcholine receptors (LinAChRs) functioned well in *Xenopus* oocytes but are yet to be implemented in neurons. $GABA_A$ receptors, P2X2 receptors and NMDA receptors have also been converted to photoreceptors using PTLs (Yue et al. 2012; Lemoine et al. 2013; Berlin et al. 2016).

1.4 The nematode *Caenorhabditis elegans* as a model organism

1.4.1 *Caenorhabditis elegans*

Caenorhabditis elegans is a free living (non-parasitic) roundworm. Though often wrongly described as a soil nematode, it can be most easily isolated from naturally decaying vegetal matter like fruits and flowers (Barrière and Félix 2014). In the laboratory, it is reared on a bacterial diet of OP-50 (a uracil auxotroph of *E. coli*) on standard agar plates (Brenner 1974). *C. elegans* has a generation time of 3 days at 25° C from egg to egg-laying adult and primarily occurs in nature as a self-fertilizing hermaphrodite, although males arise at a frequency of <0.2%. Before attaining the adulthood, the animals go through four larval stages namely L1, L2, L3, L4 (**Figure I-7**), each terminated by a period of sleep-like inactivity called lethargus followed by the molting of the old cuticle (Raizen et al. 2008). Under adverse environmental conditions, such as insufficient food, crowding, etc. which is sensed by the chemosensory systems, an alternative developmental stage can occur. Here, at the L2 to L3 molt, a resistant 'dauer' larval form is produced, which can last several months, or until the conditions become favourable again (Golden and Riddle 1984; Corsi et al. 2015).

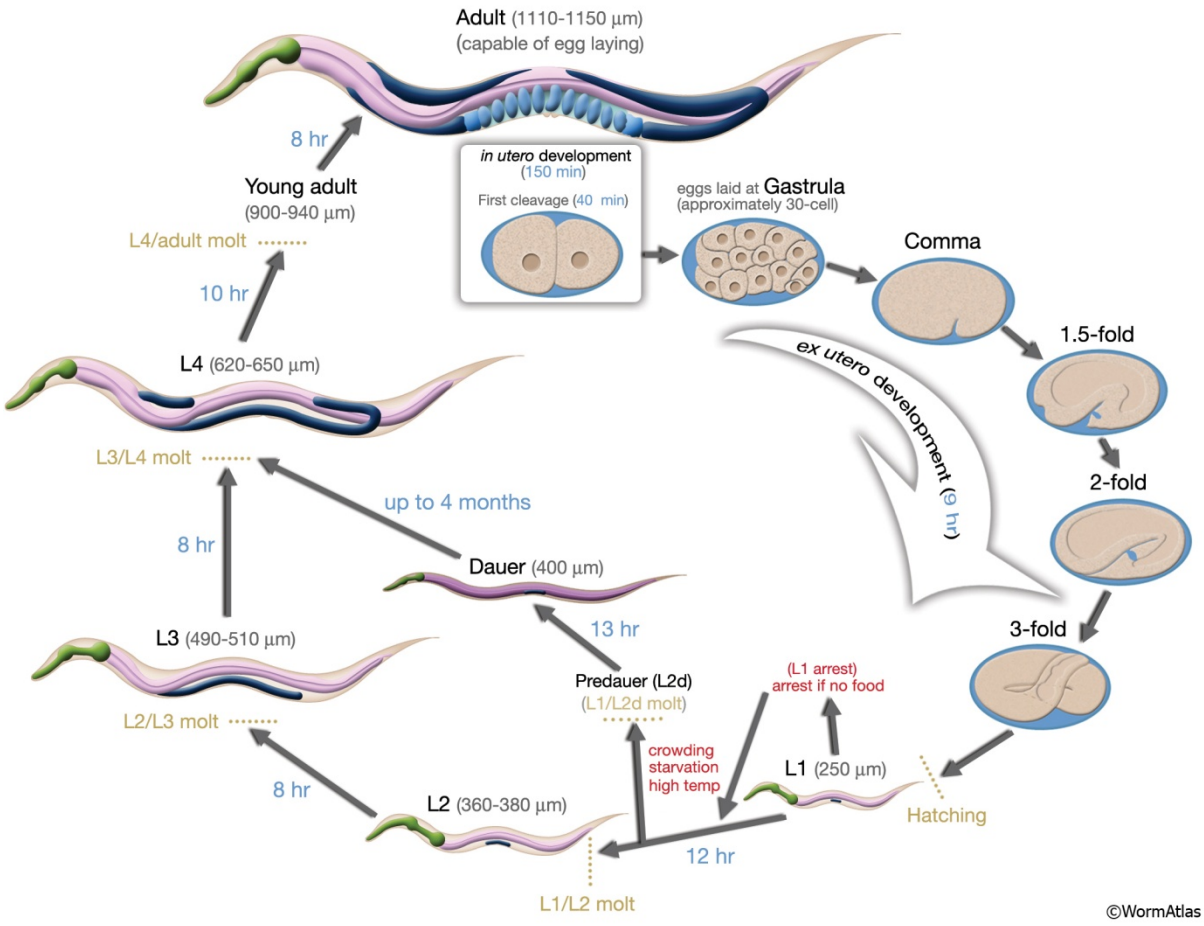

FIGURE I-7: Life cycle of *Caenorhabditis elegans* at 22^{0}C (from WormAtlas, Altun, Z.F. and Hall 2011)

C. elegans, as a model organism, has been the focus of a lot of seminal discoveries and achievements: the first metazoan organism to have the complete cell lineage deciphered (Sulston and Horvitz 1977; Kimble and Hirsh 1979; Sulston et al. 1983); first complete wiring diagram of a nervous system (White et al. 1986; Jarrell et al. 2012; White 2013); discovery of the first axon guidance genes (Hedgecock et al. 1987; Hedgecock et al. 1990; Culotti 1994); first description of microRNA (Lee et al. 1993; Wightman et al. 1993); introduction of GFP as a biological marker (Chalfie et al. 1994; Boulin et al. 2006); first metazoan genome sequenced (*C. elegans* Sequencing Consortium 1998; Schwarz 2005); Discovery of RNA interference (RNAi) (Fire et al. 1998); and the first use of microbial rhodopsin based optogenetics in an intact animal (Nagel et al. 2005).

The 100 Mb *C. elegans* genome has 20,444 protein encoding genes (*C. elegans* Sequencing Consortium 1998, WormBase release WS245, Oct. 2014) organized into

five pairs of autosomal chromosomes and two X chromosomes (males have a single X chromosome). The majority of the protein-coding mRNAs undergo *trans*-splicing, which refers to the addition of one of two 22-nucleotide long leader sequences (SL1 and SL2) at the 5' end of the mRNA, and to downstream translational start sites in mRNAs originating from operons. The leader sequence is known to help in translational initiation. The operon-like pre-mRNA (multigenic transcript) is cleaved into several transcripts. This is effected by trans-splicing i.e. the spliced leader being added to the 'internal' (downstream) start sites and the mRNA cleaved by the nature of the splicing reaction. These transcripts are encoded by genes that are closely spaced together in tandem and are expressed from a single promoter. This operon like organization is a unique feature found in the *C. elegans* genome (Blumenthal 2005).

C. elegans is an attractive model system for comprehensive analyses of neural circuits underlying behavior using optogenetic approaches since:

a) It has a transparent body, thereby allowing illumination to every neuron for optogenetic analysis. b) It is highly amenable to genetics and neural genes are well conserved between *C. elegans* and humans. c) It has a highly stereotyped nervous system with 302 neurons mapped to single cell and even synapse resolution (White et al. 1986). Many neurons are well studied in a functional manner, thus enabling reliable predictions so as to which (behavioural) effect is evoked by a certain light-switch in a particular cell. Even more interesting, optogenetic manipulation of previously unstudied neurons allows deducing the function of these cells in a straightforward fashion. d) Processes of signal transduction and integration in sensory neurons and their downstream interneurons are only partially understood, such that using light-switches may allow for a better understanding of these cells and circuits.

1.4.2 Overview of the *C. elegans* nervous system

The nervous system of an adult hermaphrodite *C. elegans* comprises of 302 neurons (White et al. 1986), while an adult male possesses 383 neurons (the extra neurons are primarily located in the specialized male tail). Every *C. elegans* neuron has a 2- or 3-letter name indicating class and in certain cases has a number indicating the neuron number within one class. If the neurons are radially symmetrical, the 3-letter name is followed by L (left), R (right), D (dorsal), or V (ventral) to specify anatomical

position. The neurons communicate with each other through 6400 chemical synapses, 900 gap junctions, and 1500 neuromuscular junctions (NMJs). The synapses are located in four major areas: the nerve ring encircling the pharynx, the ventral nerve cord, the dorsal nerve cord, and the neuropil in the tail. Most of the synapses are *en-passant* (side by side as neurites pass each other). Instead of processes being sent to muscle cells from motor neurons, the muscles send specialized cellular projections called as muscle arms to motor neurons to receive synapses (**Figure I-8**).

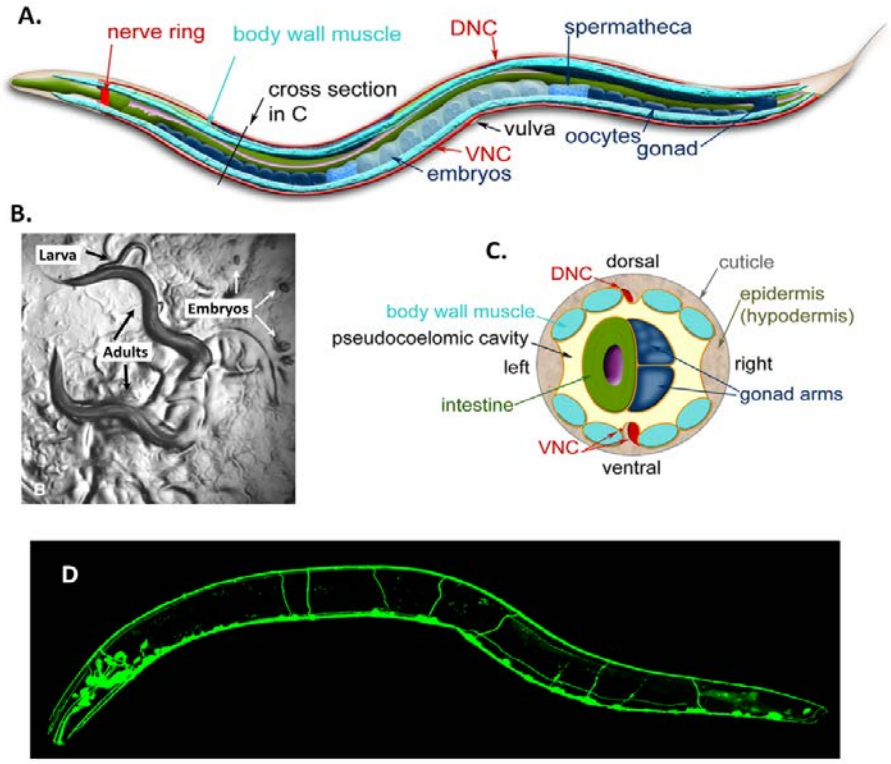

FIGURE I-8: A. Anatomy of adult hermaphrodite worm. The dorsal nerve cord (DNC) and ventral nerve cord (VNC) extend along the entire length of the animal from the nerve ring. **B.** *C. elegans* viewed through the dissecting microscope. **C.** Cross-section through the anterior region of the hermaphrodite (indiacted with a black line in A) **D.** Fluorescent image showing the nervous system labelled with a GFP reporter (sto-6::gfp).(Adapted from Corsi et al. 2015)

Apart from the neurons, the nervous system also has several glia-like cells which are primarily associated with the sensory neurons (Oikonomou and Shaham 2011). The nerve conduction through neurons is through passive graded potentials. No voltage gated sodium channels have been found in the *C. elegans* genome (Bargmann 1998) and no action potentials have been detected in the neurons (Goodman et al.

1998). Although bi-stable plateau potentials have been observed in the RMD motor neurons (Mellem et al. 2008), they may not classify as action potentials due to the following reasons: the amplitude of the transients varies according to the amplitude and duration of the stimulus; there is no proof that they are terminated intrinsically and the waveform of the transients responds to changes in the stimulus (Lockery et al. 2009).

The *C. elegans* nervous system can be broadly classified into: sensory neurons, command (pre-motor) interneurons and motor neurons, based on their anatomical features and synaptic connectivity. The sensory nerve cells respond to a variety of environmental cues - chemicals, touch, temperature, oxygen and carbon dioxide concentrations, UV light, and magnetic field. The interneurons integrate signals coming from sensory neurons and synapse onto motor neurons that trigger the appropriate locomotory response via the musculature. This forms a hierarchical organization of neuronal network employed to respond to a variety of environmental and proprioceptive stimuli.

1.4.3 The sensory systems

C. elegans sense a wide variety of environmental stimuli such as chemicals, temperature, gases, touch, light and magnetic field. They use chemotaxis, thermotaxis, and aerotaxis to escape from harmful and noxious stimuli and to move to favorable surroundings by showing avoidance/escape behaviors. Laser ablation and genetic experiments have played an important role in dissecting sensory modalities in the worm. The sensory neurons are organized in sensory organs known as sensilla comprising of ciliated nerve endings of one or more neurons and two non-neuronal cells: socket cells and sheath cells. The two amphid sensilla contain 12 associated chemosensory or thermosensory neurons each. The two phasmid sensilla contain 2 chemosensory neurons, PHA and PHB. There are six inner labial organs, each of which contains one IL2 chemosensory and one IL1 mechanosensory neuron. There are two URX neurons, one AQR neuron, and one PQR neuron; the endings of these neurons are within the animal, and not exposed. FLP and BAG are ciliated receptors that are free inside the head and are not part of a sensillum (White et al. 1986; Altun, Z.F. and Hall 2011).

1.4.3.1 cGMP mediated signal transduction in sensory neurons of *C. elegans*

C. elegans possesses a highly developed chemosensory system that helps it to respond to a variety of olfactory (volatile) and gustatory (water soluble) stimuli associated with food, danger, or other animals. The chemosensory cues can evoke chemotaxis, rapid avoidance, changes in overall locomotion, and entry into and exit from the alternative dauer developmental stage. These behaviors are regulated by chemosensory neurons and are regulated by 500–1000 different G protein-coupled receptors (GPCRs). One of the most prominent signal transduction systems working downstream of the GPCRs in chemosensation uses cGMP as a second messenger to open cGMP-gated channels (Bargmann 2006).

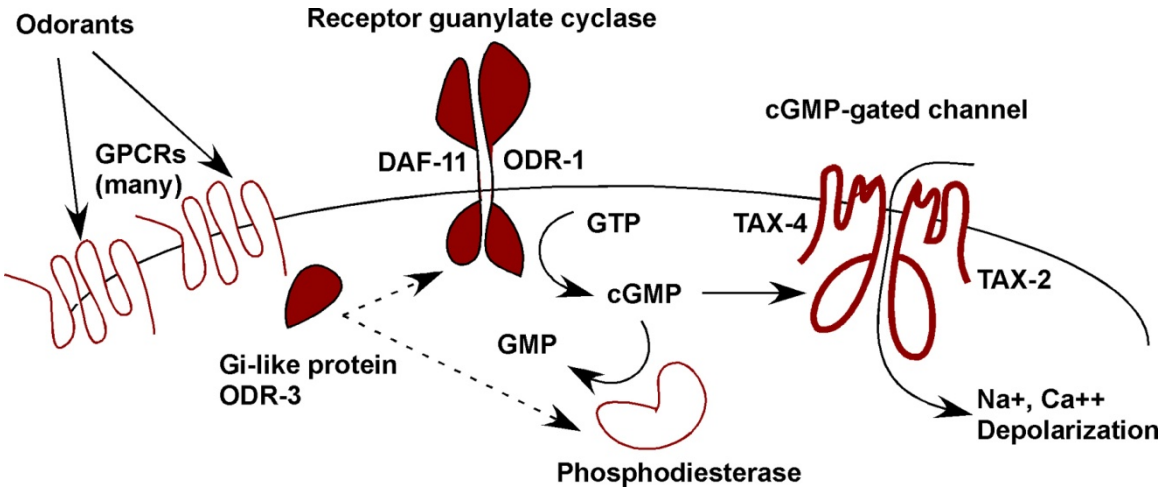

Figure I-9: Signal transduction pathway for chemosensation in AWC neuron cilia and other cGMP dependent sensory neurons. The sensory stimuli are sensed by GPCRs which activate downstream G proteins leading to either cGMP production by receptor-like guanylyl cyclases (ODR-1, DAF-11), or cGMP consumption by phosphodiesterases (PDEs). However , it still remains to be elucidated if there is a direct activation of the GCs or PDEs by G proteins or if this involves additional proteins. cGMP opens the cGMP-gated channels encoded by *tax-2* and *tax-4* to depolarize the cell (modified from Bargmann 2006).

A cyclic nucleotide-gated channel encoded by the *tax-4* and *tax-2* genes is the sensory transduction channel activated by cGMP, which is produced by downstream GPCR signaling involving guanylyl cyclase (**Figure I-9**). TAX-2 and TAX-4 are expressed in a subset of sensory neurons (for e.g. ASE, AWC, AWB, AFD, ASJ, ASI, ASG, ASK, URX, AQR, PQR, BAG) and are localized to sensory cilia (Coburn and Bargmann 1996; Komatsu et al. 1996). Animals mutant for *tax-4* or *tax-2* are

defective in ASE mediated chemotaxis to water-soluble compounds, AWC mediated chemotaxis to volatile odors, AWB mediated avoidance of volatile repellents, and AFD regulated thermotaxis. They are also weakly dauer-constitutive, especially at high temperatures (Coburn and Bargmann 1996; Komatsu et al. 1996). Heterologous expression of TAX-4 and TAX-2 in HEK293 cells produces a heteromeric non-specific cation channel that is highly sensitive to cGMP and about 40-fold less sensitive to cAMP, like the mammalian phototransduction channel (Komatsu et al. 1999). *tax-4* encodes an alpha subunit that can form a channel on its own, while *tax-2* encodes a beta subunit that enhances TAX-4 activity and does not form a channel on its own. The *C. elegans* genome encodes 34 guanylyl cyclases that are potential sources of cGMP in TAX-4/TAX-2 neurons (Ortiz et al. 2006). 27 of these cyclases are transmembrane proteins, or receptor-like guanylyl cyclases (RGCs), and 7 are cytosolic soluble guanylyl cyclases (sGCs).

C. elegans olfactory and pheromone-sensing neurons employ DAF-11 and ODR-1 as ligand-independent RGCs downstream of GPCR signaling. *daf-11*, which is essential to prevent dauer development, is expressed in the ASI and ASJ neurons that govern dauer formation and recovery. *daf-11* also shows expression in AWC, AWB, and ASK neurons, and is required for AWC and AWB chemosensory behaviors (Vowels and Thomas 1994; Birnby et al. 2000). Another RGC, *odr-1,* is expressed in the same neurons that express *daf-11* (L'Etoile and Bargmann 2000). *odr-1* mutants have been shown to have impaired AWC and AWB olfactory responses, but are normal for dauer formation. Mammalian RGCs are known to be obligate dimers where the amino acid residues at the dimer interface coming from both the subunits form the active site. Both ODR-1 and DAF-11 miss important residues required for catalysis, indicating that they usually function as ODR-1/DAF-11 heterodimers (Morton 2004). Since *daf-11* mutants are constitutively dauer while *odr-1* mutants are normal for dauer formation, DAF-11 might dimerize with other guanylyl cyclases in ASI or ASJ neurons. Photoactivation of a 'slow' long open ChR2 variant (C128S) in ASJ neurons bypassed the constitutive dauer entry phenotype in *daf-11* mutants, illustrating long term manipulation of animal development using microbial rhodopsins. Moreover, light stimulated ASJ neurons could also acutely trigger dauer-exit (Schultheis et al. 2011b). Three other RGC genes, *gcy-5*, *gcy-6*, and *gcy-7*, are known to be expressed only in ASE neurons, and each one of them is

expressed exclusively either in ASEL or ASER (Yu et al. 1997). ASEL and ASER detect different gustatory cues, so the GCY expression patterns may have a direct relevance to the different sensory functions of these neurons. However, so far, no sensory defect has been reported because of lack of function of these GCY cyclases in ASE (Ortiz et al. 2006).

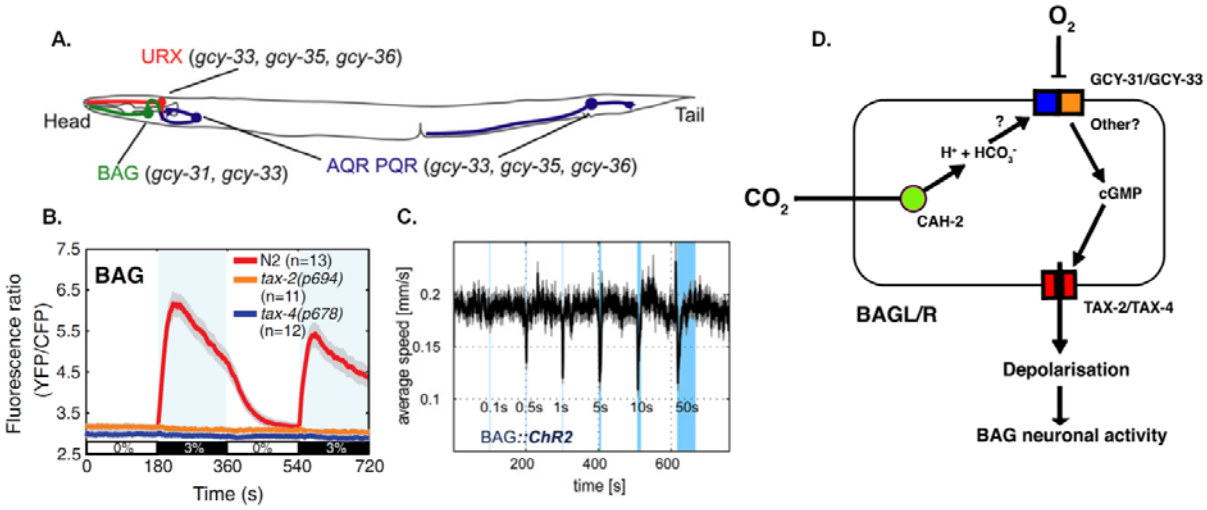

FIGURE I-10: Oxygen/Carbon dioxide sensing in *C. elegans.* **A.** The key sensory neurons along with their respective guanylyl cyclases involved in O_2/CO_2 sensation. **B.** Mutations in the *tax-2* and *tax-4* cGMP-gated ion channel subunits abolish BAG responses to 3% CO_2 as shown by ratiometic calcium imaging. **C.** Optogenetic activation of BAG (pflp-17:ChR2:mCherry) led to transiently slowed locomotion. **D.** BAG pair of sensory neurons detect decrease in [O_2] and increase of [CO_2] in the environment through the cGMP mediated depolarization (modified from Zimmer et al. 2009; Bretscher et al. 2011).

The seven soluble guanylyl cyclases encoded by *gcy-31* to *gcy-37* show expression primarily in neurons involved in oxygen and carbon dioxide sensing: *gcy-31* and *gcy-33* are co-expressed in the two BAG neurons in the head that sense carbon dioxide and oxygen, while the other five *gcy* genes are expressed in the URX, AQR, and PQR neurons that sense oxygen (Yu et al. 1997; Cheung et al. 2004; Gray et al. 2004). The ambient oxygen concentration ranges from 2% and 21% within which *C. elegans* can sustain a normal rate of metabolism due to diffusion of oxygen to its tissues through the pseudocoelomic fluid, which surrounds all tissues (Van Voorhies and Ward 2000). When grown under standard laboratory conditions, worms quickly move to an intermediate preferred oxygen concentration of between 7% and 14%, avoiding both high and low oxygen levels, although this response can be regulated by food, genotype and an animal's previous experience (Gray et al. 2004; Cheung et

al. 2005; Rogers et al. 2006). Additional neurons like *gcy-35* expressing SDQ, BDU, ALN, PLN and nociceptive ADF and ASH neurons also respond to oxygen directly or are modulatory in function (Gray et al. 2004; Chang et al. 2006). The output of the aerotaxis neuron network converges on AVA, the command interneuron responsible for generating backward motion and, hence, avoidance.

High CO_2 levels (above 9%) are known to be toxic to worms resulting in deterioration of muscles, reducing fertility and slowing development (Bretscher et al. 2008; Hallem and Sternberg 2008; Sharabi et al. 2009). A well-fed worm typically shows an acute avoidance response to CO_2 when its level rises above 0.5% (Bretscher et al. 2008). Apart from BAG, AFD and ASE neurons have also been implicated in CO_2 response (Bretscher et al. 2011). The signal transduction pathway for CO_2 response includes the TAX-2/TAX-4 cGMP-gated heteromeric channel. BAG neurons are activated transiently by decrease in O_2 levels below 10% (mediated by GCY-31 and GCY-33) and increase in CO_2 concentration and remain tonically active while high CO_2 persists (Zimmer et al. 2009; Bretscher et al. 2011) (**Figure I-10**). Optogenetic activation of BAG neurons using ChR2 resulted in the transient slowing behavior reminiscent of the slowed locomotion upon an O_2 downshift (Zimmer et al. 2009). Although both O_2 and CO_2 sensation by BAG require the cGMP-gated channel subunit TAX-4, there are a couple of differences between these sensory properties. Sensing O_2 requires GCY-31 and GCY-33, but CO_2 sensing does not (Hallem and Sternberg 2008); O_2 sensing is increased by starvation, but CO_2 sensing is suppressed by starvation (Bretscher et al. 2008). In general, the CO_2 response is modulated by the physiological state of the worm, the neuropeptide Y receptor, NPR-1, and calcineurin subunits, TAX-6 and CNB-1 (Hallem and Sternberg 2008).

GCs are heme-binding proteins and can potentially interact with gases through the heme-nitric oxide and oxygen (O_2) binding (H-NOX) domains and synthesize the second messenger cGMP from GTP. Mammalian homologs of this family (α1β1 sGCs) are directly activated by the gaseous ligand NO whereas the H-NOX domain of GCY-35 binds O_2 indicating that GCY-35 is a primary receptor for oxygen in aerotaxis (Denninger and Marletta 1999; Gray et al. 2004; Derbyshire and Marletta 2012). Mutations in *gcy-35* and *gcy-36* lead to aerotaxis defects as well as strong suppression of oxygen dependent social behavior mediated by URX, AQR, and PQR neurons (Gray et al. 2004; Cheung et al. 2005). Ectopic expression of *gcy-35* and *gcy-36* in AWB neurons that do not normally express sGCs alters O_2 preference in

aerotaxis assays (Cheung et al. 2005). All these observations suggest that sGCs have a direct role in O_2 sensation in *C. elegans*.

C. elegans can accurately detect temperatures within the ~12-27°C range and migrate to the cultivation temperature on a temperature gradient. This thermotaxis behaviour is mediated primarily by the amphid AFD neurons (along with ASI and AWC neurons) using three receptor-type guanylyl cyclases which function redundantly (GCY-8, GCY-18, and GCY-23), and cGMP-dependent TAX-2/TAX-4 cation channel (Mori and Ohshima 1995; Komatsu et al. 1996; Inada et al. 2006; Garrity et al. 2010).

1.4.4 Interneurons and Motor neurons

The interneurons operate as information processors, receiving inputs from one or more classes of neurons and relaying outputs onto other neurons. The interneurons process and integrate sensory inputs coming from individual neuronal circuits to 'command' the decision to execute a specific motor program by the motor neurons. The majority of motor neurons are located in the ventral nerve cord, innervate the body wall muscles (and other motor neurons) and affect worm locomotion. Additional motor neurons are involved in controlling head movements, pharyngeal muscles, defecation and the egg-laying musculature (de Bono and Maricq 2005).

While foraging, worms exhibit long, forward movements interrupted by brief reversals. The crucial neurons for controlling forward and backward locomotion were identified from the worm's wiring diagram and genetic and laser ablation studies (Chalfie et al. 1985; Zheng et al. 1999). Based on these studies, the interneurons AVA, AVD and AVE were shown to be regulating the reverse locomotion while interneurons PVC and AVB are associated with forward locomotion. Downstream of the shallow network of interneurons, A-type motor neurons carry out reversals while B-type motor neurons execute forward motion (**Figure I-11**). The interneuron RIM also interacts with these forward and reverse interneurons and is important for head bending and reversals (Alkema et al. 2005; Pirri et al. 2009). The command interneurons for forward and backward locomotion receive primarily glutamatergic input from the sensory neurons.

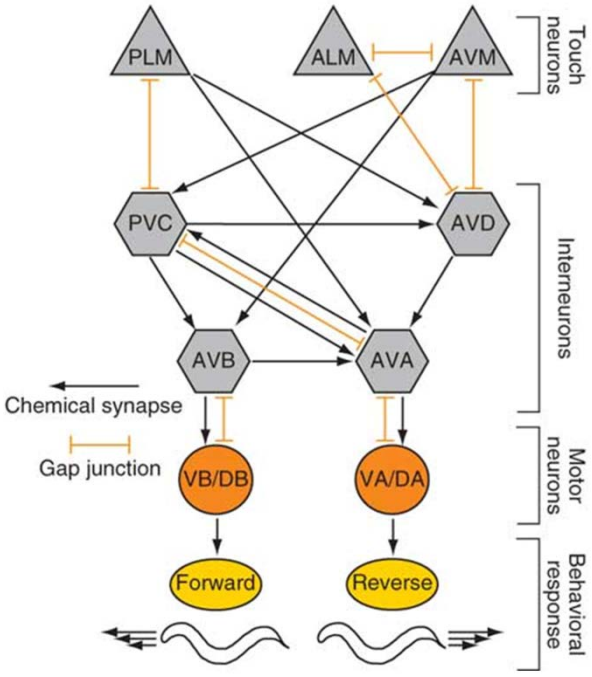

FIGURE I-11: The mechanosensory circuit, showing command neurons and the resulting behaviours. (from Stirman et al. 2011).

1.4.4.1 Ionotropic glutamatergic neurotransmission in *C. elegans*

Ionotropic glutamate receptors (iGluRs) constitute the major class of ligand gated ion channels that mediate the majority of the excitatory neurotransmission in the vertebrate central nervous system. These transmembrane proteins are broadly classified on the basis of pharmacological specificity: N-methyl-D-aspartate (NMDA) class or the non-NMDA class (further divided into two:α-amino-3-hydroxy-5-methyl-4-isoxazole propionic acid (AMPA) and kainate (KA)). These are tetrameric cation channels, with each subunit containing an extracellular ligand binding region (S1 and S2 domains), four hydrophobic segments, three transmembrane domains, and the P loop that is involved in forming the pore (Dingledine et al. 1999; Mayer 2011) (**Figure I-12A and B**).

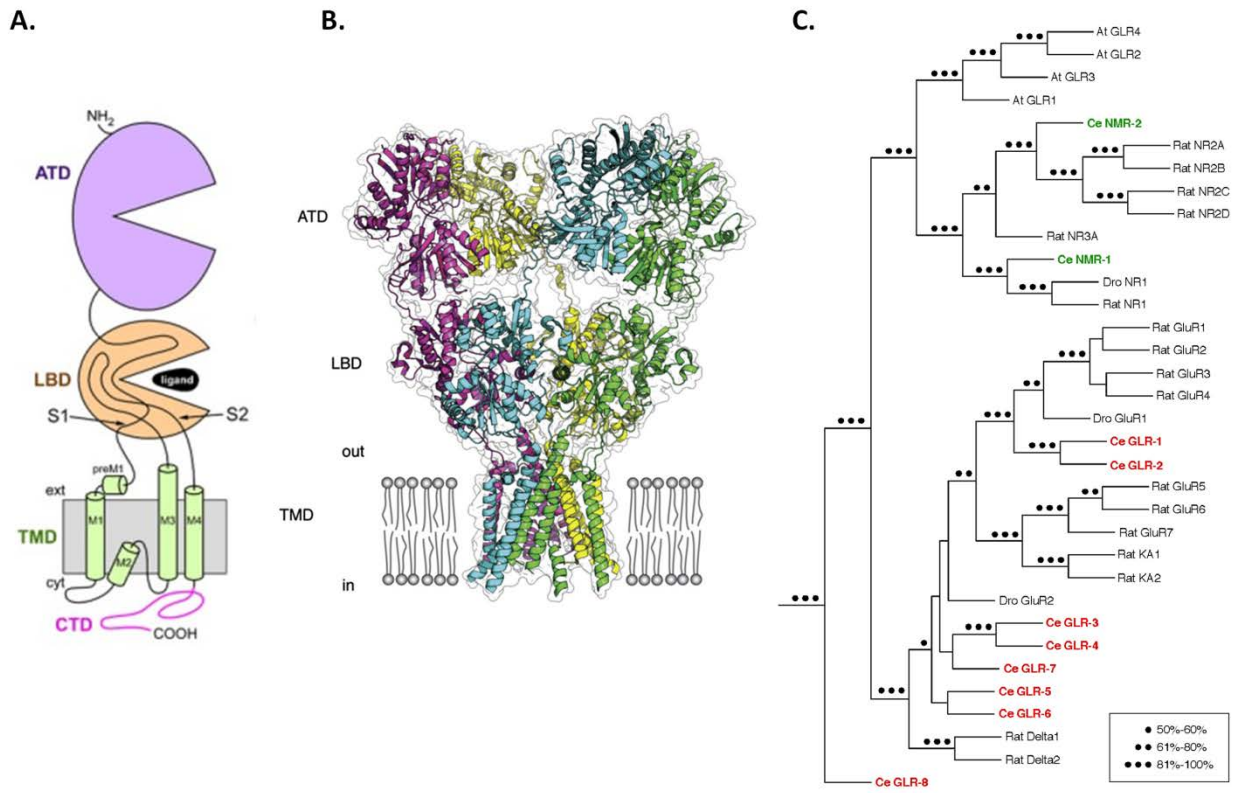

FIGURE I-12: **A.** Topology of iGluR subunit (Sobolevsky et al. 2009) **B.** Overall structure of iGluRs exemplified by GluA2 (pdb 3KG2) (Stawski et al. 2010) **C.** Phylogenetic tree of iGluR subunits from rat, *Drosophila* (*Dro*), *Arabidopsis* (*At*),and *C.elegans* (*Ce*). *C.elegans* non-NMDA and NMDA subunits are shown in red and green, respectively (Brockie and Maricq 2006).

There are at least 10 putative iGluR subunits encoded in the *C. elegans* genome (**Figure I-12C**). Two of them form NMDA receptor-type channels (encoded by *nmr-1* and *nmr-2*) and eight form non-NMDA-type channels (encoded by *glr-1* through *glr-8*) (Brockie et al. 2001a; Brockie and Maricq 2006). Six of the subunits: 4 non-NMDA (*glr-1, glr-2, glr-4* and *glr-5*) and 2 NMDA (*nmr-1* and *nmr-2*) have been shown to be expressed in many of the command interneurons - AVA, AVB, AVD, AVE and PVC - which control forward and backward movement. The distribution of NMDA receptors is almost exclusive to these interneurons. Both *glr-3* and *glr-6* are expressed in a single interneuron pair, the RIA neurons, which is involved in the thermotaxis neural circuit (Mori and Ohshima 1995). *glr-7* and *glr-8*, are expressed in partially overlapping sets of neurons in the pharyngeal nervous system, suggesting roles in food sensing. *glr-1, glr-2* and *nmr-1* have been implicated in a variety of behavioural paradigms: switch from forward to backward locomotion (Zheng et al. 1999; Brockie et al. 2001b), foraging behaviour (Hills et al. 2004), avoidance of

hyperosmotic stimuli (Mellem et al. 2002) and octanol (Chao et al. 2004), and habituation and learning (Rose et al. 2002; Rose et al. 2003). For the trafficking, scaffolding, stability, signalling, and turnover of ionotropic glutamate receptors, they are assisted by a number of distinct auxiliary transmembrane proteins collectively called TARPs (for transmembrane AMPA receptor regulatory proteins) (Jackson and Nicoll 2011). The *C. elegans* genome contains the TARPs *sol-1* and *sol-2*, which are CUB domain proteins, and *stg-1* and *stg-2*, which are proteins closely related to the vertebrate TARP stargazin. The CUB domain (for complement C1r/C1s, Uegf, Bmp1) is an evolutionarily conserved protein domain with immunoglobulin-like folds found almost exclusively in extracellular and plasma membrane-associated proteins, many of which are developmentally regulated (Bork and Beckmann 1993). These proteins are involved in a variety of processes, including complement activation, developmental patterning, tissue repair, axon guidance and angiogenesis, neurotransmission, receptor-mediated endocytosis, and tumour suppression (Bork and Beckmann 1993).

Based on genetic, pharmacological and electrophysiology evidence, SOL-1 and SOL-2 have been shown to slow the rate and limit the extent of receptor desensitization as well as to enhance the recovery from desensitization, while STG-1 promotes the surface expression of GLR-1 (Zheng et al. 2004; Walker et al. 2006a; Walker et al. 2006b; Wang et al. 2012). The vertebrate CUB/LDL/TM proteins Neto-1 and Neto-2 also operate as TARPs and there are a total of four Neto1/2-like proteins encoded in the *C. elegans* genome (*neto-1* (Neto1/2 ortholog), *lev-10*, *mig-3* and *K05C4.11*) (Wang et al. 2012; Hobert 2013). *C. elegans* genome also possesses an uncharacterized homolog of the vertebrate TARP Cornichon (Jackson and Nicoll 2011), *cni-1*, but lacks obvious homologs of the SynDIG1 or CKAMP44 TARPs (Hobert 2013).

1.4.4.2 Glutamate-gated chloride channels: distribution and function in *C. elegans*

Apart from the cation selective iGluRs, another type of glutamate gated ion channels has been identified in *C. elegans*: glutamate-gated chloride channels (GluCl). The invertebrate specific family of inhibitory GluCls form channels that are permeant to chloride ions and are sensitive to the antihelmintic drug avermectin (Cully et al. 1994;

Wolstenholme 2012). GluCls belong to the pentameric Cys-loop ligand-gated ion channel superfamily that includes the excitatory acetylcholine and serotonin receptors and the inhibitory GABA and glycine receptors (Ortells and Lunt 1995). The ability of glutamate to potentiate glycine receptor currents reflect close evolutionary relationship between GluCls and glycine receptors (Liu et al. 2010). There are 6 GluCl subunits encoded in *C. elegans* genome- *glc-1, glc-2, glc-3, glc-4, avr-14/gbr-2 and avr-15* (Cully et al. 1994; Dent et al. 1997; Laughton et al. 1997a; Vassilatis et al. 1997; Dent et al. 2000; Horoszok et al. 2001).

C. elegans glc-1 (GluClα1) and *glc-2* (GluClβ) were the first genes encoding GluCl subunits to be identified by functional expression in *Xenopus* oocytes (Cully et al. 1994). GluClα1 and GluClβ hetero-dimerize in oocytes to form a chloride channel that is also sensitive to the anti-parasitic drug ivermectin, a derivative of avermectin; the discovery of which was awarded with the 2015 Nobel prize in physiology and medicine. Although less well studied than the cationic iGluRs, genetic and electrophysiological investigations have provided some insight into the role of GluCls in control and modulation of locomotion, the regulation of feeding, and the mediation of sensory inputs (Yates et al. 2003; Brockie and Maricq 2006; Wolstenholme 2012).

Based on reporter GFP expression, GluCls have been shown to be expressed in muscle cells, intestine and neurons. *avr-14* is expressed in a subset of neurons in the ring ganglia, ventral cord, and some mechanosensory neurons ALM, PLM and PVD (Dent et al. 2000). *avr-15* is expressed in the extrapharyngeal nervous system and the pm4 (metacorpus) and pm5 (isthmus) pharyngeal muscle cells (Dent et al. 1997). GLC-2 expression is limited to the pm4 muscle cells (Laughton et al. 1997a) where it is likely to form functional heteromeric channels with AVR-15 (Vassilatis et al. 1997). As is illustrated by the pharynx dominated expression pattern, GluCls play a dominant role in controlling nematode pharyngeal pumping. The glutamatergic M3 motor neurons primarily synapse onto the pm4 pharyngeal muscle cells (Albertson and Thomson, 1976) and facilitate rapid relaxation of the pharyngeal muscle (Avery 1993; Raizen and Avery 1994) via a chloride-dependent hyperpolarization (Pemberton et al. 2001). This response is mediated by an AVR-15-containing GluCl (Dent et al. 1997; Pemberton et al. 2001) expressed on the pharyngeal muscle cells. GLC-2, and possibly an additional subunit, may also be involved (Laughton et al. 1997b).

GLC-3 is expressed in the AIY interneurons, where it receives glutamate input signals from the chemo-sensory AWC (Chalasani et al. 2007) and thermo-sensory AFD neurons (Ohnishi et al. 2011). The AWC neuron inhibits AIY interneurons through GLC-3 mediated hyperpolarization; odour presentation relieves this inhibition resulting in the activation of AIY interneurons, leading to reduction in the frequency of turns and thus promotes chemotaxis (Chalasani et al. 2007). Glutamate release from AFD neurons inhibits the postsynaptic AIY interneurons through activation of GLC-3 resulting in migration towards colder temperatures (Ohnishi et al. 2011).

In the extrapharyngeal nervous system, AVR-14, AVR-15 and GLC-1 have been identified to be responsible for sensitivity to ivermectin (Dent et al. 2000). Apart from inhibiting pharyngeal pumping, ivermectin also causes paralysis of the mid-body region leading to reduced mobility. GluCl channels have also been speculated to function antagonistically to the excitatory iGluR subunits GLR-1, GLR-2 and NMR-1in the command interneurons to drive forward rather than backward locomotion. A glutamate-gated chloride current has been observed in the AVA command interneurons in the absence of GLR-1/GLR-2 and NMR-1 mediated cationic currents (Mellem et al. 2002); however, the exact GluCl subunits responsible for this current have not been identified yet. Also, worms carrying mutations in *avr-15* exhibited a dramatic reduction in the fidelity of the anterior touch response after AVD laser ablation (Lee et al. 1999), suggesting that some of the chemical synapses between the anterior touch cells (ALM and AVM) and the command interneurons might be inhibitory and AVR-15 might play a role in inhibiting forward movement in response to mechanical stimuli. Intriguingly, mechanical stimulation of the tail reduces the rate of pharyngeal pumping in adult worms; and mutations in both *avr-14* and *avr-15* decrease these inhibitory effects (Keane and Avery 2003). This indicates that there exists a flow of information from the extrapharyngeal nervous system to the pharynx. This notion is further supported by the observation that ivermectin inhibits pharyngeal pumping in *avr-15* mutants; however, normal pumping is restored when the pharynx is dissected out (Dent et al. 2000).

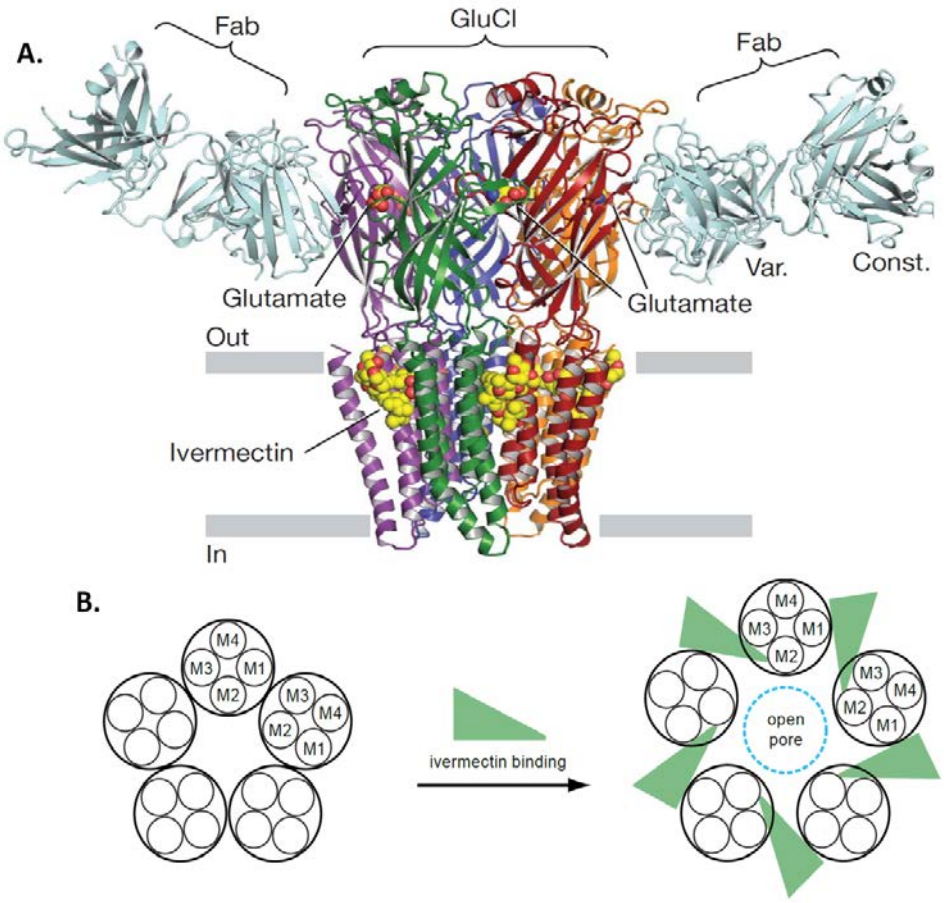

FIGURE I-13: Structure of GLC-1. **A.** X-ray structure of GLC-1 determined with allosteric agonist ivermectin binding in the transmembrane domain and native agonist glutamate binding at the subunit interfaces. **B.** Binding of ivermectin at subunit interface spreads apart M3 and M1 α-helices and stabilizes the apical portion of M2 in an orientation tilted away from the pore, allowing for ion conductance (modified from Hibbs and Gouaux 2011).

In 2011, the X-ray structure of GLC-1 was determined, making it the first three-dimensional structure of an inhibitory anion-selective Cys-loop receptor (Hibbs and Gouaux 2011) to be solved (**Figure I-13**). The structure was determined with the allosteric agonist ivermectin and in additional structures with glutamate and the open-channel blocker picrotoxin. Ivermectin binds in the transmembrane domain of the receptor and stabilizes an open pore conformation while glutamate binds in the classical agonist site at subunit interfaces in the extracellular domain of the receptor in a similar position to that of the nicotinic acetylcholine-binding sites (Unwin 2005). Each subunit of the pentamer consists of a large amino-terminal extracellular domain of mostly β structure, though with an additional helix at the N-terminus reminiscent of acetylcholine binding protein (AChBP) (Brejc et al. 2001) and Torpedo nictonic acetylcholine receptor (nAChR) structures (Unwin 2005), followed by four α-helical

transmembrane spans (M1-M4). Interestingly, heterologously glutamate binds to the homomeric GLC-1 receptor only in the presence of ivermectin, though substituting the naturally occurring threonine in M2 to a proline, glycine, or alanine enabled glutamate gating of GLC-1 homomeric channels without a prior ivermectin potentiation (Etter et al. 1996). Recently, 3D structures of GLC-1 were obtained by supplementing GLC-1 with 1-palmitoyl-2-oleoyl-sn-glycero-3-phosphocholine (POPC) in the absence of ivermectin (Althoff et al. 2014).

Since vertebrates do not have GluCls, attempts have been made to develop them as tools for the selective silencing of genetically defined neurons by supplementing low concentrations of ivermectin (Slimko et al. 2002; Frazier et al. 2013). GLC-1 and GLC-2 subunits have been expressed in mammalian neurons using recombinant viral vectors resulting in the formation of functional GluCls, which can then be selectively silenced by injecting ivermectin. The subunits have been modified to eliminate activation by glutamate while retaining ivermectin activation and GFP has been introduced in the M3-M4 loop as fluorescent marker (Li et al. 2002). GLC-1 and GLC-2 have been successfully employed *in-vivo* to identify an aggression locus in the mammalian hypothalamus (Lerchner et al. 2007; Lin et al. 2011)

Natural variation in the form of a four-amino acid deletion in the ligand binding domain of GLC-1 has been shown to confer resistance to avermectins in *C. elegans* (Ghosh et al. 2012). Interestingly, the deletion does not lie in the glutamate or ivermectin binding site region but rather toward the extreme N-terminus. Unfortunately, since the deletion happens to be within the first N-terminal 40 amino acids, which were removed for crystallization and structure determination (Hibbs and Gouaux 2011), the structural explanation for ivermectin resistance remains unclear. The *glr-1* promoter-GFP fusion reveals expression in intestine, pharyngeal muscle, head neurons and body wall muscle (Ghosh et al. 2012). However, the normal physiological role of the channel remains to be understood. The structure elucidation of GLC-1 renders it accessible to the opto-chemical genetic approach to activate it using light, thereby aiding in the investigation of the physiological role of GLC-1 in *C. elegans.*

1.4.5 Muscles and the neuro-muscular junction

As in vertebrates, *C. elegans* has both striated and non-striated muscles. The body wall musculature comprises of striated muscle cells that have their sarcomeres

oriented in an oblique conformation with respect to the actomyosin filaments (Rosenbluth 1965; Waterston et al. 1980). There are 95 body-wall muscle cells in the adult hermaphrodite with the left ventral quadrant containing 23 cells and the other quadrants have 24 cells each (Sulston and Horvitz 1977). Within each quadrant, the anterior 4 muscles are innervated by the motor neurons in the nerve ring, the next 4 is dually innervated by the motor neurons in the nerve ring and the ventral cord, and the remaining muscles are innervated solely by the motor neurons of the ventral cord (White et al. 1986).The motor neurons of the ventral cord innervate either both dorsal or both ventral quadrants of muscle thereby causing dorso-ventral propagation of body contraction waves during locomotion. However, the head can make lateral as well as dorso-ventral movements owing to the fact that motor neurons in the nerve ring synapse onto two adjacent rows of head muscles which are not necessarily in the same quadrant.

Unlike other organisms, nematode muscles have processes called as muscle arms that run from the muscle cell bellies to the neuron process bundles in which motor neuron axons are located. Neuro-muscular junctions (NMJs) are made by motor neuron processes that sporadically move to the outside of the bundle through the basal lamina to become accessible to muscle arms in synaptic regions (Stretton 1976; Sulston and Horvitz 1977; Sulston et al. 1983; White et al. 1986; Dixon and Roy 2005; Dixon et al. 2006).

The excitatory neurotransmission at the NMJs of *C. elegans* is cholinergic in nature. The opening of acetylcholine receptors on the post-synaptic muscle membrane leads to the initiation of graded action potentials in muscle arms which then converge and propagate to the contractile machinery of the muscle (Richmond and Jorgensen 1999; Jospin et al. 2002; Schafer 2002). In the absence of voltage gated sodium channels, the action potentials in the muscle are postulated to be mediated by the EGL-19 which is the pore-forming alpha1 subunit of a voltage-gated calcium channel orthologous to the alpha subunit of mammalian L-type calcium ion channels (Gao and Zhen 2011). The Ca^{2+} influx from extracellular compartment is thought to be sufficient to directly initiate a contraction in the worm body wall muscle where the sarcomeres are located in close proximity to the plasma membrane (Lee et al. 1997; Maryon et al. 1998; Jospin et al. 2002) and the synchronization of action potentials

through the muscle tissue has been shown to depend on gap junction coupling between muscle cells (Liu et al. 2011).

1.4.5.1 Cholinergic neuro-transmission at the *C. elegans* NMJ

Acetylcholine (ACh) was the first substance shown to be a neurotransmitter (Loewi 1921). It was identified in Ascaris and other nematodes in 1955 (Mellanby 1955) and was later identified as an excitatory transmitter at nematode neuromuscular junctions (Del Castillo et al. 1963; Del Castillo et al. 1967). ACh is synthesized by choline acetyltransferase encoded by *cha-1* in *C. elegans*, and is loaded into synaptic vesicles by the vesicular acetylcholine transporter which is encoded by the gene *unc-17.* Subsequent to the fusion of synaptic vesicles on the pre-synaptic membrane and transmitter release, the ACh diffuses in the synaptic cleft and binds to acetylcholine receptors (AChRs), usually located on post-synaptic cells or at muscle arms in case of NMJs. Acetylcholine is removed from the synaptic cleft by acetylcholinesterases (AChE, *ace* genes) which hydrolyse the neurotransmitter and the resulting choline is then transported back into the presynaptic neuron by choline transporter encoded by *cho-1* (Rand 2007; Hobert 2013).

The body wall muscles of *C. elegans* express two major types of Cys-loop pentameric ACh receptors: one type is sensitive to levamisole and the other type responds to nicotine, but not levamisole (Richmond and Jorgensen 1999). The levamisole-sensitive AChR (L-AChR) is heteromeric, comprising of three essential subunits: UNC-29, UNC-38, and UNC-63 (Fleming et al. 1997; Richmond and Jorgensen 1999; Culetto et al. 2004; Gottschalk et al. 2005; Boulin et al. 2008). LEV-1 and LEV-8 are also found to be subunits of L-AChR, but they are either non-essential for the response to levamisole, or they are only found in a subset of the receptors (Fleming et al. 1997; Towers et al. 2005; Gottschalk et al. 2005). The nicotine-sensitive receptors (N-AChR) are homomeric, containing only the ACR-16 α subunit (Francis et al. 2005; Touroutine et al. 2005). ACR-16 is orthologous to the human nicotinic cholinergic receptor alpha 7.

Loss-of-function mutations in *unc-29*, *unc-38*, and *unc-63* cause a strong levamisole resistance and an uncoordinated locomotion phenotype, while mutations in *lev-1* and *lev-8* result in mild levamisole resistance and almost normal locomotion (Lewis et al. 1980). Animals with loss of function mutations in *acr-16*, which eliminates the function of N-AChR, have essentially wild-type locomotion (Francis et al. 2005;

Touroutine et al. 2005). Interestingly, while genomic deletion of the L-AChR has strong behavioural effects, NMJ currents are only mildly reduced in these mutants. In contrast, ACR-16 mediates 2/3 of the currents, but *acr-16* mutants have no severe behavioural defects at all. Eliminating the function of both receptors (e.g., an *unc-29; acr-16* double mutant or an *unc-63;acr-16* double mutant) leads to a synthetic severe uncoordinated phenotype (Francis et al. 2005; Touroutine et al. 2005). Also, the levamisole-sensitive receptors present in *acr-16* mutants have been shown to desensitize at a much slower rate than the levamisole-insensitive receptors present in *unc-63* mutants (Culetto et al. 2004; Touroutine et al. 2005). This difference in desensitization rates may well affect *in-vivo* roles of the two receptors. Nonetheless, the *in-vivo* function of the ACR-16 containing N-AChR in driving locomotion and other physiological functions, if any, remains rather poorly understood.

1.4.6 Optogenetic tools and methods in *C. elegans*

The transparency, genetic amenability and an anatomically well-defined nervous system that regulates quantifiable behaviors has made *C. elegans* an ideal model system for the development and application of optogenetic methods. In the past decade, researchers have utilized optogenetic tools and techniques to manipulate numerous excitable cell types in the worm, ranging from sensory neurons, to interneurons, to motor neurons and muscles (Husson et al. 2013; Fang-Yen et al. 2015).

Primarily, microbial rhodopsins like ChR2, NpHR, Mac and Arch have been employed to activate or inhibit optogenetically modified neurons and concomitantly record the acute effects on behaviour or physiology through trackers monitoring the movement or reporters of neuronal activity (Stirman et al. 2011; Akerboom et al. 2013). These optogenetic activators and inhibitors are expressed using known promoters which can drive expression specifically in many if not all tissues and cell types in *C. elegans*. However, single (pairs of) neuron(s) specific promoters are few, which can be a bottleneck to study a small nervous system, where every single neuron is expected to have a distinct role or even multiple roles. Thus, for optogenetic manipulation of a single cell or cell type, either combinatorial genetic approaches using intersectional promoter strategies with Cre or FLP recombinases have been used (Davis et al. 2008; Macosko et al. 2009; Schmitt et al. 2012) or in

combination, patterned illumination with digital micromirror devices (DMDs), LCD projectors, etc. have been employed (Guo et al. 2009; Stirman et al. 2011; Leifer et al. 2011). The *myo-3* promoter, driving expression in body wall muscle cells, has been commonly used to express and assess the performance of new optogenetic proteins (Nagel et al. 2005; Zhang et al. 2007; Erbguth et al. 2012; Husson et al. 2012b). This is because of the fact that the photoactivation or inhibition of muscle cells leads to a straightforward behavioral readout (body contraction or elongation, respectively). Also, muscle cells are relatively more accessible than neurons to electrophysiological characterization of the optogenetic proteins (Richmond et al. 1999; Liewald et al. 2008). Unlike mammals, *C. elegans* does not synthesize retinal and hence it must be supplemented in its bacterial diet for the microbial rhodopsins to be functional. This provides an ideal internal control for any optogenetic experiment with ChR2 or any retinal based rhodopsin in *C. elegans.*

Furthermore, light-inducible enzymes, e.g., adenylate cyclases (euPAC and bPAC), have been implemented (Weissenberger et al. 2011; Flavell et al. 2013) and light-inducible protein–protein interactions have been established (Ohno et al. 2014). Optogenetic actuators like ChR2 have been combined with red shifted genetically encoded Ca^{2+} sensors which allows to image neural activity without concomitantly activating the ChR2. In 2012, Husson and colleagues used RCaMP as an optical readout for the excitation of the forward command neuron PVC by upstream photoactivation of the sensory PVD neuron (Husson et al. 2012a). The combination of ChR2 and RCaMP opens new avenues to analyse neuron to neuron and neuron to muscle communications. The combination of optogenetic manipulation with calcium imaging in freely moving worms has also been recently achieved (Shipley et al. 2014). With these advances, closed loop optogenetics with online tracking of behavior becomes conceivable in the near future.

1.5 Objectives of the thesis

This thesis aims at developing and implementing novel optogenetic tools in *C. elegans* that are more-suited to the native physiology of the excitable cell targeted and are capable of answering questions pertaining to the endogenous role of receptors and channels in an *in-vivo* context. These are: photo-activated guanylyl cyclases (PGC like bPGC and BeGC1) in sensory neurons, light-activated glutamate receptor (LiGluR) for interneurons, light-activated glutamate gated chloride channel (LiGluCl) and light-activated N-AChR (Li-N-AChR) to better understand the physiological roles of *glc-1* and *acr-16*, respectively (**Figure I-14**).

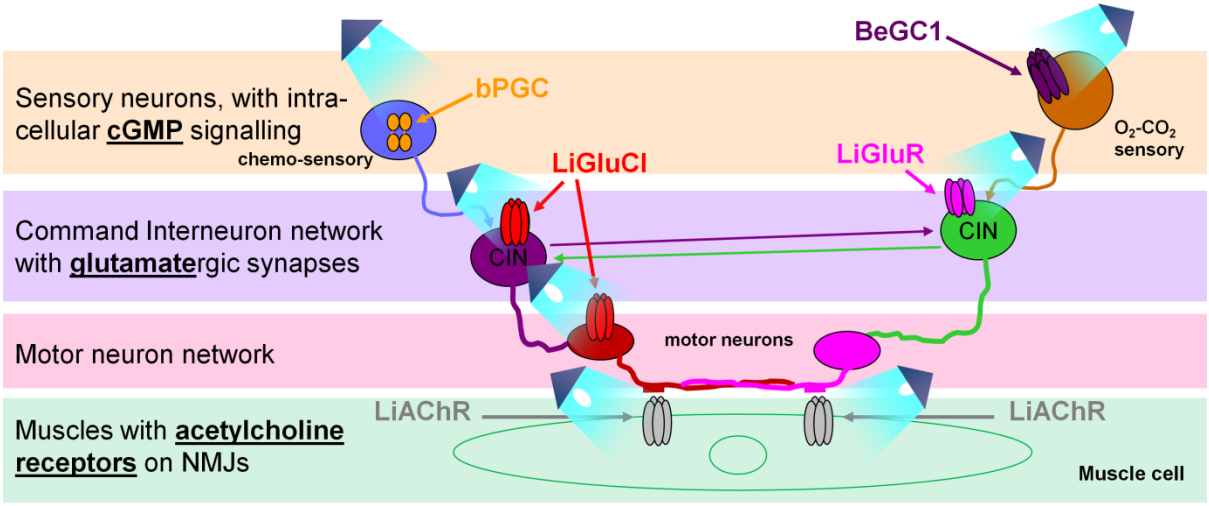

FIGURE I-14: Implementation of novel optogenetic tools in the different levels of the hierarchical organization of the *C. elegans* nervous system.

The sensory neurons in *C. elegans* have a pre-dominantly cGMP based signal transduction. To study the intracellular sensory processing and its potential role in learning and habituation, PGCs present a far better option than ChR2 as ChR2 activation leads to the overall depolarization of the cell, completely over-riding the intrinsic activity within the cell. Prior to implementation in sensory neurons, a simpler heterologous system with co-expression of the cationic TAX-2/-4 CNG channel in *C. elegans* body wall muscle needs to be tested as the muscle depolarization leading to changes in body length can be easily scored. The efficiency of bPGC and BeGC1 as light activated cGMP generators can be evaluated and compared using the muscle depolarization and body contraction set-up as well as by using genetically encoded

cGMP indicator (FlincG3 modified for worms) in muscle cells which provide a large area for signal measurement.

While ChR2 reliably activates neurons in *C. elegans*, it does not allow particularly accurate local control of membrane potential, i.e. at post-synaptic specializations or in dendritic spines, as these "foreign" proteins are not localizing to any specific site, but are rather found all over the plasma membrane. Moreover, ChR2 has a comparably low conductance, thus to attain enough photocurrent for efficient neuronal depolarization, one needs to achieve high expression levels. Due to the limited choice of (strong) promoters for a given cell type, this may not always be possible. LiGluR scores over ChR2 on both these counts: being a native protein it localizes to the synapses and has a much larger single-channel conductance than ChR2 (~250 fS versus ~40 fS) (Howe 1996; Feldbauer et al. 2009), and can be particularly useful for investigating command interneurons which receive glutamatergic innervation. To this end, cysteine mutations homologous to the original LiGluR (Szobota et al. 2007a) need to be introduced to the endogenous *C. elegans* kainate receptor and MAG conjugation to LiGluR needs to be accomplished. Body wall muscles are the ‘heterologous’ test system of choice before going to the neurons owing to their accessability to electrophysiology and relatively easy scoring of locomotory phenotypes available upon successful constitution of LiGluR.

Nematodes express glutamate-gated chloride channels (GluCls), used for fast inhibitory transmission from otherwise excitatory, glutamatergic neurons. They are found in several parts of the nervous system, but their functions are only partially understood. GluCls are strongly and specifically activated by ivermectin. GluCl is a high conductance channel, and the structure of *C. elegans* GLC-1 has been solved (Hibbs and Gouaux 2011). Thus, this provides ideal prerequisites to turn it into a light-activated channel using the PTL approach. It is aimed to establish LiGLC-1 and use it to analyze GLC-1 functions in *C. elegans*. The cysteine introduction sites need to be identified using docking studies with MAG and functional studies need to be performed to ascertain the efficiency of cysteine mutants before transferring the system to worms.

Cholinergic signalling at the NMJ utilizes two nAChRs. While the function of the L-AChR is crucial for normal locomotion behaviour of *C. elegans*, lack of the N-AChR has no discernible behavioural phenotypes. Nevertheless, its properties, i.e. large

peak currents during electrophysiological experiments and fast desensitization (Touroutine et al. 2005; Almedom et al. 2009) hint at specific functions. As the knockout of ACR-16 does not reveal them, possibly as the L-AChR undergoes compensatory changes when ACR-16 is missing, an acute, specific activation of the Li-N-AChr may very well reveal particular effects that are unlikely to be compensated for by the L-AChR. The cysteine introduction sites need to be chosen on the basis of previous molecular modelling studies on AChBP and introduced in *acr-16.* The functionality of the cysteine mutants needs to be assessed using locomotory assays like swimming and electrophysiology. The PTL capable of activating *acr-16* without being hydrolysed by the acetylcholinesterases in the synaptic cleft needs to be designed and finally the PTL needs to be tested with the cysteine mutants to check for light dependent switching before performing detailed analysis on the behaviour.

2 MATERIALS AND METHODS

2.1 Material

2.1.1 Equipment

Table 2-1| Used equipment.

Description	Type	Manufacturer
Autoclave	Serie FVS 5075 ELVC	Fedgari Tuttnauser
Bunsen burner	Labogaz 470	Campingaz
Cameras	ORCA-Flash 4.0 V2 C11440-22CU	Hamamatsu
Centrifuges	Mikro 200R Pico 17 Microcentrifuge Centrifuge 5810R	Hettich Heraeus Carl Roth Eppendorf
Compressor	BT-AC 200/24 OF	Einhell
ddH_2O equipment	Milli-Q Plus	Millipore
Dual view	DV2^{TM}	Photometrics
Electrophoresis chamber	Varia 1	Carl Roth
Filter sets	F36-525 HC Filter (EGFP) F41-007 HC Filter (mCherry) F74-423 479/585 HC Dualband Filter (FITC/TxRed) F37-647 BrightLine HC 647/57 BP 515-565 (447744-8001) 21001 - 80/20 Beamsplitter FF493/574-Di01 BrightLine dual-edge dichroic beamsplitter 493/574 nm	AHF Analysentechnik AHF Analysentechnik AHF Analysentechnik AHF Analysentechnik AHF Analysentechnik Zeiss Chroma Technology Corp. Semrock
Gel documentation system	Dark Hood DH-40 EOS 500D	Biostep Canon
Heat block	AccuBlock^{TM} Digital Dry Bath	Labnet
Incubator	DF8528GL Slimvip (-80 °C) Vinothek (16 °C)	Skadi Liebherr

Description	Type	Manufacturer
	FKS 3600 Index 20B (20 °C)	Liebherr
	Ecotron (37 °C)	Infors HT
	INB 400 basic convection 53L (37 °C)	Memmert
Lamps	HBO 100	Osram
	KL 200 cold-light source	Schott
Dual LED System	KSL-Duo (470 nm / 590 nm)	Rapp OptoElectronic
LED Power Supply	KSL 70	Rapp OptoElectronic
Magnetic stirrer	Stuart™ CB162	Bibby Scientific
Micromanipulator	MMJ right-sided, with clamp ½"	Märzhäuser
Micropipette puller	P-97 Flaming/Brown	Sutter Instrument
Microscopes	Stemi 2000-C	Zeiss
	Axiovert 40 CFL	Zeiss
	Axio Observer.Z1	Zeiss
	Leica MZ 16F	Leica
	SMZ 645	Nikon
Microwave oven	MM 41580	Micromaxx
Optical power meter	PM 100	Thorlabs
	S120UV	Thorlabs
pH meter	Cyberscan pH 510	Eutech
Photometer	Genova	Jenway
	TrayCell (1:10, 1:50 virtual dilution factor)	Hellma Analytics
Power supplies	VP231-2	Eplax
	FluoArc/001.26D	LEJ
	Enduro™ power supplies 300V	Labnet
	TN-PSE30	Nikon
Shutter	*Smart*Shutters™	Sutter Instrument
Shutter controller	Lambda SC *Smart*Shutter™ Controller	Sutter Instrument
Thermal cycler	MyCycler™ Thermal Cycler	Bio-Rad
Vortexer	Vortex Genie 2	Scientific Industries
Weighing machines	EMB 600-2	Kern
	Analysewaage 770	Kern

2.1.2 Chemicals

Table 2-2|Chemicals used

Chemical substances	Manufacturer
Acetic acid	Carl Roth
Acetone	Carl Roth
Agar	Carl Roth
Agarose	Carl Roth/ Sigma Aldrich
Ampicillin sodium salt	AppliChem
Bovine serum albumin (BSA)	New England Biolabs
Calcium chloride	Carl Roth
Cholesterol	AppliChem
dNTP	Thermo Scientific
Dipotassium phosphate	Carl Roth
Disodium phosphate	Carl Roth
Ethanol	Carl Roth
Ethanol (AR grade)	Carl Roth
Ethidium bromide	Carl Roth
Ethylene-Diamine-Tetra-acetic-Acid (EDTA)	Carl Roth
GeneRuler 1kb and 1kb Plus DNA Ladder	Thermo Scientific
Glycerin	Carl Roth
Halocarbon oil	Halocarbon
Hydrochloric acid (37 %)	AppliChem
Isopropanol	Carl Roth
Magnesium chloride	Carl Roth
Magnesium sulfate	Carl Roth
Monopotassium phosphate	Carl Roth
Nitrogen	Linde
Nystatin	AppliChem
Polyethylene glycol (PEG 4000)	Carl Roth
Potassium chloride	Carl Roth
Potassium citrate	Carl Roth
Sodium acetate	Carl Roth
Sodium azide	Carl Roth
Sodium chloride	Carl Roth
Streptomycin sulfate	AppliChem

Chemical substances	Manufacturer
Tripotassium phosphate	Carl Roth
Tris(hydroxymethyl)aminomethane (TRIS)	Carl Roth
Tryptone/Peptone from Casein	Carl Roth
Yeast extract	Carl Roth

2.1.3 Buffers and Media

Buffers and media mentioned subsequently are produced with sterile ddH_2O as a solvent. If necessary the pH was adjusted afterwards. LB-medium was additionally autoclaved.

Table 2-3| Used buffers and media.

Buffer / Media	Manufacturer / Content
Antarctic Phosphatase Reaction Buffer (10x)	New England Biolabs
DNA loading dye (6x)	New England Biolabs
dNTP-Mix (50x)	10 mM dATP 10 mM dCTP 10 mM dGTP 10 mM dTTP
Injection buffer (10x, pH 7.5)	20% (w/v) Polyethylene glycol (6000g/mol) 200 mM Tripotassium phosphate 30 mM Potassium citrate
LB medium	0.5% (w/v) Yeast extract 1% (w/v) Tryptone/Peptone 1% (w/v) Sodium chloride + 1.5% (w/v) Agar (only at LB agar) Optional, after autoclaved: + 100 µg/ml Ampicillin + 200µg/ml Streptomycin
M9 buffer	1 mM Magnesium sulfate 20 mM Monopotassium phosphate 40 mM Disodium phosphate 85 mM Sodium chloride
Restriction Enzyme Buffers (10x)	New England Biolabs
Restriction Enzyme Buffers (10x)	Fermentas

Buffer / Media	Manufacturer / Content
Nematode Growth Medium (NGM)	1.7% (w/v) Agar 0.24% (w/v) Tryptone/Peptone 0.08% (w/v) Yeast extract 0.3% (w/v) Sodium chloride 1 mM Calcium chloride 1 mM Magnesium sulfate 25 mM Tripotassium phosphate 0.001% (v/v) Cholesterol solution (0.5% in ethanol) 0.01% (v/v) Nystatin (1% solution) 0.0376% (v/v) Streptomycin sulfate (5% solution)
Single egg worm lysis buffer (SEWLB)	10 mM Tris/HCl pH 8.3 50 mM KCl 2.5 mM $MgCl_2$ 0.45 % Tween-20 0.05 % Gelantine
Phusion HF-buffer (5x)	New England Biolabs
T4 DNA-Ligase buffer (10x)	Fermentas
TRIS acetic acid EDTA buffer (TAE, 50x, pH 8.5)	40 mM Tris/Acetic acid 2mM EDTA
TRIS EDTA buffer (TE, pH8)	10 mM Tris-HCl 1 mM EDTA

2.1.4 Kits

Table 2-4| Used kits.

Usage	Kit	Manufacturer
In-fusion HD Cloning	In-Fusion® HD EcoDry™ Cloning Plus	Clontech
Gel extraction and PCR purification	Gel/PCR DNA Fragments Extraction Kit	Avegene Life Science and Geneaid
Plasmid DNA preparation (Mini)	NucleoSpin® Plasmid Kit Roti-Prep Plasmid Mini	Macherey-Nagel Roth
Plasmid DNA preparation (Midi)	NucleoBond® PC 100	Macherey-Nagel
Site directed Mutagenesis	Q5®	NEB

2.1.5 Miscellaneous Materials

Table 2-5| Used miscellaneous materials.

Description	Type	Manufacturer
Conical centrifuge tubes	15 and 50 mL	Greiner Bio-One
Cover slip	Cover slip 22x22 mm	Carl Roth
Glass capillary	1B 100F-4	World Precision Instruments
Glass pipets	5, 10, 25 mL	Brand
Microcentrifuge tube	200µL Row of 8x or 12x 200 µL 1.5 and 2 mL	Sarstedt NeoLab Carl Roth
Microscope slide	Microscope slide 76x26 mm	Carl Roth
Objective immersion oil	Immersol 518F	Zeiss
Parafilm	Parafilm M	Alcan
Petri dish	Different sizes	Greiner Bio-One
Pipets	LabMate Optima single channel (0.1-2/2-20/20-200/100-1000 µL)	Abimed
Pipet controller	Pipetus®	Hirschmann
Pipet tips	Different sizes	Carl Roth
Polystyrene beads	0.1 µm, 2.6 % solid-latex	Polysciences
Protective gloves	Rotiprotect® latex and nitrile gloves	Carl Roth
Software	Argus X1 V.3 Clone Manager 9.0 Office GraphPad Prism 5.0 ImageJ KNIME Analytics Platform 2.10.0 Micro Manager Mendeley	Biostep Sci Ed Central Microsoft GraphPad Inkscape Community Knime.com AG Vale lab Elsevier

2.1.6 Enzymes

Table 2-6| Enzymes

Enzyme	Manufacturer	Buffer
Antarctic Phosphatase	NEB	Antarctic Phosphatase

		Reaction Buffer
Phusion DNA polymerase	NEB	Phusion HF-Buffer
Taq DNA Polymerase	Fermentas	Taq Buffer
T4 DNA ligase	Fermentas	T4 DNA Ligase Buffer
Restriction Enzymes	NEB and Fermentas	Respective Buffers
Proteinase K	Sigma	

2.1.7 Plasmids

bPGC/WincG2 plasmids:

pJN48 **[ptrx-1::trx-1(first-exon)::BICIS::bPGC::eYFP]**: Bicistronic fragment was amplified using oJN101,102 primers and pENTR as template and digested with BamHI-HF and ligated into BamHI-HF digested pWSC-14 (ptrx-1::trx-1(first exon)::bPGC::eYFP).

pJN49 **[pstr-2:: bPGC::eYFP]** : ~2 kb of pstr-2 was amplified from genomic DNA using outer nested primers oWSC-48,49; after which oWSC46 and oJN102 were used for inner nested pcr and HindIII-HF digestion to get 1935bp long pstr-2, which was ligated into 5.7kb fragment obtained by HindIII-HF digestion of pWSC13 (pmyo-3::bPGC::eYFP)

pJN51**[pgcy-31:: bPGC::eYFP]** : ~3 kb of pgcy-31 was amplified from genomic DNA using outer nested primers oWSC67, 68; after which oWSC66 and oWSC65 were used for inner nested pcr and HindIII-HF digestion to get 2.3 kb long pgcy-31, which was ligated into 5.7kb fragment obtained by HindIII-HF digestion of pWSC13 (pmyo-3::bPGC::eYFP).

pJN55 **[pmyo-3::tax-2::GFP]**: A 2415 bp long pmyo-3 fragment was amplified using primers oJN144 and oJN145 .This was ligated into pgcy-8::tax-2::GFP (pBY3117 in ref. 46), digested with SphI and XmaI (resulting in a 6,790 bp long DNA fragment) using 'in-fusion cloning' (Clontech).

pJN59 **[pmyo-3::bPGC(K265D)::eYFP]** : K265D was introduced in the parent plasmid pWSC13 (pmyo-3::bPGC::eYFP) using the Q5 site-directed mutagenesis (New England Biolabs Inc.) kit and primers oJN146 and oJN147.

For pJN58 **[pmyo-3::tax-4::GFP]**, the strategy was as for pJN55, but taking a 6,589 bp long fragment obtained upon digestion of pgcy-8::tax-4::GFP (pBY2974 in ref. 46) with SphI and XmaI was used as the vector backbone. We also removed a mutation,

T724A, which we found in the parent plasmid pBY2974, using the Q5 site-directed mutagenesis (New England Biolabs Inc.) kit and primers oJN154 and oJN155.

pMS05 **[pmyo-3::bPAC::SL2::mCherry]**: A 1193 bp long bPAC fragment was amplified using primers oMS01 and oMS02. This was ligated into pmyo-3::SL2::mCherry backbone (pCG05 [p*ggr-2*::LoxP::GCaMP6::SL2::mCherry]), obtained by digestion with BamHI and SalI, using 'in-fusion cloning'(Clontech).

pMS04 **[pmyo-3::bPGC::SL2::mCherry]** : A 3486 bp long pmyo-3::bPGC fragment was amplified using primers oJN168 and oJN169. This was ligated into a SL2::mCherry backbone (pCG05 [p*ggr-2*::LoxP::GCaMP6::SL2::mCherry]), obtained by digestion with NheI and SphI, using 'in-fusion cloning'(Clontech).

pMS06 **[pmyo-3::bPAC::YFP]** : 'in-fusion cloning' performed with insert: pcr fragment obtained using punc-17::bPAC::YFP (pWSC22) as template and oMS01 and oMS03 as primers ; vector: pMS04(pmyo-3::bPGC::SL2::mCherry) restricted with BamHI and EcoRI.

pMS03 **[pmyo-3::WincG2]**: The plasmid pgcy-5::WincG2 (obtained from Noelle D'Etoile, UCSF, USA) was digested with XbaI and PciI and pgcy-5 promoter fragment was replaced with pmyo-3 obtained by the digextion of pWSC13 (pmyo-3::bPGC::eYFP) (2872 bp) to yield the pmyo-3::WincG2 plasmid construct.

pCFJ104 **[pmyo-3::mCherry]** : pmyo-3::mCherry::unc-54 was a gift from Erik Jorgensen (Addgene plasmid # 19328) (Frøkjær-Jensen et al., 2008).

BeCyclOp plasmids:

For pJN63 [**pmyo-3::BeCyclOp::SL2::mCherry**], cDNA encoding BeGC1 (B. emersonii rhodopsin/guanylyl cyclase 1, GenBank:KF309499.1; equivalent of BeCyclOp) was codon optimized for expression in *C. elegans* using the web-tool: http://worm-srv3.mpi-cbg.de/codons/cgi-bin/optimize.py47. Three artificial introns were added to the sequence for mRNA stabilization. The resulting gene was synthesized by Eurofins Genomics (Ebersberg, Germany) in a pUC57 vector. BeCyclOp was sub-cloned into pmyo-3::SL2::mCherry vector backbone using KpnI and XbaI.

For pJN66 [**pflp-17::BeCyclOp::SL2::mCherry**], the 3.3 kb of pflp-17 (ref. 42) was amplified from genomic DNA using primers oJN195 and oJN196. The PCR fragment

was cloned into pmyo-3::BeCyclOp::SL2::mCherry following digestion with XbaI and PciI, thus replacing pmyo-3 with pflp-17 using 'in-fusion' cloning.

GLC-1 plasmids:

pJN42 [**pmyo-3::glc-1::eYFP**] : 2.8kb fragment of glc-1(genomic) with EYFP in M3-M4 loop was amplified using oJN141,142 primers and pJN40 [pglc-1::glc-1::eYFP] as template and digested with XbaI,SacI and ligated with 5.7kb fragment obtained upon BamHI-HF, SacII digestion of pCFJ104 (pmyo-3:: mcherry).

pJN43 [**pCMV::glc-1(T308P)::YFP**] : glc-1(T308P) cDNA mammalian codon optimized, YFP tagged (M3-M4 loop) in pcDNA3.1 was cloned by PCR mutagenesis (oJN132,133) and replacing the corresponding fragment using KpnI,PasI sites in the Plasmid 15104 (Addgene).

pJN44 [**pCMV::glc-1(T308P,L96C)::YFP**] : glc-1 cDNA mammalian codon optimized,YFP tagged (M3-M4 loop) in pcDNA3.1 (T308P,L96C) was cloned by PCR mutagenesis (oJN132, oJN134, oJN135, oJN143) and replacing the corresponding fragment using HindIII, HpaI sites in the pJN43 [pCMV::glc-1(T308P)::YFP].

pJN45 [**pCMV::glc-1(T308P,Q230C)::YFP**] : glc-1 cDNA mammalian codon optimized,YFP tagged (M3-M4 loop) in pcDNA3.1 (T308P,Q230C) was cloned by PCR mutagenesis (oJN132,136,oJN137,oJN143) and replacing the corresponding fragment using HindIII,HpaI sites in the pJN43 [pCMV::glc-1(T308P)::YFP].

pJN46 [**pCMV::glc-1(T308P,Q230C)::YFP**] was cloned by PCR mutagenesis (oJN132,oJN138,oJN139,oJN143) and replacing the corresponding fragment using HindIII,HpaI sites in the pJN43 [pCMV::glc-1(T308P)::YFP].

GLR-3/-6 plasmids:

pDM1769 [**pmyo-3::glr-3**] and pDM1773 [pmyo-3::glr-6] were presents from Prof. AV Maricq, University of Utah, USA.

pJN2 **[pmyo-3::glr-3(L409C)]** : L409C mutation was created by PCR mutagenesis (oJN21-24) and replacing the corresponding fragment by EcoRI and XhoI sites into the pDM1769. Subsequently, 'A' deletion was observed in the original construct provided by Maricq lab, 15 bp downstream of start codon, resulting in a frameshift.

This was corrected by PCR mutagenesis (oJN51-54) and replacing the corresponding fragment by EcoRI and XhoI sites into the pmyo-3::glr-3 and pmyo-3::glr-3(L409C) constructs.

pJN5 **[pmyo-3::glr-3(L409C)::eGFP]**: The glr-3(L409C) fragment was taken out by PCR (oJN35, oJN36) and then subcloned with AgeI and KpnI in the fire vector (pCK1/ pPD96.52).

pJN7 **[pmyo-3::glr-6(H417C)]** : H417C mutation was created by PCR mutagenesis (oJN25-28) and replacing the corresponding fragment by EcoRI and NheI sites into the pDM1773.

pJN8 **[pmyo-3::glr-6::eGFP]** and pJN9 **[pmyo-3::glr-6(H417C)::eGFP]**: The glr-6 and glr-6(H417C) fragment was taken out by PCR (oJN37, oJN38) and then subcloned with AgeI and KpnI in the fire vector (pCK1/ pPD96.52).

ACR-16 plasmids:

pJN22-28 [**pmyo-3::acr-16::GFP**] - T78C, N80C, T49C, H51C, S131C, T132C, L134C cysteine variants of ACR-16 : T78C, N80C, T49C, H51C, S131C, T132C, L134C mutations in pDM906 (pmyo-3::acr-16::GFP) (Francis et al. 2005) were incorporated by PCR mutagenesis (oJN15-20, oJN72-81) and replacing the corresponding fragment using XbaI and KpnI sites in the pDM906.

2.1.8 Oligonucleotides

Table 2-7| Oligonucleotides

Name	Comment	Sequence (5' - 3')
oJN15	acr-16 outer fwd primer	GATCCATCTAGAGGATCCCCGGGATTG
oJN16	acr-16 outer reverse primer	TTCTACCGGTACCAACCCATTACTAACAGATTG
oJN17	T78C acr-16 fwd primer	GCATGGCTGGATTATTGTTGGAACGACTATAATTTGG
oJN18	T78C acr-16 rev primer	CCAAATTATAGTCGTTCCAACAATAATCCAGCCATGC
oJN19	N80C acr-16 fwd primer	GCATGGCTGGATTATACATGGTGTGACTATAATTTGG
oJN20	N80C acr-16 rev primer	CCAAATTATAGTCACACCATGTATAATCCAGCCATGC
oJN21	glr-3 outer fwd primer	GAAGCAGTTGTGATAGCGAATTCAAGTG
oJN22	glr-3 outer rev primer	GTCGAAGCTGCTCGAGGACAAAGTTCAC
oJN23	L409C glr-3 fwd primer	CAGTTTATTGTGAAGCGCCATTTGTTATGATTAC
oJN24	L409C glr-3 rev primer	GTAATCATAACAAATGGCGCTTCACAATAAACTG
oJN25	glr-6 outer fwd primer	GGAGTTGACTATGCTAGCCAAAAACATTC
oJN26	glr-6 outer rev primer	GAATTTTGAATTCGGCTGTAGACTCTTTTGG
oJN27	H417C glr-6 fwd primer	GTGACATCGATTTGTGAAAAACCTTACGTGATTGAG
oJN28	H417C glr-6 rev primer	CTCAATCACGTAAGGTTTTTCACAAATCGATGTC

Name	Comment	Sequence (5' - 3')
oJN35	glr-3::gfp sub cloning fwd primer	GGTACCAAAAATGTTCTGGATTGCCAAAACTC
oJN36	glr-3::gfp sub cloning rev primer	ACCGGTCCATTCACATTCCATCGGAAAAATCC
oJN37	glr-6::gfp sub cloning fwd primer	GGATCGGTACCAAAAATGCTCAACATCTTCAG
oJN38	glr-6::gfp sub cloning rev primer	GGATCACCGGTCCAAATTTAGGCGAATTGCGAATTTC
oJN50	inner fwd primer for correcting glr-3/L409C	ATGTTCTGGATTGCCAAAACTCTCATCGCTTTTTTG
oJN51	inner rev primer for correcting glr-3/L409C	CAAAAAAGCGATGAGAGTTTTGGCAATCCAGAACAT
oJN52	outer fwd primer for correcting glr-3/L409C	CTAGATCCATCTAGAGGATCCCCGGGATTG
oJN53	outer rev primer for correcting glr-3/L409C	TTCACTTGAATTCGCTATCACAACTGCTTCAG
oJN72	T49C acr-16 fwd primer	ATCATTCCGAGCCAGTTTGTGTACATCTAAAGGTAGC
oJN73	T49C acr-16 rev primer	GCTACCTTTAGATGTACACAAACTGGCTCGGAATG
oJN74	H51C acr-16 fwd primer	GAGCCAGTTACAGTATGTCTAAAGGTAGCCCTC
oJN75	H51C acr-16 rev primer	GGAGGGCTACCTTTAGACATACTGTAACTGGCTCGG
oJN76	S131C acr-16 fwd primer	CCAATATGATTGTGTATTGTACTGGCTTGGTGCATTGG
oJN77	S131C acr-16 rev primer	CCAATGCACCAAGCCAGTACAATACACAATCATATTG G
oJN78	T132C acr-16 fwd primer	GATTGTGTATTCATGTGGCTTGGTGCATTGGGTTCC
oJN79	T132C acr-16 rev primer	GGAACCCAATGCACCAAGCCACATGAATACACAATC
oJN80	L134C acr-16 fwd primer	GTGTATTCAACTGGCTGTGTGCATTGGGTTCCACCG
oJN81	L134C acr-16 rev primer	CGGTGGAACCCAATGCACACAGCCAGTTGAATACAC
oJN132	glc-1 HEK cell exp. SDM fwd primer	GGCTAGTTAAGCTTGGTACCGAGCTCGGATC
oJN133	T308P glc-1 rev primer	GGTCACGCCCAGGGGGACGCG
oJN134	L96C glc-1 fwd primer	GAGCGTGAACATGTGCCTGCGCACCATCAG
oJN135	L96C glc-1 rev primer	CTGATGGTGCGCAGGCACATGTTCACGCTC
oJN136	Q230C glc-1 fwd primer	AGCACAGCCCCCTGTGCCTGAAGGTCGGC
oJN137	Q230C glc-1 rev primer	GCCGACCTTCAGGCACAGGGGGCTGTGCTC
oJN138	K232C glc-1 fwd primer	CCCCTGCAGCTGTGCGTCGGCCTGTCCTC
oJN139	K232C glc-1 rev primer	AGGACAGGCCGACGCACAGCTGCAGGGG
oJN141	pmyo-3 glc-1 fwd primer	ACCGTTCTAGAATGGCTACCTGGATTGTCGGAAAG
oJN142	pmyo-3 glc-1 rev primer	GTAGCGAGCTCCTAAAATAATACGTTCTGCTGGC
oJN143	glc-1 HEK cell exp. SDM rev primer	GATGTGGTTAACCAGGGCGAACTC
oJN144	pmyo-3 fwd primer	AATGAAATAAGCTTGCGGCTATAATAAGTTCTTGAA
oJN145	pmyo-3 rev primer	TGATACATATCCCGGTCTAGATGGATCTAGTGGTC
oJN146	fwd primer for K265D bPGC	CCTGAAGATGGACCACGGCCTGC
oJN147	Rev primer for K265D bPGC	CTGCTGCCCATGTTGCCC
oJN154	Removing T724A in tax-4	TGATCTACCAACGGGAACTGA
oJN155	Removing T724A in tax-4	ATTGTTTTTGTTTGTCGGAGAC
oJN168	bPGC fwd primer	ATTACGCCAAGCTTGCGGCTATAATAAGTTCTTGAA
oJN169	bPGC rev primer	TACCGTCGACGCTAGTTACTTGTCGTTTTCCAGGG

Name	Comment	Sequence (5' - 3')
oJN195	pflp-17 fwd primer	CCTTTTGCTCACATGCCTTGA
oJN196	pflp-17 rev primer	GTCCTTCATTCTAGACTGGAAAAATAAAGTTTTGCG
oJN101	ASJ bicis fwd primer	AGTGCTGGATCCTACCGCTGTCTCATCC
oJN102	ASJ bicis rev primer	ACTGCTGGATCCCGGTACAGCAGTTTCC
oWSC48	pstr-2 nested fwd primer	ACCGGTCCTGCAAACAGGTTCA
oWSC49	pstr-2 nested rev primer	CTCGTGCAGCCACACCAGGC
oWSC46	pstr-2 inner nested forward primer	GAAATGAAATAAGCTTAGAAACTTCGGGTTACTCAGCGT
oWSC65	pgcy-31 fwd primer	AATAAGCTTTCACGCCCGTCCGGTGAAAC
oWSC66	pgcy-31 rev primer	CGGAAGCTTGGCGGTGTGAAAATTGAAAATGAAAATGTTG
oWSC67	pgcy-31 fwd nested	GCCCGTATTGCCCACGCGA
oWSC68	pgcy-31 rev nested	TCGGTGACCCCCGACACGAA
oMS01	bPAC fwd primer	TCCATCTAGAGGATCCTTCCGCATCTCTTGTTCAAGGG
oMS02	bPAC rev primer	CAGCGGTACCGTCGACTTACTTGTCGTTTTCCAGGGTCTG
oMS03	bPAC rev primer for pmyo-3::bPAC::YFP	CGCTCAGTTGGAATTCTTACTTGTACAGCTCGTCCATGCC

2.1.9 Organisms

Table 2-8| Organisms

Species	Strain	Source
Caenorhabditis elegans	Bristol N2 wild-type (N2)	CGC
Escherichia coli	DH5α	Invitrogen
Escherichia coli	OP50-1	CGC

2.1.10 Transgenic *C. elegans* strains

Table 2-9| C. elegans strains used in the thesis

Strain number	Genotype	Generated in this thesis
ZX116	*unc-63(x37) I.*	
ZX235	*acr-16(ok789)V*	
ZX399	*lite-1(ce314) X.*	
ZX401	*unc-63(x37); acr-16(ok789)*	
ZX886	*daf-11(m84)*	
ZX1201	*N2;* zxIs80[pmyo-3::glr-3(L409C)::eGFP, pmyo-3::glr-6(H417C), pmyo-2::mCherry]	X

Strain number	Genotype	Generated in this thesis
ZX1202	*lite-1(ce314)*; zxIs81[pmyo-3::glr-3(L409C)::eGFP, pmyo-3::glr-6(H417C), pmyo-2::mCherry]	X
ZX1203	*lite-1(ce314)*; zxIs82[pmyo-3::glr-3(L409C)::eGFP, pmyo-3::glr-6(H417C), pmyo-2::mCherry]	X
ZX1204	*unc-63(x37); acr-16(ok789);* zxIs83[pmyo-3::acr-16(T78C)::GFP,pmyo-2::mCherry]	X
ZX1213 (CX10293)	*N2; kyEx2416 [flp-17::ChR2::mCherry,unc-122::gfp]*	(Zimmer et al. 2009)
ZX1214	*lite-1(ce314)*; zxIs84[pstr-2::bPGC::EYFP,pmyo-2::mCherry]	X
ZX1218	*unc-63(x37); acr-16(ok789);* zxEx854[pmyo-3::acr-16::GFP,pmyo-2::mCherry]	X
ZX1220	*daf-11(m84)*; zxIs88[ptrx-1::trx-1::BICIS::bPGC::eYFP]	X
ZX1222	*lite-1(ce314);* zxIs87[pgcy-31::bPGC::EYFP, pmyo-2::mCherry]	X
ZX1224	*unc-63(x37); acr-16(ok789);* zxEx855[pmyo-3::acr-16(T49C)::GFP,pmyo-2::mCherry] line-1	X
ZX1225	*unc-63(x37); acr-16(ok789);* zxEx855[pmyo-3::acr-16(T49C)::GFP,pmyo-2::mCherry] line-2	X
ZX1226	*unc-63(x37); acr-16(ok789);* zxEx856[pmyo-3::acr-16(H51C)::GFP,pmyo-2::mCherry] line-1	X
ZX1227	*unc-63(x37); acr-16(ok789);* zxEx856[pmyo-3::acr-16(H51C)::GFP,pmyo-2::mCherry] line-2	X
ZX1228	*unc-63(x37); acr-16(ok789);* zxEx857[pmyo-3::acr-16(N80C)::GFP,pmyo-2::mCherry] line-1	X
ZX1229	*unc-63(x37); acr-16(ok789);* zxEx857[pmyo-3::acr-16(N80C)::GFP,pmyo-2::mCherry] line-2	X
ZX1230	*unc-63(x37); acr-16(ok789);* zxEx858[pmyo-3::acr-16(S131C)::GFP,pmyo-2::mCherry] line-1	X
ZX1231	*unc-63(x37); acr-16(ok789);* zxEx858[pmyo-3::acr-16(S131C)::GFP,pmyo-2::mCherry] line-2	X
ZX1232	*unc-63(x37); acr-16(ok789);* zxEx859[pmyo-3::acr-16(T132C)::GFP,pmyo-2::mCherry] line-1	X
ZX1233	*unc-63(x37); acr-16(ok789);* zxEx860[pmyo-3::acr-	X

Strain number	Genotype	Generated in this thesis
	16(L134C)::GFP,pmyo-2::mCherry] line-1	
ZX1234	*unc-63(x37); acr-16(ok789);* zxEx860[pmyo-3::acr-16(L134C)::GFP,pmyo-2::mCherry] line-3	X
ZX1250	*unc-63(x37); acr-16(ok789);* zxIs85[pmyo-3::acr-16(S131C)::GFP,pmyo-2::mCherry]	X
ZX1703	*lite-1(ce314)*; zxEx862[pmyo-3::glr-3,pmyo-3::glr-6::GFP,pmyo-2::mCherry]	X
ZX1705	*lite-1(ce314)*; zxEx862[pmyo-3::glr-3(L409C),pmyo-3::glr-6::GFP,pmyo-2::mCherry]	X
ZX1727	*lite-1(ce314)*; zxEx877[pmyo-3::glc-1::YFP,pmyo-2::mCherry]	X
ZX1728	*lite-1(ce314)*; zxEx878[pmyo-3::glc-1::YFP,pmyo-2::mCherry]	X
ZX1729	*lite-1(ce314)*; zxEx879[pmyo-3::glc-1::YFP,pmyo-2::mCherry]	X
ZX1737	*lite-1(ce314)*; zxIs82[pmyo-3::glr-3(L409C)::eGFP, pmyo-3::glr-6(H417C), pmyo-2::mCherry], ZxEx885[pmyo-3::sol-1,pmyo-3::sol-2, pges-1::GFP]	X
ZX1738	*lite-1(ce314)*; zxEx886[pmyo-3::bPGC::YFP, pmyo-3::tax-2::GFP, pmyo-3::tax-4::GFP]	X
ZX1739	*lite-1(ce314)*; *zxEx887*[pmyo-3::bPGC(K265D)::YFP, pmyo-3::tax-2::GFP, pmyo-3::tax-4::GFP]	X
ZX1740	*lite-1(ce314)*; zxEx888[pmyo-3::bPGC::YFP]	X
ZX1741	*lite-1(ce314)*; zxEx889[pmyo-3::tax-2::GFP, pmyo-3::tax-4::GFP, pmyo-2::mCherry]	X
ZX1743	*lite-1(ce314)*; zxEx851 [pmyo-3::BeGC1::SL2::mCherry, pmyo-3::tax-2::GFP, pmyo-3::tax-4::GFP]	X
ZX1745	N2; zxEx852 [pflp-17::BeGC1::SL2::mCherry, elt-2::GFP]	X
ZX1746	*lite-1(ce314)*; zxEx853 [pmyo-3:: BeGC1::SL2::mCherry]	X
ZX1756	N2; zxEx892[pmyo-3::bPGC::SL2::mCherry,pmyo-3::WincG2]	X
ZX1757	N2; zxEx893[pmyo-3::mCherry,pmyo-3::WincG2]	X
ZX1921	N2; zxEx895[pmyo-3::BeGC1::SL2::mCherry,pmyo-	X

Strain number	Genotype	Generated in this thesis
	3::WincG2]	
ZX1922	N2; zxEx896[pmyo-3::bPAC::SL2::mCherry,pmyo-3::WincG2]	X
ZX1923	*lite-1(ce314)*; zxEx897[pmyo-3::bPAC::YFP, pmyo-3::tax-2::GFP, pmyo-3::tax-4::GFP]	X
ZX1924	*lite-1(ce314)*; zxEx898[pmyo-3::bPAC::YFP, pmyo-3::tax-2::GFP, pmyo-3::tax-4::GFP]	X
ZX1925	*lite-1(ce314)*; zxEx899[pmyo-3::bPAC::YFP]	X

2.2 Molecular biological methods

Molecular biological methods described below were used for cloning, preparation and purification of plasmid DNA. After *in-silico* planning the cloning using Clone Manager, Restriction enzyme based cloning or in-fusion cloning in cases where suitable restriction sites were unavailable were used to bring the DNA fragments together and the ligated product was transformed into *E. coli* to obtain the desired final plasmid.

2.2.1 Polymerase Chain Reaction (PCR)

The polymerase chain reaction (PCR) is a method for exponentially amplifying a specific DNA-sequences *in vitro* (Lorenz 2012). Here, two oligonucleotides called primers are designed so as to flank the target sequence in a template DNA molecule. The primer that binds complementary to the antisense strand at the 5'-end of the target sequence is known as the forward primer whereas the reverse primer binds complementary to the sense strand at the 3'-end. Both of them are mixed to gether with a thermostable DNA polymerase, deoxynucleoside triphosphates (dNTPs) and a buffer for the polymerase in a water solution. The subsequent reaction can be distributed into three basic steps - denaturation leading to the opening of the double helical template, primer-template hybridization (annealing) and elongation by the polymerase.

The temperatures at which these steps are performed depend on the polymerase used and the binding ability of the oligonucleotides which in turn depends on their length and GC content; while the duration of the steps varies according to the size of

the desired amplified DNA product and the polymerase used. Phusion high-fidelity DNA polymerase was used because of its additional proof-reading 3' → 5' exonuclease activity, allowing error correction during polymerization. Furthermore it is fused to a double-strand DNA binding domain that leads to a higher processivity compared to other DNA polymerases. These two properties make Phusion DNA polymerase more suitable for cloning and for amplification of long fragments. In a two step PCR protocol, the annealing temperature is same as the elongation temperature, which minimizes the false priming of the oligonucleotides.

2.2.2 Phenol/chloroform extraction

Phenol Chloroform Isoamyl Alcohol (PCA) extraction is a method to separate DNA from salts and proteins. It was performed to purify the DNA from a PCR reaction mix when a restriction digest was performed afterwards. First 0.5 volumes of a phenol:chloroform:isoamyl alcohol mixture in the proportions 25:24:1 were added to the DNA containing solution. The solution was vortexed for one minute, enough to produce an emulsion. This was then centrifuged for five minutes at full speed (16200 rcf) using the centrifuge Micro 200R (Hettich). This procedure separated the protein containing, denser phase (bottom) from the DNA containing water phase (top). The water phase was separated and 2.5 volumes of ethanol sodium acetate (100 % ethanol with 0.12 M sodium acetate) were added. After mixing this solution thoroughly it was centrifuged at 4 °C for 30 minutes at full speed (16200 rcf) to pelletize the DNA. The supernatant was carefully removed and 250 µL 70% ethanol were added to the pellet in order to wash it. After the last centrifugation at 4 °C for 10 minutes at full speed (16200 rcf) again the supernatant was removed carefully and the pellet was allowed to dry at room temperature for 10 minutes. Finally the pellet was reconstituted in ddH_2O.

2.2.3 DNA Restriction digest

The DNA restriction digest allows to specifically cut DNA according to the recognition site of the restriction enzyme, producing linear DNA that can be used for ligation. Type II restriction enzymes are the most interesting for molecular biology since their restriction site is usually within the recognition site. The recognition site is a palindromic DNA sequence of about 4 – 8 bp. After cleavage, Type II restrictions enzymes can leave blunt ends or sticky ends. This allows cutting two different DNA molecules with the same restriction enzymes and ligating them specifically by using

the complementarity of the sticky ends. Restriction digestions were performed with the plasmid DNA and PCA purified PCR fragments for cloning. The buffer conditions were checked with NEB Double Digest Finder tool and the restriction sides were checked for Dam/Dcm methylation sites. Typically, a preparative digest of 15 to 20 µg of the plasmid DNA was performed to obtain the vector backbone for cloning. Furthermore analytical control digests were performed of plasmid DNA preparations (Mini) to analyze the results of molecular cloning and hence select clones that contain the correct vector construct. The purification of the preparative digest and the analysis of the analytical digest were both achieved through gel electrophoresis.

2.2.4 DNA gel electrophoresis

DNA gel electrophoresis is a method to purify DNA fragments or to measure DNA length in base pairs (bp). As the phosphate backbone of DNA molecules is negatively charged they move in an agarose gel under an electrical field in direction of the anode. DNA gel electrophoresis was used for the analytical and preparative separation of DNA fragments. 1% agarose (w/v) was dissolved in 1x TAE buffer in a microwave oven. After cooling the solution to a temperature of about 40 °C it was poured to a chamber. The size of the pockets was adjusted due to the volume of each sample. To each sample one fifth in volume of loading dye (6x) was added before loading the sample into the pockets. Electrophoresis was performed under a voltage of 120 V to 160 V (6.5±1.5 V/cm) for 45 to 60 min in 1x TAE buffer. After electrophoresis the DNA in the gel was stained with Ethidium Bromide (EtBr) in a 0.1% (v/v) water solution for 15 to 30 minutes, which was subsequently visualized using the trans-illuminator.

2.2.5 DNA Gel extraction

DNA gel extraction was performed to purify specific DNA fragments, which were separated by DNA gel electrophoresis, from components of preceding reactions. In this study it was primary used for purification of preparative restriction digests. The respective DNA fragment was excised from the agarose gel with a scalpel at the minimum of UV illumination to reduce damage of the DNA molecules. The extraction was performed as it is described in the manual of the Gel/PCR DNA Fragments Extraction Kit. During this process, the DNA binds selectively and reversible to a silica membrane and is separated from proteins, salts, dyes, nucleotides and agarose. In order to increase the amount of extracted DNA from the gel, the

following changes were made to the protocol: all centrifugation steps are done at 1500 RCF except for the drying (3000 RCF, 4 min) and the elution step (16200 RCF, 2 min). The step of DNA binding was repeated two to three times. The incubation with 20 µL ddH_2O in the elution step was increased to five to seven minutes.

2.2.6 Dephosphorylation

The DNA Dephosphorylation was achieved using the enzyme Antarctic Phosphatase (AP). Since dephosphorylated backbone cannot be religated through T4 DNA Ligase, the procedure prevents vector re-ligations and false positive clones. AP dephosphorylates specifically the 5'-end of linear DNA fragments.. The reaction mixture was incubated for 20 minutes at 37 °C followed by an inactivation of the AP at 70 °C for 5 minutes. The DNA solution could be used without further purification for the ligation of the insert to the backbone, as mentioned in the accompanying manual.

2.2.7 Ligation

Two linear DNA molecules with complementary sticky ends or blunt ends are ligated to a recombinant DNA plasmid using bacteriophage T4 ligase that needs ATP to catalyze the ligation reaction. The molar ratio of insert to vector DNA was varied from 2:1 to 6:1. Different amounts of vector DNA (20 and 50 fmol) were used to increase the probability of successful DNA ligation. Ligation mixture that was incubated for 1 h at room temperature. After 5 µL of the mixture were used for *E. coli* transformation, the remaining reaction volume was left over night at 16 °C. If the transformation was not successful, this would be used for another transformation. The T4 ligase was then inactivated during an incubation period of 10 min at 65 °C.

2.2.8 In-Fusion HD Cloning

In-Fusion HD Cloning allows the integration of a PCR product into a linearized vector by homologue sequence overlap. Thus no additional treatment of the PCR fragment such as restrictions digestion or ligation is necessary. The primers for PCR amplification were designed by using the online Primer Design Tool provided by Clontech. The cloning procedure was performed as per the In-Fusion® HD Cloning Kit User Manual.

2.2.9 Heat shock transformation of competent E. coli cells

The transformation of plasmid DNA into the chemical competent *E. coli* DH5α strain was used to amplify recombinant plasmids and screen for correct plasmid constructs from molecular cloning. Chemical competent bacteria were previously prepared by rubidium chloride method and frozen in aliquots of 100 µL at –80 °C. For each transformation, one aliquot was taken and thawed on ice. Then an appropriate amount of plasmid (re-transformation 1 µL, ligation mixture 5 to 20 µL) was carefully mixed with the bacteria and incubated for 30 min on ice. Then a heat shock was applied for 1 min at 42 °C. Afterwards the cells were again incubated on ice for 3 minutes. Then 500 µL of LB medium was added to the bacteria, followed by an incubation in the shaker for 1h at 37 °C. The bacteria were than centrifuged at 2500g for 5 minutes. After 500 µL of the supernatant was removed the pellet of bacteria was resuspended in the remaining medium and plated on a LB agar plate containing the antibiotic corresponding to the resistance marker present in the transformed strain (ampicillin for *E. coli* DH5α). The plates were incubated at 37°C for 16 h and stored at 4 °C after the colonies had been selected for further experiments.

2.2.10 Plasmid DNA preparation (Miniprep/Midiprep)

Plasmid DNA was extracted from *E. coli* DH5α cultures for analytical and preparative purpose by using the NucleoSpin® Plasmid kits. The kits are based on alkaline lysis of bacterial cells with a subsequent separation of genomic and plasmid DNA via centrifugation or filtration. The small-scale preparation was used to screen colonies for positively recombined plasmids after transformation. For this, bacteria were grown in 4 ml of LB medium containing the appropriate antibiotic for 16 h at 37 °C. Large-scale bacteria cultures were prepared to yield great quantities of a plasmid for further experiments, as in *C. elegans* micro injection. Those plasmids were already verified by restriction digest and sequencing. For preparation a 100 mL LB medium with the appropriate antibiotic was inoculated with bacteria from a preculture and incubated for 16h at 37 °C. The protocols were performed as described in the supplied manual.

2.2.11 Plasmid DNA sequencing and alignment

DNA sequencing was used to verify newly created plasmids. All sequencing assignments were sent to the company Eurofins MWG GmbH in Ebersberg. For this

purpose a premix of 15 µL of the DNA solution with a DNA concentration of 50 to 100 ng/µL and 2 µL of the sequencing primer (10 µM) were prepared. The sequencing results were compared to the *in silico* plasmid sequence to verify the correctness of the recombinant plasmid using Clone Manager 9.0.

2.2.12 Site-directed mutagenesis

The introduction of point mutations was achieved using the commercially available Q5 mutagenesis kit (NEB) or using an overlap extension PCR method (Heckman and Pease 2007). For the overlap PCR based method, three PCRs are carried out (**Figure M1**). The first primer (outer fwd primer) binds a position a few hundred base pairs in front of the position to be mutated and includes a useful restriction site. The next pair of primers (inner fwd and inner rev) bind to the region containing the site to be mutated. In this case care is taken that the mutation is located in the middle of the primer, it is flanked by 15 bp of each original sequence and the primers overlap each other. The final primer (outer rev primer) binds the complementary strand, again a few hundred base pairs away from the mutation site and also includes a restriction site, which should, however, be different from the first. The first two PCRs are performed with outer fwd and inner rev, and inner fwd and outer rev, primers pairs using the original plasmid as template. After the isolation of these PCR products by means of gel extraction, they are used as template for the final PCR using the outer fwd and outer rev primers. This is followed by digestion, ligation and transformation into DH5α, and a sequencing for verification of the point mutation.

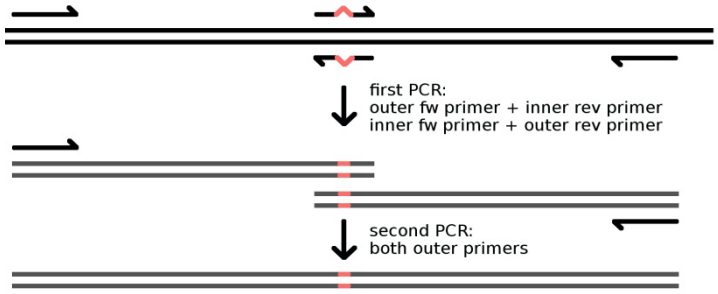

FIGURE M1: Overlap PCR based method for site directed mutagenesis. In red is marked the site for introduction of the desired mutation.

2.3 *Caenorhabditis elegans* Methods

2.3.1 Cultivation of *C. elegans*

C. elegans were grown on Nematode Growth Media (NGM) agar plates with *E. coli* OP50-1 bacteria as a food source. Depending on the desired growth period, the animals were stored at 16 °C, 20 °C or 25 °C. Contamination by foreign bacteria, yeasts or molds were removed by a bleaching solution. For this 10-20 adult animals were placed in a drop (~ 50 µL) of the bleach solution beyond the bacterial lawn on a NGM plate. The solution causes decomposition of the contaminants and of the animals until the eggs remain whose shell is resistant to the bleaching solution. The new generation hatched from these eggs is then free from contamination.

2.3.2 Microinjection of plasmid DNA into *C. elegans*

The DNA micro injection into *C. elegans* is a standard technique to obtain transgenic animals. For this purpose a solution containing foreign plasmid DNA is injected into the distal arm of the gonads of young adult hermaphrodites. Since in this specific area the oocytes create a syncytium during maturation, the exogenous DNA plasmids are engulfed by the dissolved nuclear envelope. Thus homologous recombination takes place that results in the formation of a so-called extrachromosomal array, which contains multiple copies of the injected DNA plasmid (Stinchcomb et al. 1985). This extrachromosomal array can be transmitted to the F1-generation. However the DNA array may not be transmitted into all cells of F1-generation which leads to mosaic expression. Furthermore, only the arrays that have sufficient multiple copies of the introduced DNA become heritable and are expressed also in the F2 generation (Mello et al. 1991).

The transgenic animals used in this study were created by microinjection (Mello et al., 1991) of the respective DNA construct injected in the gonads of young adult hermaphrodites. The DNA to be micro injected was prepared into injection mixes of 30 µL volume. The total DNA concentration of injection mixes was at least 100 ng/µL in order to facilitate the formation of an extrachromosomal array. The injection mix was centrifuged for 10 minutes at 16200 rcf and 15 µL of the supernatant was used for injection.

Prior to microinjection, glass needles were pulled with a P-97 microelectrode puller. Around 0.5 µL of the injection mix was pipetted over the opening of the needle which

gets filled due to the capillary forces. In the meanwhile a cover slip with a dry agar pad (2% (w/v) agar in ddH_2O) was fixed to a microscope slide. The agar pad was carved at one edge and a drop of halocarbon oil was applied on this place. The filled needle was mounted to the air pressure outlet, which was connected to the micro manipulator. Afterwards the microscope slide containing the agar pad was placed on the stage of the Zeiss Axiovert 40 CFL and the tip of the needle was broken by gently touching it to o one of the carvings in the agar pad.

A young adult hermaphrodite was transferred to the halocarbon oil with a worm pick. After cleaning the worm from bacteria, it was transferred on a clean part on the agar pad. The glued worm was then injected as described. After successful injection a drop of M9-buffer was applied over the worm body to release the worm form the agar pad and recover them from the oil. Finally the worm is picked and transferred to a fresh NGM-plate with seeded OP50-1 bacteria. The NGM-plate was cultivated at room temperature for 3-5 days. The selection was done base on the marker used in the injection mix.

2.3.3 Genomic integration of extrachromosomal DNA in *C. elegans*

Since the transmission of an extrachromosomal multicopy tandem transgene does not take place to all the progeny of a transgenic strain and there exists mosaicism in the expression, a method for genomic integration of the transgene was chosen. For this purpose, 100 transgenic animals at L4 larval stage were transferred to 55 mm NGM plates without OP50 bacterial lawn and irradiated with 66.6 mJ UV light. The irradiated animals were transferred in lots of 10 to OP50 seeded 55 mm NGM plates and incubated until the bacteria lawn was completely eroded and the F2 generation was transferred to fresh plates. Around 1000 transgenic animals were singled on fresh plates and were checked in the next generation for 100% presence of the transgene. The successfully integrated animals were subsequently out-crossed 4 times with wild-type animals to eliminate background mutations in other regions of the genome. For integration of ACR-16(S131C)::GFP extrachromosomal transgene into the genome, UV irradiation in the presence of trimethylpsoralen (TMP) was used as the mutagen.

2.3.4 Microscopy

2.3.4.1 Stereo microscopy

A stereo microscope is an optical device that allows that analysis of samples on low magnification. In this work a SMZ 645 stereo microscope (Nikon) was used for *C. elegans* handling during cultivation and preparation of experiments.

2.3.4.2 Fluorescence microscopy

Fluorescence microscopy was used to study the expression of fluorescent protein in transgenic animals. A Leica MZ 16F fluorescence stereomicroscope was used to identify transgenic animals as they carry the DNA array encoding for a fluorescent marker.

The fluorescence microscope Axio Observer Z.1 was used for analysis of the fluorescence expression pattern of transgenic animals. For this, transgenic animals were picked onto 10 % agar pads (10% (w/v) agar in M9 buffer) and were immobilized with 50 mM sodium azide. Images were acquired with an ORCA-Flash 4.0 (Hamamatsu) camera or Coolsnap HQ (Roper scientific) camera. The expression pattern of transgenic animals was imaged with a 10x objective (Zeiss A-Plan 10x / 0.25), 40x oil immersion objective (Zeiss EC-Plan 40x / 1.3 oil) and 100x oil immersion objective (Zeiss EC-Plan 100x / 1.3 oil). The HBO-100 lamp was used for excitation of fluorescence. For adjusting the exposure time and acquiring the images Micro Manager was used. As transmission light image, DIC (Differential Interference Contrast) was used.

2.3.4.3 *In vivo* cGMP imaging with simultaneous activation of light activated cyclases

Transgenic strains were kept in dark on standard NGM plates (5.5 cm diameter; 8ml NGM) with OP50-1 bacteria without or with ATR at 20 degree Celsius. Plates containing ATR were prepared by spreading 200 µl of OP50-1 culture containing 100 mM of ATR (diluted in ethanol). L4 animals were put on ATR plates overnight and young adults were used for imaging the following day.

For cGMP/cAMP imaging, animals were immobilized on 10% M9 agar pads with polystyrene beads (Polysciences, USA). The fluorescence measurements were performed with a 25 x oil objective (Zeiss 25x LCI-Plan / 0.8 Imm Corr DIC) on the inverted microscope Axio Observer Z.1 equipped with two high-power light emitting

diodes (LEDs; 470 and 590 nm wavelength, KSL 70, Rapp Optoelektronik, Germany) coupled via a beam splitter and a double band pass excitation filter permitting wavelengths of 479/21 nm and 585/19 (F74-423 479/585 HC Dualband Filter AHF Analysentechnik) to obtain simultaneous dual-wavelength illumination. The transmission light filtered with a red optical filter was used to focus on the muscle cells prior to video acquisition. The 470nm and 590nm excitation was switched on simultaneously after the start of video acquisition. In case of bPGC experiments, yellow light was used to focus the cells and therafter the blue illumination was turned on. The emission light was fed to the camera (ORCA-Flash 4.0, Hamamatsu) through a Dual-View beamsplitter (DV2, Photometrics) with 540/25 nm emission filter used for WincG2 green channel and a 647/57 emission filter for mCherry channel. Videos were acquired using Micro-Manager (Edelstein et al.,2010) and frames were taken at 100Hz (corresponding to exposure times of 10 ms) or 20 Hz (for bPGC experiments) with 4×4 spatial binning. The optical power was 3.3 mW/mm^2 at 470 nm and 2.6 mW/mm^2 at 590 nm.

Image analysis was performed in ImageJ (NIH). Regions of interest (ROIs) were drawn around single body wall muscle cells that did not show major movement and a region outside the animals was chosen as background ROI. The mean fluorescence intensity of the ROIs for both channels was analyzed with ImageJ. Background subtracted values were used to calculate the change in fluorescence intensity for each time point: $(F-F_o)/F_o$ where F represents the intensity at this time point and F_o represents the peak intensity at the onset of light stimulation.

2.3.5 Electrophysiology in *C. elegans* (by Dr. Jana Liewald)

Electrophysiology of *C. elegans* body wall muscle cells was done as previously described (Richmond and Jorgensen, 1999; Nagel *et al.*, 2005). Animals were immobilized with Histoacryl glue (B. Braun Surgical, Spain) and a lateral incision was made to access neuromuscular junctions along the ventral nerve cord. The basement membrane overlying the muscles was enzymatically removed by incubation in 0.5 mg ml^{-1} collagenase for 10 s (type IV, C5138, Sigma-Aldrich, Germany).

Currents were measured in whole-cell voltage clamp mode at room temperature (20-22°C) using fire-polished borosilicate pipettes (1B100F-4; outer diameter: 1.0 mm; World Precision Instruments, USA) of 4- to 7-MΩ resistance. The bath solution

contained (in mM): NaCl 150; KCl 5; $CaCl_2$ 5; $MgCl_2$ 1; glucose 10; sucrose 5; HEPES 15, pH7.3 with NaOH, ~330 mOsm. The pipette solution contained (in mM): KCl 120; KOH 20; $MgCl_2$ 4; N-tris[Hydroxymethyl]methyl-2-aminoethane-sulfonic acid 5; $CaCl_2$ 0.25; sucrose 36; EGTA 5; Na_2ATP 4, pH7.2 with KOH, ~315 mOsm. Muscle cells were patch clamped at a holding potential of -60 mV using an EPC10 amplifier with head stage connected to a standard pipette holder (HEKA Electronics, Germany). Data were analyzed by Patchmaster software (HEKA Electronics, Germany).

Test substances were pressure-applied onto the muscle cells (Picospritzer III, Parker Hannifin, New Hampshire, USA), triggered by the Patchmaster software. Carbachol (C4382, Sigma-Aldrich, Germany) was applied at a concentration of 500 µM for 1s. L-Glutamate (G1626, Sigma-Aldrich, Germany) was applied at a concentration of 1 mM for 1s. Pre-illumination of animals that were incubated with MAC or MAG took place for 2 minutes with UV light (NU-8 KL, Benda, Germany; 366nm, 8.06 mW/mm^2) before patch clamping the muscle cells. Light activation in whole-cell voltage clamp mode was performed using a LumenLED lamp (Prior Scientific, Germany) at a wavelength of 385 nm or 505 nm and was controlled by the Patchmaster software.

2.3.6. Swimming behavior analysis of *C. elegans*

For the analysis of the behavior of *C. elegans* in liquid, thrashing (swimming) assays of young adult hermaphrodites were carried out in 96-well microtiter plates, containing 100 µL of NGM and 100 µL of M9 saline solution. For experiments with azocholine, 1mM AzoCholine per well was used. For the control condition (without AzoCholine), M9 was supplemented with 1% DMSO (carrier solvent for AzoCholine). The animals were incubated in the buffer solution for 15 min under low-intensity UV light from a UV lamp (366 nm, 16 $\mu W/mm^2$, Benda, Wiesloch, Germany). Subsequent UV and blue light illumination of the worms was provided through a 4× magnification objective. During the assay, a HBO lamp was used with UV and blue light filters (Zeiss; 325−375 nm, 0.26 mW/mm^2; 450−490 nm, 0.6 mW/mm^2). Assays were recorded with a Powershot G9 camera (Canon, Krefeld, Germany) on a SMZ645 stereo microscope (For ACR-16) or an AxioScope fluorescence microscope, and swimming cycles (the worm's body bends forth and back per each

cycle) were counted for defined time intervals during the UV and blue light illumination.

2.3.7 Speed analysis of *C. elegans*

For the speed assay for BeCyclOp experiments, L4 stage animals were picked onto NGM agar plates supplemented with 100 mM of ATR. After 10–24 h of feeding in the dark, 15–20 young adults were transferred to an NGM plate and starved for 1 h. A multiworm tracker, which can analyse ~100 animals simultaneously (Swierczek et al. 2011) was used to follow behavior by video tracking. Blue light illumination was provided with a custom-made ring of high power 470 nm blue light-emitting diodes. The transmission light source was covered with a red film that cuts off all wavelengths below 590 nm. The NGM plate was covered with a lid, on top of which a neutral density filter was placed such that the blue light intensity incident on worms was 70 $\mu W/mm^2$. Speed was computed using 'Choreography', an additional programme for off-line analysis of different behavioural parameters (Swierczek et al. 2011).

For speed measurements for bPGC experiment, a single worm tracker(SWT) (Stirman et al. 2011) was used which enables simultaneous tracking and illumination of single animals. The animals were reared in dark and for the experiment they were placed on NGM plates without OP50 and starved for 1 h. Afterwards they were tracked on the SWT. The transmission light was filtered with the red filter and the light from the projector was shut off with the help of a shutter until the 470 nm blue illumination was turned on. This was done to prevent any pre-activation of bPGC. The speed data as computed by the Labview script in the SWT was further analysed and plotted using MS Excel 2007.

2.3.8. Body length measurement of *C. elegans* in contraction assays.

For BeCyclOp experiments, transgenic strains were kept in dark on standard NGM plates (5.5 cm diameter; 8ml NGM) with OP50-1 bacteria without or with ATR at 20 degree Celsius. Plates containing ATR were prepared by spreading 200 µl of OP50 - 1 culture containing 100 mM of ATR (diluted in ethanol). For the contraction assay, transgenic L2–L3 larvae were selected for muscle fluorescence under a Leica MZ16F dissection scope and transferred to freshly seeded ATR plates and thereafter

kept in the dark. Measurements of contractions and elongations were performed as described in (Liewald et al. 2008). L4 larvae (young adult animals for data in BeCyclOp alone data figure) were individually placed on plain NGM plates and assayed on an AxioScope.A1 microscope (Zeiss, Germany) with a 10x objective and transmission light filtered through a red 675±50nm bandpass filter. For colour illumination, the light of a 50W HBO lamp was channelled through excitation bandpass filters of 470±20nm (blue illumination) and 535±15nm (green illumination). Both blue and green illumination had an intensity of 0.9 mW mm^{-2}. For the intensity profile, 530±7.5nm (green illumination) from a monochromator (Polychrom V) was used. Intensities were individually adjusted using the neutral density filters (Zeiss, Germany); intensity was measured using an S120UV Sensor with PM 100 power metre (Thorlabs, Dachau, Germany). Video recordings of worms were done using a CMOS camera (DCC1545M, Thorlabs, Dachau, Germany). Duration of illumination was defined by a computer-controlled shutter (Sutter Instruments, USA) using a custom written LabView script (Stirman et al. 2011). Consecutive frames were extracted from video micrographs of behaving worms for body length analysis using a custom written LabView script (Stirman et al. 2011). Measured length of individual animals was normalized by the mean length (averaged over 20 frames) before the photostimulation and followed over hundreds of consecutive movie frames (at 10 Hz). Length chronograms of multiple worms were then averaged. Displayed are means±s.e.m. In case of bPGC experiments, the excitation was achieved with bandpass filters of 470±20nm while the transmission light being red-filtered to prevent any pre-activation of bPGC.

For LiGluR and LiAChR experiments, the illumination was achieved with 370-390nm (UV illumination) and 490-510nm (green illumination) band pass filters using the light of a 50W HBO lamp or with the help of Prior LED system (385 and 505 nm). The young adult hermaphrodite animals were bathed in a solution of 250-500 µM MAGs or 500 µM MAC in 4% DMSO in dark for 45 minutes (MAGs and MAC were synthesized in the lab of Prof. Dr. Dirk Trauner, University of Munich, Germany). The compounds were pre-illuminated with the low intensity UV lamp for 5 minutes to have pre-dominantly the cis-form so as to aid the process of affinity labelling. After the incubation, the animals were washed with M9 buffer for 3 times and were

allowed to recover for an hour. Afterwards, they were tested for contraction according to the procedure described above.

2.3.9. *C. elegans* extract preparation for in-vivo cGMP or CAMP assays

30 L4 larvae (strain ZX1746, worms expressing BeCyclOp only in BWMs) were picked onto NGM plates supplemented with OP50-1 with or without 100 mM ATR each. The plates were kept in a 20°C incubator for 3 days. Afterwards, the animals were rinsed off the plates with M9 buffer, subsequently washed with M9 buffer 4–5 times to remove bacteria and transferred into 24-well plates. The animals were illuminated with green light (540–580 nm, 150 mWmm_2) using a Leica fluorescence stereomicroscope for 15 min. Following illumination, the M9 buffer was substituted by 0.1M HCl (1:10 dilution to the worm pellet) and the animals were subjected to three freeze-thaw cycles with liquid nitrogen. Afterwards, the animals were vortexed with 0.25–0.5mm glass beads in 0.1M HCl for 1min. The supernatant after centrifugation (2,000 r.p.m., 1min) was used for the cGMP (or cAMP) assay performed with DetectX High Sensitivity Direct cGMP (or cAMP) Chemiluminescent Immunoassay Kit (Arbor assays) by Shiqiang Gao, Prof. Georg Nagel's lab at the University of Wuerzburg.

2.3.9. Photoactivation of ASJ neurons by bPGC and effects on dauer entry

To observe effects on dauer-entry, *daf-11(m84)* and ZX1220 strains were grown for in the dark. Then, young adults were placed on seeded plates and were allowed to lay eggs for 10–12 h, and then removed. Afterwards, the plates were exposed to continuous illumination of blue LED for three days (blue light intensity: 5 μW/mm^2 at the NGM agar surface). The fraction of adults and dauers was scored.

2.3.10. Aldicarb assays to asses the effect of PhoDAG in *C. elegans*

Caenorhabditis elegans wild-type (N2) strain was cultivated at 20°C on nematode growth medium (NGM) plates seeded with *E. coli* strain OP50-1 (Brenner 1974). A 10 mM stock solution of PhoDAG-3 was prepared in 100% Ethanol. For application to *C. elegans,* the stock solution was diluted to the working concentration of 1mM PhoDAG-3 using OP50-1 and 200 µl of the resultant solution was applied to the NGM plate. For the carrier solvent control, an equivalent volume of 100% EtOH was used instead of the stock solution. L4 stage larvae were picked onto 1mM PhoDAG-3/EtOH NGM plates and left overnight. The young adult hermaphrodites were used

on the following day for the Aldicarb and Levamisole -sensitivity assays (Mahoney et al., 2006; Lewis et al.,1980). The assay was performed in dark except for the picking and counting of animals which was performed under red light. To study Aldicarb sensitivity, 20 animals were transferred onto NGM plates containing 1 mM Aldicarb (Sigma) or 0.1mM Tetramisole hydrochloride (Racemic form of levamisole, Sigma) and the fraction of animals paralysed was scored every 15 minutes by assessing movement, following three gentle touches with a platinum wire. The animals were illuminated with UV light (366 nm, 18 μW/mm^2) provided by a UV lamp (Benda, Wiesloch, Germany) for the first five minutes after being placed on the Aldicarb plates and then subsequently for the last 3 minutes of each 15 minute time interval. The assays were performed blinded regarding the absence/presence of PhoDAG-3, and on the same day with the same batch of aldicarb or levamisole plates.

2.4 Methods for GLC-1 experiments in mammalian cells

2.4.1 Molecular docking

The software VMD() and PyMol()were used to visualize and prepare pdb files. D-MAG-0 was docked to the crystal structure of GLC-1 (PDBid: 3RIF; (Hibbs and Gouaux 2011)) using AutoDock Vina(). The ligand and receptor structures were converted from pdb into pdbqt format using Autodock tools. A grid box was centered at the 8.38, 51.03 ,38.43 coordinates in the x, y, and z directions to cover the ligand binding pocket at the interface of two subunits in GLC-1 structure. The lowest energy conformations reported by AutoDock Vina were inspected using the PyMol software.

2.4.2 Cell culture

HEK293T cells were maintained at 37°C in a 10% CO2 atmosphere in Dulbecco's modified Eagle medium (DMEM, Merk Millipore, Germany) containing 10% FBS (Merk Millipore, Germany). For electrophysiological measurements cells were plated on coverslips treated with 0.1 mg/ml poly-L-lysine (Sigma-Aldrich, Germany) in a density of 40,000 cells per coverslip. HEK293T cells were transfected using JetPrime (Polyplus-transfections, France) according to manufacturer's instructions 24 h before measurements.

2.4.3 Electrophysiology

Patch clamp measurements were performed in whole-cell mode at room temperature and recorded using the EPC10 USB patch clamp amplifier and PatchMaster software (HEKA Elektronik, Germany). Bath solution for HEK-293T cells contained in mM: 140 NaCl, 2 KCl, 2 $MgCl_2$, 2 $CaCl_2$, 10 HEPES, 10 glucose (NaOH to pH 7.3). Pipette solution contained in mM: 140 $CsCl_2$, 10 HEPES, 2 Na_2ATP, 10 EGTA (CsOH to pH 7.3). Illumination during electrophysiology experiments was performed using a TILL Photonics monochromator (Polychrome 5000) operated with the patch clamp amplifier (HEKA Elektronik, Germany).

3. RESULTS

3.1 bPGC in body wall muscle (BWM) cells and in sensory neurons of *C. elegans*

bPGC - *Beggiatoa* photoactivated guanylyl cyclase which catalyses the synthesis of cGMP from GTP upon blue light illumination was generated by performing 3 point mutations in the substrate binding pocket of bPAC (Ryu et al. 2010). As an *in-vivo* test system for cGMP generation, we expressed the bPGC in BWMs using the *myo-3* promoter, along with an intrinsic cGMP-gated heteromeric CNG channel found in many *C. elegans* neurons, consisting of TAX-2 and TAX-4 subunits. TAX-2/-4 form a non-specific cation channel both *in-vitro* (Komatsu et al. 1999) and *in-vivo* (Ramot et al. 2008). The activation of this CNG channel is expected to lead to muscle depolarization and contraction **(Figure R1)**. Since BWMs are large, the contraction evoked is macroscopic and can be scored as a reduction in the body length. This is the first instance of using this approach of coupled optogenetics in *C.elegans*.

Apart from BWMs, bPGC was subsequently expressed in sensory neurons- ASJ, AWC and BAG which use cGMP signalling to transduce the extracellular signals and evoke behavioral outcomes.

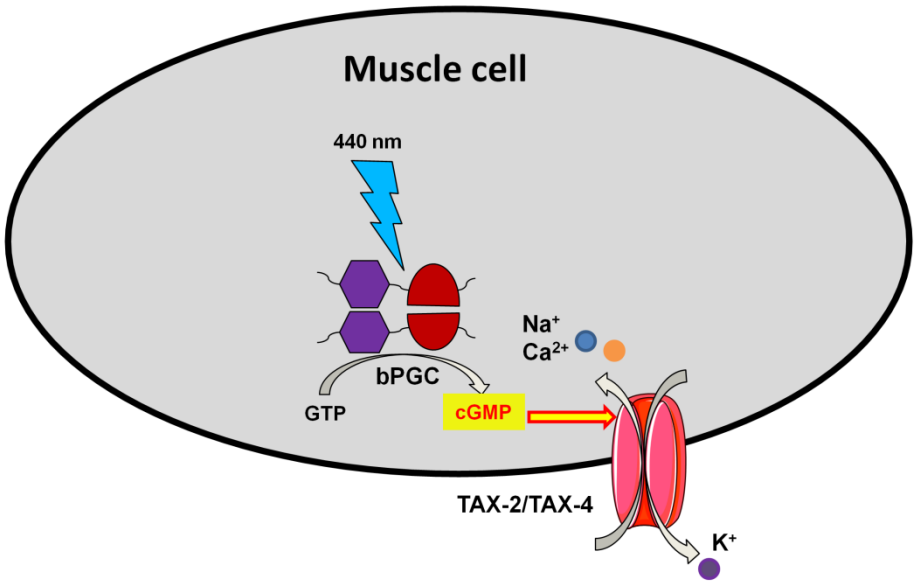

FIGURE R1: An *in-vivo* test system to assess the efficacy of cGMP generation in *C.elegans*. bPGC, TAX-2, TAX-4 are co-expressed in BWM cells and upon blue light illumination, cGMP thus generated leads to the opening of TAX-2/-4 causing the cellular depolarisation. As a result, the muscles contract leading to the shortening of body length or contraction of the body.

3.1.1. Function of bPGC in muscle cells of live *C. elegans*

Transgenic *C. elegans* strains were generated with BWM specific expression of bPGC tagged with eYFP, TAX-2/-4 tagged with GFP, bPGC::eYFP along with TAX-2/-4::GFP. A mutated version of bPGC - bPGC(K265D) (Ryu et al. 2010) with no cyclase activity was also co-expressed with TAX-2/-4 as a negative control for cGMP mediated depolarization and contraction (**Figure R2**). As with BeCyclOp/TAX-2/TAX-4 animals, the bPGC strains were also generated in a *lite-1* background to eliminate the intrinsic photophobic response of the animal and true light evoked response to the optogenetic tool can be observed.

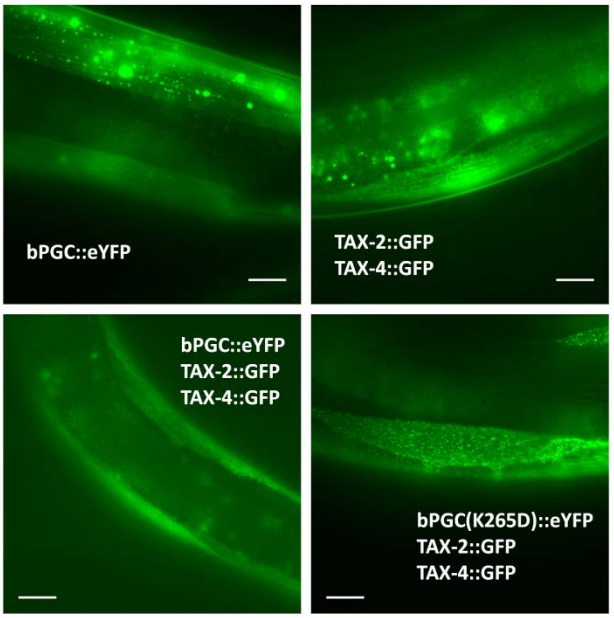

FIGURE R2: Fluorescent micrographs of transgenic *C.elegans* strains expressing bPGC::eYFP, TAX-2/-4::GFP, bPGC::eYFP along with TAX-2/-4::GFP and bPGC (K265D)::eYFP along with TAX-2/-4::GFP in BWMs using *myo-3* promoter in *lite-1(ce314)* background. The scale bar represents 20 µm.

bPGC::eYFP,TAX-2/-4::GFP expressing animals upon 5s blue light illumination (450-490 nm, 0.5 mW mm^{-2}) showed a slowly developing contraction of about 2% while the other strains tested (*lite-1(ce314)*, bPGC::eYFP only, TAX-2/-4::GFP only and bPGC(K265D)::eYFP along with TAX-2/-4::GFP) did not show any obvious contraction (**Figure R3 A**). In a subsequent experiment with a longer illumination period of 20 s and higher blue light intensity of 0.9 mW mm^{-2}, bPGC::eYFP,TAX-2/-4::GFP animals reached a maximum contraction of about 3% after 10 s of the start of the illumination (**Figure R3 B**).

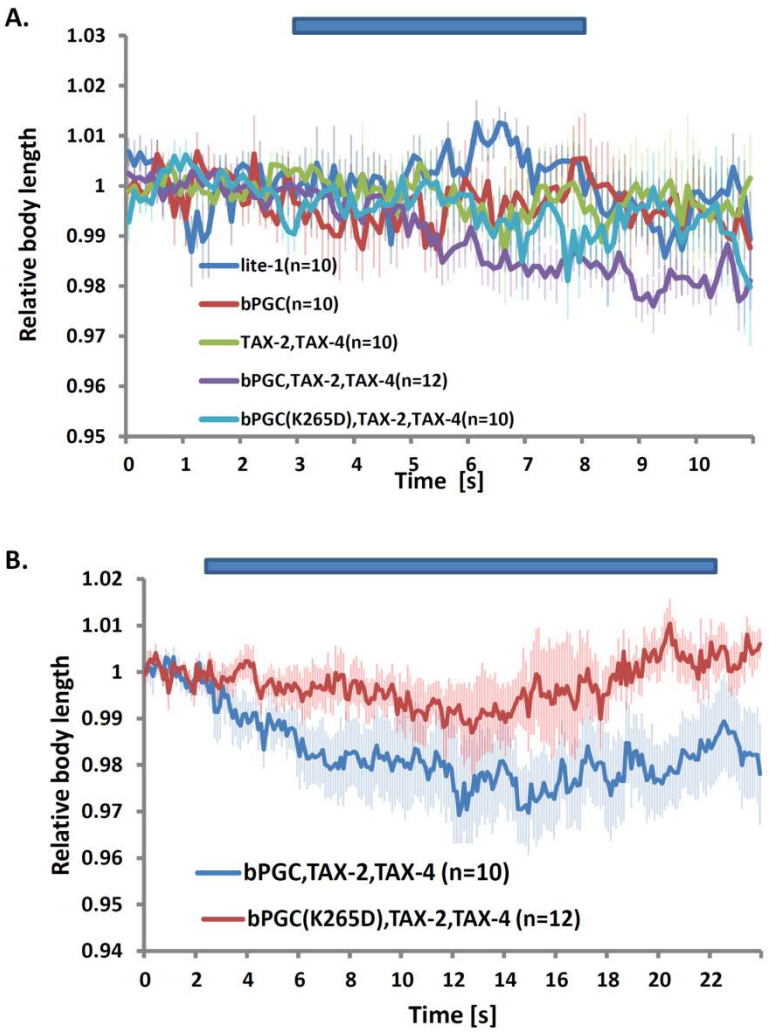

FIGURE R3: Body length measurements of animals (*lite-1(ce314)* background) with BWM expression of bPGC::eYFP, TAX-2/-4::GFP, bPGC::eYFP along with TAX-2/-4::GFP, and bPGC(K265D)::eYFP along with TAX-2/-4::GFP with blue light illumination of **A.** 5s and 0.5 mW mm^{-2} and **B.** 20s and 0.9 mW mm^{-2}. Bars represent the illumination period, error reported as S.E.M., number of animals tested, n are in the parenthesis for each strain.

To ascertain the cGMP specificity for the TAX-2/-4 mediated depolarization-contraction set up, transgenic lines expressing bPAC (*Beggiatoa* photoactivated adenylyl cyclase) instead of bPGC in BWMs along with TAX-2/-4 were generated Surprisingly, upon illumination with 20 s blue light (0.9 mW mm^{-2}), two independent lines showed a sustained contraction of 5-6% (**Figure R4 A**). Transgenic line with lower injected concentration of bPGC::eYFP (2 ng/µl instead of 15 ng/µl) also showed a contraction of about 4%, however the body length returned back to the base line at the end of 20 s illumination period (**Figure R4 B**). To check if cAMP by

itself has an effect on muscle physiology, bPAC::eYFP alone was expressed in BWMs and subjected to blue light illumination. However, with bPAC alone, no light induced contraction was observed indicating cAMP itself has no effect on the state of muscle cell (de-)polarization (**Figure R4 C**).

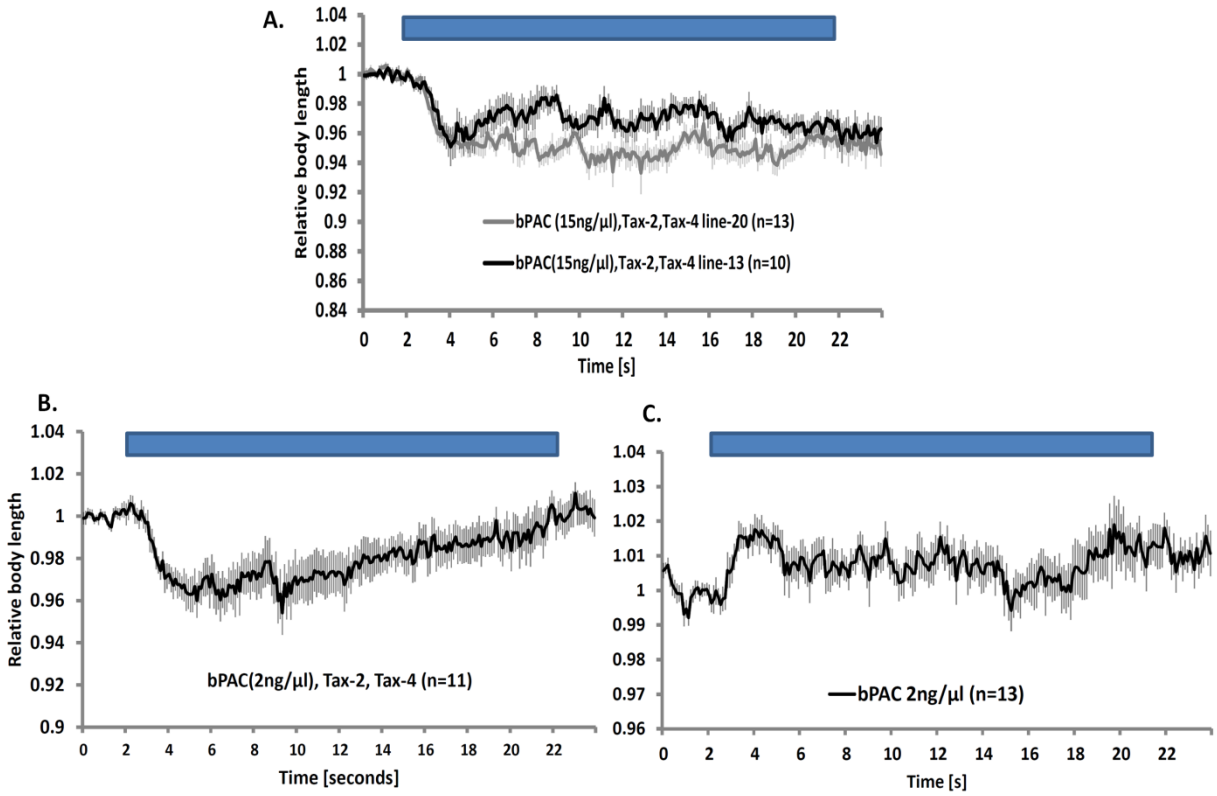

FIGURE R4: Body length measurements of animals (*lite-1*(ce314) background) with BWM expression of bPAC::eYFP,TAX-2/-4::GFP (**A** with bPGC 15 ng/µl **,B** with bPGC 2 ng/µl) and bPAC::eYFP (**C**) upon blue light illumination (20s and 0.9 mW mm^{-2}). Bars represent the illumination period, error reported as S.E.M., number of animals tested, n are in the parenthesis for each strain.

3.1.2. Expression of bPGC in the pheromone sensing ASJ neurons.

ASJ sensory neurons govern dauer formation and recovery through a receptor-like guanylyl cyclase DAF-11. Dauer-pheromones and environmental signals (i.e. absence of food, high temperature) inhibit DAF-11, thus causing dauer-entry by blocking release of ASJ signals. *daf-11(m84)* mutants display a constitutive dauer-phenotype i.e. most larvae become dauers even under favourable environmental conditions. Under such conditions, ASJ is depolarized via cGMP-gated TAX-2/-4 channels thereby releasing signals causing dauer-repression and dauer-exit. Photoactivation of TRX-1B::ChR2(C128S) in ASJ was able to prevent dauer-entry of

daf-11(m84) mutant animals (Schultheis et al. 2011b). We aimed to recapitulate this behavioural rescue using the light activation of bPGC in ASJ neurons which would lead to cGMP mediated TAX-2/TAX-4 depolarization of neurons causing dauer rescue (**Figure R5**).

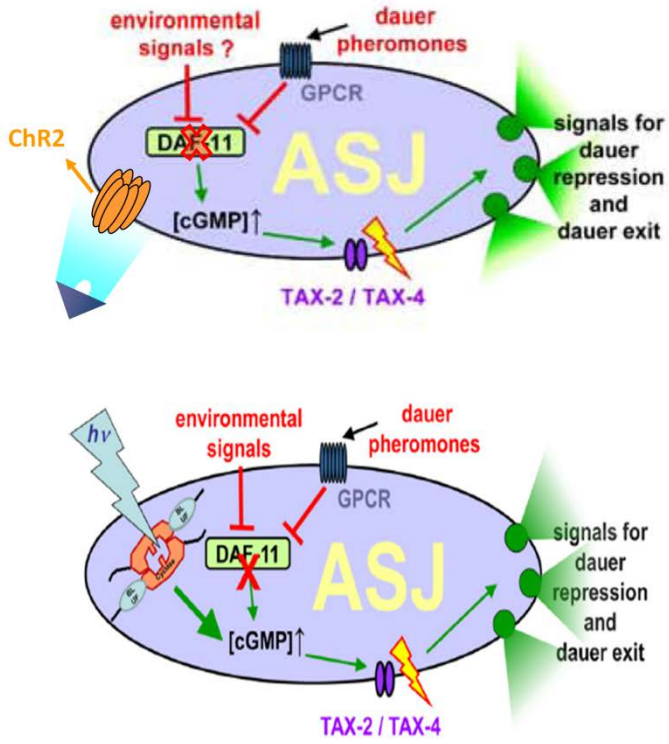

FIGURE R5: The molecular mechanisms of dauer formation and recovery as governed by DAF-11 signalling in ASJ, and ChR2 and bPGC being used as two ways of suppressing the constitutive dauer-phenotype displayed by *daf-11(m84)* mutants.

To this end, ASJ specific expression of bPGC::eYFP was achieved using ptrx-1::TRX-1B promoter fragment and the transgene was crossed into *daf-11(m84)* background (**Figure R6A**). Eggs (from mothers that were kept in the dark at all times) were incubated in the presence of bacterial food under constant low illumination (5 µW mm^{-2} blue light). After 3 days, the fraction of worms in dauer and adult states was scored. Of the *daf-11(m84)* mutant animals, almost 100% of animals stayed in the dauer state irrespective of the illumination. However, when ptrx-1::TRX-1B::bPGC::eYFP was expressed in *daf-11(m84)* mutants, photo-activation prevented dauer formation in 30% of *daf-11(m84)* animals (**Figure R6B**). In spite of the promising results, it also must be noted that the experiment was

difficult to reproduce in subsequent trials owing to possibly high sensitivity of *daf-11* mutants to external environmental conditions like temperature and low dark activity of bPGC.

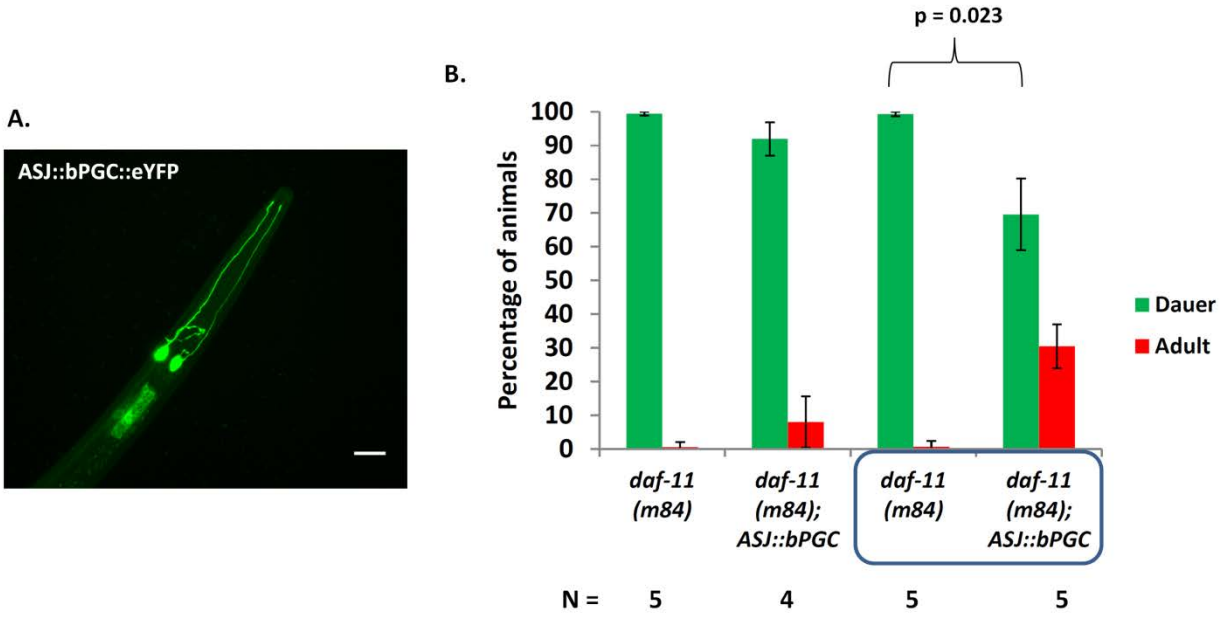

FIGURE R6: **A.** ASJ specific expression of bPGC in *daf-11(m84)* mutants achieved using ptrx-1::TRX-1B::bPGC::eYFP. The scale bar represents 20 µm. **B.** Long-term photoactivation of ASJ neurons by bPGC caused partial suppression of the constitutive entry into the dauer larval state in *daf-11* mutants. The blue box represents the blue light illuminated set of animals and N represents the number of individual experiments performed (the number of observed animals for each condition was more than 30).

3.1.3. Expression of bPGC in the chemosensory AWC-ON neuron.

AWC chemosensory neurons employ cGMP/TAX-2/-4 signalling downstream of GPCR activation by different odorants (Bargmann 2006) to respond to the olfactory cues. It has been shown that optogenetic activation of AWC-on using ChR2 increases the reversal frequency of the animals (Kocabas et al. 2012).

We reasoned that bPGC generated cGMP would lead to depolarization of AWC-on, and that this could evoke a similar effect. We achieved expression of bPGC in AWC-on using the promoter *pstr-2* (**Figure R7A**) and thus generated an integrated array of bPGC::eYFP in AWC-on in *lite-1(ce314)* background. We next counted the number

of reversals shown by these animals upon 3 different blue light illumination intensities.

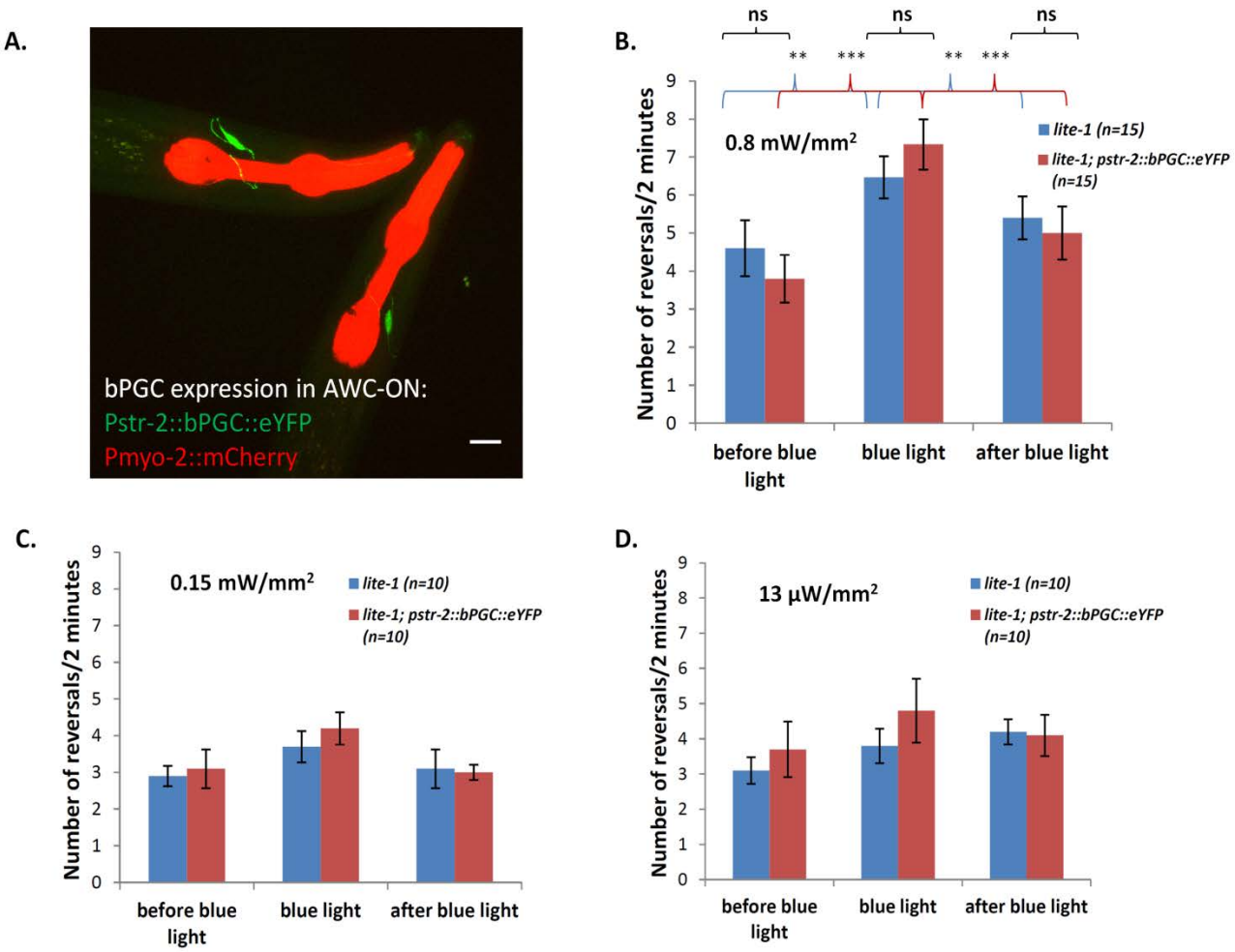

FIGURE R7: **A.** AWC-ON specific expression of bPGC in achieved in *lite-1(ce314)* using pstr-2::bPGC::eYFP integrated array. The scale bar represents 20 µm. **B-D.** The number of reversals exhibited by animals expressing an integrated array of bPGC::eYFP in AWC-on in *lite-1(ce314)* background in a 2 minute interval before, during and after the blue light illumination (450-490 nm) at three different intensities (0.8, 0.15 and 0.013 mW mm^{-2}). Statistically significant differences were tested using paired 2-tailed t-test (*** $p<0.001$, ** $p<0.01$).

At the highest light intensity used (0.8 mW mm^{-2}), the transgenic animals showed a highly significant increase in the number of reversals during the 2 minute illumination period which returned back to pre-illumination levels after the blue light stimulus ended. However, the control animals - *lite-1(ce314)* also exhibited the same phenotype, possibly owing to the high light intensity used even though the *lite-*

1(ce314) mutation should substantially reduce the intrinsic photophobic effect exhibited by the worms (**Figure R7B**).

To reduce the non-specific photophobic responses, two lower light intensities (0.15 mW mm^{-2} and 0.013 mW mm^{-2}) were tested. At both these intensities, the transgenic animals did show a tendency towards increase in the number of reversals during the blue light illumination, however the differences were non-significant (**Figure R7 C and D**).

3.1.4. Expression of bPGC in the O_2/CO_2 sensing BAG neurons.

O_2/CO_2 sensing BAG neurons use guanylyl cyclases GCY-31 and GCY-33 along with TAX-2/-4 to detect drop in oxygen and increase in carbon dioxide concentrations (Zimmer et al. 2009; Bretscher et al. 2011). Optogenetic activation of BAG using ChR2 led to transiently slowed locomotion in *C. elegans* mimicking a drop in oxygen response (Zimmer et al. 2009).

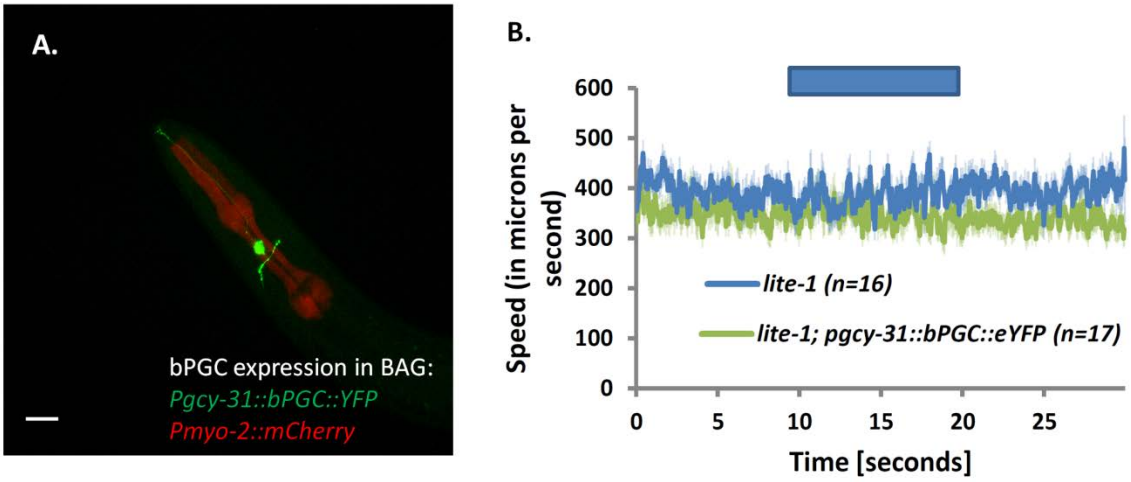

FIGURE R8: **A.** BAG specific expression of bPGC in achieved in *lite-1(ce314)* using pgcy-31::bPGC::eYFP transgene. The scale bar represents 20 µm. **B.** Locomotion speed exhibited by animals expressing bPGC::eYFP in BAG neurons in lite-*1(ce314) background* in a 10 s interval before, during and after the blue light illumination (450-490 nm) performed at the single worm tracker (Stirman et al. 2011).

We aimed to recapitulate the slowing response by expressing bPGC in BAG neurons using the *pgcy-31* promoter (**Figure R8A**). 10 s blue light illumination showed no discernible effect on the locomotion speed between the bPGC expressing animals and control *lite-1(ce314)* animals (**Figure R8B**).

3.2 BeCyclOp in body wall muscles and in O_2/CO_2 sensory neurons of *C. elegans*

Since bPGC showed only moderate effects as an optogenetic tool for cGMP production, we looked for a more efficient alternative. In 2014, Avelar et al. identified a microbial rhodopsin sequence in the genome of fungus *Blastocladiella emersonii* and showed that the protein functions as a phototaxis photoreceptor (Avelar et al. 2014). Furthermore, sequence analysis revealed that the Blastocladiella rhodopsin (named as BeGC1) is directly connected to a putative guanylyl cyclase (GC) domain.

We implemented BeGC1 (renamed as BeCyclOp - ***B****lastocladiella* ***e****mersonii* derived guanylyl **cycl**ase **op**sin) in *C. elegans* body wall muscle cells (BWMs) along with the *C. elegans* CNG channel comprising of TAX-2 and TAX-4 subunits (as a heterologous system to check their functionality) as well as in O_2/CO_2 sensory neurons of *C. elegans.*

BeCyclOp comprises of a microbial opsin domain near the N- terminal and a guanylyl cyclase domain in the C-terminal part. Based on transmembrane helix prediction, BeCyclop seems to have 8 transmembrane helices, unlike all other opsins which are seven transmembrane proteins. Another feature which distinguishes BeCyclOp from other microbial opsins is both the N and C - termini appear to be cytosolic while all other opsins known so far have extracellular N and cytosolic C termini, respectively. The fourth helix (aa 249-270) in BeCyclOp shows high conservation with the transmembrane helix 3 in other microbial opsins and the conserved lysine for retinal binding is in the last helix (**Figure R9**).

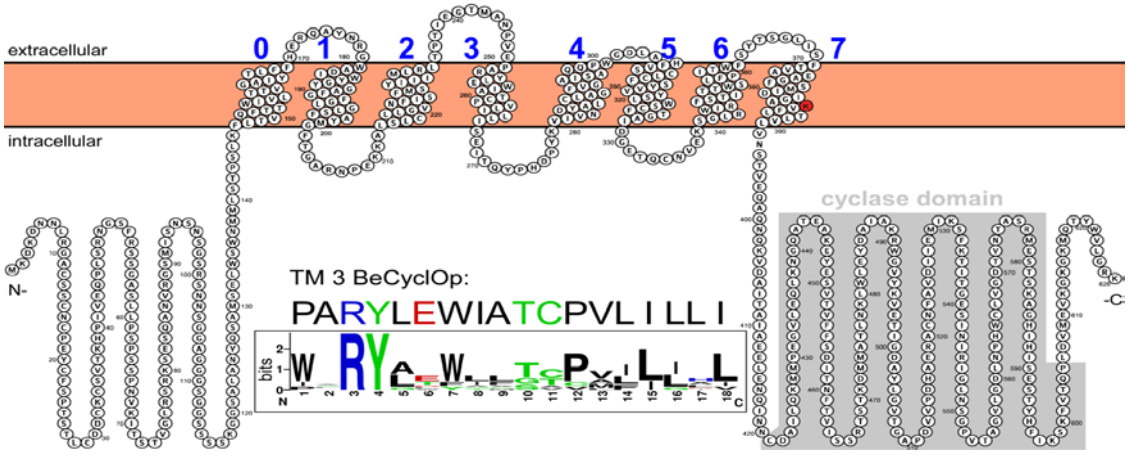

FIGURE R9: Domain architecture of BeCyclOp based on transmembrane helix prediction using TMHMM (Krogh et al. 2001) in combination with sequence alignment. Picture drawn using Protter (Omasits et al. 2014).

3.2.1. Function of BeCyclOp in muscle cells of live *C. elegans*

C. elegans codon optimized synthetic cDNA encoding for BeCyclOp was expressed in the BWMs using the *myo-3* promoter, along with an intrinsic cGMP-gated heteromeric CNG channel found in many *C. elegans* neurons, consisting of TAX-2 and TAX-4 subunits. TAX-2/-4 form a non-specific cation channel both *in-vitro* (Komatsu et al. 1999) and *in-vivo* (Ramot et al. 2008). The activation of this CNG channel is expected to lead to muscle depolarization and contraction **(Figure R10)**. Since BWMs are large, the contraction evoked is macroscopic and can be scored as a reduction in the body length.

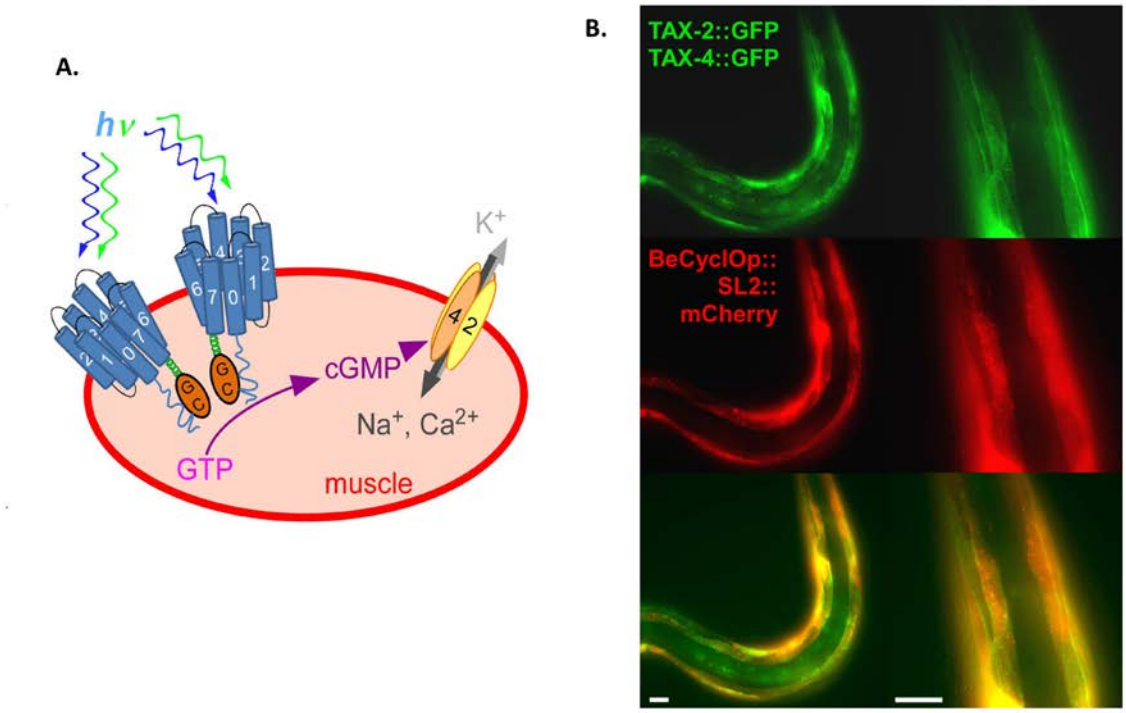

FIGURE R10: A. A light-activated system for cell depolarization and muscle activation: Co-expression of BeCyclOp and the *C. elegans* CNG channel consisting of TAX-2 and TAX-4 subunits. **B.** Fluorescent micrographs of an animal expressing BeCyclOp from a bicistronic construct with mCherry, in body wall muscles, and co-expressing TAX-2::GFP/TAX-4::GFP. Scale bar, 20 µm. Membrane expression of TAX-2/4 is clearly visible as well as cytosolic mCherry.

Animals expressing BeCyclOp::SL2::mCherry/TAX-2::GFP/TAX-4::GFP in BWMs in presence of ATR, and 100 ms illumination with blue (450 - 490 nm) or green (520-550 nm) light showed body contractions of about 9-10% of the initial body length within 1-1.5 s (rise time constant ~ 0.36-0.38 s (n= 10-13 animals) **(Figure R11A,B)**. These effects are comparable to the muscle contraction caused by photostimulation

of ChR2 expressed in BWMs (Nagel et al. 2005; Liewald et al. 2008; AzimiHashemi et al. 2014). No contraction was observed for animals raised without ATR as the opsin optogenetic tools are non-functional without their chromophore ATR, which is not endogenously synthesized by the worms.

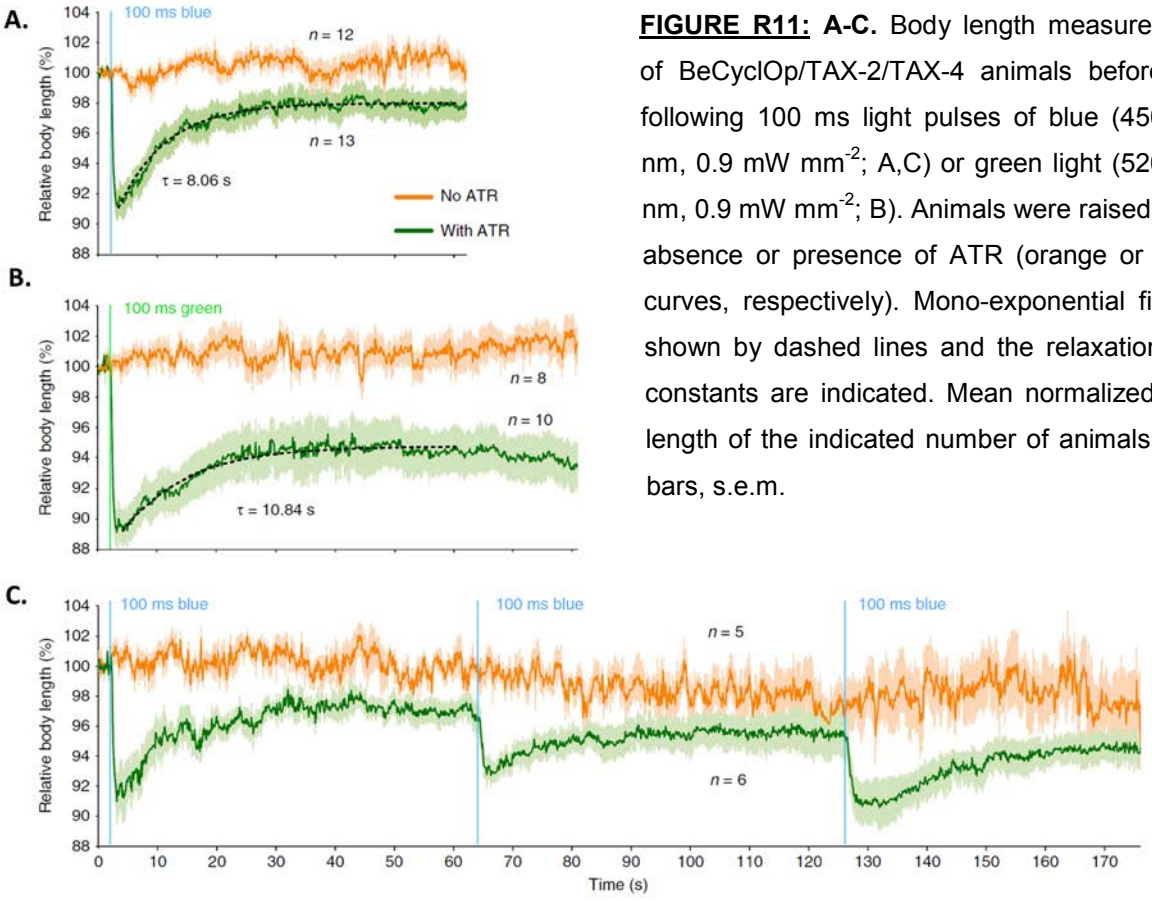

FIGURE R11: A-C. Body length measurements of BeCyclOp/TAX-2/TAX-4 animals before and following 100 ms light pulses of blue (450–490 nm, 0.9 mW mm^{-2}; A,C) or green light (520–550 nm, 0.9 mW mm^{-2}; B). Animals were raised in the absence or presence of ATR (orange or green curves, respectively). Mono-exponential fits are shown by dashed lines and the relaxation time constants are indicated. Mean normalized body length of the indicated number of animals; error bars, s.e.m.

Contractions were long-lasting and recovered to a plateau of about 3% within 30 s ('off' time constant ~ 8.1 s (n=13 animals)) for blue light while for green light illumination, the plateau was about at 6% contraction ('off' time constant ~ 10.8 s (n=10 animals)). This highlights increased cGMP production when BeCyclOp is stimulated in the green wavelengths which lie at its peak excitation maxima (Avelar et al. 2014). In comparison, ChR2 evoked contractions recover within 1-1.5 s (AzimiHashemi et al. 2014) indicating cGMP levels may be increased for a sustained time following BeCyclOp activation, likely due to low phosphodiesterase activity in BWM. Three consecutive blue light pulses over 3 minutes evoked similar effects showing that BeCyclOp can be repetitively activated without any apparent desensitization **(Figure R11C).** Light-induced contractions were not observed when

BeCyclOp alone was expressed in BWMs without the TAX-2/-4 channel indicating increase in cGMP alone does not cause BWM contractions **(Figure R12).**

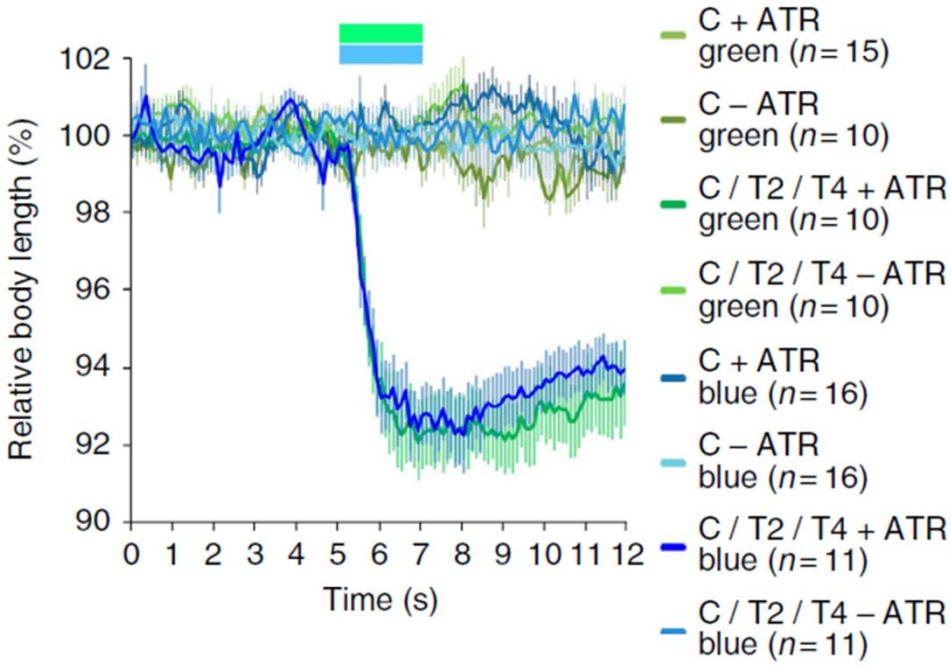

FIGURE R12: Changes in body length were caused only when BeCyclOp ('C') was co-expressed with TAX-2/TAX-4 ('T2/T4') and animals were cultivated in the presence of ATR. Illumination was either with blue light (blue graphs), or with green light (green graphs). Bars indicate 2 s illumination period.

To determine the light intensity required to evoke full effects (experiments done partly by Marin Schneider), 1 s light pulses of 530 nm wavelength, at intensities between 0.02–1.52 µW mm^{-2} (n=10 animals each; **Figure R13A**) were used with BeCyclOp/TAX-2/4 animals. The peak contractions at each of the corresponding light intensities showed a negative linear correlation with the log of the light intensity (**Figure R13B**). Illumination of animals cultivated in the absence of ATR (1.52 µW mm^{-2}) caused no contraction. The optogenetic ensemble of BeCyclOp/TAX-2/TAX-44 evokes muscle activation at 200-fold lower light intensity than ChR2 (Nagel et al. 2005; AzimiHashemi et al. 2014). However, this may be an apparently higher light sensitivity, as BeCyclOp/TAX-2/4 system uses second messenger amplification, and a high conductance channel constituted by TAX-2/4, unlike ChR2 photocurrents that need to trigger muscle contraction directly.

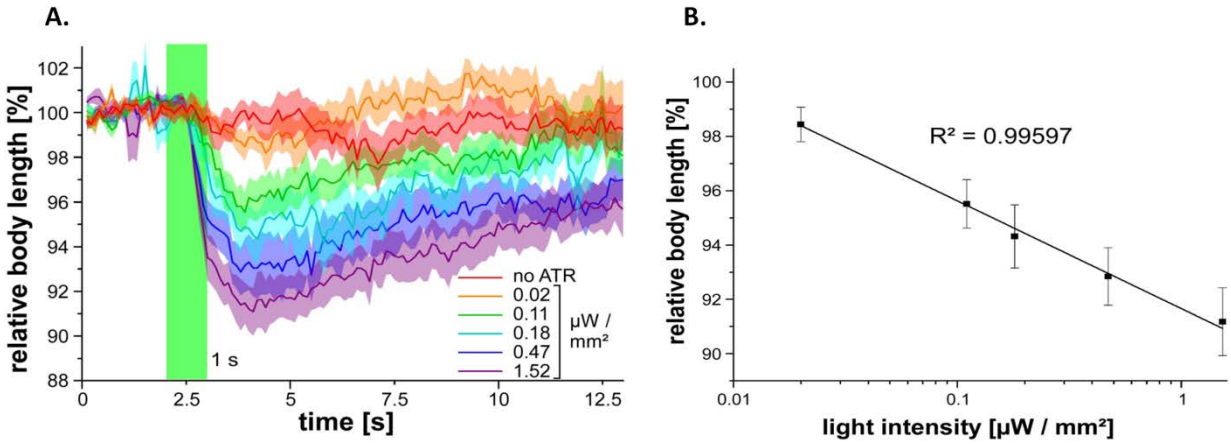

FIGURE R13: Light dose-response characterization of BeCyclOp-evoked body contractions in *C. elegans*. **A.** Mean normalized body length chronograms of animals before, during and after 1 s green light stimuli (green bar) of the indicated light intensities. The negative control (no ATR) was performed at 1.52 µW mm^{-2} (n=10 each, error bars, s.e.m.). **B.** Dose-response graph (linear fit of contraction and the log of the light intensities used) shows a negative correlation.

To ascertain the specificity of BeCyclOp for cGMP over cAMP, *in vivo* cGMP and cAMP concentrations were assessed in crude extracts derived from whole animals expressing BeCyclOp in BWMs (measurement of the prepared samples was done by Shiqiang Gao and Georg Nagel, Uni-Würzburg). Green light (540-580 nm) evoked almost 12-fold increase in cGMP concentration, as determined from crude whole-animal extracts, compared with the dark condition (N=6; **Figure R14**). No evidence for BeCyclOp mediated cAMP generation was found (N=4), although illuminated samples showed a trend to increased cAMP. This was independent of ATR (and thus, functional BeCyclOp).

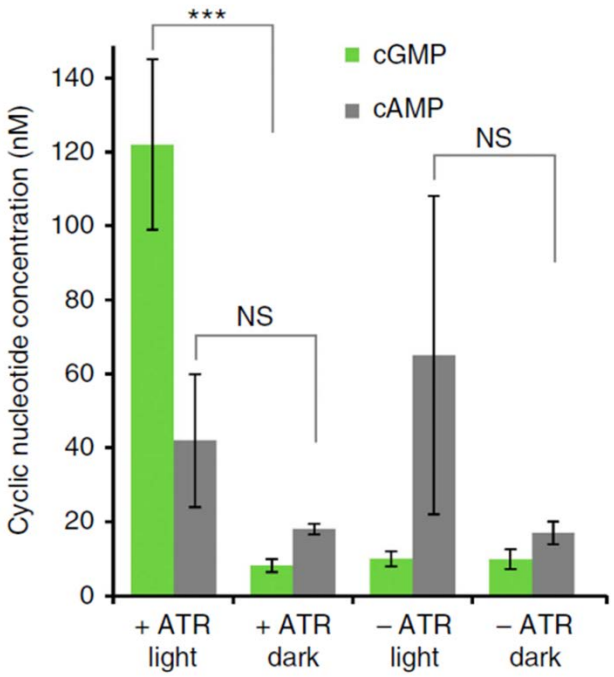

FIGURE R14: In vivo cGMP and cAMP concentration assessed in crude extracts derived from whole animals expressing BeCyclOp in muscle cells. The animals were raised in the absence or presence of all-trans retinal (ATR) and were illuminated with green light (540–580 nm, 150 µW mm^{-2}, 15 min) or were kept in the dark during extract preparation. N=6 experiments; Error bars, s.d. Statistically significant differences: one-way ANOVA (***P<0.001).

3.2.2. Activating BeCyclOp in O_2 sensors slows down locomotion in *C. elegans*

BAG (cell **b**ody in **a**nterior **g**anglion) neurons located in the head of *C. elegans* are O_2/CO_2 sensors that detect a fall in O_2 concentration as well as increases in CO_2 concentration and as a result evoke a transient slowing response (Bretscher et al. 2008; Zimmer et al. 2009; Bretscher et al. 2011). BAG neurons employ O_2-binding soluble receptor guanylyl cyclases, GCY-31 and GCY-33, as well as the TAX-2/4 channel to detect O_2. BeCyclOp was expressed in the BAG neurons using the *flp-17* promoter (**Figure R15A**; (Zimmer et al. 2009)).

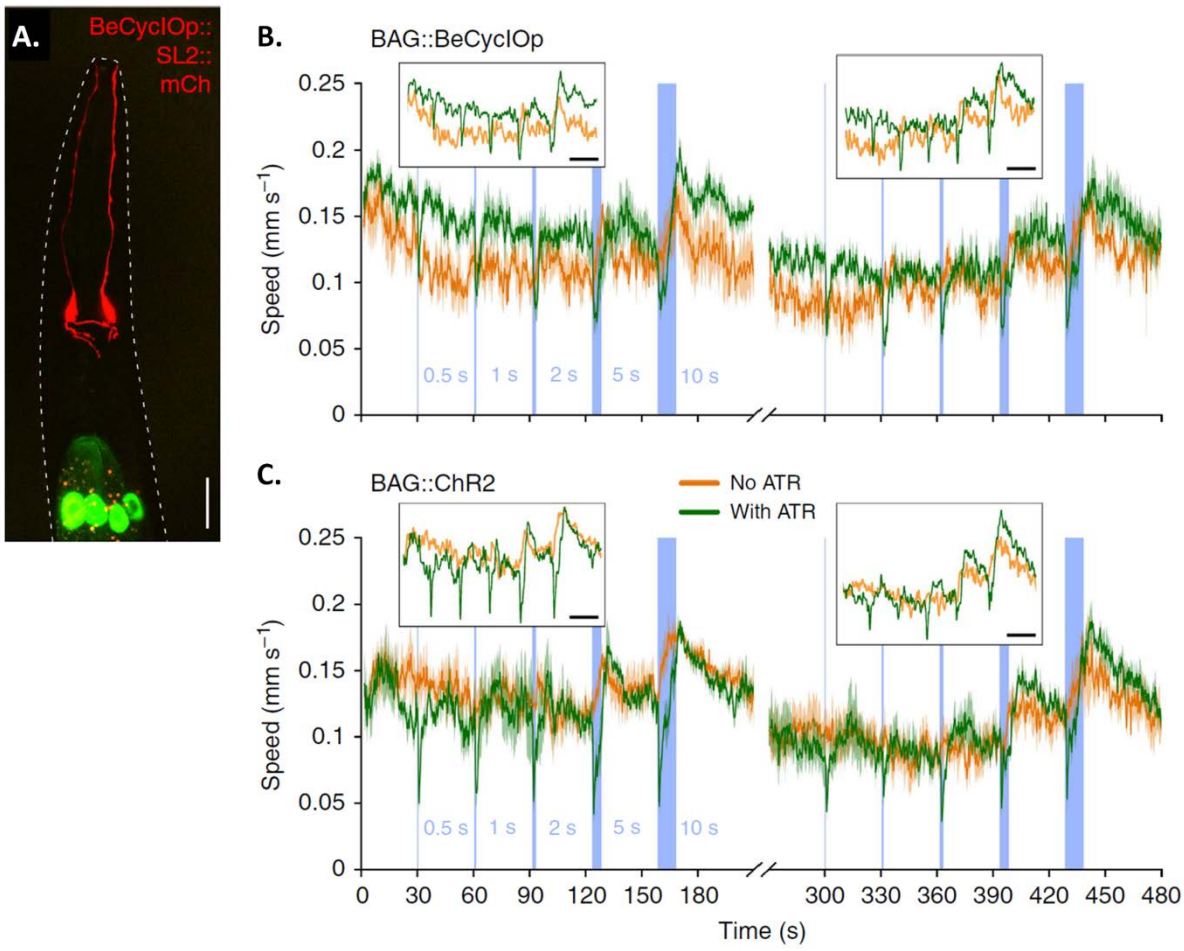

FIGURE R15: BeCyclOp triggers CO_2/O_2 sensory BAG neurons that intrinsically use cGMP signalling. **A.** Confocal picture of expression of BeCyclOp::SL2::mCherry bicistronic construct in the BAG neuron pair in the head of *C. elegans*. Cell bodies, nerve ring processes and sensory dendrites reaching the nose can be seen. Outline of the animal indicated by a dashed white line, anterior is up. Green fluorescence: GFP co-expression marker localized to intestinal cell nuclei. Scale bar, 20 μm. **B.** Mean absolute locomotion speed of animals expressing BeCyclOp in BAG neurons, during repeated blue light exposure (470 nm, 70 μW mm^{-2}) for the indicated periods (blue bars), with 30 s interstimulus intervals, as deduced from videoanalysis using a multiworm tracker. Animals in the absence (orange curves) or presence of ATR (green curves) in the culture media are compared. Speed increase in animals without ATR is due to photophobic behavior. N=5 (4 for no ATR) experiments with n=15–20 animals each; error bars, s.e.m. **C.** As in B, but animals expressing ChR2 in BAG neurons were used instead. N=3 experiments with n=15–20 animals each; error bars, s.e.m. The insets show mean speeds, as a moving average, using a sliding window bin corresponding to 1 s for smoothing the data. Black bars, 30 s.

The measurement of locomotion speed was done using a multiworm tracker (Swierczek et al. 2011), combined with a ring of blue light emitting diodes which provide light of sufficient intensity to a whole-culture dish. Photostimulation of BeCyclOp in BAG led to transient slowing responses (**Figure R15B**). Stimuli of increasing duration (500 ms, 1, 2, 5 and 10 s; 30 s intervals; N=5 (4 for no ATR) experiments; n=15–20 animals each) caused significant slowing responses of increasing duration. Each of the slowing response was characterized by a transient minimum followed by a gradual increase in speed, despite ongoing light stimulation (see insets in **Figure R15B** and **Figure R16** for analysis of speed changes within 1 s before and during the light stimuli).

The transient slowing behaviour was similarly observed for animals expressing ChR2 in BAG (N=3 experiments; n=15–20 animals each; Figure 19B; ref. (Zimmer et al. 2009)). For both optogenetic tools, stimulus protocols could be repeated, leading to similar results. In control experiments with animals raised without ATR, light illumination for more than 2 s evoked a transient increase in locomotion speed. This may be because of the *C. elegans* ultraviolet/blue-light sensor, LITE-1, which evoked escape behaviour (Edwards et al. 2008). This photophobic response is overcome by the slowing responses evoked by light activation of BeCyclOp or ChR2. When the prolonged blue-light stimuli ended, animals displayed a rebound speed increase that was more pronounced for longer stimuli; locomotion speed then returned back to initial speeds within ~20–30 s.

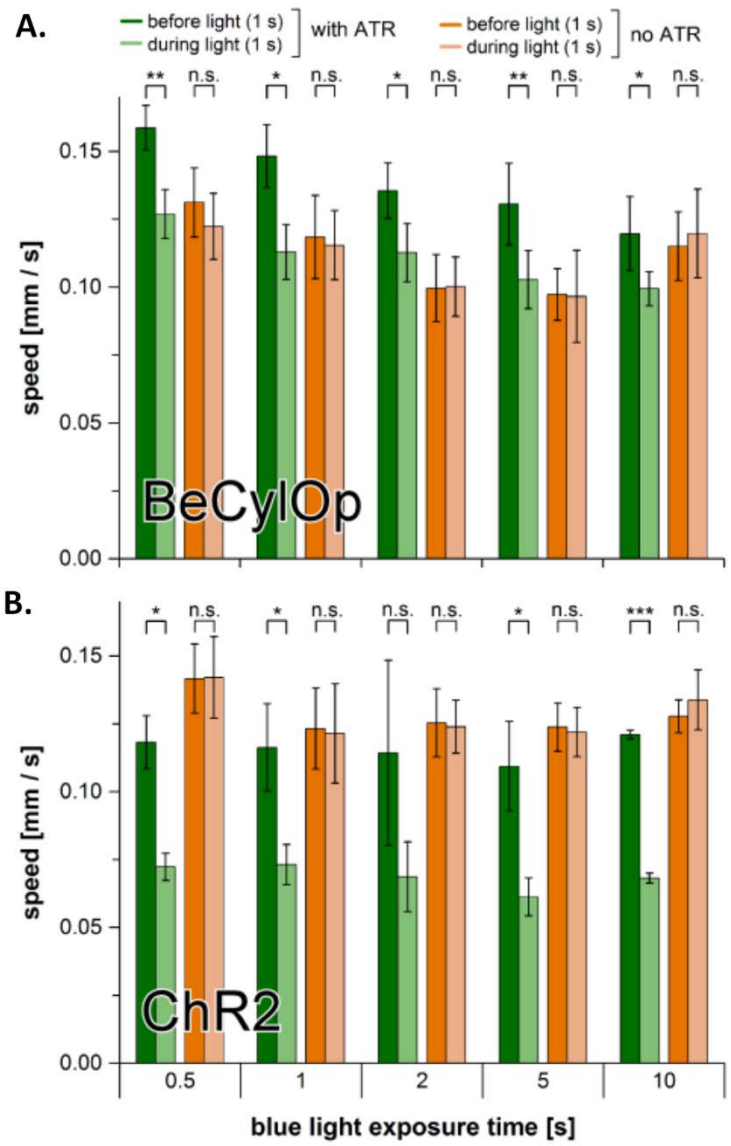

FIGURE R16: Speed changes following the activation of BeCyclOp and ChR2 in CO_2/O_2 sensing BAG neurons of *C. elegans* **A**) Average speed 1 second before and after the onset of the blue light illumination of varying durations (0.5, 1, 2, 5, and 10 s) in the locomotion speed assay performed with animals expressing BeCyclOp in BAG neurons in the absence and presence of ATR. N=5(4 for no ATR) experiments with n=15-20 animals each; error bars: SEM. **B**) As in A), but animals expressing ChR2 in BAG neurons were used instead. N=3 experiments with n=15-20 animals each; error bars: SEM. Statistically significant differences determined by paired 2-tailed Student's t-test * P<0.05, ** P<0.01, *** P<0.001.

3.3 All-optical generation and detection of cGMP

Genetically encoded fluorescent indicators of cGMP have been used to study spatial and temporal dynamics of second messenger signalling in cells and animals (Nikolaev et al. 2006b; Sprenger and Nikolaev 2013). Both Förster resonance energy transfer (FRET) and GFP based visual reporters for cGMP have been developed (Nausch et al. 2008; Bhargava et al. 2013; Couto et al. 2013). The FRET based tool was implemented in *C. elegans*, but the low signal and computationally heavy imaging limit its utility. To address this, a circularly permutated GFP-based cGMP reporter, namely FlincG3 (Bhargava et al. 2013), was adapted to obtain a *C. elegans* suitable sensor, WincG2 (**W**orm **In**dicator of **cG**MP-2) by the laboratory of Noelle L'Etoile at the University of California, San Francisco, USA.

To further characterize the kinetics and efficiency of cGMP production by the light activated cyclases - BeCyclOp and bPGC, we co-expressed WincG2 along with the cyclases in BWMs and investigated the cGMP dynamics as evoked by the cyclases in intact *C. elegans* using the fluorescence reporting by WincG2. BWMs were chosen as the cells are relatively large in size, thus large fluorescent signals should be obtained relatively conveniently. Moreover, the apparent lack of strong endogenous cyclase activity as can be interpreted by the lack of obvious effects of cAMP or cGMP in muscle in the absence of TAX-2/-4, should be favourable to enable precise measurements.

3.3.1 WincG2 is a codon-optimized circularly permutated cGMP sensor derived from the mammalian sensor FlincG3

WincG2 (developed by Noelle L'Etoile at University of California San Francisco, USA) is based on FlincG3, a genetically encoded, circularly permutated GFP based cGMP sensor that was characterized both in vitro and in mammalian cell lines and primary cell culture (Bhargava et al. 2013). FlincG3 possesses two in-tandem protein kinase G (PKG) I cGMP binding domains that bind cGMP cooperatively, attached to the N terminus of circularly permutated EGFP (cpEGFP) (**Figure R17**). In the presence of cGMP, the fluorescence emission intensity of FlincG3 increases, presumably due to the conformational changes of the sensor upon cGMP binding (Nausch et al. 2008; Bhargava et al. 2013). In FlincG3, mutating methionine at

position 335, located outside the beta barrel of the cpEGFP domain, to lysine (M335K), improved the response amplitude of the sensor to cGMP.

FlincG3 was codon optimized for use in *C. elegans* and inserted it into a worm specific expression vector, pPD95.75 (Boulin et al. 2006), which facilitates transcription and translation of the sensor (**Figure R17**). This construct can be modified to contain any *C. elegans* promoter so that the sensor can be expressed in almost any cell of interest.

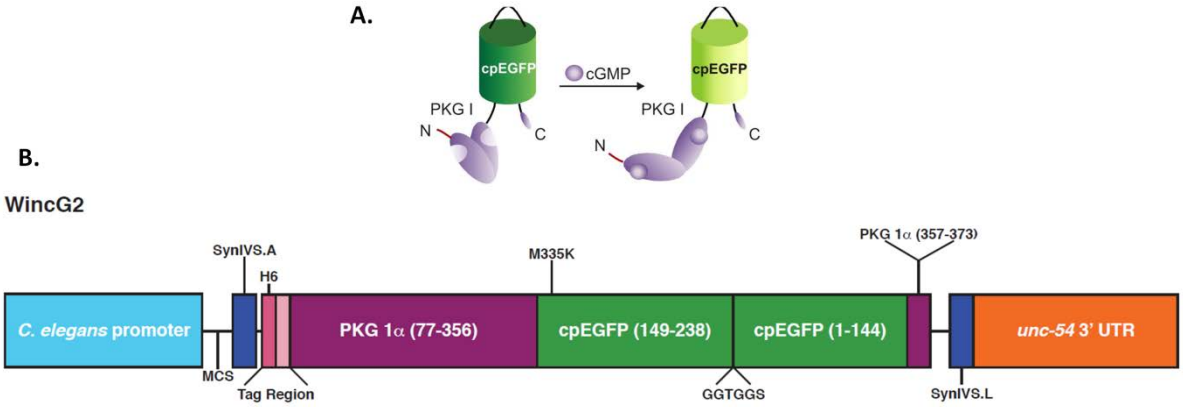

FIGURE R17: A. The predicted unbound and bound state of WincG2. The tandem cGMP binding sites of PKG Iα is fused on the N-terminus of cpEGFP. cGMP binding leads to a change of the protein conformation, closing the beta barrel of cpEGFP which causes the chromophore to increase its fluorescence intensity (Nausch et al. 2008). **B.** WincG2 is a non FRET based cGMP sensor codon optimized for use in *C. elegans*. WincG2 is based on the mammalian cGMP sensor FlincG3 (Bhargava et al. 2013). The figure was kindly provided by Noelle L'Etoile.

3.3.2 The fluorescence emission intensity of WincG2 increases upon stimulation of blue light activatable guanylyl cyclases - BeCyclOp and bPGC when coexpressed in BWMs.

WincG2 was expressed in body wall muscle cells to report on the cGMP levels in-vivo using fluorescence readout upon cGMP production in a light-regulated fashion by co-expression of either BeCyclOp or bPGC. BeCyclOp and bPGC were tagged with a bicistronic mCherry sequence so as to control for changes in fluorescence arising because of movement artefacts. This is convenient as changes arising purely because of cGMP rise will be detected as rise in the signal in the green channel for WincG fluorescence and no such increase would be evident in the red channel for mCherry fluorescence.

WincG2 and BeCyclOp were co-expressed in body wall muscle cells (**Figure R18A**). The red transmission light was used to focus on the muscle cells and then simultaneous acquisition of signals in the green and red channel was started. An acute increase in WincG2 fluorescence emission intensity was observed upon blue light illumination (**Figure R18B**).

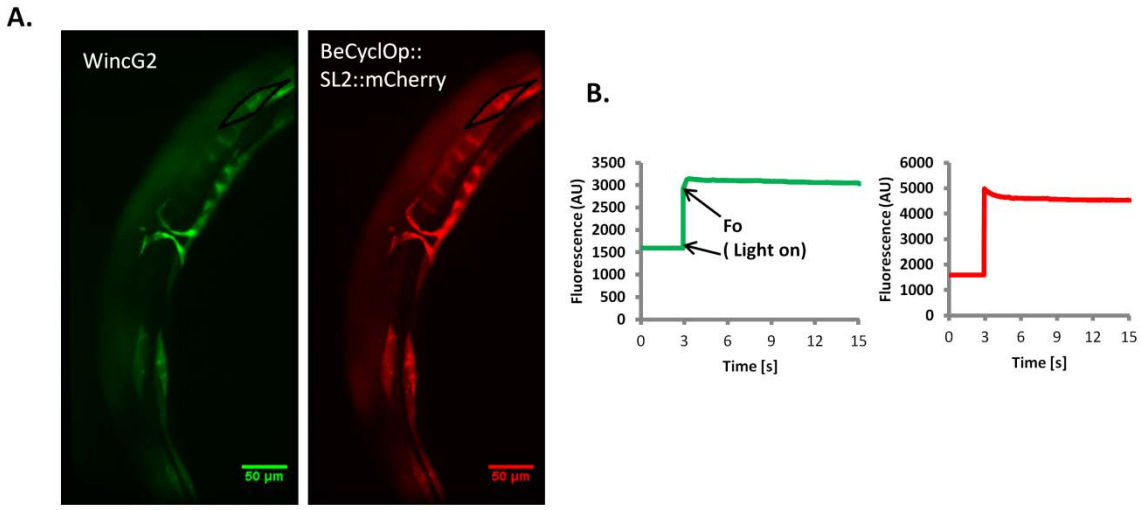

FIGURE R18: **A.** Fluorescent micrographs of animals expressing BeCyclOp::SL2::mCherry and WincG2 in BWMs. **B.** Time course of green and red fluorescence intensities upon BeCyclOp and WincG2 activation for the defined ROI The fluorescence intensity at the peak upon light onset was used as F_0 to normalize for subsequently calculating $(F-F_0)/F_0$ after subtracting the background.

This experiment is complicated by the fact that blue light used to image WincG2 also activates BeCyclOp simultaneously. To test whether changes in WincG2 fluorescence emission intensity and dynamics correspond with cGMP production by BeCyclOp, animals coexpressing WincG2 and BeCyclOp were grown with or without all-trans retinal (ATR), which is required for BeCyclOp activity. Animals grown in the absence of ATR showed an apparent decrease in WincG2 fluorescence emission intensity (dark green trace in **Figure R19**; $(F-F_o)/F_o$ plateaued at -0.312 beginning at 9s) when exposed to blue light. The sudden drop from the initial fluorescence intensity F_o may be due to apparent photobleaching or photoswitching like phenomenon in the WincG2 fluorescence dynamics. In contrast, for animals that were grown with ATR, the drop in signal due to photobleaching is not visible at all, as it is immediately obscured by the rising fluorescence emission signal (light green

trace in **Figure R18**; peak $(F-F_o)/F_o$ = 0.218 ± 0.023 at 0.49s). The fluorescence in the red channel (red traces) showed a decrease in the intensity for both with and without ATR

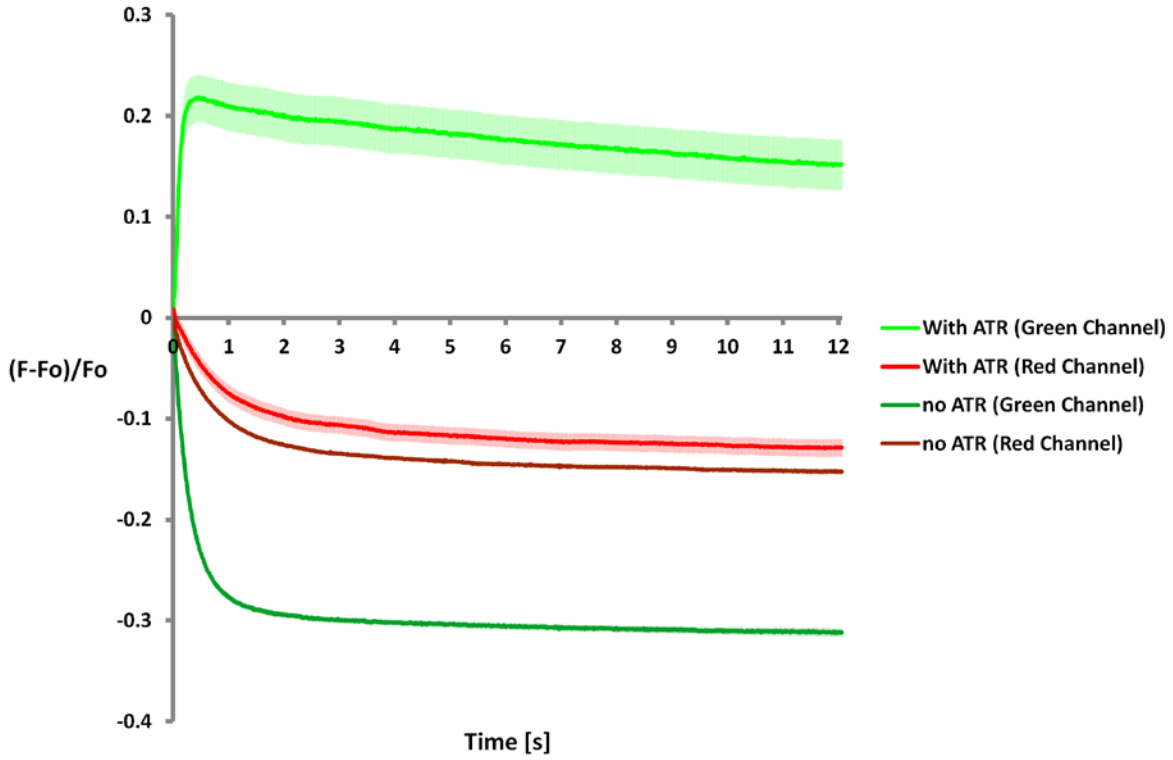

FIGURE R19: (F-Fo)/Fo for the green and red channel for pmyo-3::BeCyclOp::SL2::mCherry, pmyo-3::WincG2 animals grown in the absence and presence of all-*trans* retinal (ATR). n=6 (21 ROIs) without ATR; n=5 (28 ROIs) with ATR. Acquisition done at 100 frames/s. Error bars: SEM.

WincG2 and bPGC tagged with SL2::mCherry were co-expressed in body wall muscle cells (**Figure R20A**). The muscle cells were identified and focussed using the mCherry fluorescence in the red channel and the blue light to excite WincG2 as well as bPGC was switched on. The fast 'photoswitching' drop of WincG2 fluorescence was followed by a slow increase in the fluorescence taking ~140 seconds to reach a plateau (**Figure R20A,** upper panel-green trace).

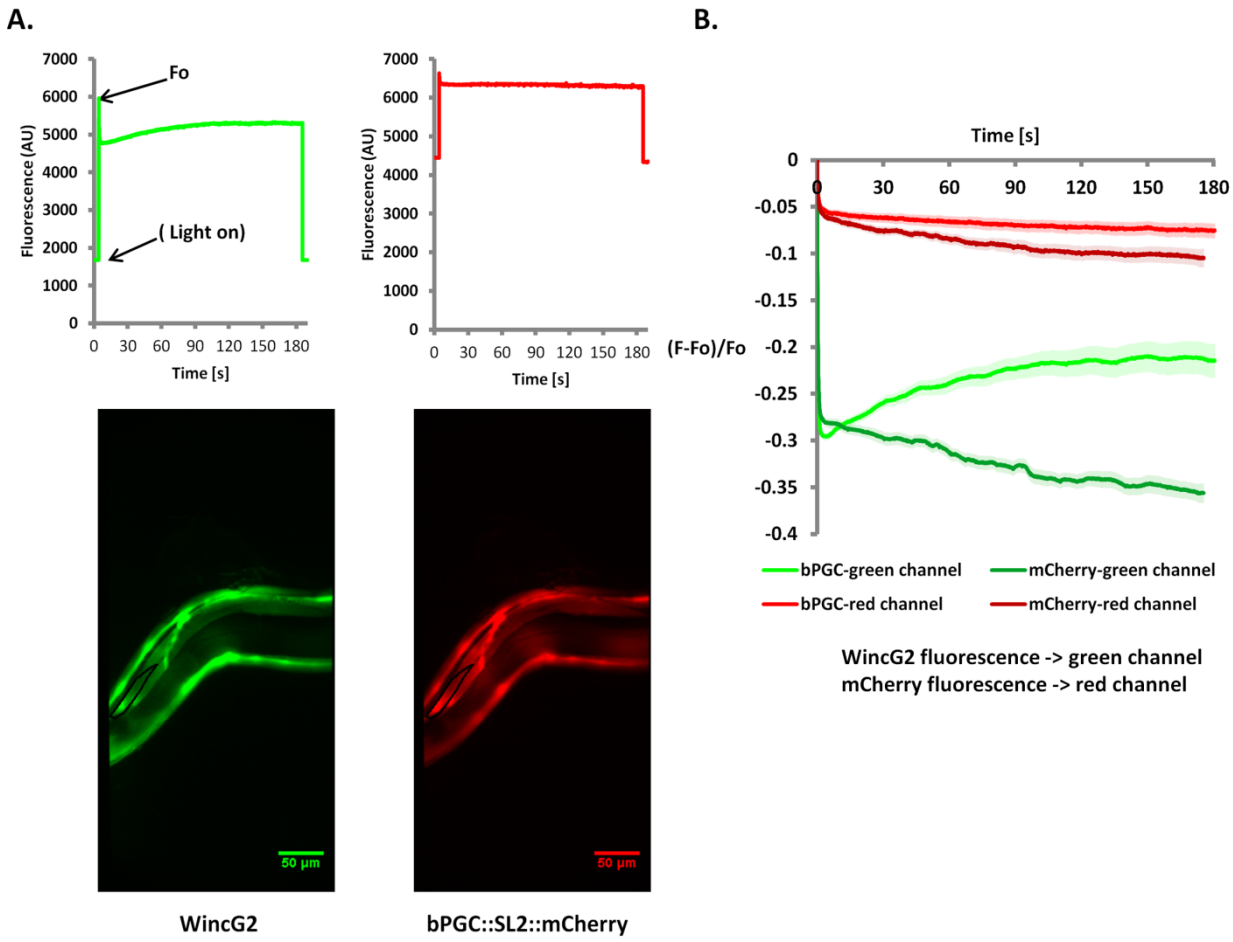

FIGURE R20: **A.** Fluorescent micrographs of pmyo-3::bPGC::SL2::mCherry, pmyo-3::WincG2 animals along with time course of green and red fluorescence intensities upon bPGC and WincG2 activation for the defined ROI. **B)** (F-Fo)/Fo for the green and red channel for pmyo-3::bPGC::SL2::mCherry,pmyo-3::WincG2 (5 animals, 27 ROIs) and pmyo-3::mCherry,pmyo-3::WincG2 (5 animals , 30 ROIs). Acquisition done at 20 frames/s. Error bars: SEM.

As can also be seen from the normalized curve from multiple animals, the fluorescence emission intensity of WincG2 when coexpressed with bPGC increased in the order of minutes upon activation of bPGC, with the maximum increase in $(F-F_o)/F_o$ being around 10% (above from the minimum value) (**Figure R20B**). In contrast, the fluorescence emission intensity of WincG2 increased acutely upon activation of BeCyclOp and the magnitude of increase in fluorescence was twice as much. As a control, mCherry alone was co-expressed with WincG2 in the BWMs. The signal in the green channel displayed the fast 'photoswitching' drop followed by the gradual bleaching decay (**Figure R20B**). The red channel for both the strains exhibited decline in the fluorescence intensity owing to the bleaching of mCherry.

Bhargava et al. showed that FlincG3 has 230-fold lower EC50 for cGMP as compared to cAMP (Bhargava et al. 2013). To understand how the fluorescence emission intensity of WincG2 changes with increases in cAMP levels in vivo and compare with the BeCyclOp mediated increase, WincG2 fluorescence emission intensity was examined in animals co-expressing WincG2 and bPAC, the blue light activatable adenylyl cyclase (**Figure R21**). After the initial drop in the WincG2 fluorescence emission intensity due to the photoswitching (though only till 10 percent of the peak intensity at light onset), the cAMP kicks in to raise the WincG2 signal. This indicates WincG2 does respond to changes in cAMP concentration.

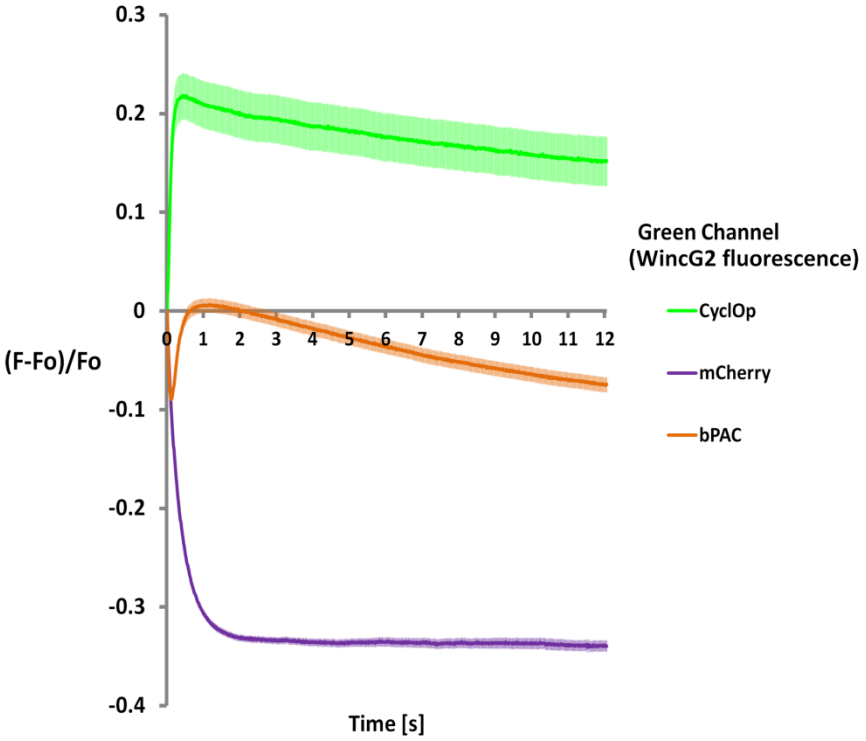

FIGURE R21: (F-Fo)/Fo for the green channel for pmyo-3::BeCyclOp::SL2::mCherry,pmyo-3::WincG2 with ATR (5 animals, 28 ROIs), pmyo-3::mCherry,pmyo-3::WincG2 (6 animals, 38 ROIs) and pmyo-3::bPAC::SL2::mCherry,pmyo-3::WincG2 (7 animals, 50 ROIs). Acquisition done at 100 frames/s with red transmission light being used to focus on the muscle cells. Error bars: SEM.

In order to better understand the underlying dynamics of cGMP/cAMP mediated increase in WincG2 fluorescence and to objectively compare the efficiency and kinetics of the different cyclases - BeCyclOp, bPGC, bPAC; we performed the following subtractions of the respective green channel WincG2 $(F-F_o)/F_o$ values: BeCyclOp::SL2::mCherry without ATR from BeCyclOp::SL2::mCherry with ATR, mCherry (corresponding to WincG2 only) from bPAC::SL2::mCherry and mCherry (corresponding to WincG2 only) from bPGC::SL2::mCherry (**Figure R22**). Such a comparison clearly highlights that BeCyclOp is a much more efficient cyclase as compared to bPGC with 30 percent increase in intensity within a second for BeCyclOp while 10 percent increase in intensity within a couple of minutes for bPGC. Interestingly for bPAC, the magnitude of peak increase is comparable to BeCyclOp but it is a little slower (see inset) than BeCyclOp and the intensity sharply dips after the maximum rise.

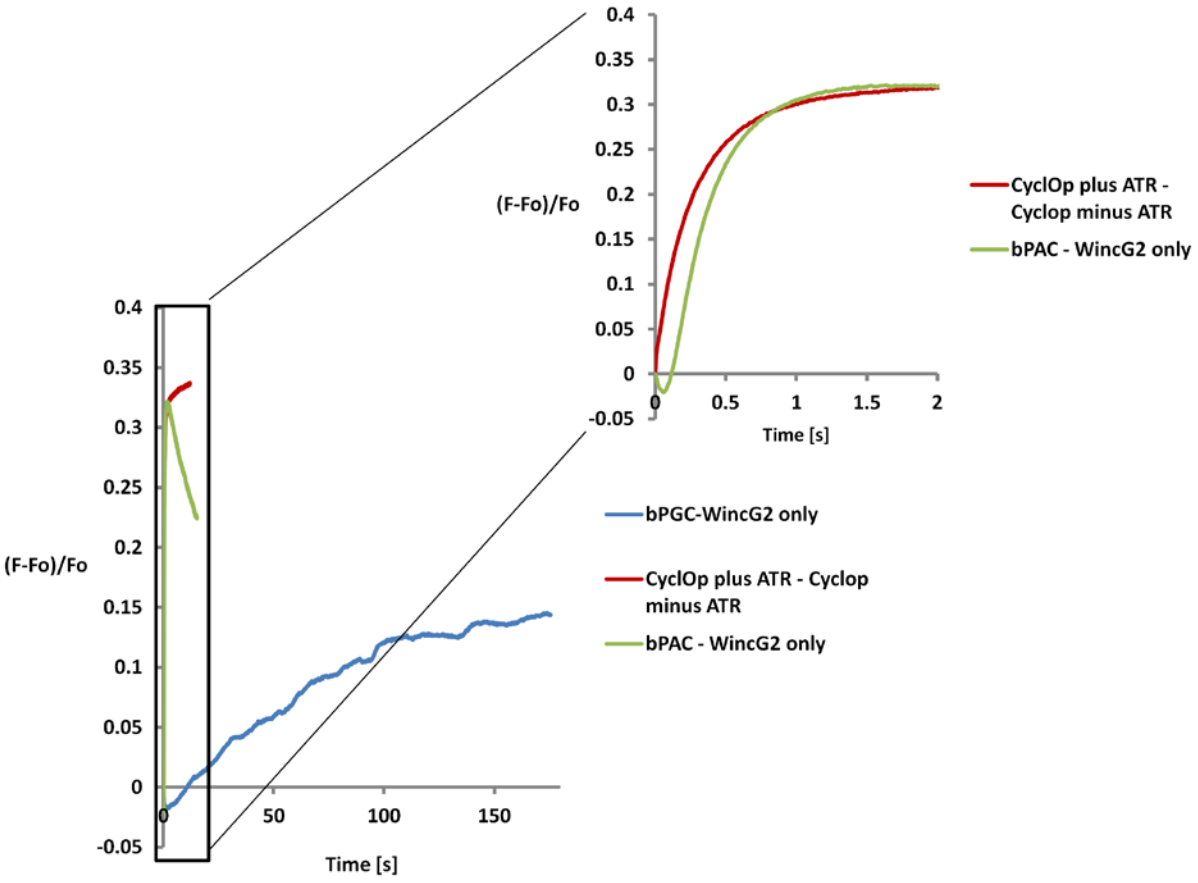

FIGURE R22: Subtracted (F-Fo)/Fo profiles for the green channel for: (i) pmyo-3::BeCyclOp::SL2::mCherry,pmyo-3::WincG2 with ATR (5 animals, 28 ROIs) minus pmyo-3::BeCyclOp::SL2::mCherry,pmyo-3::WincG2 without ATR (6 animals, 21 ROIs), (ii) pmyo-3::bPAC::SL2::mCherry,pmyo-3::WincG2 (7 animals, 50 ROIs) minus pmyo-3::mCherry,pmyo-

3::WincG2 (no ATR) (7 animals, 29 ROIs) and (iii) pmyo-3::bPGC::SL2::mCherry,pmyo-3::WincG2 (5 animals, 27 ROIs) minus pmyo-3::mCherry,pmyo-3::WincG2 (6 animals, 30 ROIs). Acquisition done at 100 frames/s with red transmission light being used to focus on the muscle cells for (i) and (ii) and 20 frames/s with yellow light for red channel being used to focus on the muscle cells for (iii).

To check for the comparability of different transgenic strains with respect to pure WincG2 response, green channel $(F-F_o)/F_o$ values corresponding to WincG2 fluorescence in the absence of any cyclase were plotted together (**Figure R23**). These are: BeCyclOp::SL2::mCherry without ATR leading to a non-functional cyclase, mCherry only with and without ATR, and mCherry only without ATR albeit at 20 frames per second with yellow light used to focus on the red fluorescent muscle cells while for the other three the acquisition was at 100 frames per second and red transmission light was used to focus on the cells. In all cases, there was a fast drop indicating a rapid 'photo-switching' or photo-bleaching event and then a subsequent stationary plateau phase starting from 1s onwards where the $(F-F_o)/F_o$ values ranged from about 27 to 34 percent.

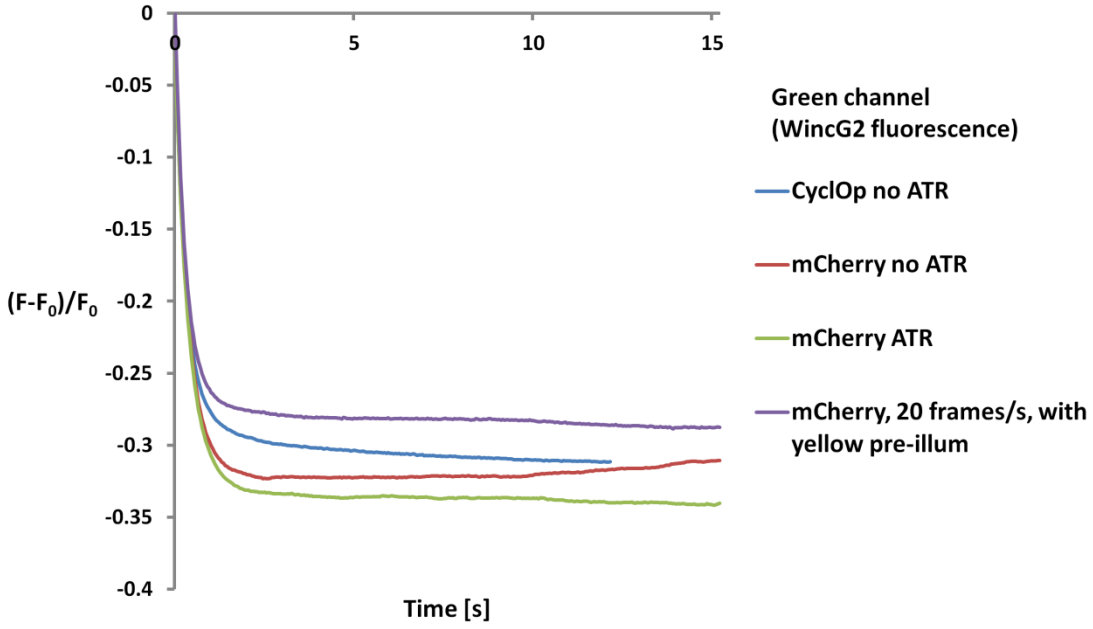

FIGURE R23: Mean (F-Fo)/Fo for the green channel for transgenic animals with pmyo-3::BeCyclOp::SL2::mCherry,pmyo-3::WincG2 without ATR (5 animals, 28 ROIs) , pmyo-3::mCherry,pmyo-3::WincG2 without ATR (7 animals, 29 ROIs), pmyo-3::mCherry,pmyo-3::WincG2 with ATR (6 animals, 38 ROIs) - videos acquired at 100 frames per second (condensed to 20 frames per second) and with no yellow pre-illumination and pmyo-3::mCherry,pmyo-3::WincG2 with ATR (5 animals, 30 ROIs) - acquisition done at 20 frames/s with yellow light being used to focus on the muscle cells.

3.4 Implementation of LiGluR in *C. elegans*

Downstream of the sensory neurons, the interneurons occupy the next level in the hierarchy of neurons processing the sensory information in the nervous system of *C.elegans.* The interneurons receive largely a glutamatergic input from the sensory neurons and relay the information using the glutamate receptors. A light activated glutamate receptor in the command interneurons would be highly useful to understand the dynamics of sensory processing at this vital layer of information flow in the nervous system of the worm.

3.4.1 Identification of a *C. elegans* Kainate receptor

The LiGluR which has been established to work in mammalian hippocampal neurons and in zebrafish is a Kainate-type Glutamate receptor, encoded by the rat iGluR6 gene. It was modified with cysteine at position 439, for the attachment of the photo-switchable maleimide-azobenzene-glutamate (MAG) reagent (Szobota et al. 2007b). In first experiments in the Gottschalk lab, it was tried to express iGluR6 in *C. elegans* muscles and neurons, but it was found that rat iGluR6 was not functionally expressed in this host. Thus, it appeared more appropriate to modify a *C. elegans* intrinsic channel for this purpose. The first step was thus to identify Kainate-type receptors in *C. elegans*. Bioinformatic analysis revealed GLR-3, GLR-4, GLR-5, and GLR-6 as the putative candidates homologous to the mammalian Kainate-type receptor. From electrophysiological studies in the lab of Prof. A. V. Maricq (University of Utah, Salt Lake City, USA), we learned that GLR-3 and GLR-6 may indeed be forming a heteromeric kainate-type receptor (personal communication).

3.4.2 Expression of GLR-3 and GLR-6 with cysteine substitutions in *C. elegans* BWM and contraction experiments with MAGs (Maleimide-Azobenzene-Glutamate)

Following the sequence alignment for *C. elegans* GLR-3, -6 and iGluR6 in the amino acid stretches including the analogous L439 positions, the sites for cysteine substitution were chosen and using site directed mutagenesis, cysteine mutants for GLR-3(L409C) and GLR-6(H417C) were generated (**Figure R24A**)

These cysteine mutants for GLR-3 and GLR-6 were first expressed in *C. elegans* BWM cells using the *myo-3* promoter since BWMs are accessible to electrophysiology and the scoring of the expected macroscopically observable phenotypes upon successful constitution and activation of LiGluR (i.e. contraction and subsequent decrease in body length) is relatively easy. Expression of combination of GFP tagged/non-tagged and mutated/non-mutated versions of both subunits was achieved in BWMs in a *lite-1(ce314)* background (**Figure R24B**).

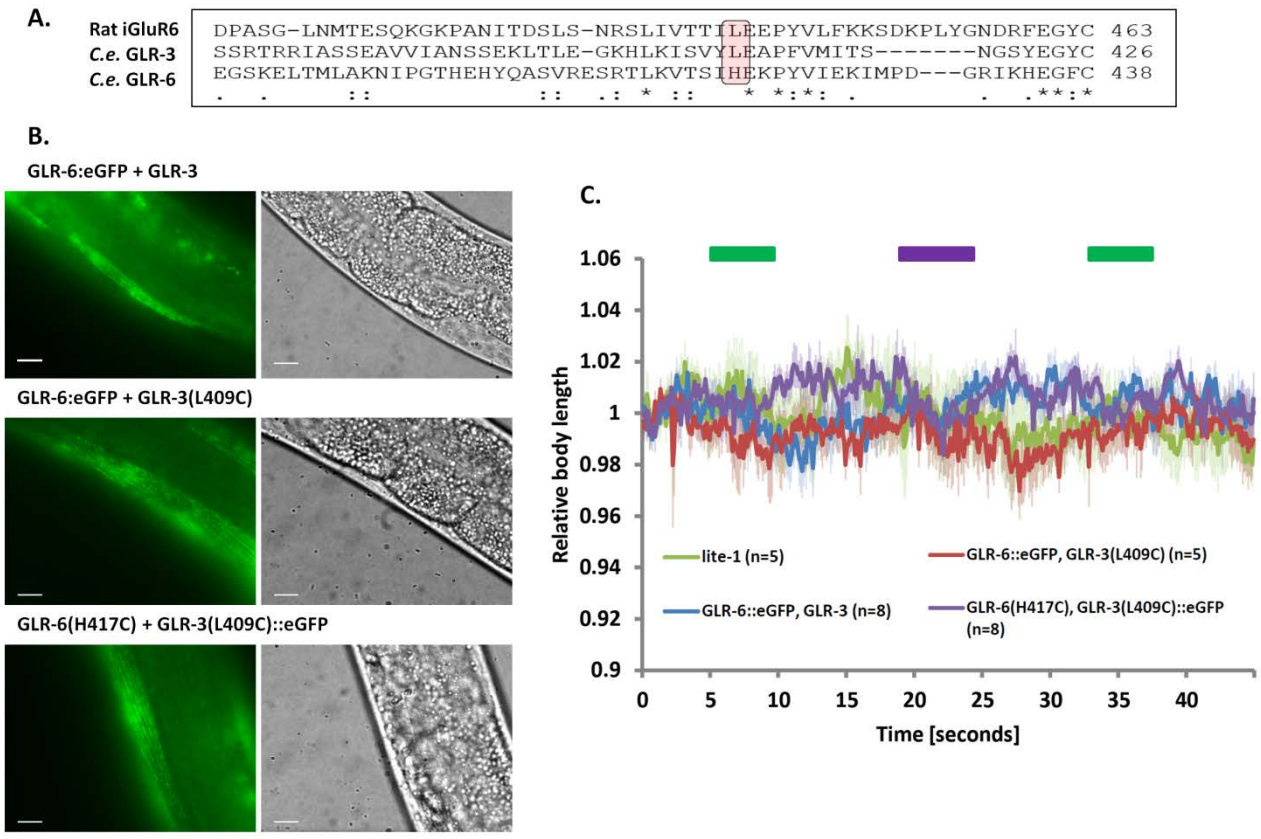

FIGURE R24: **A.** L409C and H417C cysteine substitutions were chosen for GLR-3 and GLR-6, respectively based on sequence alignment for LiGluR constitution in *C. elegans.* **B.** Expression of GFP-tagged GLR subunits in body wall muscles of *C. elegans*. Scale bar - 20 µm. **C.** Body length measurement of worms incubated with 250 µM MAG-1 in 4% DMSO Light intensity at 380nm: 0.88 mW/mm^2 and 500nm: 0.26 mW/mm^2. Green and violet bars represent green (490-505 nm) and UV illumination respectively (370-390 nm). The number of animals is represented as n in the parentheses. Error bars: SEM.

The transgenic worms expressing GLR-6::eGFP,GLR-3(L409C); GLR-6::eGFP,GLR-3; GLR-6(H417C),GLR-3(L409C)::eGFP under the *myo-3* promoter in a *lite-1(ce314)*

background were incubated with 250 µM MAG-1 (MAGs were provided by Prof. Dirk Trauner, University of Munich, Germany) in 4% DMSO and subjected to green-UV-green illumination to switch LiGluR from non-conducting to the conducting state. The transgenic line with both subunits point mutated - GLR-6(H417C), GLR-3(L409C)::eGFP showed a minor hint of contraction coinciding with the UV illumination and was subsequently integrated to eliminate mosaicisms in expression (**Figure R24C**).

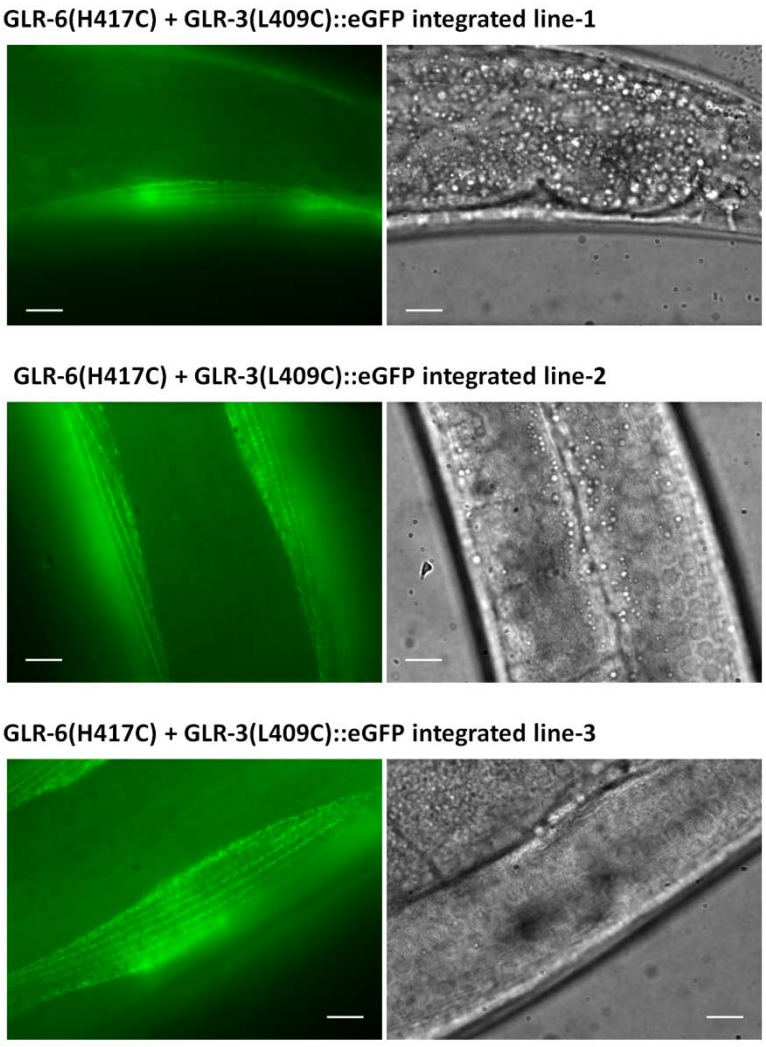

FIGURE R25: Expression of GFP-tagged GLR-3(L409C) and GLR-6(H417C) in body wall muscles of *C. elegans* in 3 independent integrated lines. Scale bar - 20 µm.

Following integration, 3 independent lines were obtained which showed uniform expression of GFP-tagged GLR-3(L409C) and GLR-6(H417C) across the body wall

musculature (**Figure R25**). One of the integrated lines was further tested with MAG-1 (incubated with 250 µM MAG-1 in 4% DMSO or injected directly into the body cavity) and seamless transition between the two wavelengths without any time interval between them. However, none of the conditions seemed to evoke any substantial contraction of the body length (**Figure R26**).

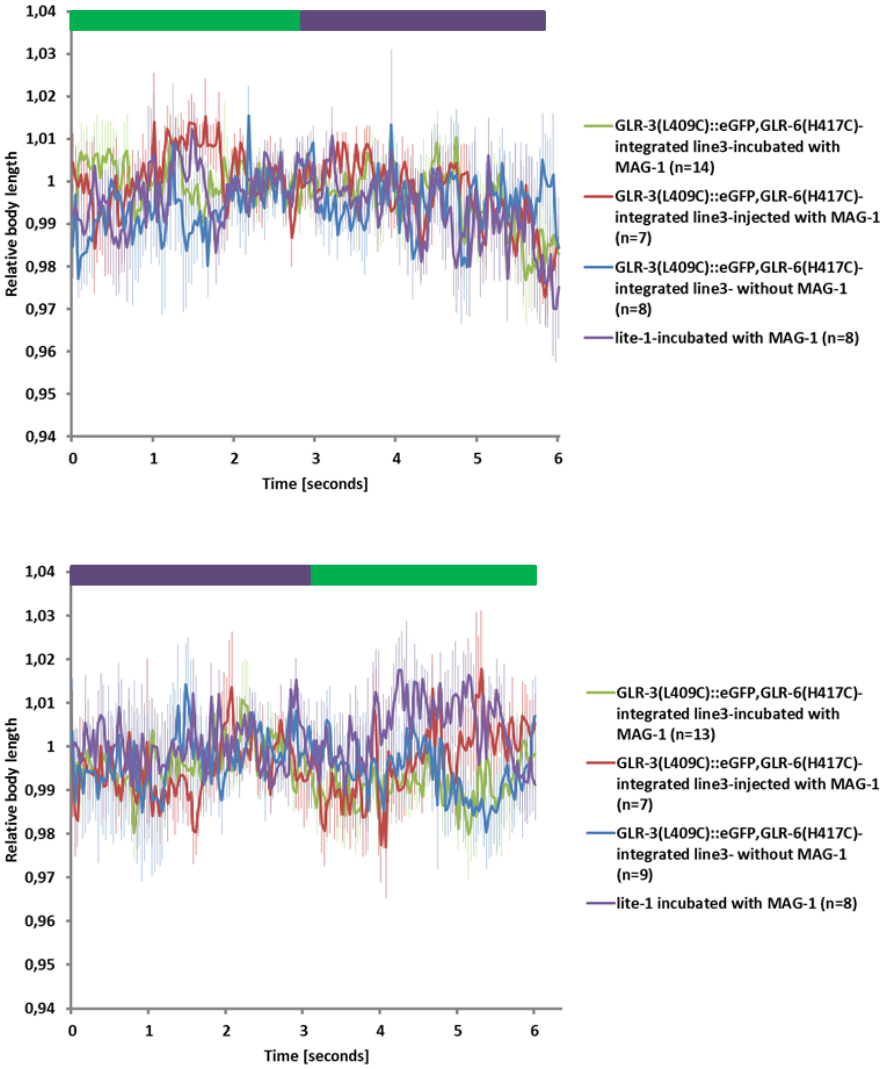

FIGURE R26: Body length measurement of 'worm LiGluR' expressing worms incubated or injected with 250 µM MAG-1 in 4% DMSO. Light intensity at 380nm: 0.84 mW/mm^2 and 500nm: 0.28 mW/mm^2. Green and violet bars represent green (490-505 nm) and UV illumination respectively (370-390 nm). The number of animals represented as n in the parentheses. Error bars: SEM.

The 3 integrated lines were again tested with a new LED illumination system from Prior Scientific Instruments GmbH, Jena, Germany which was procured

subsequently. The experiments were done with incubation of animals with 250 µM MAG-1 in 4% DMSO Light intensity at 365nm: 0.41 mW/mm^2 and 525nm: 0.81 mW/mm^2. Also, another shorter variant of MAG ,MAG-0 was tested to see if that would provide a better fit into the ligand binding domain of the glutamate receptor constituted by GLR-3 and GLR-6. However, no substantial UV or green light induced contractions could be observed (**Figure R27 and R28)**.

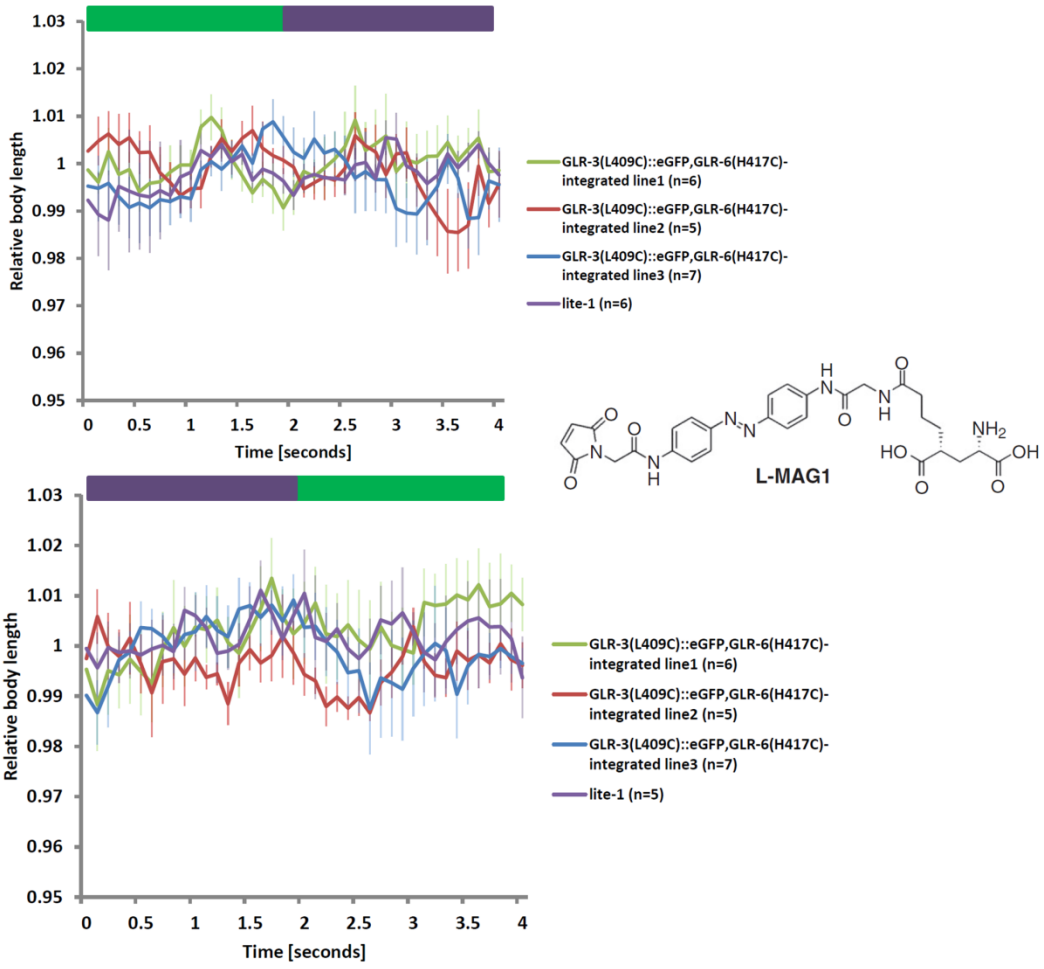

FIGURE R27: Body length measurement of integrated GLR-3,-6 lines incubated with 250 µM MAG-1 in 4% DMSO Light intensity at 365nm: 0.41 mW/mm^2 and 505nm: 0.81 mW/mm^2. Green and violet bars represent green and UV illumination respectively obtained using Prior LED system. The number of animals represented as n in the parentheses.

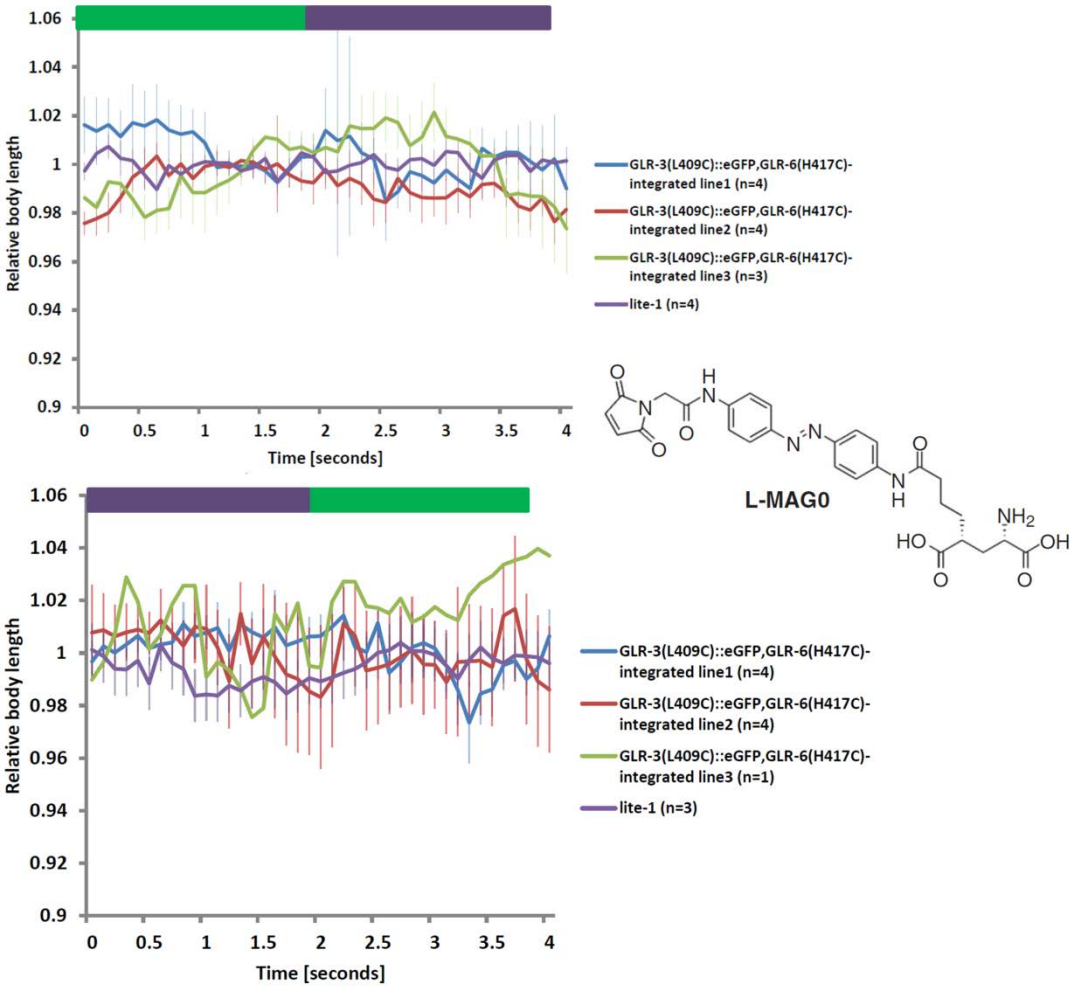

FIGURE R28: Body length measurement of integrated GLR-3,-6 lines incubated with MAG-0 in 4% DMSO Light intensity at 365nm: 0.41 mW/mm^2 and 505nm: 0.81 mW/mm^2. Green and violet bars represent green and UV illumination respectively obtained using Prior LED system. The number of animals represented as n in the parentheses.

3.4.3 Whole cell patch clamp electrophysiology on BWM with MAGs (performed by J. Liewald)

In order to ascertain the functionality of GLR-3/GLR-6 heterologously expressed in BWMs, patch clamp electrophysiological recordings were performed on the BWM cells of *C.elegans* (**Figure R29B**) by Dr. Jana Liewald in the our lab. N2 control animals did not show any current response to the application of 1mM Glutamate. For the transgenic line expressing GLR-6::eGFP+GLR-3 in BWMs, glutamate application elicited a peak current response of ~100 pA indicating a functional glutamate receptor being constituted on the muscle membrane. In comparison, the integrated

transgenic line expressing GLR-3(L409C)::eGFP+GLR-6(H417C) in BWMs showed around a 50 pA response (**Figure R29A,C**).

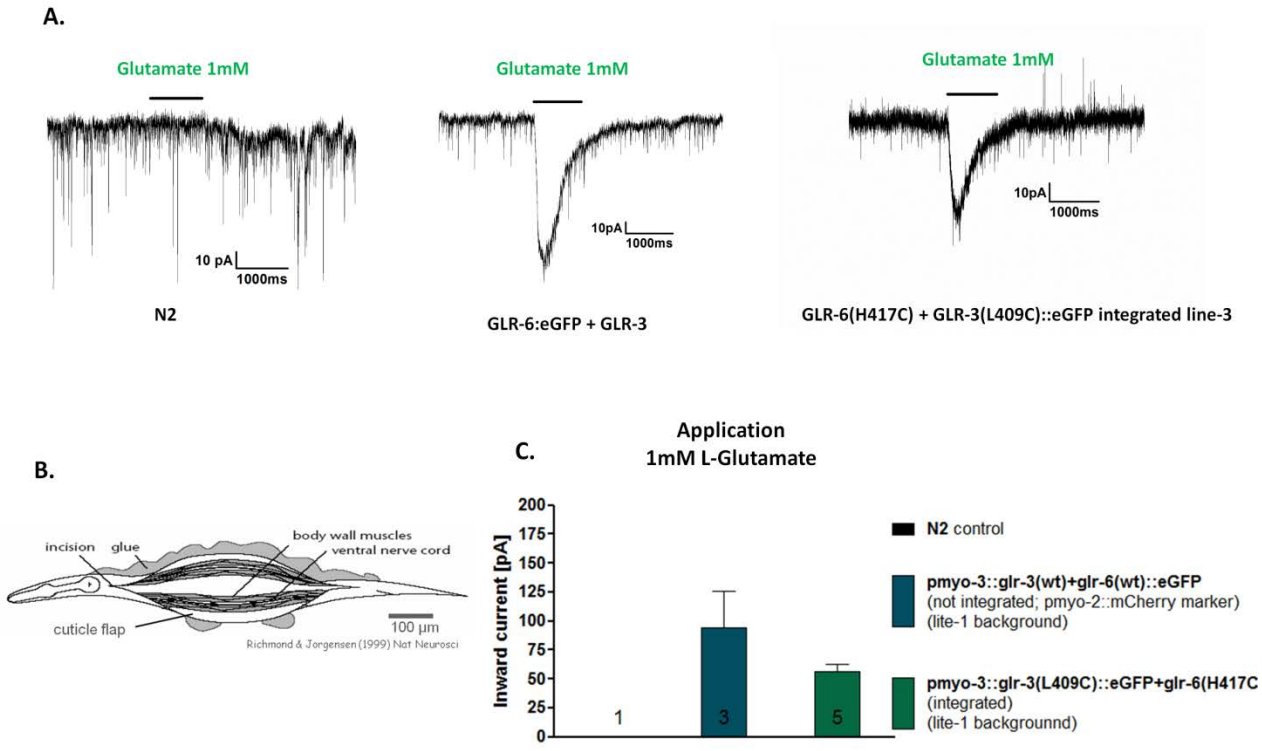

FIGURE R29: Whole-cell patch clamp recordings of the body wall muscle cells of *C. elegans*, provided by Dr. J. Liewald. **A.** and **C**. Original traces and summary of electrophysiological recordings of application of 1mM glutamate to the exposed BWM cells of control N2 strain, transgenic line expressing GLR-6::eGFP+GLR-3 and the integrated GLR-3(L409C):eGFP+GLR-6(H417C) line. **B.** An illustration of the preparation of *C. elegans* BWM cells for patch clamp recording from Richmond and Jorgensen 1999.

Since the behavioural experiments did not show any contraction which could be because of MAG not being able to reach the desired site in sufficient amounts, it was envisaged that direct application and photoswitching of MAG while recording the electrical activity of the muscle cell would provide the conclusive answer. The whole cell patch clamp experiment wherein 10 µM MAG-0 and MAG-1 were incubated with the exposed BWMs of the integrated transgenic line expressing GLR-3(L409C)::eGFP+GLR-6(H417C) in BWMs was performed by Dr. Jana Liewald. MAG-1 incubation and subsequent photoswitching from trans to cis state by switching from green to UV wavelength showed a hint of light evoked current (~ 5

pA) while MAG-0 incubated BWM cells did not show any photo-currents (**Figure R30**).

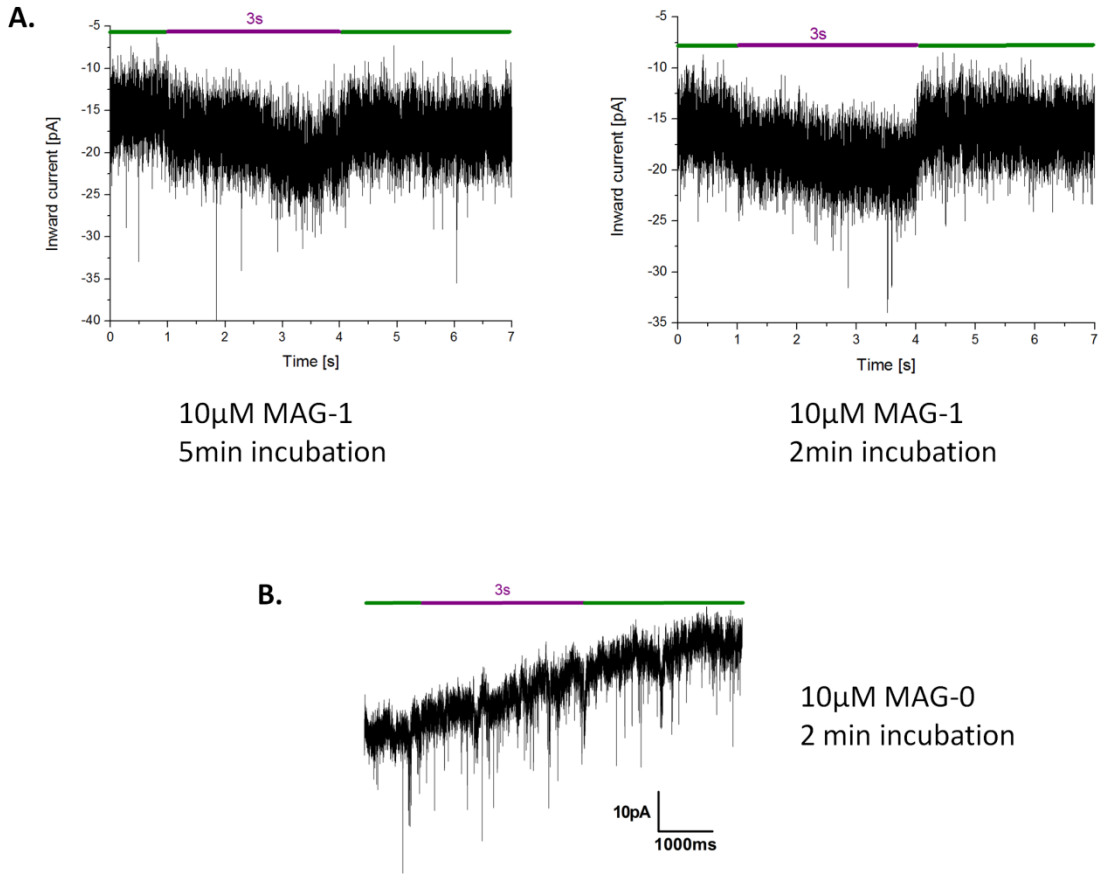

FIGURE R30: Whole-cell patch clamp recordings of the body wall muscle cells of *C. elegans* (integrated GLR-3(L409C):eGFP+ GLR-6(H417C) line) with simultaneous green-UV-green wavelength photoswitching after incubation of the preparation with 10 µM MAG-1 (**A**) and MAG-0 for 2-5 minutes (**B**). The illumination was done with the Prior LED system (505nm Prior LED 60x Objective: 10,3 mW/mm^2 , 385nm Prior LED 60x Objective: 9,0 mW/mm^2)

3.4.4 Co-expression of SOL-1 and SOL-2 in BWM and contraction experiments with MAG-2

Transmembrane AMPA receptor regulatory proteins (TARPs) - SOL-1 and SOL-2, have been shown to slow the rate and limit the extent of receptor desensitization, as well as to enhance the recovery from desensitization. It has further been shown that TARPs play a key role in trafficking, scaffolding, stability, signalling, and turnover of ionotropic glutamate receptors (Jackson and Nicoll 2011). SOL-1 and SOL-2 were co-expressed in BWMs in the integrated transgenic line expressing GLR-

3(L409C)::eGFP+GLR-6(H417C) in BWMs to boost the membrane insertion and aid the receptor functionality. Also a longer tether length variant of MAG, MAG-2 was used to see if a longer linker length might have better access to the ligand binding pocket. The worms with co-expression of SOL-1 and SOL-2 and incubation with MAG-2 did not show any strong contraction upon photoswitching from green to UV or back to green wavelengths of light (**Figure R31**).

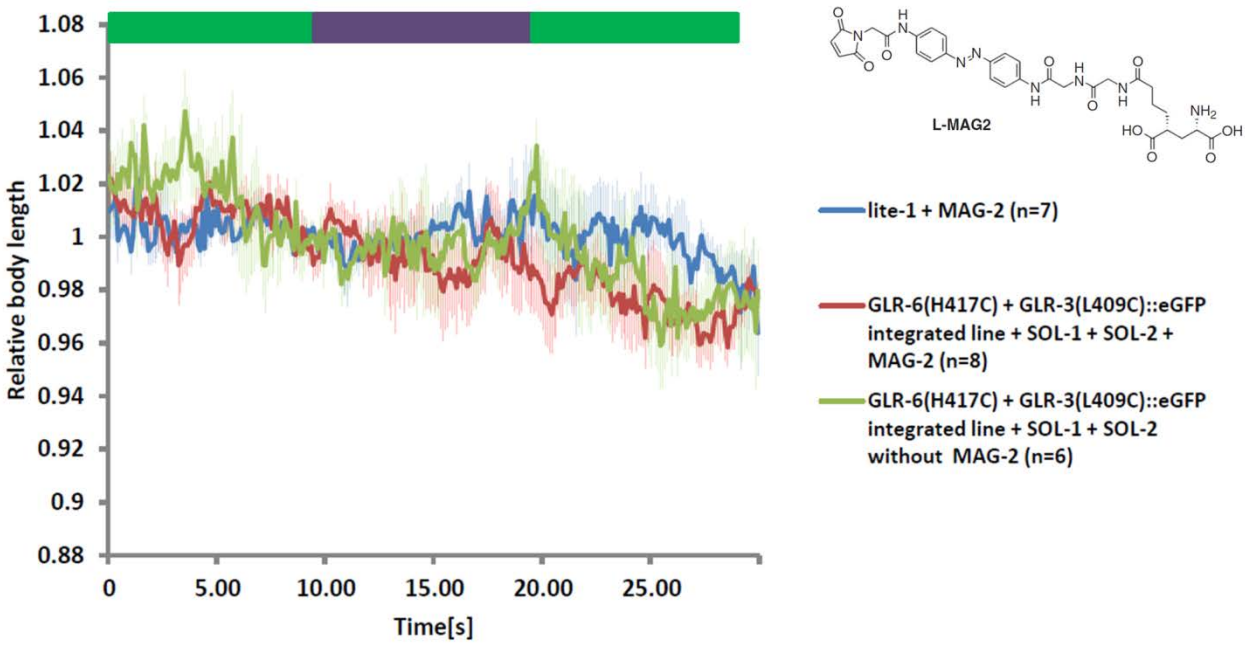

FIGURE R31: Body length measurement of worms incubated 500 µM MAG-2 in 4% DMSO. Light intensity at 380nm: 0.35 mW/mm^2 and 505nm: 0.33 mW/mm^2. Green and violet bars represent green and UV illumination respectively using Prior LED system. The number of animals represented as n in the parentheses and error bars represent SEM.

3.5 Implementation of Light activated Glutamate gated chloride channel, GLC-1 (Li-GLC-1) in *C. elegans*

Glutamate-gated chloride channels (GluCls), used for fast inhibitory transmission from otherwise excitatory, glutamatergic neurons, are found in several parts of the *C. elegans* nervous system particularly the motor neurons, but their functions are only partially understood. The structure of *C. elegans* GLC-1 has been solved (Hibbs and Gouaux 2011). Thus, this provides ideal prerequisites to turn it into a light-activated channel using the PTL approach and use it to analyze GLC-1 functions in *C. elega0ns* (**Figure R32**). Instead of L-MAGs which were used for LiGluR, the stereoisomer D-MAG-0 was predicted to have best accessibility to the glutamate binding site in GLC-1 structure (personal communication, Prof. Dirk Trauner)

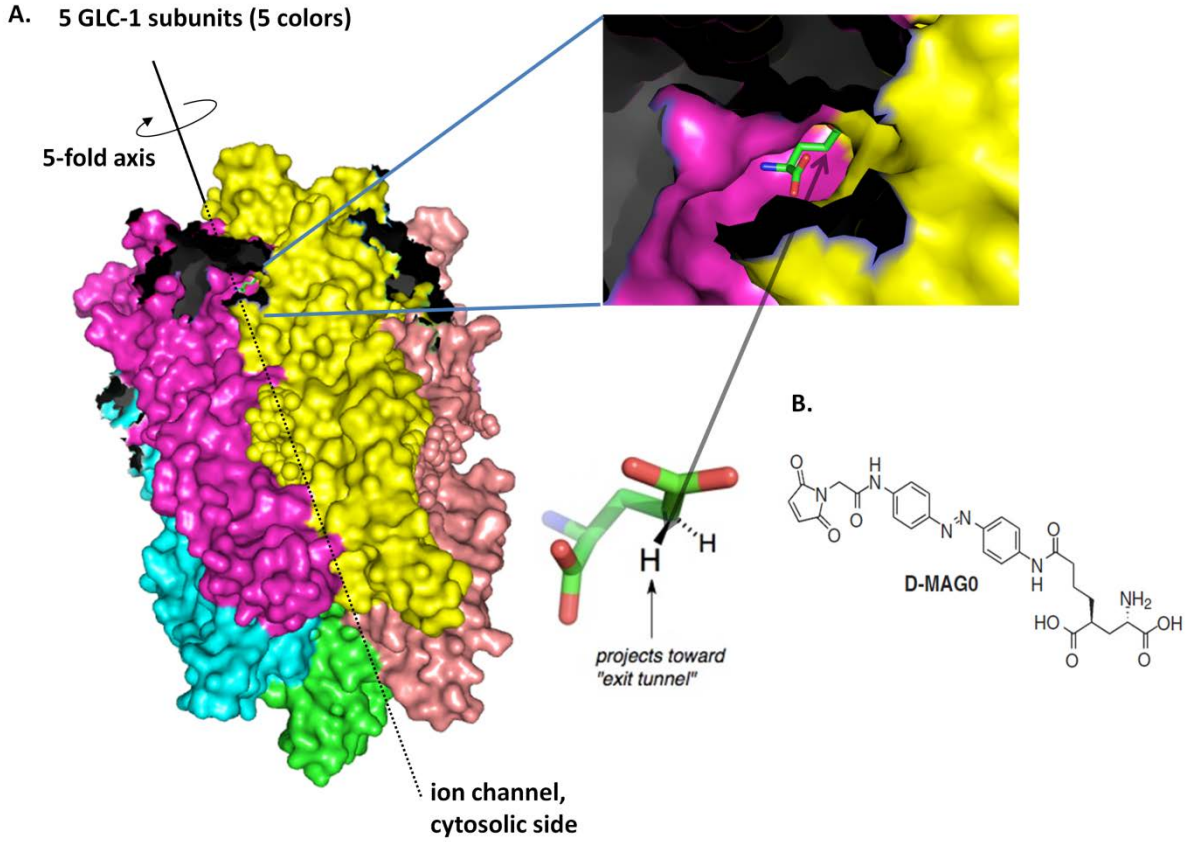

FIGURE R32: **A.** Pentameric structure of GLC-1 as revealed by (Hibbs and Gouaux 2011) with glutamate at the ligand binding site at the interface of two subunits on the extracellular side. **B**. The structure of D-MAG0. The inset shows the suitability of D-stereoisomer to have a better access to flip in and out through the exit tunnel upon photo-switching.

3.5.1 Identification of residues for cysteine introduction in GLC-1

To identify the putative amino acid residues of GLC-1 to be mutated to cysteines for the attachment of the PTL- D-MAG-0, in-silico docking studies were carried out (in collaboration with Dr. Antoine Taly at IBPC, Paris, France. Using the molecular docking and virtual screening program, Autodock Vina (Trott and Olson 2010), D-MAG-0 was docked onto the GLC-1 structure with glutamate of the MAG placed in the ligand binding pocket at the interface of two subunits of GLC-1. Based on the best predicted binding mode, the residues which when mutated to cysteine came in close proximity to the extended maleimide of the docked MAG were L96, T115, R117, Q230, K232 (**Figure R33**).

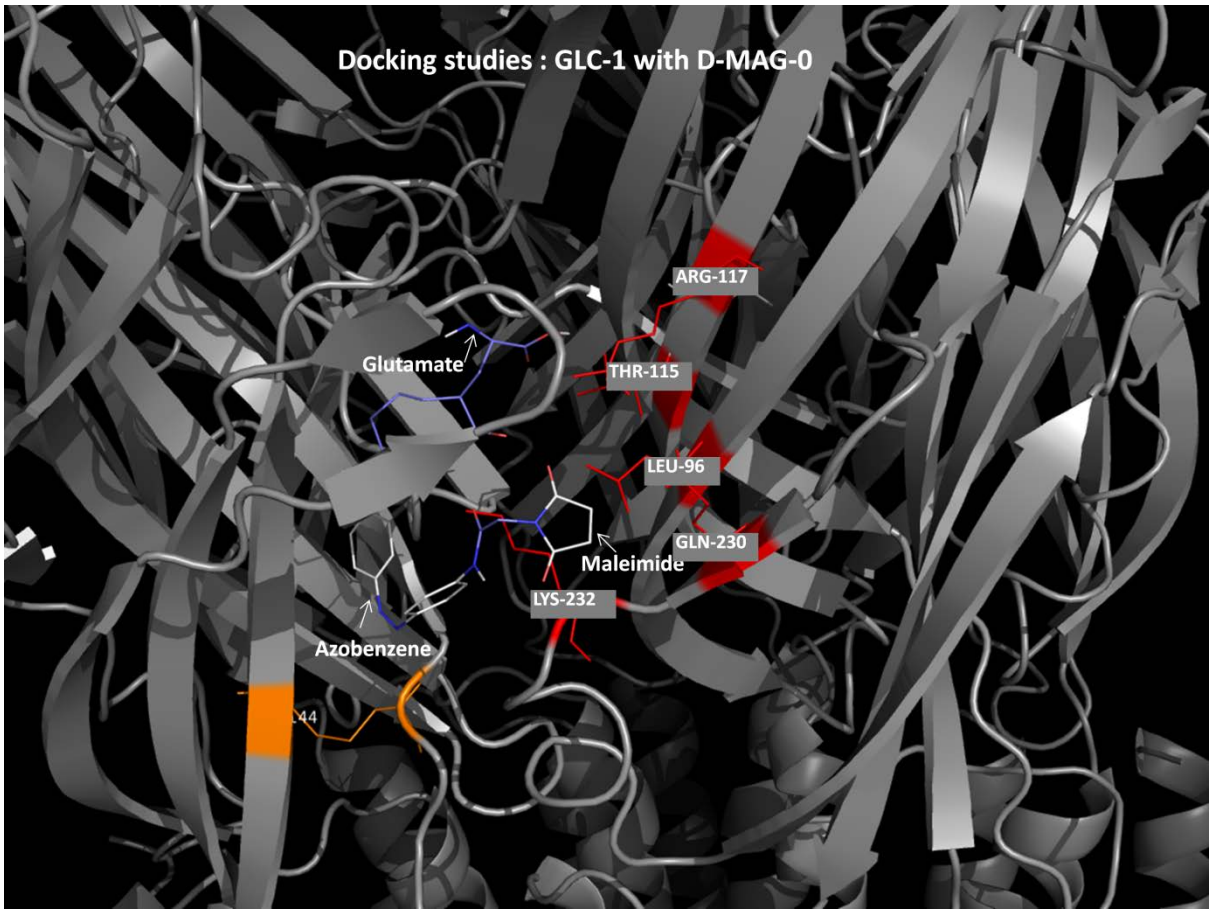

FIGURE R33:. Docking of D-MAG-0 to the GLC-1 structure. Maleimide, azobenezene and glutamate of the MAG are labelled. Maleimide comes in close vicinity with the residues L96, T115, R117, Q230, K232 indicated in red. In orange is depicted the characteristic Cys loop of the GLC-1. Representation done using Pymol.

A closer look at the Q230 residue in the docked model reveals Maleimide-Azobenzene sticking out of the 'exit tunnel' seen in the GLC-1 structure and 3.7

Angstrom distance between the maleimide and the thiol of the intended cysteine at the position (**Figure R34**), making Q230 a more probable candidate for cysteine introduction in GLC-1 for covalent attachment of the PTL- D-MAG0.

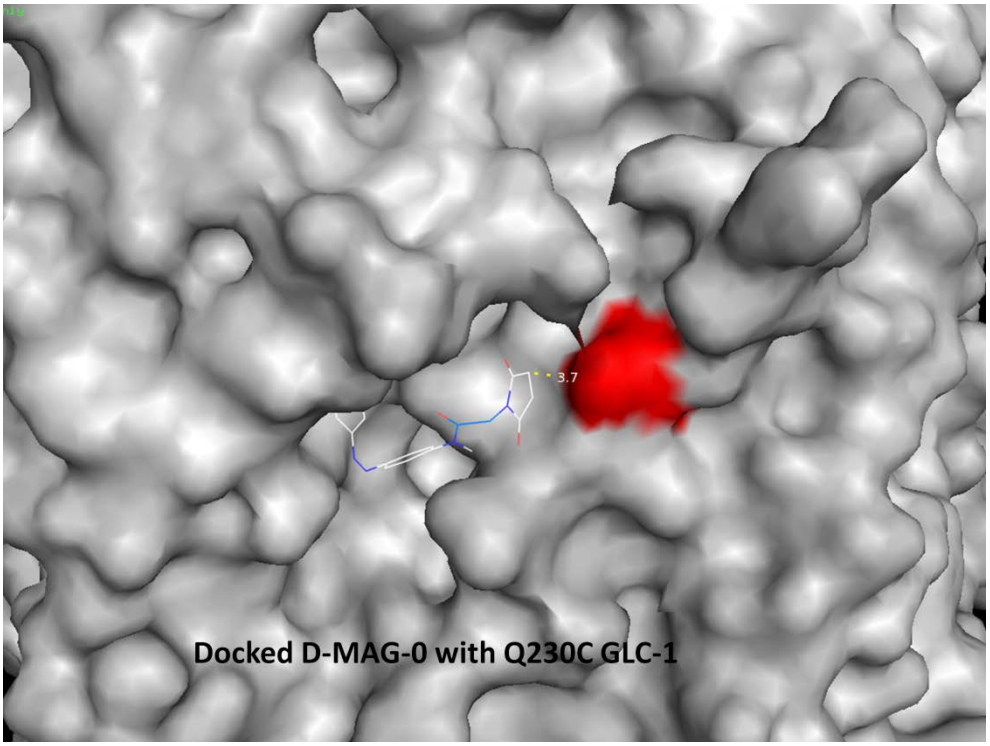

FIGURE R34:. Surface view rendering of the GLC-1 (Q230C) docked with D-MAG-0. Docking performed with Autodock Vina and visualization is done using Pymol.

3.5.2 Electrophysiological assessment of cysteine mutants of GLC-1

With the key candidate residues identified, we aimed to first check for functional coupling and photoswitching of D-MAG-0 using electrophysiology experiments performed on HEK293 cells transiently transfected to express GLC-1. These experiments were performed in collaboration with Arunas Damijonaitis in the laboratory of Prof. Dirk Trauner at the University of Munich, Germany. Heterologously glutamate binds to the homomeric GLC-1 receptor only in the presence of ivermectin, though it has been shown that substituting the naturally occurring threonine (T308) in M2 loop to a proline enabled glutamate gating of GLC-1 homomeric channels without a prior ivermectin potentiation (Etter et al. 1996). For this reason, we introduced T308P mutation in the mammalian expression vector containing mammalian codon optimized GLC-1 tagged with eYFP in its M3-M4 loop

(Li et al. 2002) and on top of the 'T308P background' of GLC-1, we introduced the cysteine mutations L96C, Q230C, and K232C separately and expressed these constructs in HEK 293 cells by transient transfection (**Figure R35**).

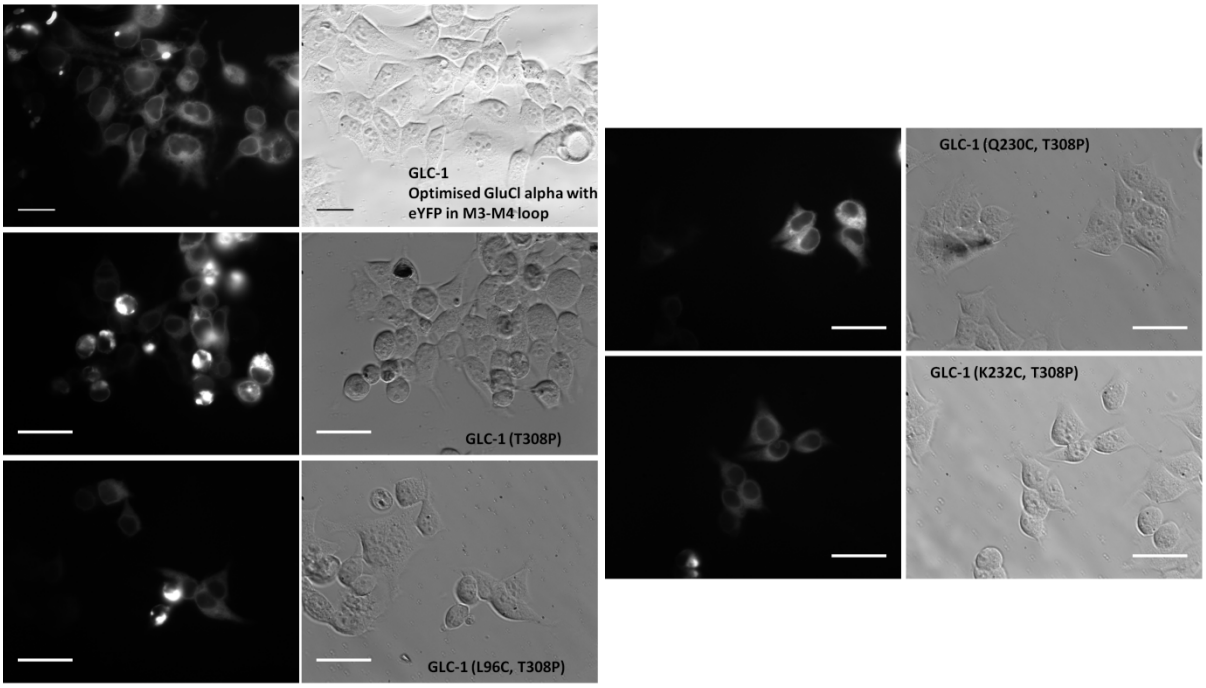

FIGURE R35:.Flourescence and transmission light micrographs of HEK 293 cells expressing GLC-1, GLC-1(T308P), GLC-1(L96C,T308P), GLC-1(Q230C,T308P), and GLC-1(K232C,T308P). Scale bar 20 µm.

To test for the functionality of the constructs, HEK 293 cells were subjected to application of 6 mM glutamate or glutamate potentiated with 10 µM ivermectin. HEK 293 cells expressing GLC-1(T308P) evoked a huge 800 pA current response in response to glutamate application in whole cell patch clamp electrophysiology experiments as compared to less than 100 pA for wildtype GLC-1 indicating GLC-1(T308P) forms a functional glutamate receptor. The application of ivermectin in combination with glutamate caused a prolonged open channel response without fast inactivation post the application of the stimulus.

Of the three candidate mutations, only K232(T308P) resulted in GLC-1 responding to glutamate application with ~500 pA current response, while L96C, T308P and Q230C, T308P combinations did not give any current response to glutamate application and a small response to glutamate with ivermectin potentiation (**Figure R36**).

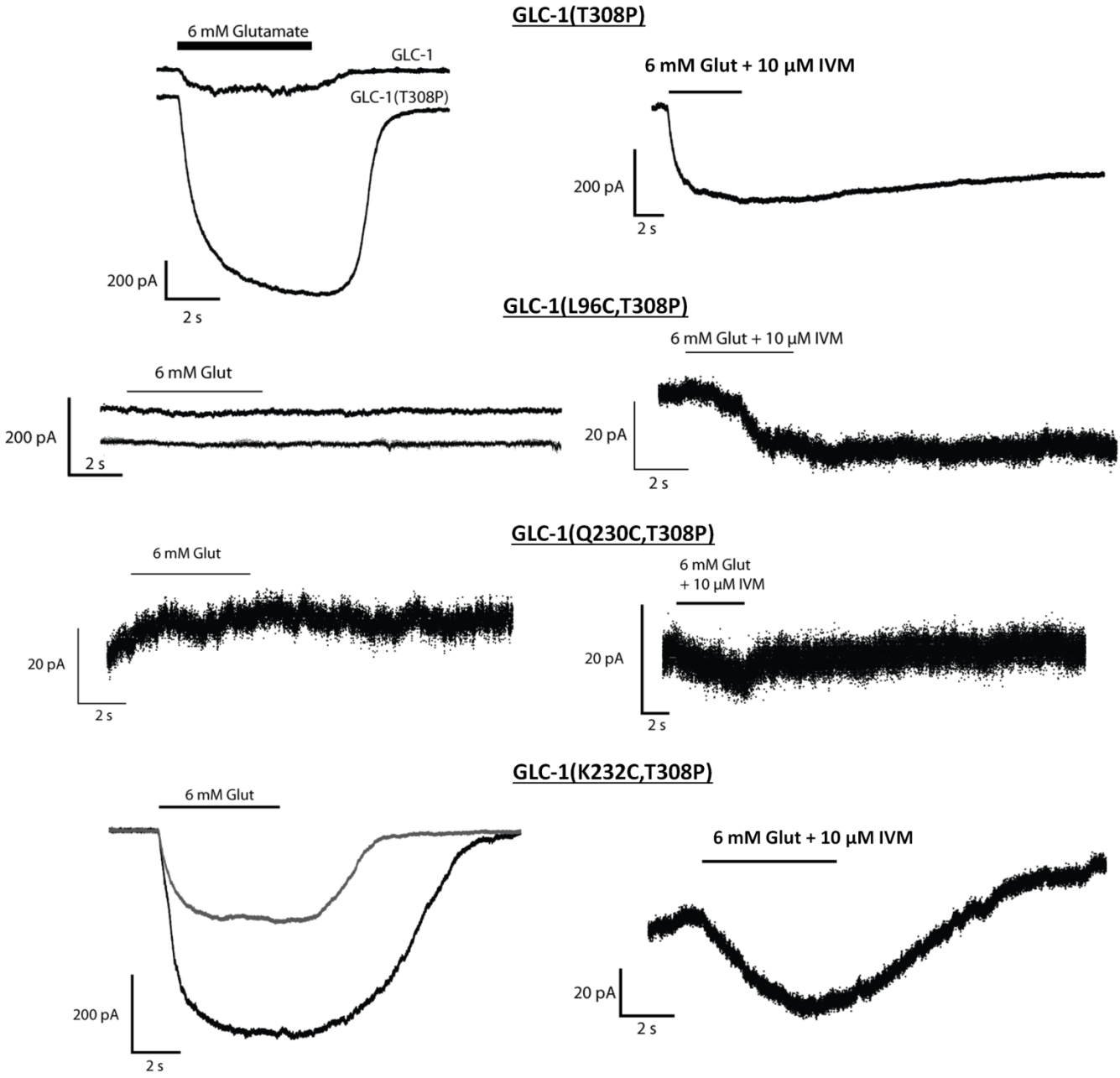

FIGURE R36: Representative whole cell patch clamp electrophysiology experiments with HEK 293 cells expressing GLC-1, GLC-1(T308P), GLC-1(L96C,T308P), GLC-1(Q230C,T308P), and GLC-1(K232C,T308P) subjected to 6mM glutamate and 6mM glutamate potentiated with 10 µM ivermectin application. Experiments performed in collaboration with Arunas Damijonaitis.

Before testing the PTL, its non-tethering freely diffusible version D-AG-0 (**Figure R37A**) which lacks the maleimide moiety was applied to the GLC-1(T308P) to check if it can confer photoswitchability to it with alternate 360 and 440 nm illumination (the

wavelengths for cis-trans switching for D-AG-0). Unfortunately no current response could be observed upon the D-AG-0 application, and also 360-440 nm photoswitching did not evoke any response (**Figure R37B**). However the same cell responded to bath perfusion of 6 mM glutamate (albeit with a delay because of the time taken by the glutamate to perfuse in) with a current response (**Figure R37C**).

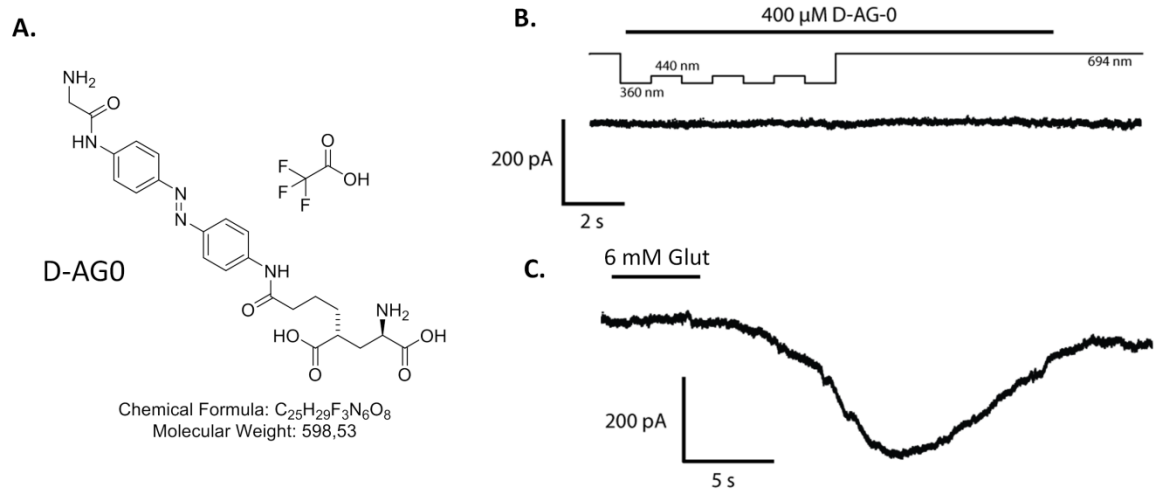

FIGURE R37: **A.** Chemical structure of D-AG-0, photochromic ligand version of the PTL, D-MAG-0. **B.** No current response observed with whole cell patch clamp electrophysiology experiments with HEK 293 cells expressing GLC-1(T308P) subjected to 0.4 mM D-AG-0 application and 360-440 nm alternate photoswitching using the monochromator. **C.** Current response of the same cell perfused with 6mM Glutamate in the bath. Experiments performed in collaboration with Arunas Damijonaitis.

We next proceeded to test D-MAG-0 with the GLC-1(K232C, T308P) mutant in the electrophysiology experiments. We incubated the cells with 50 µM D-MAG-0 for an hour and subsequently checked for current responses upon photoswitching with 500 nm and 380 nm wavelength illumination. Unfortunately, no light evoked current response could be observed (**Figure R38A**). Although, the same cell did show a current response to glutamate being washed into the bath (**Figure R38B**). We also performed a wavelength screen (360-370-380-390-400 nm) to check for altered wavelength specificity for the cis-isoform if any. However, no substantial current response could be observed in response to any of the wavelengths (**Figure R38C**).

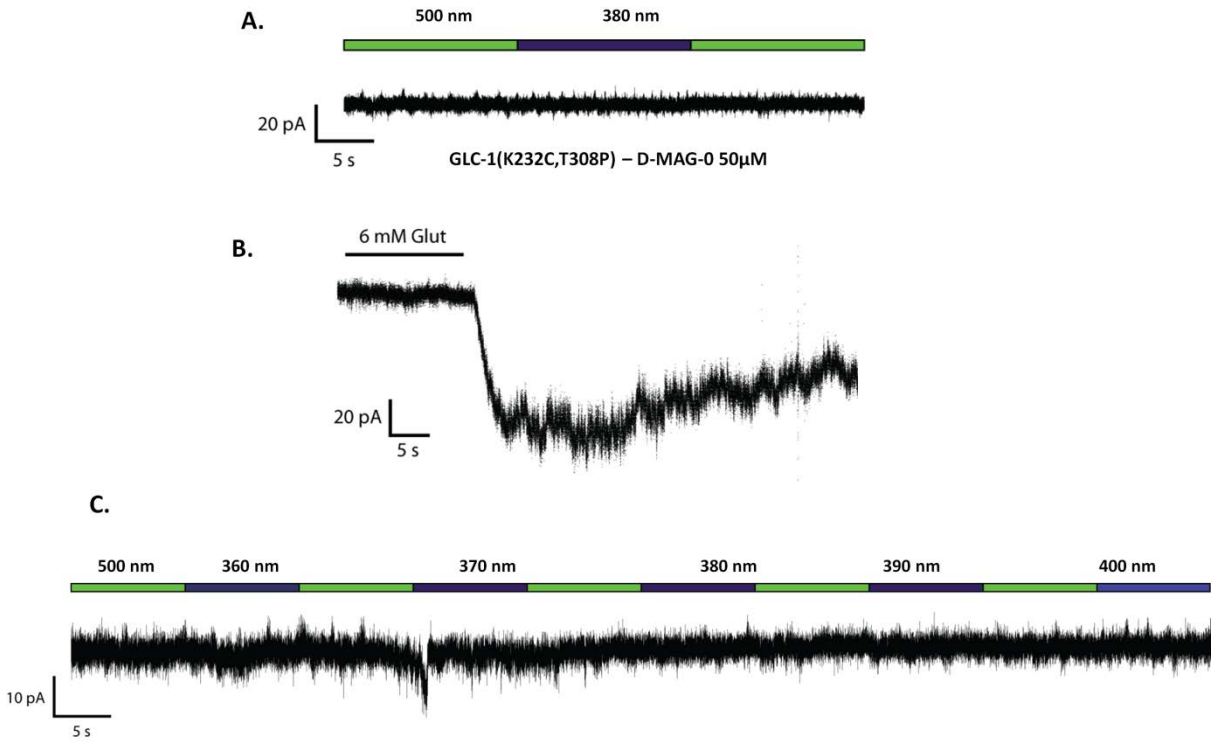

FIGURE R38: **A.** Whole cell patch clamp electrophysiology response of HEK 293 cell transfected with GLC-1(K232C, T308P) incubated with 50 µM D-MAG-0 and subjected to 500-380-500 nm light illumination. **B.** Current response of the same cell perfused with 6 mM Glutamate in the bath. **C.** Response to different wavelengths of light (360-370-380-390-400 nm) with alternating 500 nm illumination. Experiments performed in collaboration with Arunas Damijonaitis.

In parallel, the possibility of developing GLC-1 as a heterologous optogenetic hyperpolarizing tool in *C.elegans* was explored. To this end, GLC-1 was expressed in BWMs since they provide an easy readout as muscle hyperpolarization would lead to relaxation and consequent elongation of body length. In the first step, GLC-1 tagged with YFP in its M3-M4 loop was expressed in BWMs using *myo-3* promoter at three different concentrations (10, 2, and 1 ng/µl). At 1 ng/µl, membranous expression can be seen while at higher concentrations, the tendency to form aggregates is visible (**Figure R39**).

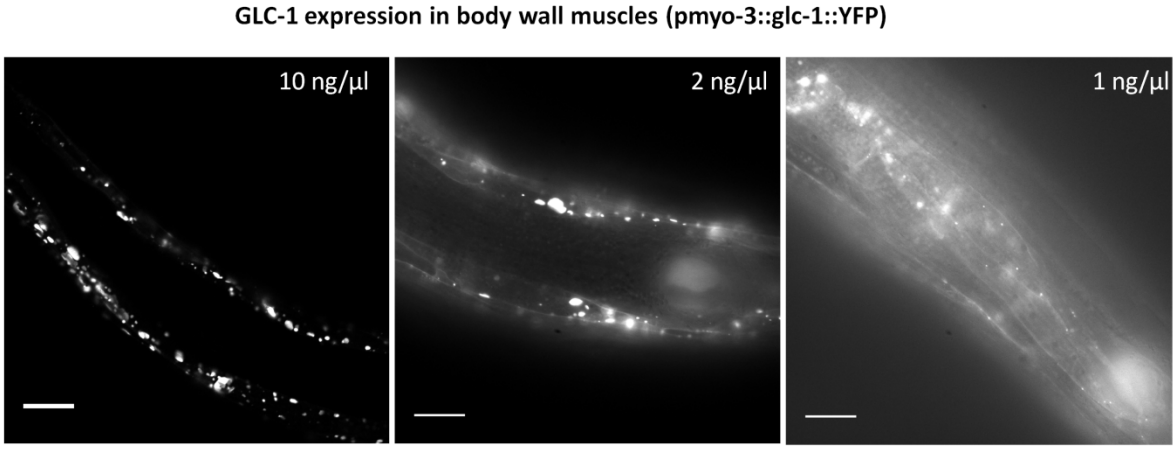

FIGURE R39: Fluorescent micrographs of *C. elegans* BWMs expressing GLC-1 tagged with YFP in the M3-M4 loop injected at three different concentrations-10,2,1ng/µl. Scale bar 20 µm.

3.6 Implementation of light-activated N-AChR (Li-N-AChR) in *C. elegans*

The two nAChRs at the *C. elegans* NMJ - N-AChR (ACR-16 homo-pentamer) and L-AChR (hetero-pentamer comprising of UNC-29, UNC-38, UNC-63, LEV-1, LEV-8) (Gottschalk et al. 2005; Touroutine et al. 2005) seem to be involved in different facets of physiology as loss of ACR-16 eliminates majority of the current at NMJ while the animals do not have a strong behavioural phenotype. On the other hand, loss of L-AChR leaves the animals highly uncoordinated in locomotion while the currents are largely unaltered (**Figure R40**). To better understand the in-vivo role of ACR-16 at the NMJ and in general in the locomotion behaviour of *C. elegans,* the PTL approach to obtain a Li-N-AChR is highly suitable as an acute, specific activation of the Li-N-AChR can reveal particular effects that are unlikely to be compensated for by the L-AChR.

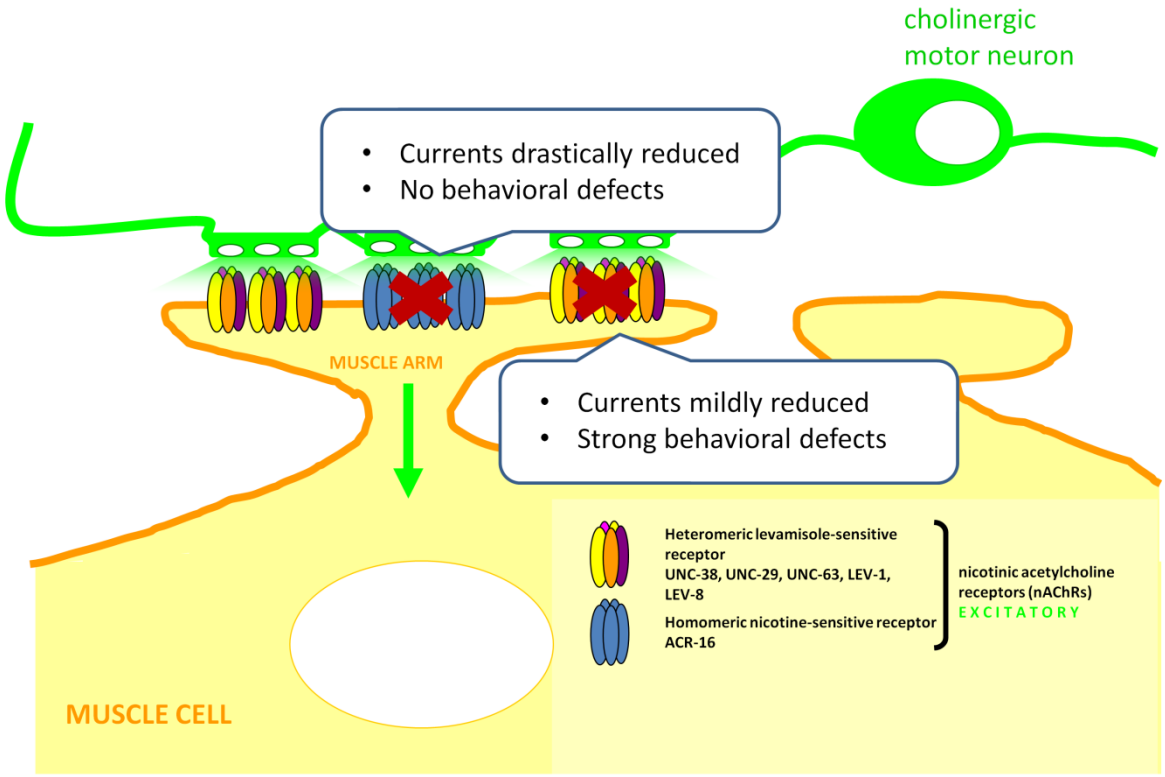

FIGURE R40: Scheme of cholinergic neurotransmission at the *C. elegans* NMJ.

3.6.1 The PTL - maleimide-azobenzene-carbachol (MAC)

The PTL to be used for Li-N-AChR was designed to comprise of maleimide, azobenzene and an agonist of acetylcholine called as carbachol (in collaboration with Prof. Dirk Trauner). Carbachol also known as carbamyl choline is a positively charged quarternary ammonium compound that stimulates both muscarinic and nicotinic receptors and is not readily hydrolysed by acetylcholinesterase (Rosenberry et al. 2008). Acetylcholinesterase is a very fast enzyme operating at a rate approaching that of a diffusion-controlled reaction and is responsible for rapid hydrolysis of acetylcholine thereby terminating neurotransmission at cholinergic synapses (Dvir et al. 2010). This resistance towards hydrolysis by acetylcholinesterase makes carbachol more suitable than the endogenous agonist acetylcholine as the PTL, since the acetylcholine moiety may be rapidly hydrolysed before having the opportunity to covalently bind to the cysteine introduced in the ACR-16 and be able to photo-activate it.

Although carbachol has been shown to work as cholinergic agonist, however its ability to bind and activate nAChRs at the *C. elegans* NMJ remains to be verified. To this end, Dr. Jana Liewald from our lab performed whole cell patch clamp electrophysiology recordings on dissected preparations of the *C. elegans* NMJ and measured current responses to application of 500 µM carbachol (**Figure R41**). The wildtype N2 worms responded with ~ 900 pA current response, animals carrying a non-functional mutant UNC-63 (core constituent of L-AChR) showed 500 pA response and worms with disabling mutations in both ACR-16 and UNC-63 did not elicit any response to carbachol. The current responses to carbachol make maleimide-azobenzene-carbachol (MAC) an ideal PTL to render ACR-16 photo-switchable.

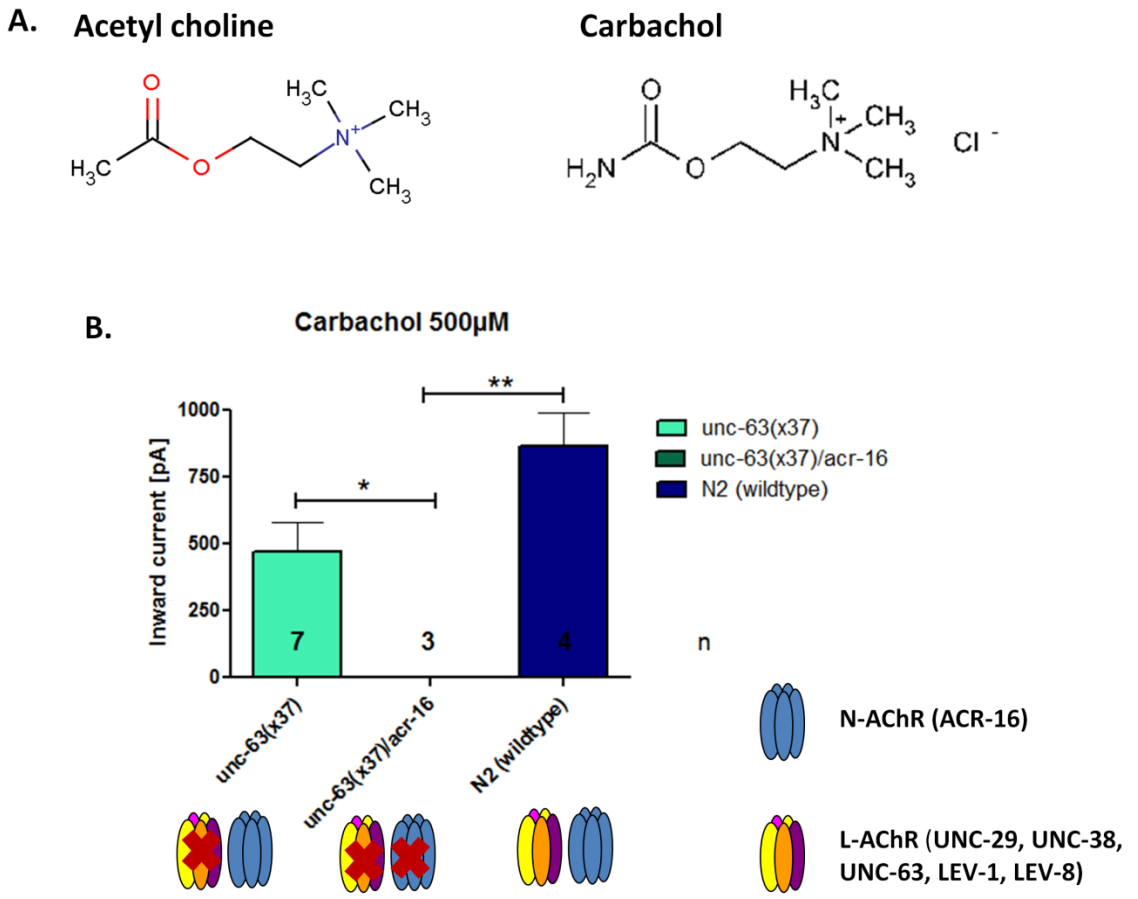

FIGURE R41: **A.** The structures of acetylcholine and carbachol. The acetoxy group with the ester bond subjected to hydrolysis is shown in red and the quarternary ammonium in blue. **B.** Peak inward current responses measured by Dr. Jana Liewald in whole cell patch clamp electrophysiology recordings on dissected preparations of N2 wildtype, *unc-63(x37)* and *unc-63(x37),acr-16(ok789)*. Statistically significant differences were tested using unpaired 2-tailed t-test (*** p<0.001, ** p<0.01, * p<0.05, ns p>0.05).

3.6.2 Introduction of cysteine mutations in ACR-16

For the 'PTL-ready' ACR-16, the cysteine introduction sites were chosen on the basis of previous modelling and docking studies on AChBP performed in the laboratory of Prof. Dirk Trauner (**Figure R42A**). Sequence alignment of AChBP and ACR-16 indicated the following residues as probable candidates for introduction of cysteine in ACR-16: THR49, HIS51, THR78, ASN80, SER131, THR132, and LEU134 (**Figure R42B**).

A.

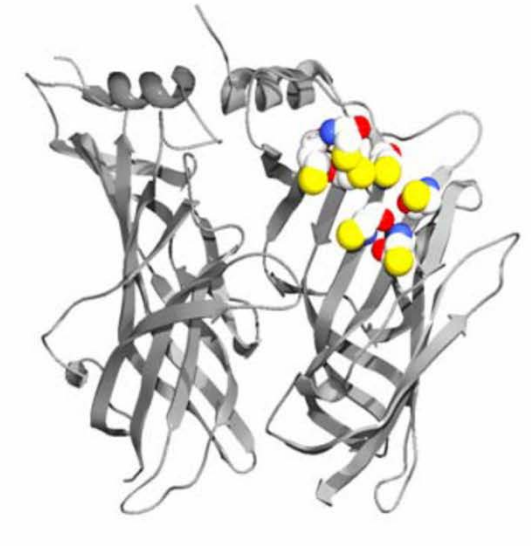

B.

	43 52	72 83	121 133
AChBP:	DRPV**A**V**S**VSL	WQQT**T**W**S**DRTLA	LARVV-**SD**G**E**VLYM
ACR-16:	SEPV**T**V**H**LKV	WLDY**T**W**N**DYNLV	TNMIVY**ST**G**L**VHWV

FIGURE R42: **A.** The candidate cysteine residues for PTL attachment modelled onto acetylcholine binding protein structure (PhD thesis, M Banghart, performed in the lab of Prof. Dirk Trauner, then at U. California, Berkeley). **B.** Sequence alignment of AChBP and ACR-16. Candidate cysteine mutant sites shown on AChBP in **A.** are indicated with blue arrows above the sequences.

3.6.3 Functional assessment of cysteine mutants using swimming assays and electrophysiology measurements

In liquid medium, *C. elegans* exhibits a dorso-ventrally alternating C-shaped body movement to achieve swimming locomotion. These thrashing movements can be used to quantify locomotion behaviour. *C. elegans* with loss of function mutation in *acr-16* have essentially wild type thrashing behaviour (Francis et al. 2005; Touroutine et al. 2005). Thus, to score a visible behavioural rescue phenotype for the cysteine mutants of ACR-16, fused to GFP, we expressed them in BWMs under the *myo-3* promoter in the double mutant background of *acr-16(ok689); unc-63(x37)* where the animals have a severely impaired thrashing behaviour. We first assessed the expression pattern to see if all proteins were produced and showed a comparable localization as the non-mutated ACR-16::GFP protein (**Figure R43)**.

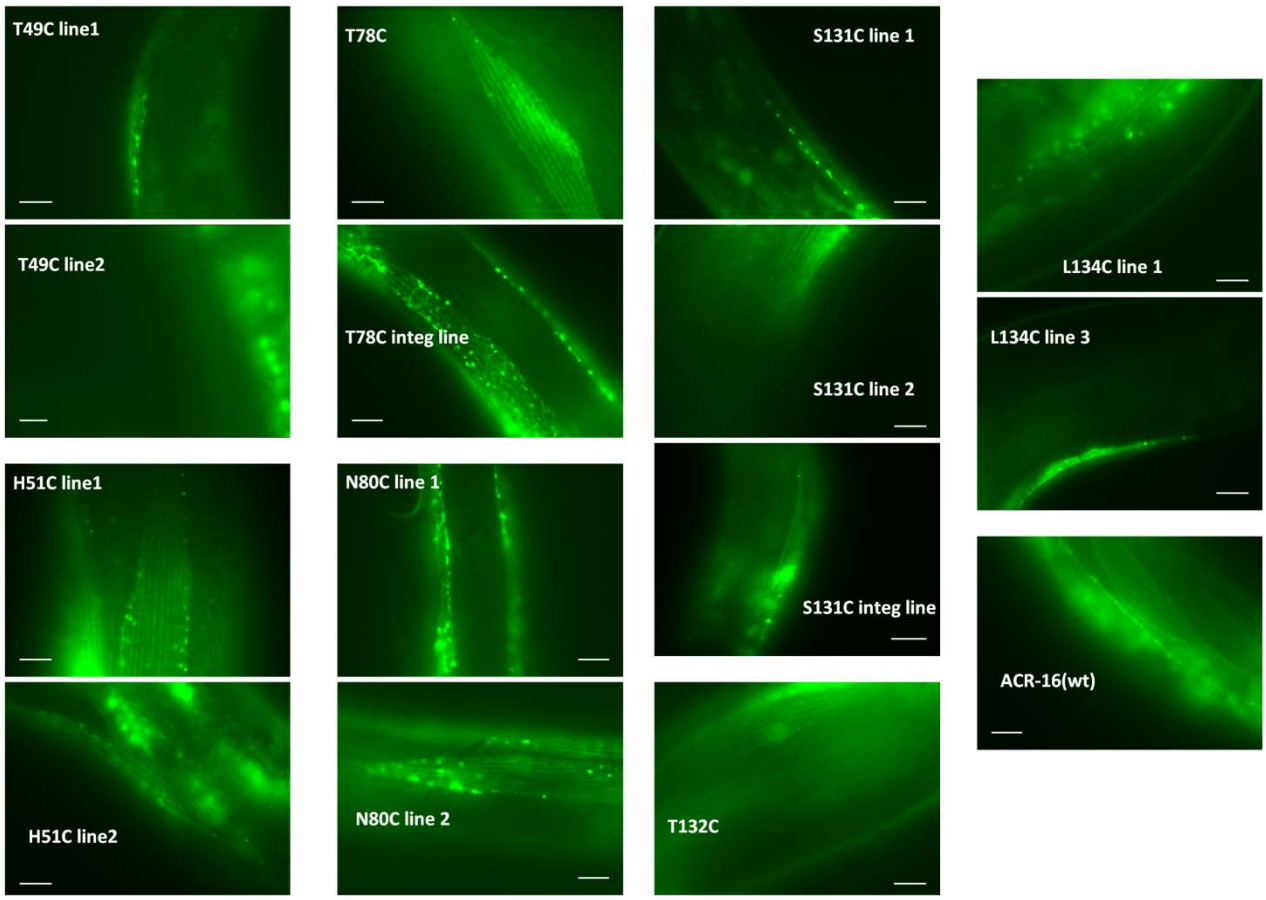

FIGURE R43: Fluorescent micrographs showing expression of the various cysteine mutants of ACR-16 tagged with GFP (inserted in the large cytosolic loop between TM1 and TM2 of the protein) expressed in BWMs in *acr-16 (ok689); unc-63(x37)* background. Scale bar 20 µm.

The swimming behaviour in terms of the number of thrashes executed by the worms per minute was assessed (**Figure R44**). The wildtype N2 worms performed ~115 thrashes/min which was matched by the *acr-16(ok789)* worms as had been reported earlier (Francis et al. 2005; Touroutine et al. 2005). *unc-63(x37)* worms thrashed ~70 times a minute while the worms carrying both *acr-16(ok789), unc-63(x37)* mutations were highly compromised in swimming, thrashing ~16 times a minute.

The transgenic worms expressing non-mutated ACR-16 (tagged with GFP in the cytosolic loop) in BWMs in the *acr-16(ok789), unc-63(x37)* background only partially rescued the loss of ACR-16, thrashing 55 times a minute. The loss of full rescue can

be ascribed to the fact that the GFP tagged subunits may not be able to make a completely functional ACR-16 homopentamer owing to steric conflicts. Also, the over-expression in muscles may lead to non-endogenous expression of ACR-16, which is natively localized to the muscle arms. This may affect normal muscle physiology and hence locomotion.

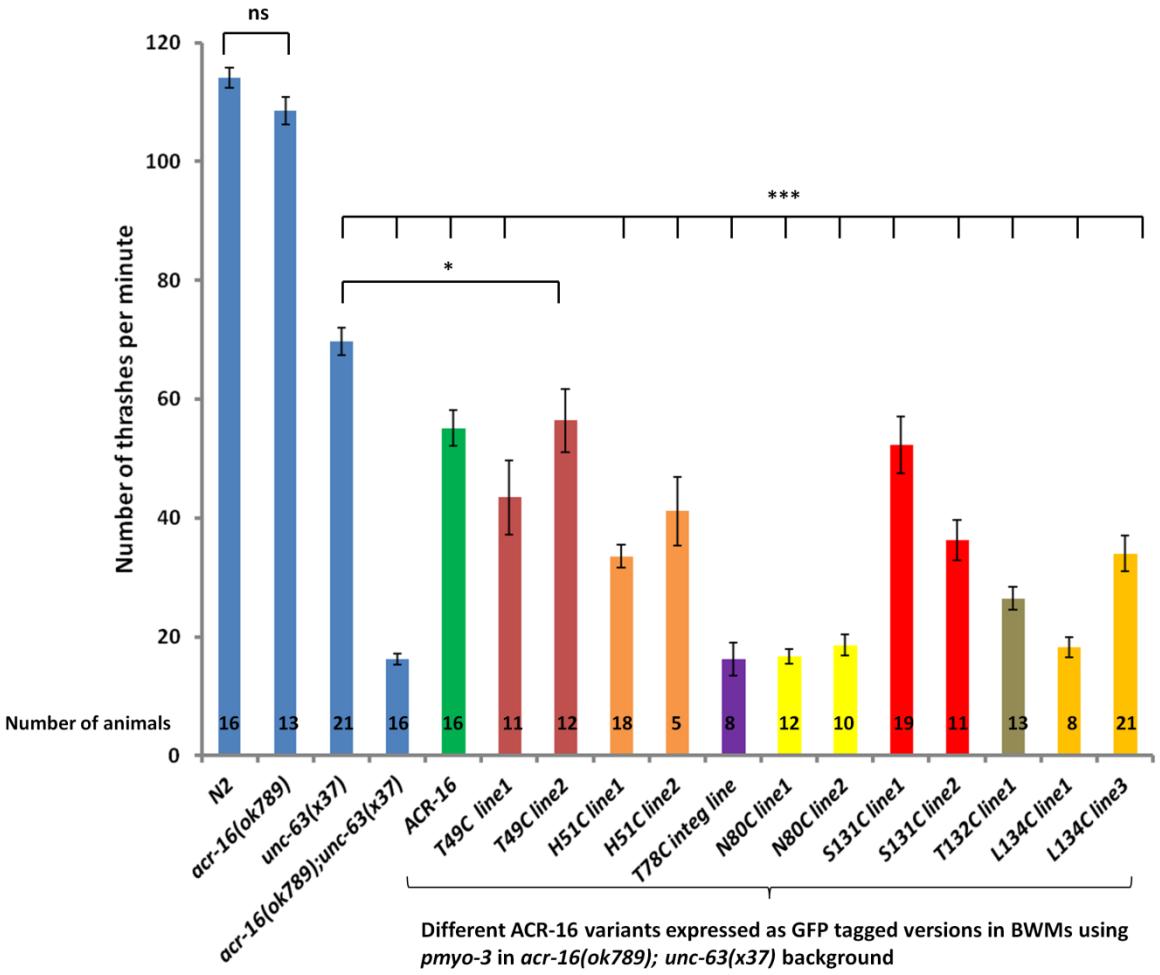

FIGURE R44: Swimming behaviour of *C. elegans* strains (wildtype N2; *acr-16(ok789); unc-63(x37)*; *acr-16(ok789),unc-63(x37),* non-mutated ACR-16::GFP and the different cysteine mutants in *acr-16(ok789),unc-63(x37)* background*)* as assessed by the number of thrashes swam per minute by the worms. The number of worms for which the thrashing rate was counted is shown in the figure. Statistical significance of the differences in the thrashing rate was tested using unpaired 2-tailed t-test (*** p<0.001, ** p<0.01, * p<0.05, not significant ns p>0.05).

The transgenic worms with T78C and N80C mutations in ACR-16 did not show a rescue for ACR-16 functionality. H51C, T132C, and L134C showed a moderate rescue of ACR-16 functionality. The transgenic worms with T49C and S131C mutations with the thrashing rates of about ~56 a minute were the most promising among all the mutations, with thrashing rates comparable to non-mutated ACR-16 (in *acr-16(ok789), unc-63(x37)* background) in thrashing rate.

The T78C mutation had been pursued first since the transgenic line with extrachromosomal array of ACR-16(T78C) expressed in BWMs in *acr-16(ok789), unc-63(x37)* background showed a minor contraction response to UV illumination upon incubation with Maleimide-Azobenzene-Acetylcholine (MAA; prior to the development of MAC). As a result, an integrated transgenic line was created so as to boost the expression of ACR-16(T78C) and the response properties. Unfortunately, the integrated line thrashed as poorly as the *acr-16(ok789), unc-63(x37)* double mutant indicating a non-functional ACR-16 as far as the thrashing behaviour was concerned.

Nonetheless, the T78C transgenic lines were subjected to carbachol exposure in whole cell patch clamp electrophysiology experiments performed by Dr. Jana Liewald (**Figure R45**). The transgenic line expressing wildtype ACR-16 in *acr-16(ok789), unc-63(x37)* showed almost N2 like inward current responses while the ACR-16(T78C) in *acr-16(ok789), unc-63(x37)* exhibited current responses smaller in magnitude almost comparable to *unc-63(x37)* and ACR-16(S131C) in *acr-16(ok789), unc-63(x37)* displayed relatively meagre peak inward currents of ~100pA.

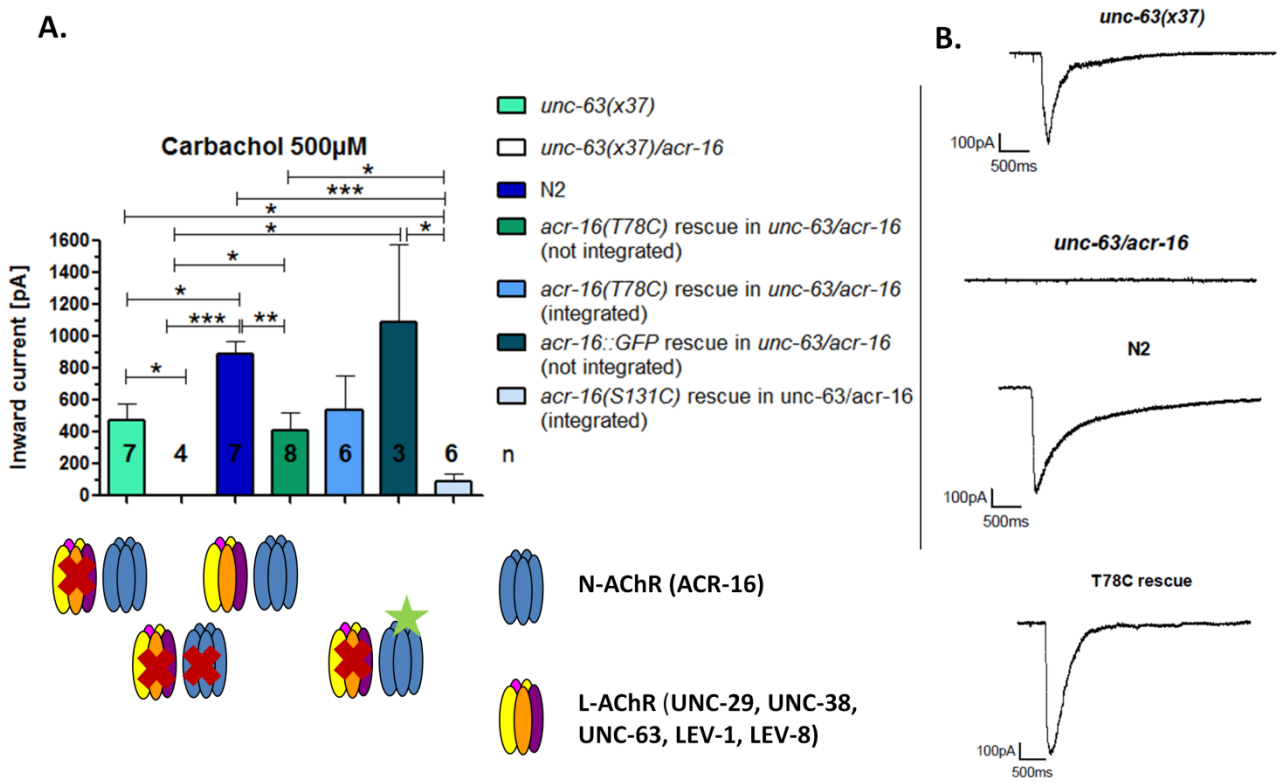

FIGURE R45: **A.** Peak inward current responses measured by Dr. Jana Liewald in whole cell patch clamp electrophysiology recordings on dissected preparation of N2 wildtype; *unc-63(x37)*; *unc-63(x37),acr-16(ok789);* wildtype ACR-16 and T78C and S131C cysteine mutants in *acr-16(ok789),unc-63(x37)* background in response to 500 µM carbachol application. Statistically significant differences were tested using unpaired 2-tailed t-test (*** p<0.001, ** p<0.01, * p<0.05, ns p>0.05). **B.** Representative traces of the corresponding inward current responses.

To check if T78C mutation allows for the PTL, MAC to bind and photoswitch ACR-16, the integrated ACR-16(T78C) in *acr-16(ok789), unc-63(x37)* transgenic line was prepared for whole cell patch clamp experiments (BWMs exposed), incubated with 100 µM MAC for 5 minutes and current responses were measured while illuminating the preparation with green(505 nm)-UV(385 nm)-green(505 nm) light (performed by Dr. Jana Liewald). Acute fast onset current response was observed upon switching to UV light (trans to cis shift of the PTL-MAC) indicating MAC rendered the ACR-16(T78C) photoswitchable. The magnitude of peak current response was relatively small (**Figure R46**).

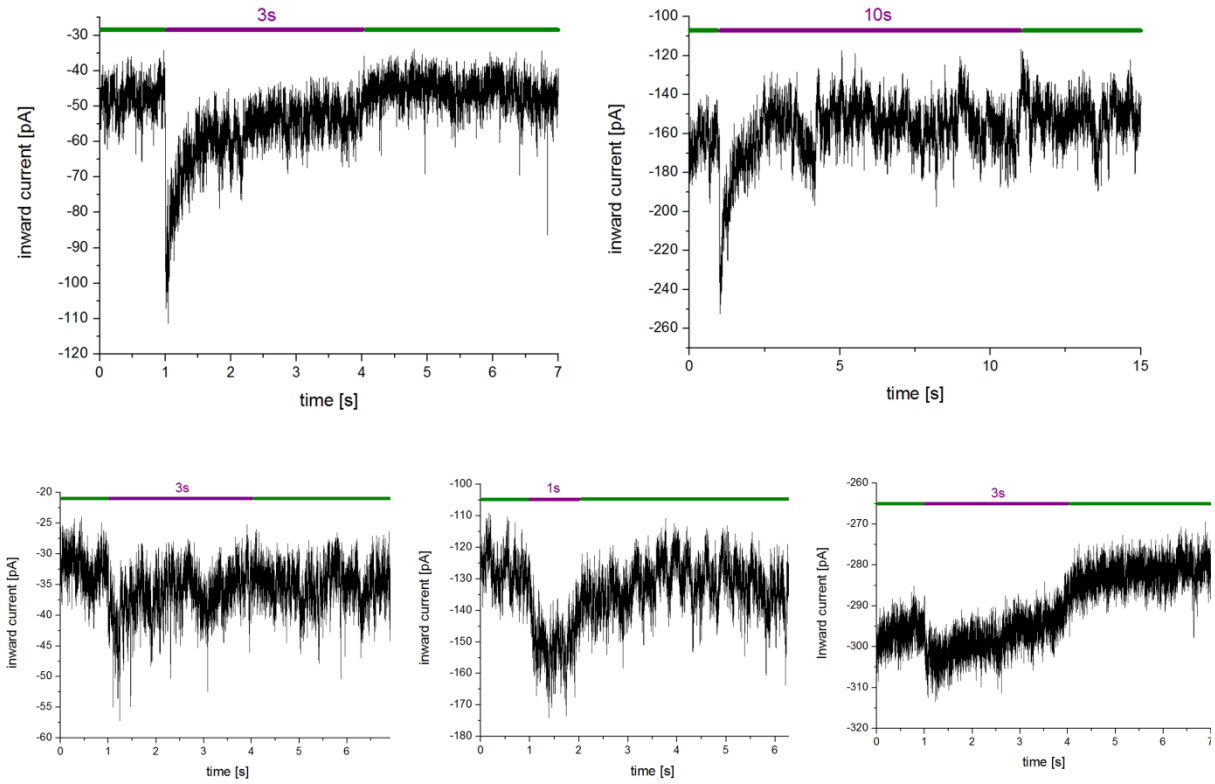

FIGURE R46: Representative whole-cell patch clamp recordings of the body wall muscle cells of *C. elegans* (integrated strain: ACR-16(T78C)::GFP expressing in BWMs in *acr-16(ok789),unc-63(x37)* background) with simultaneous green-UV-green wavelength photoswitching after incubation of the preparation with 100 µM MAC for 5 minutes. The traces in the upper panel come from the same cell. The illumination was done with the Prior LED system (505nm Prior LED 60x Objective: 10,3 mW/mm^2, 385nm Prior LED 60x Objective: 9,0 mW/mm^2).

Apart from the electrophysiological verification, the integrated ACR-16(T78C) in *acr-16(ok789); unc-63(x37)* transgenic line was incubated with 250 µM MAC and behaviour (contraction) was checked while illuminating the animals with green (505 nm) - UV (385 nm) - green (505 nm) light (**Figure R47A**). No UV light induced contraction could be observed in the ACR-16(T78C) expressing animals. The other cysteine mutants were also tested in the similar set up. While there was a contraction tendency (most pronounced with L134C), it could still be an attribute of the intrinsic UV avoidance of the animals (**Figure R47B**).

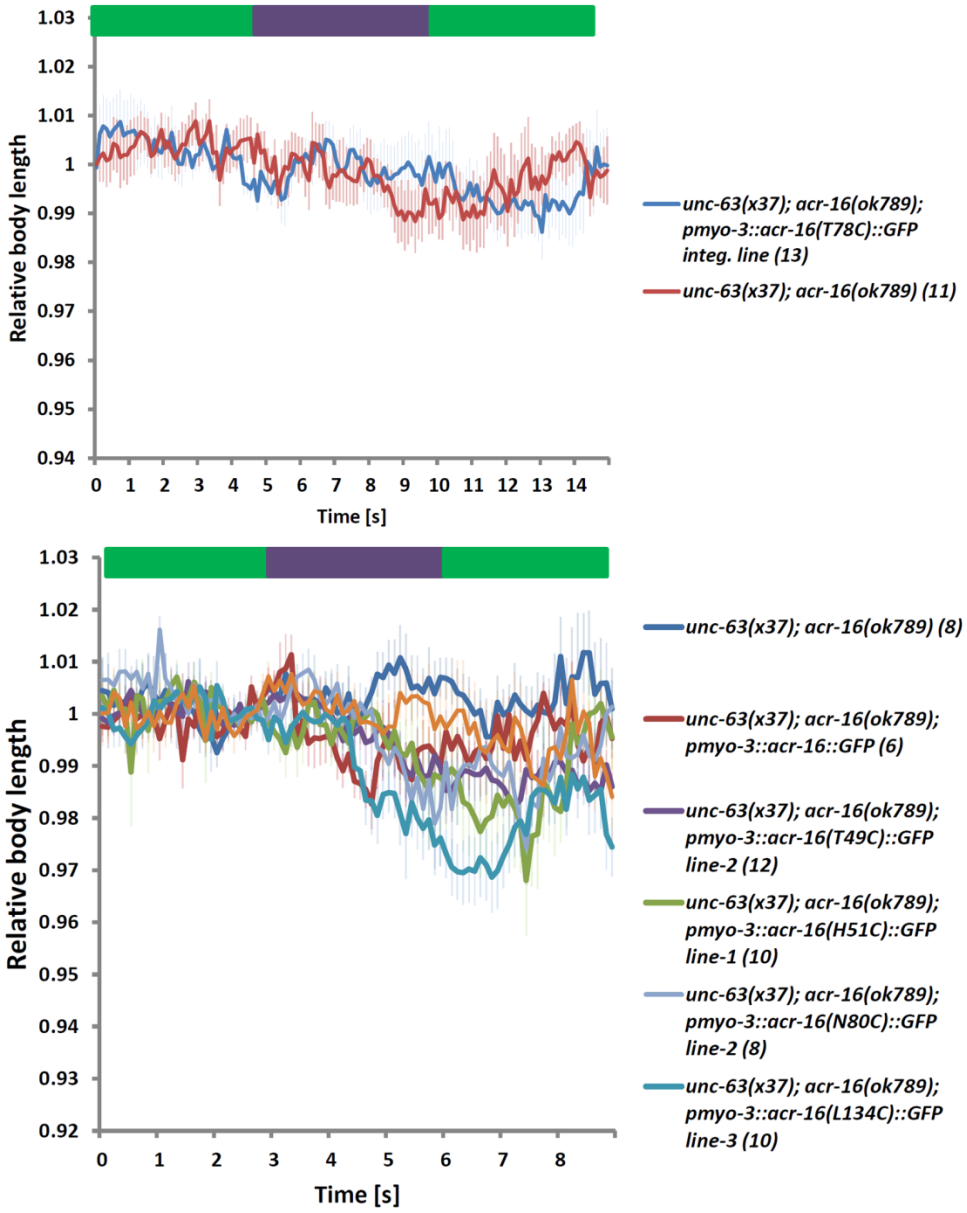

FIGURE R47: Body length measurement of worms incubated 250 µM MAC in 4% DMSO. Light intensity at 380nm: 3.13 mW/mm^2 and 505nm: 1.96 mW/mm^2. Green and violet bars represent green and UV illumination respectively using Prior LED system. The number of animals represented as n in the parentheses and error bar represent SEM.

3.7 Implementation of non-tethered Photochromic ligands (PCLs) - AzoCholine and PhoDAG in *C. elegans*

The synthetic photoswitches used in photo-pharmacological approaches can either be covalently attached to their target (photoswitchable tethered ligands, PTLs) or be tightly bound through noncovalent interactions (photochromic ligands). Both classes of photoswitchable ligands have been applied to a wide variety of biological targets (Fehrentz et al. 2011; Broichhagen et al. 2015b). In case of PCLs, the freely diffusible ligand carries a photoswitchable side chain, usually an azobenzene moiety, that can be toggled between two configurations - on and off states, thereby triggering the desired biological effect in a reversible fashion.

Here, two such PCLs were implemented in *C.elegans.* The first is AzoCholine, a photo-switchable agonist for neuronal α7 nAChRs and the second is a light sensitive second messenger lipid diacylglycerol featuring a photo-switchable acyl chain termed as PhoDAG (photo-switchable diacylglycerol). Both these compounds were synthesized in the laboratory of Prof. Dirk Trauner and were validated in other systems like cultured mammalian cells before being implemented in worms.

3.7.1 AzoCholine evokes light-dependent perturbation of swimming behavior in *C. elegans*

Azocholine enabled optical control of heterologously expressed α7 nAChR/glycine receptor chimera in HEK293T cells. Upon blue light illumination (440 nm), the trans-state of azocholine could evoke currents in the electrophysiology patch clamp experiments. This process was found to be reversible by alternating the switching wavelengths (360 and 440 nm) over many cycles (results from Arunas Damijonaitis in the lab of Prof. Dirk Trauner).

We aimed to see if Azocholine could evoke any light-dependent perturbations in the behaviour of *C.elegans.* For this, we investigated the swimming (or thrashing) behaviour of *lite-1* animals in the presence and absence of Azocholine upon switching between UV and blue light illumination. Thrashing of *lite-1* animals in physiological buffer (M9) was not affected when switching from UV (350 nm) to blue (470 nm) light illumination. However, upon supplementing the buffer with 1 mM AzoCholine, the worms displayed a sharp decline in thrashing frequency upon switching from UV to blue light. The thrashing frequency recovered during the

second half of the blue light pulse and was fully back to baseline after switching to UV light (**Figure R48A**).

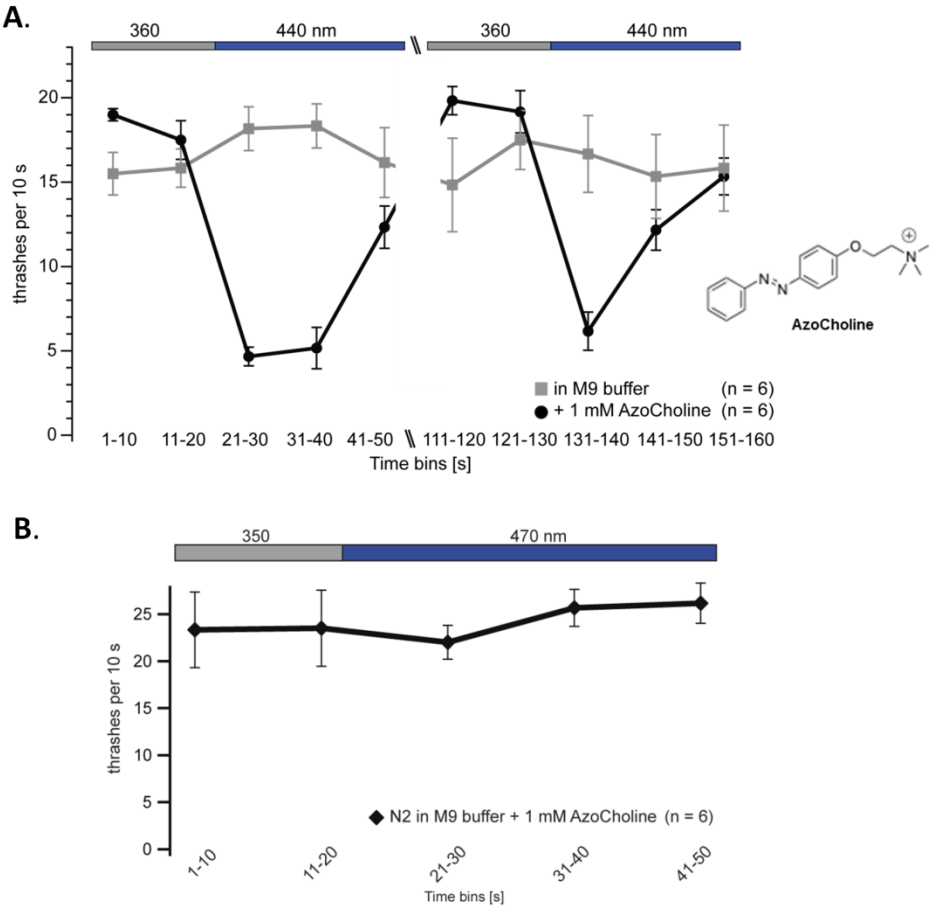

FIGURE R48: Quantification of C. elegans swimming cycles. Nematodes (**A.** *lite-1* worms and **B.** N2 worms) swimming in M9 buffer (gray boxes) and in M9 with AzoCholine (1 mM, black circles) (n = 6, mean with S.E.M.). When switching from UV (350 nm) to blue (470 nm) light (bar), trans-AzoCholine induces stopping/freezing behavior in *lite-1* animals.

This indicates that AzoCholine in the *trans*-state may have activated nAChRs in the motor nervous system, possibly evoking inhibition, e.g., through GABAergic motoneurons. Surprisingly, when tested on wild-type worms (strain N2, with normal LITE-1 function) the immediate drop in the thrashing rate due to the light-effect of AzoCholine photoswitching did not appear (**Figure R48B**). This unexpected result is difficult to rationalize given the complexity of the system. However, it can be envisaged that the UV pre-exposure leads to a LITE-1-dependent signal that could put wild-type animals into a state where AzoCholine cannot exert full effects.

Possible scenarios could be that the general excitability of the motor system is reduced or AChRs are modified such that they desensitize more readily upon AzoCholine binding. Since AzoCholine has been shown to be specific for α7 nAChRs in mammalian cells, the observed effects in *C. elegans* are likely affected via nAChRs. However, the putative target receptor activated by AzoCholine in *C. elegans* remains to be identified.

3.7.2 PhoDAG-3 evokes light-dependent hypersensitivity to Aldicarb, an acetylcholinesterase inhibitor in C. elegans.

Elevated levels of the second messenger lipid diacylglycerol (DAG) induce downstream signaling events which include the translocation of C1 domain-containing proteins toward the plasma membrane. Photoactivated DAGs (PhoDAGs) were shown to promote the translocation of C1 domains containing proteins towards the plasma membrane upon a flash of UV-A light. This effect was reversed after the termination of photostimulation or by irradiation with blue light (results from James Frank in the lab of Prof. Dirk Trauner). We set out to test PhoDAG in *C. elegans* employing an assay used for analysis of synaptic transmission as described below.

C. elegans has been used extensively to study mechanisms of synaptic transmission (Bargmann 1998). In a wild-type animal, the neurotransmitter acetylcholine released from cholinergic motor neurons activates postsynaptic cholinergic receptors of the body-wall muscles leading to the contraction of the muscles (Rand 2007). A widely used assay to study chemical transmission at the *C. elegans* neuromuscular junction is the Aldicarb sensitivity assay (Mahoney et al. 2006). Aldicarb is an acetylcholinesterase inhibitor used commonly as a nematicide. Acetylcholinesterase, found in the synaptic cleft, catalyzes the hydrolysis of acetylcholine, thereby eliminating acetylcholine from the synapse. In the presence of aldicarb, acetylcholine accumulates in the synaptic cleft leading to the over-activation of cholinergic receptors, muscle hyper-contraction and paralysis. Conditions wherein there is an excess release of acetylcholine from the pre-synaptic terminal lead to a phenotype of hypersensitivity to aldicarb in a time-course assay whereas in the case of deficient acetylcholine release or dysfunctional post synaptic receptor machinery, aldicarb resistance is observed. In order to distinguish between pre-synaptic versus post-synaptic defects leading to altered aldicarb sensitivity, a levamisole-induced paralysis assay can be employed (Lewis et al. 1980). Levamisole is a cholinergic

receptor agonist that activates a class of acetylcholine receptors in the muscle cells of *C. elegans*, and thus specifically reports on post-synaptic defects. In the presence of levamisole, wild-type worms and worms with mutations resulting in gain or loss of function of presynaptic genes generally exhibit a similar rate of paralysis.

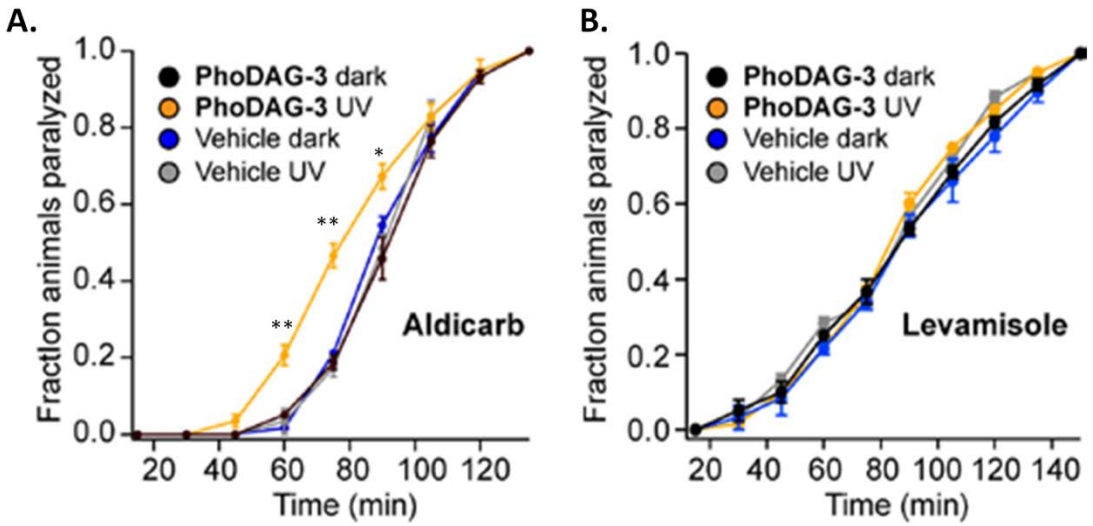

FIGURE R49: **A.** *cis*-PhoDAG-3 (1 mM) increased the rate of aldicarb-induced (1 mM) paralysis in *Caenorhabditis elegans* (n = 3 experiments, 20 animals each) when compared to animals exposed to *trans*-PhoDAG-3 (black). The paralysis rate was not affected by UV-A irradiation alone (blue, gray). *cis*-PhoDAG-3 (1 mM) did not affect the rate of levamisole-induced (0.1 mM) paralysis in *C. elegans* (n = 3 experiments, 20 animals each) when compared to animals exposed to *trans*-PhoDAG-3 (black). The paralysis rate was not affected by UV-A irradiation alone (blue, gray). The values depicted are mean with S.E.M. and statistical significance is denoted as * $p<0.05$, ** $p<0.01$ (unpaired t test).

Upon activation with UV light, animals cultivated in the presence of 1 mM PhoDAG-3 showed faster onset of paralysis and hypersensitivity to aldicarb as compared to the animals cultivated only with ethanol (vehicle) (**Figure R49A**). Moreover, the animals cultivated in the presence of PhoDAG-3 but not exposed to the UV light did not show any hypersensitivity to aldicarb. The hypersensitivity to aldicarb observed in the presence of activated PhoDAG-3 can be attributed to increased acetylcholine release from the cholinergic neurons, an effect possibly caused due to the increased activation of UNC-13, a diacylglycerol-binding pre-synaptic protein and mediator of synaptic vesicle priming (Lackner et al. 1999).

Animals grown in the absence or presence of PhoDAG-3 upon application of UV light show similar rates of paralysis in time course based levamisole induced paralysis

assays (**Figure R49B**). This excludes the possibility that the aldicarb hypersensitivity phenotype observed in animals treated with PhoDAG-3 is due to effects on the post synaptic acetylcholine receptor machinery or signalling pathways in the muscle, thereby substantiating the observation that PhoDAG-3 enhances the synaptic output due to increased transmitter release at the neuro-muscular junction of *Caenorhabditis elegans* in a light-dependent manner.

4. DISCUSSION

Since the 2005 publications of the implementation of single component optogenetics with microbal opsins (ChR2) in neurons (Boyden et al. 2005) and in an intact animal (*C. elegans*) to trigger coordinated behavior (Nagel et al. 2005), the last 10 years have witnessed a tremendous growth of optogenetics driven neuroscience research which is now making a visible impact also in the realm of cell biology (**Figure D1**).

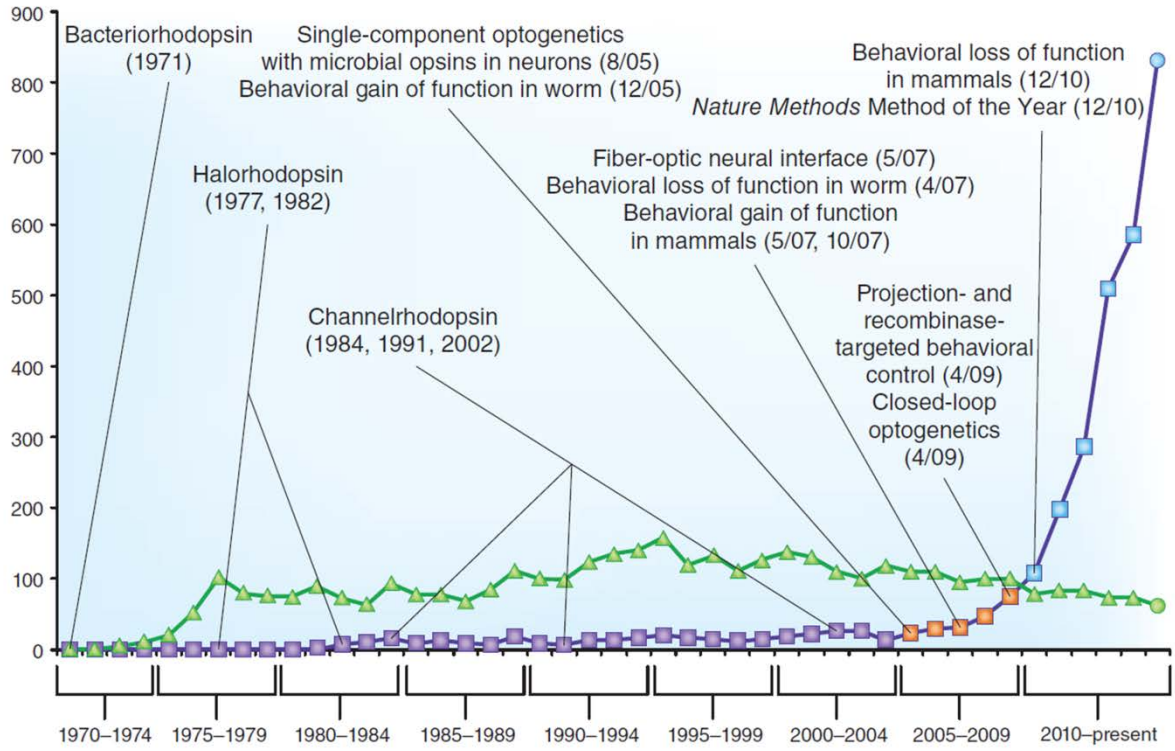

FIGURE D1: Publication timeline for microbial opsins and optogenetics as seen from the number of PubMed entries over the last 45 years. Shown are papers in Pubmed searchable by bacteriorhodopsin (triangles); halorhodopsin, channelrhodopsin or variations of optogenetics (squares). The year of publication of seminal papers in the field indicated in the parenthesis (From Deisseroth 2015).

Since these early reports, a variety of optogenetic tools have been established in *C. elegans*. These include a number of variants of ChR2 which have different properties that are useful for specific applications (Liu et al. 2009; Schultheis et al. 2011b; Schultheis et al. 2011a; Erbguth et al. 2012; Watanabe et al. 2013) as well as outward-directed proton pumps as inhibitory rhodopsins (Husson et al. 2012b) and

together have been used to dissect neural circuits underlying behaviour (Husson et al. 2013; Fang-yen et al. 2015). The inability of these microbial rhodopsins to allow for sub-cellular signalling control as well as endogenous receptor control reflect some of their biggest drawbacks. Through this thesis, it was attempted to address these problems by developing and implementing novel optogenetic tools in *C. elegans* - two light activated guanylyl cyclases (BeCyclOp and bPGC) to modify cGMP mediated signalling as well as attempts towards rendering endogenous *C. elegans* receptors GLR-3/-6, ACR-16, GLC-1 light switchable and to understand their biological function *in-vivo.*

4.1 Implementation of bPGC in *C. elegans* muscle cells and sensory neurons

Light activation of bPGC expressed in muscle cells along with TAX-2 and TAX-4 caused a relatively slower and much less pronounced contraction as compared to BeCyclOp (~ 10% peak contraction with the contraction on rate of ~350 ms for BeCyclOp vs 3% peak contraction achieved ~10 s after the onset of illumination for bPGC). This can be explained by the differences in the biophysical characteristics of the two cyclases described in the section above.

Interestingly, expression of cAMP generating bPAC along with TAX-2/-4 in BWMs evoked a stronger and fast onset contraction response as compared to bPGC, though the magnitude of peak contraction (4-6%) was still lower than what was observed with BeCyclOp. This surprising finding can be explained by the fact that the TAX-2/-4 channel, though low, indeed does possess affinity also for cAMP. The EC_{50} values of TAX-2/-4 for cGMP and cAMP are 8.4 and ≥300 µM, respectively (Komatsu et al. 1999). Coupled to that, bPAC is highly efficient in producing cAMP (L/D ratio of about ~350) (Ryu et al. 2010) and it can be envisaged that bPAC produces large amounts of cAMP very rapidly so as to partially activate TAX-2/-4 leading to depolarization of muscle cells and contraction.

Expression and activation of bPGC in the sensory neuron ASJ led to a partial suppression of the constitutive entry into the dauer larval state in *daf-11* mutants. The cGMP produced due to the continuous activation of bPGC was sufficient to overcome the absence of DAF-11in ASJ and allow the animals to enter the normal life cycle proceeding to adulthood. Though significant, the level of suppression

achieved was not high. This can be explained by low efficiency of cGMP production by bPGC. Also, the experiment was difficult to reproduce afterwards. This may be due to the dark activity of bPGC, non-specificity towards cAMP generation upon activation of bPGC for longer periods which may alter the physiology of the neurons, and *daf-11(m84)* mutants which are sensitive to mild variations in external conditions like temperature etc. as (Vowels and Thomas 1994).

The activation of bPGC in BAG and AWC did not evoke the desired behavioral responses primarily owing to low levels of cGMP produced with activation of bPGC. Longer illumination times could possibly evoke responses for BAG experiments as bPGC is relatively slow in generating cGMP but the intrinsic photo-avoidance response may very well mask the transient slowing response. Also for BAG, the *gcy-31* promoter was used to achieve the expression of bPGC instead of the *flp-17* promoter which was previously used (Zimmer et al. 2009). The reason for this choice was that *flp-17* is known to have expression in pharyngeal neuron M5 and faint or variable expression in an extra pair of cells in the head, apart from BAG (Kim and Li 2004), though for BeCyclOp, expression was observed only in BAG. For bPGC activation in AWC, the transgenic animals showed a tendency to have an increased number of reversals at the two lower light intensities tested (0.15 mW mm^{-2} and 0.013 mW mm^{-2}), however non-significant. This could be because of insufficient amounts of cGMP being generated during the 2 minute illumination period leading to only a partial depolarization of AWC (via TAX-2/-4), which may not be sufficent to relay the signal to the downstream neurons in the circuit affecting the reversal behaviour. The extent of depolarization matters in case of *C. elegans* neurons as they do not fire all or none action potentials but rather show graded potentials.

Though BeCyclOp is a superior light activated guanylyl cycase in terms of speed and magnitude of cGMP generation, bPGC could find applications wherein slow gradual increase in [cGMP] is desired over the course of several minutes or is deemed to be sufficient. Recently, bPGC was implemented in DAF-11 expressing neurons (ASI, ASJ, ASK) in *C. elegans* and shown to alter the cGMP dependent process of water sensation in worms (Wang et al. 2016).

4.2 Optogenetic manipulation of cGMP mediated signaling using BeCyclOp

BeGC1, the microbial rhodopsin of the fungus *Blastocladiella emersonii* has been shown to function as a phototaxis photoreceptor in the zoospores of the fungus which use cGMP and retinal for photo-orientation (Silverman 1976; Saranak and Foster 1997; Avelar et al. 2014). Furthermore, sequence analysis had shown that the rhodopsin domain is directly connected to a putative guanylyl cyclase domain through a 46–amino acid residue linker. Intriguingly, this molecule possesses no kinase homology domain, which in other membrane-bound guanylyl cyclases connects the cyclase domain to their trans-membrane helices (Biswas et al. 2009).

This is also the first instance among photoreceptor transduction cascades known so far wherein the function of a light-absorbing rhodopsin and cyclase is merged into a single molecule, without the requirement for an intermediary transducer module.

In this thesis, we show that BeGC1 functions as a directly light-activated guanylyl cyclase, hence we aptly renamed to BeCyclOp (guanylyl cyclase opsin from *B. emersonii*). We introduced this protein into *C. elegans* muscle cells (along with the CNG channel TAX-2/-4) and oxygen sensory neurons and assessed its potential as an optogenetic tool. It is shown that both the cell types could be photoactivated, and macroscopic behaviours were rapidly induced, making BeCyclOp a new optogenetic tool for specific cGMP manipulation in live animals.

The implementation of BeCyclOp in *C. elegans* was complemented by a collaboration with the lab of Georg Nagel (University of Würzburg), who analysed its properties in *Xenopus* oocytes and provided the biophysical insight into the functioning of CyclOp (Gao et al. 2015). In a parallel study, the protein was also characterized by the Hegemann and Oertner labs (Scheib et al. 2015). The biophysical properties of BeCyclOp as determined by the Nagel (Gao et al. 2015), Hegemann and Oertner labs (Scheib et al. 2015) are discussed in the following section, which are crucial to the understanding of the protein and its future application as an optogenetic tool in other cell types and model organisms.

4.2.1 Biophysical characterization of BeCyclOp

The transmembrane helix prediction of BeCyclOp reveals the presence of an extra N-terminal transmembrane helix, unlike any other known rhodopsin which are all 7-TM proteins. The absence of a signal peptide and the bimolecular fluorescence complementation experiment wherein strong cytoplasmic fluorescence was observed with a split YFP tag on the N and C-termini of BeCyclOp (Gao et al. 2015) indicate cytoplasmic localization of both BeCyclOp termini. This makes it the first finding of an N terminus of any rhodopsin being intracellular.

Based on studies on CyclOp-containing membranes from oocytes, it could be shown that BeCyclOp has a very high ratio of light versus dark activity (L/D) of 5000. Importantly, BeGC1 was found to be inactive in the dark. Previously the highest L/D ratio (300) was reported for the light activated adenylyl cyclase bPAC (Stierl et al. 2011). Fusion of YFP to the C terminus or truncation of the N-terminus resulted in higher dark activity and lower light-induced cGMP production indicating that the N and C termini are crucial for the tight light regulation of the guanylyl cyclase activity of BeCyclOp.

BeCyclOp has a typical broad rhodopsin action spectrum with a maximum at 530nm. The time constant for light activation of the guanylyl cyclase is expected to be faster than 1 ms while the inactivation time constant upon light-off was found to be ~ 320 ms. This is faster than what is reported for previously described adenylyl cyclases bPAC and mPAC (20 and 10 s, respectively (Stierl et al. 2011; Raffelberg et al. 2013)) endowing BeCyclOp with not only good optogenetic ON, but also OFF control. The half maximal activation intensity ($K_{0.5}$) for BeCyclOp was found to be 0.055 mW mm^{-2} while for bPAC and mPAC is 4 µW mm^{-2} and 6 µW mm^{-2}, respectively (Stierl et al. 2011; Raffelberg et al. 2013). The larger $K_{0.5}$ value for BeCyclOp indicates a faster photocycle as compared to bPAC and mPAC.

BeCyclOp did not have detectable adenylyl cyclase activity in oocytes, suggesting that it has a high selectivity for GTP. The experiments with *C. elegans* extracts also showed that BeCyclOp is significantly more specific for cGMP as compared to cAMP. The absorption wavelength, kinetic properties and light sensitivity of BeCyclOp are amenable to further tuning to suit experimental demands, an advantage of rhodopsins over flavin based photoreceptor domains. This can be envisaged to be achieved using rational mutagenesis or using retinal analogues

(Saranak and Foster 1997; Berndt et al. 2009; Bamann et al. 2010; AzimiHashemi et al. 2014). ChR2 was altered to allow long-term manipulation at low light intensities. The mutation of the residue cysteine 128 to serine (C128S) in ChR2 significantly delays the closing time of the channel, resulting in a larger proportion of channels in the open state. Similar effects were observed for the D156A mutant and C128S; D156A double mutant (Bamann et al. 2010; Yizhar et al. 2011). This effectively reduces the light intensity required to achieve activation, and both these effects allow long term stimulation of cells (even for hours) without the need for continuous intense blue light illumination that would be deleterious. As with wild-type ChR2, this variant can be switched off by yellow or green light (Berndt et al. 2009; Schultheis et al. 2011b). Similar approach could be adopted with BeCyclOp to generate a 'step-function' BeCyclOp. Like channelrhodopsins, BeCyclOp can be activated repetitively which is crucial for reproducible optical stimulation.

4.2.2 Implementation of BeCyclOp in *C. elegans* muscle cells and sensory neurons

BeCyclOp generated cGMP in *C. elegans* muscle cells, which could be photodepolarized when the TAX-2/4 CNG channel was co-expressed. The extent of photodepolarization and hence the muscle contraction was more pronounced with green as compared to blue illumination highlighting the excitation maximum of BeCyclOp. Likely due to low phosphodiesterase activity in BWM cells, cGMP levels may be persistently increased by BeCyclOp activation. The TAX-2/-4 channel is gated open and close based on the binding of the cGMP (Komatsu et al. 1999). In the background of low phosphodiesterase activity in BWM cells, the BeCyclOp activation leads to a prolonged cGMP increase which keeps the TAX-2/-4 channel open until the cGMP is cleared off or the channel desensitizes.

Due to the built-in signal amplification through second messenger generation, the combination of BeCyclOp/TAX-2/TAX-4 can also be used as multi-component optogenetic depolarizing tool, though the requirement for co-expression of three genes makes this less versatile than ChR2. In cases where the respective cell types lack or have low levels of endogenous phosphodiesterases and the signal turns off slowly, BeCyclOp may be combined with the recently described red light activated phosphodiesterase, LAPD (Gasser et al. 2014) to have a bimodal control over cGMP

levels in the cell. This may be complicated by the fact that LAPD, in its dark adapted state, also absorbs in the blue wavelength range, thereby making independent activation of light activated cyclases (bPGC and BeCyclOp) and LAPD difficult to achieve. It has also been shown to be activated potently by broad spectrum white light. The chromophore for LAPD is biliverdin, which is a product of heme catabolism, resulting from the breakdown of the heme moiety by heme oxygenase (Freitas, Alves-Filho et al. 2006). Since there is no known homologue of heme oxygenase in *C. elegans*, biliverdin like ATR has to be supplied exogenously *in C. elegans.* However, its low solubility in ethanol prompts the usage of organic solvents like DMSO for administration, which may interfere with the behaviour even at low concentrations.

The maximum utility for BeCyclOp as an optogenetic tool resides in its implementation in cell types that intrinsically signal via cGMP. The most important among such cell types are the sensory neurons which widely use guanylyl cylases to relay primary sensory signals to downstream cellular machinery (e.g. protein kinase G or CNG channels) that encodes this information for a signal output. The output of a sensory neuron is the neurotransmitter release which can be addressed by optogenetics using ChR2. However, the intracellular encoding of the primary sensory signal via cGMP cannot be addressed using ChR2. This is crucial to understand the encoding process itself which can be a control point for signal amplification or modulation. Thus, BeCyclOp in such cells would enable control over intracellular encoding events in cGMP mediated signalling.

In the *C. elegans* O_2 and CO_2 sensing BAG neurons, photostimulation of ChR2 resulted in a transient decrease in locomotion speed (Zimmer et al. 2009 and Figure R7 C), and we could re-capitulate the same behavioural effects with the activation of BeCyclOp in BAG neurons. The slowed locomotion is consistent with the natural BAG response to a drop or rise in oxygen or carbon dioxide concentration, respectively. The difference between the ChR2 and BeCyclOp mediated effect is: while ChR2 merely depolarizes the BAG neurons, BeCyclOp leads to the slowing response by triggering the cGMP second messenger upstream of the intrinsic CNG channel TAX-2/4. The cGMP signal may be utilized by the BAG neurons for the modulation of the sensory input.

For both BeCyclOp and ChR2, despite ongoing photostimulation, the slowing was transient and a quick 'recovery' of the slowing response was observed. This may hint towards desensitization or even habituation. Using ChR2, it is not possible to determine if this desensitization is due to modulation of cGMP signalling in BAG, or it is affected at BAG output synapses, or in downstream neuronal networks that cause and execute slowing (BAG is pre-synaptic to the backward command interneurons AVA and AVE with 2 and 6 synapses between them, respectively). Using BeCyclOp, it can likely be concluded that as far as the BAG mediated slowing behaviour is concerned, the desensitization response must occur downstream of BAG depolarization and prolonged stimulation of BAG does not result in modulation of intrinsic cGMP signalling. However, one can also argue that the extremely high cGMP concentrations achieved by the activation of BeCyclOp may be sufficient to override any such intrinsic mechanism, leading to the same macroscopic behavioural phenotype as observed with ChR2. In an ideal case scenario, one may compare cGMP levels in BAG induced by oxygen exposure to those evoked by BeCyclOp or Ca^{2+} levels in BAG and in downstream cells evoked by ChR2 and BeCyclOp activation to directly compare their effects.

4.3 Comparison of the two PGCs - bPGC and BeCyclOp using experiments in *Xenopus* oocytes.

BlgC or bPGC (*Beggiatoa* photoactivated guanylyl cyclase) is a mutated version of Beggiatoa sp. bacterial light-activated adenylyl cyclase (BlaC), with specificity for GTP (Ryu et al. 2010). Recently, bPGC has been implemented as 'erectile optogenetic stimulator' (EROS) in male rats to evoke penile erection following transfection and blue illumination of the *Corpora cavernosa* (Kim et al. 2015).

The efficiency of cGMP production of the two guanylyl cyclases- BeCyclOp and bPGC- was compared by the Nagel lab (Gao et al. 2015) by measuring the cGMP concentrations in the extracts prepared from *Xenopus* oocytes expressing the cyclases and illuminated with blue light (illumination conditions favoring the bPGC with its action spectrum maximum in the blue range and its higher light sensitivity). It was found that bPGC is much less active than BeCyclOp, with 50 times lower cGMP production at bPGC favouring illumination conditions.

Moreover, BeCyclOp was highly specific for cGMP production with no cAMP detected, while bPGC generated at least one cAMP for every four cGMP molecules under *in-vivo* conditions or one cAMP per seven cGMP molecules under *in-vitro* conditions (Ryu et al. 2010). BeCyclOp had a turnover of 17 cGMP per second while for bPGC, it was estimated to be 0.2 cGMP per second. Furthermore, bPGC has substantial dark activity while BeCyclOp has an undetectable activity in darkness (Gao et al. 2015; Scheib et al. 2015) making BeCyclOp a much better suited tool for optogenetic applications. To sum it up, BeCyclOp is highly active and specific for cGMP production, and it has the highest so far reported dynamic range for any photoactivated nucleotidyl cyclase with ratio of light versus dark activity (L/D) of 5000. The superior features of BeCyclOp over bPGC may be attributable to the fact that BeCyclOp (or BeGC1) is a naturally evolved light-triggered guanylyl cyclase playing a vital physiological role in the life-cycle of an aquatic fungus while bPGC is an artificial guanylyl cyclase generated by mutating three amino acid residues crucial for nucleotide specificity of an existing PAC.

4.4 Simultaneous optogenetic detection and generation of cGMP using WincG2 and light activated cyclases

WincG2 is a *C. elegans* codon optimized version of genetically encoded fluorescent cGMP sensor FlincG3 (Bhargava et al. 2013). In the absence of any cyclase activity, we observed a rapid drop of the fluorescence emission of WincG2 at the onset of blue light illumination. This rapid decline in intensity may hint towards an apparent 'photo-switching' or photo-bleaching to dim states. In two previous reports on FlincG (Batchelor et al. 2010; Bhargava et al. 2013), FlincG-transfected $HEK_{GC/PDE5}$ cells challenged with high concentrations of NO showed responses that "were sometimes followed by small, rapid undershoots" that may be reminescent of the rapid drop in fluorescence observed with WincG2. Also, like other cp-EGFP based biosensors, FlincG fluorescence is highly pH-dependent and pH induced artifacts during live imaging should be kept in mind (Nakai et al. 2001; Wang et al. 2008; Zhao et al. 2011; Bhargava et al. 2013). In experiments using FlincG-transfected $HEK_{GC/PDE5}$ cells as detectors for NO released from NMDA- stimulated brain slices, fluorescent undershoots were observed that were NO-independent (Bhargava et al. 2013) and

were attributed to transient acidifications caused by metabolic byproducts, notably lactate (Wood et al. 2011). The fluorescent photo-switching may have a similar origin.

WincG2 can detect fast and slow rises in cGMP (i.e. without bleaching) as is evident from the fluorescence rise over minutes time scale in case of bPGC as compared to BeCyclOp where the rise was more pronounced (three-fold) and is extremely fast (in milli-second time range) and saturates soon after. The kinetics and magnitude of fluorescence changes of WincG2 aptly reflect the underlying cGMP dynamics brought about by two different guanylyl cyclases - BeCyclOp being much more rapid and efficient in cGMP generation as compared to bPGC. Notably, WincG2 fluorescence emission intensity also increased in the presence of cAMP in response to the activation of bPAC. It is plausible that it may be due to an extremely large surge in cAMP concentration that saturates WincG2, despite it being 230 times more sensitive to cGMP (Bhargava et al. 2013) or even due to some minute background cGMP production by bPAC. To resolve this specificity issue, it may be worthwhile to express very little amounts of the cyclases and thereafter compare the WincG2 response.

4.5 Opto-chemical genetic approaches to understand native receptor function - studies on implementing LiGluR, Li-ACR-16 and Li-GLC-1 in *C. elegans*

PTL based photoswitches, that site-specifically attach covalently to a protein of interest and permit reversible modulation via photoisomerization of a light-sensitive moiety (like azobenzene), have been quite successful in rendering native 'blind' receptors photo-switchable (Fehrentz et al. 2011; Kramer et al. 2013; Broichhagen and Trauner 2014). The covalent attachment of the PTL to the target protein enables complete subtype specificity compared to soluble pharmacological agents, and the genetic targeting of proteins permits precise photocontrol of specific nodes within a neural circuit.

For the *in-vivo* application of PTLs, thiol-maleimide bio-conjugation has been employed as it only requires the introduction of an accessible cysteine that is

relatively slow to oxidize following surface-expression of the protein. This has the advantage that the receptor structure is not too much altered as compared to its native state, whereas a fusion protein might disrupt the function and expression of the target receptor. A potential shortcoming of cysteine labelling is the inherent instability of the maleimides and similar electrophiles in the aqueous, nucleophilic environments of animals and tissues, which could lead to non-selective labeling and destruction of the PTL. For example, maleimides may not be stable in the presence of serum albumin, which is known to have a highly reactive cysteine which evolved to inactivate electrophiles (Kratz 2008). In order to preserve the maleimide reactivity, it may be necessary to include a reducing agent, such as dithiothreitol or *tris*(2-carboxyethyl) phosphine. Apart from this, thiol-maleimide chemistry is limited to extracellular bioconjugation as high concentration of intracellular glutathione would rapidly inactivate the maleimide.

4.5.1 LiGluR in *C. elegans*

GFP tagged GLR-3(L409C) and GLR-6(H417C), when expressed in BWMs formed a functional glutamate receptor as could be demonstrated from electrophysiological recordings at the NMJ. This indicated that the cysteine mutations and C-terminal GFP tagging did not impair the glutamate gating of the receptor, though they may prevent the full response of the functional glutamate receptor. Importantly, MAG-1 incubation and subsequent photoswitching produced a small current response corresponding to the 'on' state (cis state of MAG-1) which suggests that in principle the LiGluR could be functionally re-constituted in *C. elegans*. However, in order to achieve more efficient photo-switching response, it may be required to perform a cysteine scanning for the GLR-3 and GLR-6 subunits to obtain more suitable sites for MAG conjugation.

The possibility of trying another *C. elegans* glutamate receptor homologous to iGluR6, namely GLR-4 can be explored. GLR-4 is a putative non-NMDA ionotropic glutamate receptor subunit possibly of the kainate subfamily, most closely related to GLR-3. *glr-4* is expressed in various sensory neurons and interneurons from embyrogenesis onward (Brockie et al. 2001a). *C. elegans* GLR-4 along with GLR-3 are identified as putative homologs to rat iGluR6 (Grik2) in the NCBI HomoloGene database. Furthermore, upon sequence alignment of GLR-3, GLR-4 and iGluR6 (**Figure D2**), a strong conservation of the leucine residue was found that when

mutated to cysteine rendered iGluR6 photoswitchable by MAG-1(L439C) (Volgraf et al. 2006).

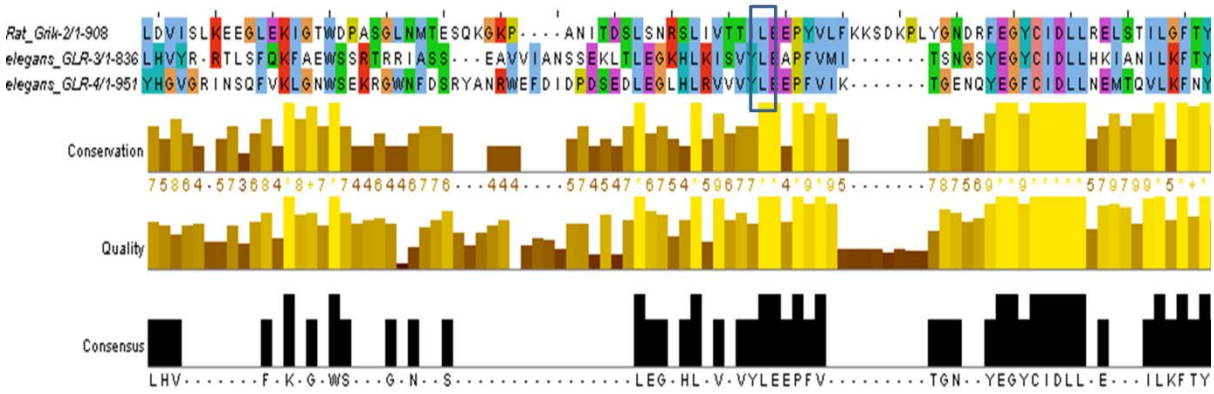

FIGURE D2: Sequence alignment of rat iGluR6 (Grik2), *C. elegans* GLR-3, GLR-4 using Clustal Omega (Sievers et al. 2011) with the boxed L439 residue of iGluR6 showing strong conservation with L409 of GLR-3 and L416 of GLR-4.

Furthermore, once a functional photo-switchable LiGluR has been identified in worms, it is desirable to have means to get sufficient amounts of the MAG and other PTLs inside the body past the relatively impermeable thick cuticle. This could be achieved by incubating worms with PTLs dissolved in solvents like methanol, ethanol, DMSO (at low concentrations so as to not alter normal physiology) to allow penetration of the compound inside the body apart from the intake by drinking. It has been reported that worms do not drink fluid while immersed and addition of dopamine significantly increases the amount of fluid consumed by drinking (Vidal-Gadea et al. 2012). This may have implications if PTLs are to make their way in through the drinking route while the worms are immersed in the PTL solution. Feeding the PTLs like ATR as for other microbial opsins may be an alternative but ATR after being ingested with the dietary microbes, being more hydrophobic may be able to cross through membranes and reach the desired site in sufficient amounts while PTLs like MAG which are relatively less hydrophobic may be quenched.

4.5.2 Li-GLC-1 in *C. elegans*

The available X-ray structure of GLC-1 (Hibbs and Gouaux 2011) presented an ideal opportunity to render it light switchable using the PTL approach. The docking studies with D-MAG-0 revealed several candidate cysteine sites of which L96C, Q230C, K232C were expressed in HEK 293 cells and checked with patch clamp electrophysiology. The L96C and Q230C mutants did not yield a current response upon glutamate application indicating the mutations dramatically impaired the functionality of GLC-1. It can also be envisaged that the introduced cysteines somehow impaired the native cysteine loop formation important for the channel function. The K232C mutation gave a robust glutamate response suggesting a functional GLC-1. However, it did not give any photo-currents with D-MAG-0 which indicates that the covalently attached MAG at K232C could not access the ligand binding pocket so as to gate the receptor. Moreover, the PCL version (D-AG-0) lacking the maleimide also could not make GLC-1 light switchable which hints towards the fact that the azobenzene-glutamate linker might not be of the right length so as to allow access of the glutamate moiety to the ligand binding site. This suggests that modifing the linker length might allow the compound a greater flexibility to access the binding site and thereby making a PTL that could render GLC-1 light activatable.

4.5.3 Li-ACR-16 in *C.elegans*

In order to achieve a light activated version of ACR-16, a new PTL with non-readily hydrolysed cholinergic agonist carbachol - MAC was developed. Carbachol could mimic acetylcholine responses on the *C.elegans* NMJ candidate indicating the PTL based on carbachol could potentially work if the correct cysteine attachment site was identified. Cysteine introduction sites were chosen based on the X-ray structure of an acetylcholine binding protein in complex with carbamylcholine (Celie et al. 2004) and the model of AC-5, a photoactivatable agonist docked into the Torpedo nAChR (Mourot et al. 2006).

The T78C mutation was the first to be tried since the residue is located on an antiparallel beta sheet in the subunit that faces the ligand-binding site which was identified as a potential region for PTL attachment. The patch clamp experiment with photoswitching performed on the NMJs of transgenic worms expressing ACR-16(T78C) (tagged with GFP in the cytosolic loop in an *acr-16, unc-63* mutant

background) showed inward currents with the PTL MAC upon UV illumination. This revealed that the receptor could indeed be photoswitched. However, in thrashing assays, the worms were phenotypically similar to *acr-16, unc-63* mutants indicating no functional rescue of ACR-16, hence these animals cannot be used to elucidate the in-*vivo* role of ACR-16. One of the reasons could be the gross over-expression of ACR-16 in an integrated transgenic strain all over the body wall muscle cells and not just at the synaptic sites. Moreover, ACR-16 forms homo-pentamers and even with GFP in the cytosolic loop, there could be steric conflicts among the subunits in the pentamer leading to reduction in the functionality of ACR-16. Also, the fact that all the subunits in the homo-pentamer carry the cysteine mutation as potential binding site to MAC may have implications in terms of formation of non-specific disulphide bridges and physical crowding at the extracellular ligand binding region.

Among a variety of other receptors (Broichhagen and Trauner 2014; Broichhagen et al. 2015b), mammalian neuronal nicotinic acetylcholine receptors (nAChRs) have also been subjected to optochemical control using PTL agonists and antagonists (Tochitsky et al. 2012). Heteromeric α3β4 and α4β2 nAChRs have been engineered with cysteine introduction in the β subunit (E61C) and have been shown to be activated or inhibited with deep-violet light using MAACh or another variant based on homocholine, MAHoCh, respectively. Using sequence alignment, it can be shown that the E61 is homologous to the T78 of ACR-16, corroborating with our electrophysiological findings that showed ACR-16(T78C) could be photo-switched with MAC (**Figure D3**).

```
ACR-16      -----MSVCTLLISCAILAAPTLGSLQERRLYEDLM--RNYNNLERPVANHSEPVTVHLK
Beta-4      MRGTP--LLLVSLFSLLQDGDCRLANAEEKLMDDLLNKTRYNNLIRPATSSSQLISIRLE
Beta-2      MAGHSNSMALFSFSLLWLCSGVLGTDTEERLVEHLLDPSRYNKLIRPATNGSELVTVQLM
                   :  . :      .    :  *.:* :.*:   .**:* **.:. *: ::::*

ACR-16      VALQQIIDVDEKNQVVYVNAWLDYTWNDYNLVWDKAEYGNITDVRFPAGKIWKPDVLLYN
Beta-4      LSLSQLISVNEREQIMTTSIWLKQEWTDYRLAWNSSCYEGVNILRIPAKRVWLPDIVLYN
Beta-2      VSLAQLISVHEREQIMTTNVWLTQEWEDYRLTWKPEDFDNMKKVRLPSKHIWLPDVVLYN
            ::* *:*.*.*::*:: .. **   * **.*.*.   :  :. :*:*: ::* **::***

ACR-16      SVDTNFDSTYQTNMIVYSTGLVHWVPPGIFKISCKIDIQWFPFDEQKCFFKFGSWTYDGY
Beta-4      NADGTYEVSVYTNVIVRSNGSIQWLPPAIYKSACKIEVKHFPFDQQNCTLKFRSWTYDHT
Beta-2      NADGMYEVSFYSNAVVSYDGSIFWLPPAIYKSACKIEVKHFPFDQQNCTMKFRSWTYDRT
            ..*  :: :  :* :*   * : *:**.*:* :***::: ****:*:* :** *****
```

FIGURE D3: Sequence alignment of ACR-16, Rat β4 and β2 nAChR subunits used in Tochitsky et al. 2012 for Li-nAChR using Clustal Omega (Sievers et al. 2011). Underlined residues (T49, H51, T78,

N80, S131, T132, L134) are the residues in ACR-16 that have been mutated to have been expressed in *acr-16, unc-63* mutant background. Highlighted residues (yellow and red) have been tested electrophysiologically in Tochitsky et al. 2012 as α3β4 and α4β2 nAChRs combinations. Yellow highlighted ones (E61, R113, S117(rat β4) corresponding to T78, Y130, L134 in *C. elegans* have shown photoswitchability with MAACh as cis-agonist. Red highlighted ones (S32, R34, T63, N115(rat β4) corresponding toT49, H51, N80, T132 in *C. elegans* did not show photoswitchability.

Apart from E61, R113 and S117(rat β4) have also shown photoswitchability with MAACh as cis-agonist (Tochitsky et al. 2012) which map onto Y130 and L134 in ACR-16, respectively. ACR-16(L134C) has been generated, produced a small response in the contraction assays with MAC but gave only a partial rescue in thrashing assays making it difficult to be used for the in-*vivo* analysis of ACR-16.The Y130 mutation in ACR-16 is yet to be explored.

An integrated line with ACR-16(S131C)::GFP gave small current responses to carbachol application at the NMJ, while it showed a rescue in thrashing behavioural assays. However, it may not be the correct candidate site as it is the next residue to Y130 (more probable to be correct being analogous to R113 in rat β4) and being on the β sheet, it will orient in the opposite direction relative to the Y130 and hence not in the right orientation for MAC binding and photo-switchability. Another mutation T49C also gave a rescue in the thrashing behaviour. It can be checked for potential photo-switching in NMJ electrophysiology experiments with MAC though the cysteine mutation of corresponding amino acids in the α3β4 (S32) could not evoke light induced currents with MAACh (Tochitsky et al. 2012).

As an outlook for the photo-switching T78C mutation or for that matter in general also, it may be better to work with single copy integrants using the MosSCI approach (Frøkjær-Jensen 2015) or even modifying the native ACR-16 using the CRISPR/Cas9 system (Dickinson and Goldstein 2016). Both these approaches will allow transgene expression at levels that approximate endogenous gene expression as well as expression in the germline. Furthermore, in the case of CRISPR/Cas9 mediated modification of ACR-16 in the genome, the protein will be expressed under its native promoter which will allow native expression dynamics as compared to the *myo-3* promoter.

It is also noteworthy that molecular dynamics simulations have facilitated the design of LiGluR (Numano et al. 2009) and LimGluR (Levitz et al. 2013) by helping to

identify the cysteine residue for attachment of the tethered ligands. Even for the development of LinAChR (Tochitsky et al. 2012), calculations of the conformational space that could be assessed by the photoswitches in their cis- and trans configurations were invaluable. MAACh and MAHoCh, photoswitchable tethered agonist and antagonist, respectively could be tethered to the same engineered cysteine residue (E61C) despite their functional differences. Though molecular docking studies correctly identified positions 61 and 117 as suitable sites of PTL attachment, the predicted site 63 turned out to be non-functional, which underlines the importance of functional screening as a complement to in silico approaches.

Finally, the goal of Li-ACR-16 is to use it to understand the in-*vivo* role of ACR-16 at the NMJ and possibly in locomotion or movement. First hints may come from a report (Jensen et al. 2012) wherein *acr-16* mutants were challenged with a more rigid substrate (worms were mounted on 5% agarose pads with 1 ml of polybead microspheres 0.625% (w/v) in M9 buffer) and it was found that their movement was diminished compared to WT controls (unlike the thrashing assays). This defect could be rescued by muscle-specific expression of ACR-16. Li-ACR-16, however, would enable an acute difference in locomotion behaviour or body posture to be evoked in the same animal, in contrast to testing two different populations of animals (as in the published experiment), provided that the Cys-mutated protein is fully functional.

4.6 Outlook

Light activated guanylyl cyclases will enable detailed mechanistic studies of sensory neuron function in *C. elegans* and other animals. The acute, non-invasive and spatiotemporally precise manipulation of cGMP levels using such cyclases especially BeCyclOp will be useful to study environmental stimuli like odorants, tastants, gases or temperature, the sensation of all of which is cGMP dependent in *C. elegans*. The intra-cellular control over [cGMP] will permit understanding of how cGMP signalling may contribute to the response of the respective sensory neurons and the behavioural outcomes of their activation.

BeCyclOp and bPGC may also be useful in other systems where cGMP signalling is involved, for example, in sperm swimming, erectile dysfunction, NO signalling, smooth muscle relaxation and animal vision (Lucas et al. 2000). Apart from the

applications in optogenetics for neuro and cell biologists, BeCyclOp also provides an interesting structure-function puzzle for biophysicists and spectroscopists to understand how the signal is relayed from the light sensing rhodopsin domain to the effector cyclase domain. An obvious line of research may attempt to reverse the specificity of BeCyclOp towards generating cAMP, thereby making a membrane-bound light-activated AC optogenetic tool which may mimic more closely the membrane originating cAMP signalling. Also, altering the functional properties (light sensitivity/photocycle dynamics, or absorption spectrum) of BeCyclOp by using retinal analogs may be assessed. Recently, a bPAC mutant with red-shifted absorbance and a decreased dark activity has been identified (Stierl et al. 2014). Transplanting the mutation to bPGC may confer similar properties which can make it highly valuable for long-term optogenetic experiments.

The first generation calcium sensors, the FRET based YC2.12 acted as a calcium sponge (Miyawaki et al. 1999) and hence affected the behavior of neurons in which they were expressed (Ferkey et al. 2007). The application of the cGMP sensor WincG2 in *C. elegans* sensory neurons will require investigation if it may alter the physiology and functionality of the neurons by acting as cGMP buffer. Mutations that increase the quantal yield of WincG2 (as has been done with GCaMP) may allow the reporter to be expressed at lower levels and thus reduce the probability of it interfering with cellular functions. The subcellular landscape of cGMP can also be probed using WincG2 by targeting it to specific microdomains. This could greatly facilitate the investigation of cGMP dynamics directly in functionally relevant subcellular compartments.

Photo-pharmacological approaches have been quite successful in employing synthetic photoswitches to optically control biological functions. For PTL based optochemical genetics, alternate ways to attach a PTL to a given protein can be explored. Apart from the classical electrophilic protein labeling with cysteine-reactive groups, such as maleimides or haloacetamides, chemically more stable electrophiles that only react with genetically encoded protein domains, such as SNAP-tags or CLIP-tags (Gautier et al. 2008; Broichhagen et al. 2015a) can be used. The introduction of unnatural amino acids via expansion of the genetic code and their labelling with in vivo-click chemistry is another alternate way to introduce PTLs. These potentially allow for milder labelling conditions as compared to maleimides.

Several variants of LiGluR such as a low affinity variant without activation by native glutamate, high and low calcium permeability variants as well as red shifted and 2-photon compatible MAGs have been developed (Carroll et al. 2015; Levitz et al. 2016). Similar transformations may also be seen for the other members of the PTL family. Finally, the realm of targets of photopharmacology is under continuous expansion; what started from ion channels, GPCRs, enzymes is now being extended to components of the cytoskeleton, as well as lipids as was demonstrated by the use of PhoDAG and it will continue to find more targets suitable to be put under optical control with photoswitchable ligands.

REFERENCES

Adamantidis A, Arber S, Bains JS, Bamberg E, Bonci A, Buzsáki G, Cardin JA, Costa RM, Dan Y, Goda Y, Graybiel AM, Häusser M, Hegemann P, Huguenard JR, Insel TR, Janak PH, Johnston D, Josselyn SA, Koch C, Kreitzer AC, Lüscher C, Malenka RC, Miesenböck G, Nagel G, Roska B, Schnitzer MJ, Shenoy K V, Soltesz I, Sternson SM, Tsien RW, Tsien RY, Turrigiano GG, Tye KM, Wilson RI (2015) Optogenetics: 10 years after ChR2 in neurons-views from the community. Nat Neurosci 18:1202–12. doi: 10.1038/nn.4106

Akerboom J, Carreras Calderón N, Tian L, Wabnig S, Prigge M, Tolö J, Gordus A, Orger MB, Severi KE, Macklin JJ, Patel R, Pulver SR, Wardill TJ, Fischer E, Schüler C, Chen T-W, Sarkisyan KS, Marvin JS, Bargmann CI, Kim DS, Kügler S, Lagnado L, Hegemann P, Gottschalk A, Schreiter ER, Looger LL (2013) Genetically encoded calcium indicators for multi-color neural activity imaging and combination with optogenetics. Front Mol Neurosci 6:2. doi: 10.3389/fnmol.2013.00002

Alkema MJ, Hunter-Ensor M, Ringstad N, Horvitz HR (2005) Tyramine Functions independently of octopamine in the Caenorhabditis elegans nervous system. Neuron 46:247–60. doi: 10.1016/j.neuron.2005.02.024

Almedom RB, Liewald JF, Hernando G, Schultheis C, Rayes D, Pan J, Schedletzky T, Hutter H, Bouzat C, Gottschalk A (2009) An ER-resident membrane protein complex regulates nicotinic acetylcholine receptor subunit composition at the synapse. EMBO J 28:2636–49. doi: 10.1038/emboj.2009.204

Althoff T, Hibbs RE, Banerjee S, Gouaux E (2014) X-ray structures of GluCl in apo states reveal a gating mechanism of Cys-loop receptors. Nature 512:333–7. doi: 10.1038/nature13669

Altun, Z.F. and Hall DH (2011) Nervous system, general description.

Avelar GM, Schumacher RI, Zaini P a., Leonard G, Richards T a., Gomes SL (2014) A Rhodopsin-Guanylyl cyclase gene fusion functions in visual perception in a fungus. Curr Biol 24:1234–1240. doi: 10.1016/j.cub.2014.04.009

Avery L (1993) Motor neuron M3 controls pharyngeal muscle relaxation timing in Caenorhabditis elegans. J Exp Biol 175:283–97.

AzimiHashemi N, Erbguth K, Vogt A, Riemensperger T, Rauch E, Woodmansee D, Nagpal J, Brauner M, Sheves M, Fiala A, Kattner L, Trauner D, Hegemann P, Gottschalk A, Liewald JF (2014) Synthetic retinal analogues modify the spectral and kinetic characteristics of microbial rhodopsin optogenetic tools. Nat Commun 5:5810. doi: 10.1038/ncomms6810

Bae G, Choi G (2008) Decoding of light signals by plant phytochromes and their interacting proteins. Annu Rev Plant Biol 59:281–311. doi: 10.1146/annurev.arplant.59.032607.092859

Bamann C, Gueta R, Kleinlogel S, Nagel G, Bamberg E (2010) Structural guidance of the photocycle of channelrhodopsin-2 by an interhelical hydrogen bond. Biochemistry 49:267–78. doi: 10.1021/bi901634p

Bamann C, Kirsch T, Nagel G, Bamberg E (2008) Spectral characteristics of the photocycle of channelrhodopsin-2 and its implication for channel function. J Mol Biol 375:686–94. doi: 10.1016/j.jmb.2007.10.072

Banghart M, Borges K, Isacoff E, Trauner D, Kramer RH (2004) Light-activated ion channels for remote control of neuronal firing. Nat Neurosci 7:1381–6. doi: 10.1038/nn1356

Bargmann CI (1998) Neurobiology of the Caenorhabditis elegans genome. Science 282:2028–33.

Bargmann CI (2006) Chemosensation in C. elegans. WormBook 1–29. doi: 10.1895/wormbook.1.123.1

Barrière A, Félix M-A (2014) Isolation of C. elegans and related nematodes. WormBook 1–19. doi: 10.1895/wormbook.1.115.2

Bartels E, Wassermann NH, Erlanger BF (1971) Photochromic activators of the acetylcholine receptor. Proc Natl Acad Sci U S A 68:1820–3.

Batchelor AM, Bartus K, Reynell C, Constantinou S, Halvey EJ, Held KF, Dostmann WR, Vernon J, Garthwaite J (2010) Exquisite sensitivity to subsecond, picomolar nitric oxide transients conferred on cells by guanylyl cyclase-coupled receptors. Proc Natl Acad Sci U S A 107:22060–5. doi: 10.1073/pnas.1013147107

Baylor D (1996) How photons start vision. Proc Natl Acad Sci U S A 93:560–5.

Berlin S, Szobota S, Reiner A, Carroll EC, Kienzler MA, Guyon A, Xiao T, Tauner D, Isacoff EY (2016) A family of photoswitchable NMDA receptors. Elife 5:e12040. doi: 10.7554/eLife.12040

Berndt A, Schoenenberger P, Mattis J, Tye KM, Deisseroth K, Hegemann P, Oertner TG (2011) High-efficiency channelrhodopsins for fast neuronal stimulation at low light levels. Proc Natl Acad Sci U S A 108:7595–7600. doi: 10.1073/pnas.1017210108

Berndt A, Yizhar O, Gunaydin LA, Hegemann P, Deisseroth K (2009) Bi-stable neural state switches. Nat Neurosci 12:229–234. doi: 10.1038/nn.2247

Bhargava Y, Hampden-Smith K, Chachlaki K, Wood KC, Vernon J, Allerston CK, Batchelor AM, Garthwaite J (2013) Improved genetically-encoded, FlincG-type fluorescent biosensors for neural cGMP imaging. Front Mol Neurosci 6:26. doi: 10.3389/fnmol.2013.00026

Birnby DA, Link EM, Vowels JJ, Tian H, Colacurcio PL, Thomas JH (2000) A transmembrane guanylyl cyclase (DAF-11) and Hsp90 (DAF-21) regulate a common set of chemosensory behaviors in caenorhabditis elegans. Genetics 155:85–104.

Biswas KH, Shenoy AR, Dutta A, Visweswariah SS (2009) The evolution of guanylyl cyclases as multidomain proteins: conserved features of kinase-cyclase domain fusions. J Mol Evol 68:587–602. doi: 10.1007/s00239-009-9242-5

Blomhoff R, Blomhoff HK (2006) Overview of retinoid metabolism and function. J Neurobiol 66:606–30. doi: 10.1002/neu.20242

Blumenthal T (2005) Trans-splicing and operons. WormBook 1–9. doi: 10.1895/wormbook.1.5.1

Bork P, Beckmann G (1993) The CUB Domain. J Mol Biol 231:539–545. doi: 10.1006/jmbi.1993.1305

Boulin T, Etchberger JF, Hobert O (2006) Reporter gene fusions. WormBook 1–23. doi: 10.1895/wormbook.1.106.1

Boulin T, Gielen M, Richmond JE, Williams DC, Paoletti P, Bessereau J-L (2008) Eight genes are required for functional reconstitution of the Caenorhabditis elegans levamisole-sensitive acetylcholine receptor. Proc Natl Acad Sci U S A 105:18590–5. doi: 10.1073/pnas.0806933105

Boyden ES (2011) A history of optogenetics: the development of tools for controlling brain circuits with light. F1000 Biol Rep 3:11. doi: 10.3410/B3-11

Boyden ES, Zhang F, Bamberg E, Nagel G, Deisseroth K (2005) Millisecond-timescale, genetically targeted optical control of neural activity. Nat Neurosci 8:1263–1268. doi: 10.1038/nn1525

Brejc K, van Dijk WJ, Klaassen R V, Schuurmans M, van Der Oost J, Smit AB, Sixma TK (2001) Crystal structure of an ACh-binding protein reveals the ligand-binding domain of nicotinic receptors. Nature 411:269–76. doi: 10.1038/35077011

Brenner S (1974) The genetics of Caenorhabditis elegans. Genetics 77:71–94.

Bretscher AJ, Busch KE, de Bono M (2008) A carbon dioxide avoidance behavior is integrated with responses to ambient oxygen and food in Caenorhabditis elegans. Proc Natl Acad Sci U S A 105:8044–9. doi: 10.1073/pnas.0707607105

Bretscher AJ, Kodama-Namba E, Busch KE, Murphy RJ, Soltesz Z, Laurent P, de Bono M (2011) Temperature, oxygen, and salt-sensing neurons in C. elegans are carbon dioxide sensors that control avoidance behavior. Neuron 69:1099–113. doi: 10.1016/j.neuron.2011.02.023

Brockie PJ, Madsen DM, Zheng Y, Mellem J, Maricq A V (2001a) Differential expression of glutamate receptor subunits in the nervous system of Caenorhabditis elegans and their regulation by the homeodomain protein UNC-42. J Neurosci 21:1510–22.

Brockie PJ, Maricq A V (2006) Ionotropic glutamate receptors: genetics, behavior and electrophysiology. WormBook 1–16. doi: 10.1895/wormbook.1.61.1

Brockie PJ, Mellem JE, Hills T, Madsen DM, Maricq A V (2001b) The C. elegans glutamate receptor subunit NMR-1 is required for slow NMDA-activated currents that regulate reversal frequency during locomotion. Neuron 31:617–30.

Broichhagen J, Damijonaitis A, Levitz J, Sokol KR, Leippe P, Konrad D, Isacoff EY, Trauner D (2015a) Orthogonal Optical Control of a G Protein-Coupled Receptor with a SNAP-Tethered Photochromic Ligand. ACS Cent Sci 1:383–93. doi: 10.1021/acscentsci.5b00260

Broichhagen J, Frank JA, Trauner D (2015b) A Roadmap to Success in Photopharmacology. Acc Chem Res 150623154001000. doi: 10.1021/acs.accounts.5b00129

Broichhagen J, Trauner D (2014) The in vivo chemistry of photoswitched tethered ligands. Curr Opin Chem Biol 21:121–127. doi: 10.1016/j.cbpa.2014.07.008

C. elegans Sequencing Consortium (1998) Genome sequence of the nematode C. elegans: a platform for investigating biology. Science 282:2012–8.

Callaway EM, Katz LC (1993) Photostimulation using caged glutamate reveals functional circuitry in

living brain slices. Proc Natl Acad Sci U S A 90:7661–5.

Canepari M, Nelson L, Papageorgiou G, Corrie JE, Ogden D (2001) Photochemical and pharmacological evaluation of 7-nitroindolinyl-and 4-methoxy-7-nitroindolinyl-amino acids as novel, fast caged neurotransmitters. J Neurosci Methods 112:29–42.

Caporale N, Kolstad KD, Lee T, Tochitsky I, Dalkara D, Trauner D, Kramer R, Dan Y, Isacoff EY, Flannery JG (2011) LiGluR restores visual responses in rodent models of inherited blindness. Mol Ther 19:1212–1219. doi: 10.1038/mt.2011.103

Carroll EC, Berlin S, Levitz J, Kienzler M a., Yuan Z, Madsen D, Larsen DS, Isacoff EY (2015) Two-photon brightness of azobenzene photoswitches designed for glutamate receptor optogenetics. Proc Natl Acad Sci 201416942. doi: 10.1073/pnas.1416942112

Celie PHN, van Rossum-Fikkert SE, van Dijk WJ, Brejc K, Smit AB, Sixma TK (2004) Nicotine and carbamylcholine binding to nicotinic acetylcholine receptors as studied in AChBP crystal structures. Neuron 41:907–14.

Chalasani SH, Chronis N, Tsunozaki M, Gray JM, Ramot D, Goodman MB, Bargmann CI (2007) Dissecting a circuit for olfactory behaviour in Caenorhabditis elegans. Nature 450:63–70. doi: 10.1038/nature06292

Chalfie M, Sulston JE, White JG, Southgate E, Thomson JN, Brenner S (1985) The neural circuit for touch sensitivity in Caenorhabditis elegans. J Neurosci 5:956–64.

Chalfie M, Tu Y, Euskirchen G, Ward WW, Prasher DC (1994) Green fluorescent protein as a marker for gene expression. Science 263:802–5.

Chambers JJ, Banghart MR, Trauner D, Kramer RH (2006) Light-induced depolarization of neurons using a modified Shaker K(+) channel and a molecular photoswitch. J Neurophysiol 96:2792–6. doi: 10.1152/jn.00318.2006

Chang AJ, Chronis N, Karow DS, Marletta MA, Bargmann CI (2006) A distributed chemosensory circuit for oxygen preference in C. elegans. PLoS Biol 4:e274. doi: 10.1371/journal.pbio.0040274

Chao MY, Komatsu H, Fukuto HS, Dionne HM, Hart AC (2004) Feeding status and serotonin rapidly and reversibly modulate a Caenorhabditis elegans chemosensory circuit. Proc Natl Acad Sci U S A 101:15512–7. doi: 10.1073/pnas.0403369101

Chen M, Tao Y, Lim J, Shaw A, Chory J (2005) Regulation of phytochrome B nuclear localization through light-dependent unmasking of nuclear-localization signals. Curr Biol 15:637–42. doi: 10.1016/j.cub.2005.02.028

Chen Z-H, Raffelberg S, Losi A, Schaap P, Gärtner W (2014) A cyanobacterial light activated adenylyl cyclase partially restores development of a Dictyostelium discoideum, adenylyl cyclase a null mutant. J Biotechnol 191:246–9. doi: 10.1016/j.jbiotec.2014.08.008

Cheung BHH, Arellano-Carbajal F, Rybicki I, de Bono M (2004) Soluble guanylate cyclases act in neurons exposed to the body fluid to promote C. elegans aggregation behavior. Curr Biol 14:1105–11. doi: 10.1016/j.cub.2004.06.027

Cheung BHH, Cohen M, Rogers C, Albayram O, de Bono M (2005) Experience-dependent modulation of C. elegans behavior by ambient oxygen. Curr Biol 15:905–17. doi: 10.1016/j.cub.2005.04.017

Chow BY, Han X, Dobry AS, Qian X, Chuong AS, Li M, Henninger M a, Belfort GM, Lin Y, Monahan PE, Boyden ES (2010) High-performance genetically targetable optical neural silencing by light-driven proton pumps. Nature 463:98–102. doi: 10.1038/nature08652

Christie JM, Gawthorne J, Young G, Fraser NJ, Roe AJ (2012) LOV to BLUF: flavoprotein contributions to the optogenetic toolkit. Mol Plant 5:533–44. doi: 10.1093/mp/sss020

Coburn CM, Bargmann CI (1996) A putative cyclic nucleotide-gated channel is required for sensory development and function in C. elegans. Neuron 17:695–706.

Corsi AK, Wightman B, Chalfie M (2015) A Transparent window into biology : A primer on Caenorhabditis elegans. 1–31. doi: 10.1895/wormbook.1.177.1

Couto A, Oda S, Nikolaev VO, Soltesz Z, de Bono M (2013) In vivo genetic dissection of O2-evoked cGMP dynamics in a Caenorhabditis elegans gas sensor. Proc Natl Acad Sci U S A 110:E3301–10. doi: 10.1073/pnas.1217428110

Crick FH (1979) Thinking about the brain. Sci Am 241:219–232. doi: 10.1038/scientificamerican0979-219

Crick FHC (1999) The impact of molecular biology on neuroscience. Philos Trans R Soc Lond B Biol Sci 354:2021–2025. doi: 10.1098/rstb.1999.0541

Crosson S, Moffat K (2001) Structure of a flavin-binding plant photoreceptor domain: insights into light-mediated signal transduction. Proc Natl Acad Sci U S A 98:2995–3000. doi: 10.1073/pnas.051520298

Crosson S, Moffat K (2002) Photoexcited structure of a plant photoreceptor domain reveals a light-driven molecular switch. Plant Cell 14:1067–75.

Culetto E, Baylis HA, Richmond JE, Jones AK, Fleming JT, Squire MD, Lewis JA, Sattelle DB (2004) The Caenorhabditis elegans unc-63 gene encodes a levamisole-sensitive nicotinic acetylcholine receptor alpha subunit. J Biol Chem 279:42476–83. doi: 10.1074/jbc.M404370200

Cully DF, Vassilatis DK, Liu KK, Paress PS, Van der Ploeg LH, Schaeffer JM, Arena JP (1994) Cloning of an avermectin-sensitive glutamate-gated chloride channel from Caenorhabditis elegans. Nature 371:707–11. doi: 10.1038/371707a0

Culotti JG (1994) Axon guidance mechanisms in Caenorhabditis elegans. Curr Opin Genet Dev 4:587–95.

Davis MW, Morton JJ, Carroll D, Jorgensen EM (2008) Gene activation using FLP recombinase in C. elegans. PLoS Genet 4:e1000028. doi: 10.1371/journal.pgen.1000028

de Bono M, Maricq AV (2005) Neuronal substrates of complex behaviors in C. elegans. Annu Rev Neurosci 28:451–501. doi: 10.1146/annurev.neuro.27.070203.144259

DeFelipe J (2002) Sesquicentenary of the birthday of Santiago Ramón y Cajal, the father of modern

neuroscience. Trends Neurosci 25:481–4.

Deisseroth K (2015) Optogenetics: 10 years of microbial opsins in neuroscience. Nat Neurosci 18:1213–25. doi: 10.1038/nn.4091

Deisseroth K, Feng G, Majewska AK, Miesenbock G, Ting A, Schnitzer MJ (2006) Next-Generation Optical Technologies for Illuminating Genetically Targeted Brain Circuits. J Neurosci 26:10380–10386. doi: 10.1523/JNEUROSCI.3863-06.2006

Dejean C, Courtin J, Rozeske RR, Bonnet MC, Dousset V, Michelet T, Herry C (2015) Neuronal Circuits for Fear Expression and Recovery: Recent Advances and Potential Therapeutic Strategies. Biol Psychiatry 78:298–306. doi: 10.1016/j.biopsych.2015.03.017

Del Castillo J, De Mello WC, Morales T (1967) The initiation of action potentials in the somatic musculature of Ascaris lumbricoides. J Exp Biol 46:263–79.

Del Castillo J, DEMELLO WC, MORALES T (1963) THE PHYSIOLOGICAL ROLE OF ACETYLCHOLINE IN THE NEUROMUSCULAR SYSTEM OF ASCARIS LUMBRICOIDES. Arch Int Physiol Biochim 71:741–57.

Denninger JW, Marletta MA (1999) Guanylate cyclase and the .NO/cGMP signaling pathway. Biochim Biophys Acta 1411:334–50.

Dent JA, Davis MW, Avery L (1997) avr-15 encodes a chloride channel subunit that mediates inhibitory glutamatergic neurotransmission and ivermectin sensitivity in Caenorhabditis elegans. EMBO J 16:5867–79. doi: 10.1093/emboj/16.19.5867

Dent JA, Smith MM, Vassilatis DK, Avery L (2000) The genetics of ivermectin resistance in Caenorhabditis elegans. Proc Natl Acad Sci U S A 97:2674–9.

Derbyshire ER, Marletta MA (2012) Structure and regulation of soluble guanylate cyclase. Annu Rev Biochem 81:533–59. doi: 10.1146/annurev-biochem-050410-100030

Dickinson DJ, Goldstein B (2016) CRISPR-Based Methods for Caenorhabditis elegans Genome Engineering. Genetics 202:885–901. doi: 10.1534/genetics.115.182162

Dingledine R, Borges K, Bowie D, Traynelis SF (1999) The glutamate receptor ion channels. Pharmacol Rev 51:7–61.

DiPilato LM, Cheng X, Zhang J (2004) Fluorescent indicators of cAMP and Epac activation reveal differential dynamics of cAMP signaling within discrete subcellular compartments. Proc Natl Acad Sci U S A 101:16513–8. doi: 10.1073/pnas.0405973101

Dixon SJ, Alexander M, Fernandes R, Ricker N, Roy PJ (2006) FGF negatively regulates muscle membrane extension in Caenorhabditis elegans. Development 133:1263–75. doi: 10.1242/dev.02300

Dixon SJ, Roy PJ (2005) Muscle arm development in Caenorhabditis elegans. Development 132:3079–92. doi: 10.1242/dev.01883

Dugué GP, Akemann W, Knöpfel T (2012) A comprehensive concept of optogenetics. Prog Brain Res 196:1–28. doi: 10.1016/B978-0-444-59426-6.00001-X

Dvir H, Silman I, Harel M, Rosenberry TL, Sussman JL (2010) Acetylcholinesterase: from 3D structure to function. Chem Biol Interact 187:10–22. doi: 10.1016/j.cbi.2010.01.042

Edwards SL, Charlie NK, Milfort MC, Brown BS, Gravlin CN, Knecht JE, Miller KG (2008) A novel molecular solution for ultraviolet light detection in Caenorhabditis elegans. PLoS Biol 6:e198. doi: 10.1371/journal.pbio.0060198

Ellis-Davies GCR (2007) Caged compounds: photorelease technology for control of cellular chemistry and physiology. Nat Methods 4:619–28. doi: 10.1038/nmeth1072

Erbguth K, Prigge M, Schneider F, Hegemann P, Gottschalk A (2012) Bimodal Activation of Different Neuron Classes with the Spectrally Red-Shifted Channelrhodopsin Chimera C1V1 in Caenorhabditis elegans. PLoS One. doi: 10.1371/journal.pone.0046827

Ernst OP, Lodowski DT, Elstner M, Hegemann P, Brown LS, Kandori H (2014) Microbial and animal rhodopsins: structures, functions, and molecular mechanisms. Chem Rev 114:126–63. doi: 10.1021/cr4003769

Etter A, Cully DF, Schaeffer JM, Liu KK, Arena JP (1996) An amino acid substitution in the pore region of a glutamate-gated chloride channel enables the coupling of ligand binding to channel gating. J Biol Chem 271:16035–16039. doi: 10.1074/jbc.271.27.16035

Fang-Yen C, Alkema MJ, Samuel ADT (2015) Illuminating neural circuits and behaviour in Caenorhabditis elegans with optogenetics. Philos Trans R Soc Lond B Biol Sci 370:20140212. doi: 10.1098/rstb.2014.0212

Fang-yen C, Alkema MJ, Samuel ADT, Fang-yen C (2015) Illuminating neural circuits and behaviour in Caenorhabditis elegans with optogenetics.

Fehrentz T, Schönberger M, Trauner D (2011) Optochemical genetics. Angew Chemie - Int Ed 50:12156–12182. doi: 10.1002/anie.201103236

Feldbauer K, Zimmermann D, Pintschovius V, Spitz J, Bamann C, Bamberg E (2009) Channelrhodopsin-2 is a leaky proton pump. Proc Natl Acad Sci U S A 106:12317–12322. doi: 10.1073/pnas.0905852106

Fenno L, Yizhar O, Deisseroth K (2011) The development and application of optogenetics. Annu Rev Neurosci 34:389–412. doi: 10.1146/annurev-neuro-061010-113817

Ferkey DM, Hyde R, Haspel G, Dionne HM, Hess HA, Suzuki H, Schafer WR, Koelle MR, Hart AC (2007) C. elegans G protein regulator RGS-3 controls sensitivity to sensory stimuli. Neuron 53:39–52. doi: 10.1016/j.neuron.2006.11.015

Fire A, Xu S, Montgomery MK, Kostas SA, Driver SE, Mello CC (1998) Potent and specific genetic interference by double-stranded RNA in Caenorhabditis elegans. Nature 391:806–11. doi: 10.1038/35888

Flavell SW, Pokala N, Macosko EZ, Albrecht DR, Larsch J, Bargmann CI (2013) Serotonin and the neuropeptide PDF initiate and extend opposing behavioral states in C. Elegans. Cell 154:1023–1035. doi: 10.1016/j.cell.2013.08.001

Fleming JT, Squire MD, Barnes TM, Tornoe C, Matsuda K, Ahnn J, Fire A, Sulston JE, Barnard EA, Sattelle DB, Lewis JA (1997) Caenorhabditis elegans levamisole resistance genes lev-1, unc-29, and unc-38 encode functional nicotinic acetylcholine receptor subunits. J Neurosci 17:5843–57.

Fortin DL, Dunn TW, Fedorchak A, Allen D, Montpetit R, Banghart MR, Trauner D, Adelman JP, Kramer RH (2011) Optogenetic photochemical control of designer K+ channels in mammalian neurons. J Neurophysiol 106:488–496. doi: 10.1152/jn.00251.2011

Francis MM, Evans SP, Jensen M, Madsen DM, Mancuso J, Norman KR, Maricq AV (2005) The Ror receptor tyrosine kinase CAM-1 is required for ACR-16-mediated synaptic transmission at the C. elegans neuromuscular junction. Neuron 46:581–94. doi: 10.1016/j.neuron.2005.04.010

Frazier SJ, Cohen BN, Lester HA (2013) An engineered glutamate-gated chloride (GLUCL) channel for sensitive, consistent neuronal silencing by ivermectin. J Biol Chem 288:21029–21042. doi: 10.1074/jbc.M112.423921

Frins S, Bönigk W, Müller F, Kellner R, Koch KW (1996) Functional characterization of a guanylyl cyclase-activating protein from vertebrate rods. Cloning, heterologous expression, and localization. J Biol Chem 271:8022–7.

Frøkjær-Jensen C (2015) Transposon-Assisted Genetic Engineering with Mos1-Mediated Single-Copy Insertion (MosSCI). Methods Mol Biol 1327:49–58. doi: 10.1007/978-1-4939-2842-2_5

Gao S, Nagpal J, Schneider MW, Kozjak-pavlovic V, Nagel G, Gottschalk A (2015) Optogenetic manipulation of cGMP in cells and animals by the tightly light-regulated guanylyl-cyclase opsin CyclOp. Nat Commun 6:1–12. doi: 10.1038/ncomms9046

Gao S, Zhen M (2011) Action potentials drive body wall muscle contractions in Caenorhabditis elegans. Proc Natl Acad Sci U S A 108:2557–62. doi: 10.1073/pnas.1012346108

Garrity PA, Goodman MB, Samuel AD, Sengupta P (2010) Running hot and cold: behavioral strategies, neural circuits, and the molecular machinery for thermotaxis in C. elegans and Drosophila. Genes Dev 24:2365–82. doi: 10.1101/gad.1953710

Gasser C, Taiber S, Yeh C-M, Wittig CH, Hegemann P, Ryu S, Wunder F, Moglich a. (2014) Engineering of a red-light-activated human cAMP/cGMP-specific phosphodiesterase. Proc Natl Acad Sci 111:8803–8808. doi: 10.1073/pnas.1321600111

Gauden M, van Stokkum IHM, Key JM, Lührs DC, van Grondelle R, Hegemann P, Kennis JTM (2006) Hydrogen-bond switching through a radical pair mechanism in a flavin-binding photoreceptor. Proc Natl Acad Sci U S A 103:10895–900. doi: 10.1073/pnas.0600720103

Gautier A, Juillerat A, Heinis C, Corrêa IR, Kindermann M, Beaufils F, Johnsson K (2008) An engineered protein tag for multiprotein labeling in living cells. Chem Biol 15:128–36. doi: 10.1016/j.chembiol.2008.01.007

Ghosh R, Andersen EC, Shapiro J a., Gerke JP, Kruglyak L (2012) Natural Variation in a Chloride Channel Subunit Confers Avermectin Resistance in C. elegans. Science (80-) 335:574–578. doi: 10.1126/science.1214318

Golden JW, Riddle DL (1984) The Caenorhabditis elegans dauer larva: developmental effects of pheromone, food, and temperature. Dev Biol 102:368–78.

Goodman MB, Hall DH, Avery L, Lockery SR (1998) Active currents regulate sensitivity and dynamic range in C. elegans neurons. Neuron 20:763–72.

Gordeliy VI, Labahn J, Moukhametzianov R, Efremov R, Granzin J, Schlesinger R, Büldt G, Savopol T, Scheidig AJ, Klare JP, Engelhard M (2002) Molecular basis of transmembrane signalling by sensory rhodopsin II-transducer complex. Nature 419:484–7. doi: 10.1038/nature01109

Gorostiza P, Volgraf M, Numano R, Szobota S, Trauner D, Isacoff EY (2007) Mechanisms of photoswitch conjugation and light activation of an ionotropic glutamate receptor. Proc Natl Acad Sci U S A 104:10865–10870. doi: 10.1073/pnas.0701274104

Gorshkov K, Zhang J (2014) Visualization of cyclic nucleotide dynamics in neurons. Front Cell Neurosci 8:395. doi: 10.3389/fncel.2014.00395

Gottschalk A, Almedom RB, Schedletzky T, Anderson SD, Yates JR, Schafer WR (2005) Identification and characterization of novel nicotinic receptor-associated proteins in Caenorhabditis elegans. EMBO J 24:2566–78. doi: 10.1038/sj.emboj.7600741

Govorunova EG, Sineshchekov OA, Janz R, Liu X, Spudich JL (2015) Natural light-gated anion channels: A family of microbial rhodopsins for advanced optogenetics. Science (80-) 349:647–650. doi: 10.1126/science.aaa7484

Gray JM, Karow DS, Lu H, Chang AJ, Chang JS, Ellis RE, Marletta MA, Bargmann CI (2004) Oxygen sensation and social feeding mediated by a C. elegans guanylate cyclase homologue. Nature 430:317–22. doi: 10.1038/nature02714

Guo Z V, Hart AC, Ramanathan S (2009) Optical interrogation of neural circuits in Caenorhabditis elegans. Nat Methods 6:891–6. doi: 10.1038/nmeth.1397

Hallem EA, Sternberg PW (2008) Acute carbon dioxide avoidance in Caenorhabditis elegans. Proc Natl Acad Sci U S A 105:8038–43. doi: 10.1073/pnas.0707469105

Hardie RC, Raghu P (2001) Visual transduction in Drosophila. Nature 413:186–93. doi: 10.1038/35093002

Harper SM, Neil LC, Gardner KH (2003) Structural basis of a phototropin light switch. Science 301:1541–4. doi: 10.1126/science.1086810

Heckman KL, Pease LR (2007) Gene splicing and mutagenesis by PCR-driven overlap extension. Nat Protoc 2:924–932. doi: 10.1038/nprot.2007.132

Hedgecock EM, Culotti JG, Hall DH (1990) The unc-5, unc-6, and unc-40 genes guide circumferential migrations of pioneer axons and mesodermal cells on the epidermis in C. elegans. Neuron 4:61–85.

Hedgecock EM, Culotti JG, Hall DH, Stern BD (1987) Genetics of cell and axon migrations in Caenorhabditis elegans. Development 100:365–82.

Hegemann P (2008) Algal Sensory Photoreceptors.pdf. Annu Rev Plant Biol 167–189. doi:

10.1146/annurev.arplant.59.032607.092847

Hibbs RE, Gouaux E (2011) Principles of activation and permeation in an anion-selective Cys-loop receptor. Nature 474:54–60. doi: 10.1038/nature10139

Hills T, Brockie PJ, Maricq A V (2004) Dopamine and glutamate control area-restricted search behavior in Caenorhabditis elegans. J Neurosci 24:1217–25. doi: 10.1523/JNEUROSCI.1569-03.2004

Hobert O (2013) The neuronal genome of Caenorhabditis elegans. WormBook 1–106. doi: 10.1895/wormbook.1.161.1

Honda A, Adams SR, Sawyer CL, Lev-Ram V, Tsien RY, Dostmann WR (2001) Spatiotemporal dynamics of guanosine 3',5'-cyclic monophosphate revealed by a genetically encoded, fluorescent indicator. Proc Natl Acad Sci U S A 98:2437–42. doi: 10.1073/pnas.051631298

Honda A, Moosmeier MA, Dostmann WR (2005a) Membrane-permeable cygnets: rapid cellular internalization of fluorescent cGMP-indicators. Front Biosci 10:1290–301.

Honda A, Sawyer CL, Cawley SM, Dostmann WRG (2005b) Cygnets: in vivo characterization of novel cGMP indicators and in vivo imaging of intracellular cGMP. Methods Mol Biol 307:27–43. doi: 10.1385/1-59259-839-0:027

Horoszok L, Raymond V, Sattelle DB, Wolstenholme AJ (2001) GLC-3: a novel fipronil and BIDN-sensitive, but picrotoxinin-insensitive, L-glutamate-gated chloride channel subunit from Caenorhabditis elegans. Br J Pharmacol 132:1247–54. doi: 10.1038/sj.bjp.0703937

Howe JR (1996) Homomeric and heteromeric ion channels formed from the kainate-type subunits GluR6 and KA2 have very small, but different, unitary conductances. J Neurophysiol 76:510–9.

Husson SJ, Costa WS, Wabnig S, Stirman JN, Watson JD, Spencer WC, Akerboom J, Looger LL, Treinin M, Miller DM, Lu H, Gottschalk A (2012a) Optogenetic analysis of a nociceptor neuron and network reveals ion channels acting downstream of primary sensors. Curr Biol 22:743–52. doi: 10.1016/j.cub.2012.02.066

Husson SJ, Gottschalk A, Leifer AM (2013) Optogenetic manipulation of neural activity in C. elegans: From synapse to circuits and behaviour. Biol Cell 105:235–250. doi: 10.1111/boc.201200069

Husson SJ, Liewald JF, Schultheis C, Stirman JN, Lu H, Gottschalk A (2012b) Microbial light-activatable proton pumps as neuronal inhibitors to functionally dissect neuronal networks in C. elegans. PLoS One. doi: 10.1371/journal.pone.0040937

Inada H, Ito H, Satterlee J, Sengupta P, Matsumoto K, Mori I (2006) Identification of guanylyl cyclases that function in thermosensory neurons of Caenorhabditis elegans. Genetics 172:2239–52. doi: 10.1534/genetics.105.050013

Isner J-C, Maathuis FJM (2011) Measurement of cellular cGMP in plant cells and tissues using the endogenous fluorescent reporter FlincG. Plant J 65:329–34. doi: 10.1111/j.1365-313X.2010.04418.x

Izquierdo-Serra M, Gascón-Moya M, Hirtz JJ, Pittolo S, Poskanzer KE, Ferrer È, Alibés R, Busqué F,

Yuste R, Hernando J, Gorostiza P (2014) Two-photon neuronal and astrocytic stimulation with azobenzene-based photoswitches. J Am Chem Soc 136:8693–701. doi: 10.1021/ja5026326

Jackson AC, Nicoll RA (2011) The expanding social network of ionotropic glutamate receptors: TARPs and other transmembrane auxiliary subunits. Neuron 70:178–99. doi: 10.1016/j.neuron.2011.04.007

Janovjak H, Szobota S, Wyart C, Trauner D, Isacoff EY (2010) A light-gated, potassium-selective glutamate receptor for the optical inhibition of neuronal firing. Nat Neurosci 13:1027–1032. doi: 10.1038/nn.2589

Jansen V, Alvarez L, Balbach M, Strünker T, Hegemann P, Kaupp UB, Wachten D (2015) Controlling fertilization and cAMP signaling in sperm by optogenetics. Elife. doi: 10.7554/eLife.05161

Jarrell TA, Wang Y, Bloniarz AE, Brittin CA, Xu M, Thomson JN, Albertson DG, Hall DH, Emmons SW (2012) The connectome of a decision-making neural network. Science 337:437–44. doi: 10.1126/science.1221762

Jensen M, Hoerndli FJ, Brockie PJ, Wang R, Johnson E, Maxfield D, Francis MM, Madsen DM, Maricq A V (2012) Wnt signaling regulates acetylcholine receptor translocation and synaptic plasticity in the adult nervous system. Cell 149:173–87. doi: 10.1016/j.cell.2011.12.038

Jospin M, Jacquemond V, Mariol M-C, Ségalat L, Allard B (2002) The L-type voltage-dependent Ca2+ channel EGL-19 controls body wall muscle function in Caenorhabditis elegans. J Cell Biol 159:337–48. doi: 10.1083/jcb.200203055

Jung K-H, Trivedi VD, Spudich JL (2003) Demonstration of a sensory rhodopsin in eubacteria. Mol Microbiol 47:1513–22.

Kaplan JH, Somlyo AP (1989) Flash photolysis of caged compounds: new tools for cellular physiology. Trends Neurosci 12:54–9.

Keane J, Avery L (2003) Mechanosensory inputs influence Caenorhabditis elegans pharyngeal activity via ivermectin sensitivity genes. Genetics 164:153–62.

Kienzler MA, Reiner A, Trautman E, Yoo S, Trauner D, Isacoff EY (2013) A red-shifted, fast-relaxing azobenzene photoswitch for visible light control of an ionotropic glutamate receptor. J Am Chem Soc 135:17683–6. doi: 10.1021/ja408104w

Kim K, Li C (2004) Expression and regulation of an FMRFamide-related neuropeptide gene family in Caenorhabditis elegans. J Comp Neurol 475:540–50. doi: 10.1002/cne.20189

Kim T, Folcher M, Doaud-El Baba M, Fussenegger M (2015) A synthetic erectile optogenetic stimulator enabling blue-light-inducible penile erection. Angew Chem Int Ed Engl 54:5933–8. doi: 10.1002/anie.201412204

Kimble J, Hirsh D (1979) The postembryonic cell lineages of the hermaphrodite and male gonads in Caenorhabditis elegans. Dev Biol 70:396–417.

Klapoetke NC, Murata Y, Kim SS, Pulver SR, Birdsey-Benson A, Cho YK, Morimoto TK, Chuong AS, Carpenter EJ, Tian Z, Wang J, Xie Y, Yan Z, Zhang Y, Chow BY, Surek B, Melkonian M,

Jayaraman V, Constantine-Paton M, Wong GK-S, Boyden ES (2014) Independent optical excitation of distinct neural populations. Nat Methods 11:338–46. doi: 10.1038/nmeth.2836

Kocabas A, Shen CH, Guo ZC V, Ramanathan S (2012) Controlling interneuron activity in Caenorhabditis elegans to evoke chemotactic behaviour. Nature 490:273–+. doi: 10.1038/nature11431

Kolbe M, Besir H, Essen LO, Oesterhelt D (2000) Structure of the light-driven chloride pump halorhodopsin at 1.8 A resolution. Science 288:1390–6.

Komatsu H, Jin YH, L'Etoile N, Mori I, Bargmann CI, Akaike N, Ohshima Y (1999) Functional reconstitution of a heteromeric cyclic nucleotide-gated channel of Caenorhabditis elegans in cultured cells. Brain Res 821:160–8.

Komatsu H, Mori I, Rhee JS, Akaike N, Ohshima Y (1996) Mutations in a cyclic nucleotide-gated channel lead to abnormal thermosensation and chemosensation in C. elegans. Neuron 17:707–18.

Kramer RH, Mourot A, Adesnik H (2013) Optogenetic pharmacology for control of native neuronal signaling proteins. Nat Neurosci 16:816–23. doi: 10.1038/nn.3424

Kratz F (2008) Albumin as a drug carrier: design of prodrugs, drug conjugates and nanoparticles. J Control Release 132:171–83. doi: 10.1016/j.jconrel.2008.05.010

Krogh A, Larsson B, von Heijne G, Sonnhammer EL (2001) Predicting transmembrane protein topology with a hidden Markov model: application to complete genomes. J Mol Biol 305:567–80. doi: 10.1006/jmbi.2000.4315

L'Etoile ND, Bargmann CI (2000) Olfaction and odor discrimination are mediated by the C. elegans guanylyl cyclase ODR-1. Neuron 25:575–86.

Lackner MR, Nurrish SJ, Kaplan JM (1999) Facilitation of synaptic transmission by EGL-30 G(q)?? and EGL-8 PLC??: DAG binding to UNC-13 is required to stimulate acetylcholine release. Neuron 24:335–346. doi: 10.1016/S0896-6273(00)80848-X

Lanyi JK (1995) Bacteriorhodopsin as a model for proton pumps. Nature 375:461–3. doi: 10.1038/375461a0

Laughton DL, Lunt GG, Wolstenholme AJ (1997a) Alternative splicing of a Caenorhabditis elegans gene produces two novel inhibitory amino acid receptor subunits with identical ligand binding domains but different ion channels. Gene 201:119–25.

Laughton DL, Lunt GG, Wolstenholme AJ (1997b) Reporter gene constructs suggest that the Caenorhabditis elegans avermectin receptor beta-subunit is expressed solely in the pharynx. J Exp Biol 200:1509–14.

Lee RC, Feinbaum RL, Ambros V (1993) The C. elegans heterochronic gene lin-4 encodes small RNAs with antisense complementarity to lin-14. Cell 75:843–54.

Lee RY, Lobel L, Hengartner M, Horvitz HR, Avery L (1997) Mutations in the alpha1 subunit of an L-type voltage-activated Ca2+ channel cause myotonia in Caenorhabditis elegans. EMBO J

16:6066–76. doi: 10.1093/emboj/16.20.6066

Lee RY, Sawin ER, Chalfie M, Horvitz HR, Avery L (1999) EAT-4, a homolog of a mammalian sodium-dependent inorganic phosphate cotransporter, is necessary for glutamatergic neurotransmission in caenorhabditis elegans. J Neurosci 19:159–67.

Lefkowitz RJ, Shenoy SK (2005) Transduction of receptor signals by beta-arrestins. Science 308:512–7. doi: 10.1126/science.1109237

Leifer AM, Fang-Yen C, Gershow M, Alkema MJ, Samuel ADT (2011) Optogenetic manipulation of neural activity in freely moving Caenorhabditis elegans. Nat Methods 8:147–52. doi: 10.1038/nmeth.1554

Lemoine D, Habermacher C, Martz A, Méry P-F, Bouquier N, Diverchy F, Taly A, Rassendren F, Specht A, Grutter T (2013) Optical control of an ion channel gate. Proc Natl Acad Sci U S A 110:20813–8. doi: 10.1073/pnas.1318715110

Lerchner W, Xiao C, Nashmi R, Slimko EM, van Trigt L, Lester HA, Anderson DJ (2007) Reversible silencing of neuronal excitability in behaving mice by a genetically targeted, ivermectin-gated Cl- channel. Neuron 54:35–49. doi: 10.1016/j.neuron.2007.02.030

Levitz J, Pantoja C, Gaub B, Janovjak H, Reiner A, Hoagland A, Schoppik D, Kane B, Stawski P, Schier AF, Trauner D, Isacoff EY (2013) Optical control of metabotropic glutamate receptors. Nat Neurosci 16:507–16. doi: 10.1038/nn.3346

Levitz J, Popescu AT, Reiner A, Isacoff EY (2016) A Toolkit for Orthogonal and in vivo Optical Manipulation of Ionotropic Glutamate Receptors. Front Mol Neurosci 9:2. doi: 10.3389/fnmol.2016.00002

Lewis JA, Wu CH, Berg H, Levine JH (1980) The genetics of levamisole resistance in the nematode Caenorhabditis elegans. Genetics 95:905–28.

Li P, Slimko EM, Lester HA (2002) Selective elimination of glutamate activation and introduction of fluorescent proteins into a Caenorhabditis elegans chloride channel. FEBS Lett 528:77–82. doi: 10.1016/S0014-5793(02)03245-3

Liewald JF, Brauner M, Stephens GJ, Bouhours M, Schultheis C, Zhen M, Gottschalk A (2008) Optogenetic analysis of synaptic function. Nat Methods 5:895–902. doi: 10.1038/nmeth.1252

Lima SQ, Miesenböck G (2005) Remote control of behavior through genetically targeted photostimulation of neurons. Cell 121:141–152. doi: 10.1016/j.cell.2005.02.004

Lin D, Boyle MP, Dollar P, Lee H, Lein ES, Perona P, Anderson DJ (2011) Functional identification of an aggression locus in the mouse hypothalamus. Nature 470:221–6. doi: 10.1038/nature09736

Lin JY (2011) A user's guide to channelrhodopsin variants: features, limitations and future developments. Exp Physiol 96:19–25. doi: 10.1113/expphysiol.2009.051961

Lin JY, Lin MZ, Steinbach P, Tsien RY (2009) Characterization of engineered channelrhodopsin variants with improved properties and kinetics. Biophys J 96:1803–1814. doi: 10.1016/j.bpj.2008.11.034

Lin W-C, Davenport CM, Mourot A, Vytla D, Smith CM, Medeiros KA, Chambers JJ, Kramer RH (2014) Engineering a light-regulated GABAA receptor for optical control of neural inhibition. ACS Chem Biol 9:1414–9. doi: 10.1021/cb500167u

Lin WC, Tsai MC, Davenport CM, Smith CM, Veit J, Wilson NM, Adesnik H, Kramer RH (2015) A Comprehensive Optogenetic Pharmacology Toolkit for In Vivo Control of GABAA Receptors and Synaptic Inhibition. Neuron 88:879–891. doi: 10.1016/j.neuron.2015.10.026

Liu J, Wu DC, Wang YT (2010) Allosteric potentiation of glycine receptor chloride currents by glutamate. Nat Neurosci 13:1225–32. doi: 10.1038/nn.2633

Liu P, Chen B, Wang Z-W (2011) Gap junctions synchronize action potentials and Ca2+ transients in Caenorhabditis elegans body wall muscle. J Biol Chem 286:44285–93. doi: 10.1074/jbc.M111.292078

Liu Q, Hollopeter G, Jorgensen EM (2009) Graded synaptic transmission at the Caenorhabditis elegans neuromuscular junction. Proc Natl Acad Sci U S A 106:10823–8. doi: 10.1073/pnas.0903570106

Lockery SR, Goodman MB, Faumont S (2009) First report of action potentials in a C. elegans neuron is premature. Nat Neurosci 12:365–6; author reply 366. doi: 10.1038/nn0409-365

Loewi O (1921) Über humorale übertragbarkeit der Herznervenwirkung. Pflugers Arch Gesamte Physiol Menschen Tiere 189:239–242. doi: 10.1007/BF01738910

Lorenz TC (2012) Polymerase chain reaction: basic protocol plus troubleshooting and optimization strategies. J Vis Exp e3998. doi: 10.3791/3998

Lucas KA, Pitari GM, Kazerounian S, Ruiz-Stewart I, Park J, Schulz S, Chepenik KP, Waldman SA (2000) Guanylyl Cyclases and Signaling by Cyclic GMP. Pharmacol Rev 52:375–414.

Lutz C, Otis TS, DeSars V, Charpak S, DiGregorio DA, Emiliani V (2008) Holographic photolysis of caged neurotransmitters. Nat Methods 5:821–7. doi: 10.1038/nmeth.1241

Macosko EZ, Pokala N, Feinberg EH, Chalasani SH, Butcher RA, Clardy J, Bargmann CI (2009) A hub-and-spoke circuit drives pheromone attraction and social behaviour in C. elegans. Nature 458:1171–5. doi: 10.1038/nature07886

Mahoney TR, Luo S, Nonet ML (2006) Analysis of synaptic transmission in Caenorhabditis elegans using an aldicarb-sensitivity assay. Nat Protoc 1:1772–1777. doi: 10.1038/nprot.2006.281

Maryon EB, Saari B, Anderson P (1998) Muscle-specific functions of ryanodine receptor channels in Caenorhabditis elegans. J Cell Sci 111 (Pt 1:2885–95.

Matsuno-Yagi A, Mukohata Y (1977) Two possible roles of bacteriorhodopsin; a comparative study of strains of Halobacterium halobium differing in pigmentation. Biochem Biophys Res Commun 78:237–43.

Mayer ML (2005) Crystal structures of the GluR5 and GluR6 ligand binding cores: Molecular mechanisms underlying kainate receptor selectivity. Neuron 45:539–552. doi: 10.1016/j.neuron.2005.01.031

Mayer ML (2011) Structure and mechanism of glutamate receptor ion channel assembly, activation and modulation. Curr Opin Neurobiol 21:283–290. doi: 10.1016/j.conb.2011.02.001

Mellanby H (1955) The identification and estimation of acetylcholine in three parasitic nematodes (Ascaris lumbricoides, Litomosoides carinii, and the microfilariae of Dirofilaria repens). Parasitology 45:287–94.

Mellem JE, Brockie PJ, Madsen DM, Maricq A V (2008) Action potentials contribute to neuronal signaling in C. elegans. Nat Neurosci 11:865–7. doi: 10.1038/nn.2131

Mellem JE, Brockie PJ, Zheng Y, Madsen DM, Maricq A V (2002) Decoding of polymodal sensory stimuli by postsynaptic glutamate receptors in C. elegans. Neuron 36:933–44.

Mello CC, Kramer JM, Stinchcomb D, Ambros V (1991) Efficient gene transfer in C.elegans: extrachromosomal maintenance and integration of transforming sequences. EMBO J 10:3959–70.

Miesenböck G (2009) The optogenetic catechism. Science 326:395–9. doi: 10.1126/science.1174520

Miesenböck G (2011) Optogenetic Control of Cells and Circuits. Annu Rev Cell Dev Biol 27:731–758. doi: 10.1146/annurev-cellbio-100109-104051

Miesenböck G, De Angelis DA, Rothman JE (1998) Visualizing secretion and synaptic transmission with pH-sensitive green fluorescent proteins. Nature 394:192–5. doi: 10.1038/28190

Miesenböck G, Rothman JE (1997) Patterns of synaptic activity in neural networks recorded by light emission from synaptolucins. Proc Natl Acad Sci U S A 94:3402–7.

Miyawaki A, Griesbeck O, Heim R, Tsien RY (1999) Dynamic and quantitative Ca2+ measurements using improved cameleons. Proc Natl Acad Sci U S A 96:2135–40.

Miyawaki A, Llopis J, Heim R, McCaffery JM, Adams JA, Ikura M, Tsien RY (1997) Fluorescent indicators for Ca2+ based on green fluorescent proteins and calmodulin. Nature 388:882–7. doi: 10.1038/42264

Möglich A, Yang X, Ayers RA, Moffat K (2010) Structure and function of plant photoreceptors. Annu Rev Plant Biol 61:21–47. doi: 10.1146/annurev-arplant-042809-112259

Mori I, Ohshima Y (1995) Neural regulation of thermotaxis in Caenorhabditis elegans. Nature 376:344–8. doi: 10.1038/376344a0

Morton DB (2004) Invertebrates yield a plethora of atypical guanylyl cyclases. Mol Neurobiol 29:97–116. doi: 10.1385/MN:29:2:097

Mourot A, Rodrigo J, Kotzyba-Hibert F, Bertrand S, Bertrand D, Goeldner M (2006) Probing the reorganization of the nicotinic acetylcholine receptor during desensitization by time-resolved covalent labeling using [3H]AC5, a photoactivatable agonist. Mol Pharmacol 69:452–61. doi: 10.1124/mol.105.017566

Nagel G, Brauner M, Liewald JF, Adeishvili N, Bamberg E, Gottschalk A (2005) Light activation of Channelrhodopsin-2 in excitable cells of caenorhabditis elegans triggers rapid behavioral responses. Curr Biol 15:2279–2284. doi: 10.1016/j.cub.2005.11.032

Nagel G, Ollig D, Fuhrmann M, Kateriya S, Musti AM, Bamberg E, Hegemann P (2002) Channelrhodopsin-1: a light-gated proton channel in green algae. Science 296:2395–8. doi: 10.1126/science.1072068

Nagel G, Szellas T, Huhn W, Kateriya S, Adeishvili N, Berthold P, Ollig D, Hegemann P, Bamberg E (2003) Channelrhodopsin-2, a directly light-gated cation-selective membrane channel. Proc Natl Acad Sci U S A 100:13940–13945. doi: 10.1073/pnas.1936192100

Nakai J, Ohkura M, Imoto K (2001) A high signal-to-noise Ca(2+) probe composed of a single green fluorescent protein. Nat Biotechnol 19:137–41. doi: 10.1038/84397

Nausch LWM, Ledoux J, Bonev AD, Nelson MT, Dostmann WR (2008) Differential patterning of cGMP in vascular smooth muscle cells revealed by single GFP-linked biosensors. Proc Natl Acad Sci U S A 105:365–70. doi: 10.1073/pnas.0710387105

Nerbonne JM (1996) Caged compounds: tools for illuminating neuronal responses and connections. Curr Opin Neurobiol 6:379–86.

Ni M, Tepperman JM, Quail PH (1999) Binding of phytochrome B to its nuclear signalling partner PIF3 is reversibly induced by light. Nature 400:781–4. doi: 10.1038/23500

Niino Y, Hotta K, Oka K (2009) Simultaneous live cell imaging using dual FRET sensors with a single excitation light. PLoS One 4:e6036. doi: 10.1371/journal.pone.0006036

Nikolaev VO, Bünemann M, Hein L, Hannawacker A, Lohse MJ (2004) Novel single chain cAMP sensors for receptor-induced signal propagation. J Biol Chem 279:37215–8. doi: 10.1074/jbc.C400302200

Nikolaev VO, Bünemann M, Schmitteckert E, Lohse MJ, Engelhardt S (2006a) Cyclic AMP imaging in adult cardiac myocytes reveals far-reaching beta1-adrenergic but locally confined beta2-adrenergic receptor-mediated signaling. Circ Res 99:1084–91. doi: 10.1161/01.RES.0000250046.69918.d5

Nikolaev VO, Gambaryan S, Lohse MJ (2006b) Fluorescent sensors for rapid monitoring of intracellular cGMP. Nat Methods 3:23–5. doi: 10.1038/nmeth816

Nikolaev VO, Lohse MJ (2009) Novel techniques for real-time monitoring of cGMP in living cells. Handb Exp Pharmacol 229–43. doi: 10.1007/978-3-540-68964-5_11

Numano R, Szobota S, Lau AY, Gorostiza P, Volgraf M, Roux B, Trauner D, Isacoff EY (2009) Nanosculpting reversed wavelength sensitivity into a photoswitchable iGluR. Proc Natl Acad Sci U S A 106:6814–6819. doi: 10.1073/pnas.0811899106

Oesterhelt D, Stoeckenius W (1971) Rhodopsin-like protein from the purple membrane of Halobacterium halobium. Nat New Biol 233:149–52.

Ohnishi N, Kuhara A, Nakamura F, Okochi Y, Mori I (2011) Bidirectional regulation of thermotaxis by glutamate transmissions in Caenorhabditis elegans. EMBO J 30:1376–88. doi: 10.1038/emboj.2011.13

Ohno H, Kato S, Naito Y, Kunitomo H, Tomioka M, Iino Y (2014) Role of synaptic phosphatidylinositol

3-kinase in a behavioral learning response in C. elegans. Science 345:313–7. doi: 10.1126/science.1250709

Oikonomou G, Shaham S (2011) The glia of Caenorhabditis elegans. Glia 59:1253–63. doi: 10.1002/glia.21084

Omasits U, Ahrens CH, Müller S, Wollscheid B (2014) Protter: interactive protein feature visualization and integration with experimental proteomic data. Bioinformatics 30:884–6. doi: 10.1093/bioinformatics/btt607

Ortells MO, Lunt GG (1995) Evolutionary history of the ligand-gated ion-channel superfamily of receptors. Trends Neurosci 18:121–7.

Ortiz CO, Etchberger JF, Posy SL, Frøkjaer-Jensen C, Lockery S, Honig B, Hobert O (2006) Searching for neuronal left/right asymmetry: genomewide analysis of nematode receptor-type guanylyl cyclases. Genetics 173:131–49. doi: 10.1534/genetics.106.055749

Owald D, Lin S, Waddell S (2015) Light, heat, action: neural control of fruit fly behaviour. Philos Trans R Soc Lond B Biol Sci 370:20140211. doi: 10.1098/rstb.2014.0211

Palczewski K (2006) G protein-coupled receptor rhodopsin. Annu Rev Biochem 75:743–67. doi: 10.1146/annurev.biochem.75.103004.142743

Partch CL, Clarkson MW, Ozgür S, Lee AL, Sancar A (2005) Role of structural plasticity in signal transduction by the cryptochrome blue-light photoreceptor. Biochemistry 44:3795–805. doi: 10.1021/bi047545g

Pemberton DJ, Franks CJ, Walker RJ, Holden-Dye L (2001) Characterization of glutamate-gated chloride channels in the pharynx of wild-type and mutant Caenorhabditis elegans delineates the role of the subunit GluCl-alpha2 in the function of the native receptor. Mol Pharmacol 59:1037–43.

Pierce KL, Premont RT, Lefkowitz RJ (2002) Signalling: Seven-transmembrane receptors. Nat Rev Mol Cell Biol 3:639–650. doi: 10.1038/nrm908

Pirri JK, McPherson AD, Donnelly JL, Francis MM, Alkema MJ (2009) A tyramine-gated chloride channel coordinates distinct motor programs of a Caenorhabditis elegans escape response. Neuron 62:526–38. doi: 10.1016/j.neuron.2009.04.013

Ponsioen B, Zhao J, Riedl J, Zwartkruis F, van der Krogt G, Zaccolo M, Moolenaar WH, Bos JL, Jalink K (2004) Detecting cAMP-induced Epac activation by fluorescence resonance energy transfer: Epac as a novel cAMP indicator. EMBO Rep 5:1176–80. doi: 10.1038/sj.embor.7400290

Raffelberg S, Wang L, Gao S, Losi A, Gärtner W, Nagel G (2013) A LOV-domain-mediated blue-light-activated adenylate (adenylyl) cyclase from the cyanobacterium Microcoleus chthonoplastes PCC 7420. Biochem J 455:359–65. doi: 10.1042/BJ20130637

Raizen DM, Avery L (1994) Electrical activity and behavior in the pharynx of Caenorhabditis elegans. Neuron 12:483–95.

Raizen DM, Zimmerman JE, Maycock MH, Ta UD, You Y, Sundaram M V, Pack AI (2008) Lethargus

is a Caenorhabditis elegans sleep-like state. Nature 451:569–72. doi: 10.1038/nature06535

Ramón Y Cajal S (1894) The Croonian Lecture: La Fine Structure des Centres Nerveux. Proc R Soc London 55:444–468. doi: 10.2307/115494

Ramot D, MacInnis BL, Goodman MB (2008) Bidirectional temperature-sensing by a single thermosensory neuron in C. elegans. Nat Neurosci 11:908–15. doi: 10.1038/nn.2157

Rand JB (2007) Acetylcholine. WormBook 1–21. doi: 10.1895/wormbook.1.131.1

Reiner A, Isacoff EY (2014) Tethered ligands reveal glutamate receptor desensitization depends on subunit occupancy. Nat Chem Biol 10:273–80. doi: 10.1038/nchembio.1458

Richmond JE, Davis WS, Jorgensen EM (1999) UNC-13 is required for synaptic vesicle fusion in C. elegans. Nat Neurosci 2:959–64. doi: 10.1038/14755

Richmond JE, Jorgensen EM (1999) One GABA and two acetylcholine receptors function at the C. elegans neuromuscular junction. Nat Neurosci 2:791–7. doi: 10.1038/12160

Rieke F, Baylor DA (1998) Origin of reproducibility in the responses of retinal rods to single photons. Biophys J 75:1836–57. doi: 10.1016/S0006-3495(98)77625-8

Ritter E, Stehfest K, Berndt A, Hegemann P, Bartl FJ (2008) Monitoring light-induced structural changes of Channelrhodopsin-2 by UV-visible and Fourier transform infrared spectroscopy. J Biol Chem 283:35033–41. doi: 10.1074/jbc.M806353200

Rogers C, Persson A, Cheung B, de Bono M (2006) Behavioral motifs and neural pathways coordinating O2 responses and aggregation in C. elegans. Curr Biol 16:649–59. doi: 10.1016/j.cub.2006.03.023

Rose JK, Kaun KR, Chen SH, Rankin CH (2003) GLR-1, a non-NMDA glutamate receptor homolog, is critical for long-term memory in Caenorhabditis elegans. J Neurosci 23:9595–9.

Rose JK, Kaun KR, Rankin CH (2002) A new group-training procedure for habituation demonstrates that presynaptic glutamate release contributes to long-term memory in Caenorhabditis elegans. Learn Mem 9:130–7. doi: 10.1101/lm.46802

Rosenbaum DM, Rasmussen SGF, Kobilka BK (2009) The structure and function of G-protein-coupled receptors. Nature 459:356–63. doi: 10.1038/nature08144

Rosenberry TL, Sonoda LK, Dekat SE, Cusack B, Johnson JL (2008) Monitoring the reaction of carbachol with acetylcholinesterase by thioflavin T fluorescence and acetylthiocholine hydrolysis. Chem Biol Interact 175:235–41. doi: 10.1016/j.cbi.2008.06.002

Rosenbluth J (1965) Ultrastructural organization of obliquely striated muscle fibers in Ascaris lumbricoides. J Cell Biol 25:495–515.

Russwurm M, Mullershausen F, Friebe A, Jäger R, Russwurm C, Koesling D (2007) Design of fluorescence resonance energy transfer (FRET)-based cGMP indicators: a systematic approach. Biochem J 407:69–77. doi: 10.1042/BJ20070348

Ryu M-H, Kang I-H, Nelson MD, Jensen TM, Lyuksyutova AI, Siltberg-Liberles J, Raizen DM, Gomelsky M (2014) Engineering adenylate cyclases regulated by near-infrared window light.

Proc Natl Acad Sci U S A 111:10167–10172. doi: 10.1073/pnas.1324301111

Ryu M-H, Moskvin O V, Siltberg-Liberles J, Gomelsky M (2010) Natural and engineered photoactivated nucleotidyl cyclases for optogenetic applications. J Biol Chem 285:41501–8. doi: 10.1074/jbc.M110.177600

Sadeghian K, Bocola M, Schütz M (2008) A conclusive mechanism of the photoinduced reaction cascade in blue light using flavin photoreceptors. J Am Chem Soc 130:12501–13. doi: 10.1021/ja803726a

Saranak J, Foster KW (1997) Rhodopsin guides fungal phototaxis. Nature 387:465–6. doi: 10.1038/387465a0

Sato M, Hida N, Ozawa T, Umezawa Y (2000) Fluorescent indicators for cyclic GMP based on cyclic GMP-dependent protein kinase Ialpha and green fluorescent proteins. Anal Chem 72:5918–24.

Schafer WR (2002) Genetic analysis of nicotinic signaling in worms and flies. J Neurobiol 53:535–41. doi: 10.1002/neu.10154

Scheib U, Stehfest K, Gee CE, Korschen HG, Fudim R, Oertner TG, Hegemann P (2015) The rhodopsin-guanylyl cyclase of the aquatic fungus Blastocladiella emersonii enables fast optical control of cGMP signaling. Sci Signal 8:1–8. doi: 10.1126/scisignal.aab0611

Schmitt C, Schultheis C, Pokala N, Husson SJ, Liewald JF, Bargmann CI, Gottschalk A (2012) Specific expression of channelrhodopsin-2 in single neurons of Caenorhabditis elegans. PLoS One 7:e43164. doi: 10.1371/journal.pone.0043164

Schobert B, Lanyi JK (1982) Halorhodopsin is a light-driven chloride pump. J Biol Chem 257:10306–13.

Schröder-Lang S, Schwärzel M, Seifert R, Strünker T, Kateriya S, Looser J, Watanabe M, Kaupp UB, Hegemann P, Nagel G (2007) Fast manipulation of cellular cAMP level by light in vivo. Nat Methods 4:39–42. doi: 10.1038/nmeth975

Schultheis C, Brauner M, Liewald JF, Gottschalk A (2011a) Optogenetic analysis of GABAB receptor signaling in Caenorhabditis elegans motor neurons. J Neurophysiol 106:817–27. doi: 10.1152/jn.00578.2010

Schultheis C, Liewald JF, Bamberg E, Nagel G, Gottschalk A (2011b) Optogenetic long-term manipulation of behavior and animal development. PLoS One. doi: 10.1371/journal.pone.0018766

Schwarz EM (2005) Genomic classification of protein-coding gene families. WormBook 1–23. doi: 10.1895/wormbook.1.29.1

Sharabi K, Lecuona E, Helenius IT, Beitel GJ, Sznajder JI, Gruenbaum Y (2009) Sensing, physiological effects and molecular response to elevated CO2 levels in eukaryotes. J Cell Mol Med 13:4304–18. doi: 10.1111/j.1582-4934.2009.00952.x

Shcherbakova DM, Shemetov AA, Kaberniuk AA, Verkhusha V V (2015) Natural photoreceptors as a source of fluorescent proteins, biosensors, and optogenetic tools. Annu Rev Biochem 84:519–

50. doi: 10.1146/annurev-biochem-060614-034411

Shipley FB, Clark CM, Alkema MJ, Leifer AM (2014) Simultaneous optogenetic manipulation and calcium imaging in freely moving C. elegans. Front Neural Circuits 8:28. doi: 10.3389/fncir.2014.00028

Siegel MS, Isacoff EY (1997) A genetically encoded optical probe of membrane voltage. Neuron 19:735–41.

Sievers F, Wilm A, Dineen D, Gibson TJ, Karplus K, Li W, Lopez R, McWilliam H, Remmert M, Söding J, Thompson JD, Higgins DG (2011) Fast, scalable generation of high-quality protein multiple sequence alignments using Clustal Omega. Mol Syst Biol 7:539. doi: 10.1038/msb.2011.75

Silverman PM (1976) Regulation of guanylate cyclase activity during cytodifferentiation of Blastocladiella emersonii. Biochem Biophys Res Commun 70:381–8.

Sineshchekov OA, Jung K-H, Spudich JL (2002) Two rhodopsins mediate phototaxis to low- and high-intensity light in Chlamydomonas reinhardtii. Proc Natl Acad Sci U S A 99:8689–94. doi: 10.1073/pnas.122243399

Slimko EM, McKinney S, Anderson DJ, Davidson N, Lester H a (2002) Selective electrical silencing of mammalian neurons in vitro by the use of invertebrate ligand-gated chloride channels. J Neurosci 22:7373–7379. doi: 20026775

Sobolevsky AI, Rosconi MP, Gouaux E (2009) X-ray structure, symmetry and mechanism of an AMPA-subtype glutamate receptor. Nature 462:745–756. doi: 10.1038/nature08624

Sprenger JU, Nikolaev VO (2013) Biophysical techniques for detection of cAMP and cGMP in living cells. Int J Mol Sci 14:8025–8046. doi: 10.3390/ijms14048025

Spudich JL, Bogomolni RA (1984) Mechanism of colour discrimination by a bacterial sensory rhodopsin. Nature 312:509–13.

Spudich JL, Yang CS, Jung KH, Spudich EN (2000) Retinylidene proteins: structures and functions from archaea to humans. Annu Rev Cell Dev Biol 16:365–392. doi: 10.1146/annurev.cellbio.16.1.365

Stawski P, Janovjak H, Trauner D (2010) Pharmacology of ionotropic glutamate receptors: A structural perspective. Bioorg Med Chem 18:7759–7772. doi: 10.1016/j.bmc.2010.09.012

Stierl M, Penzkofer A, Kennis JTM, Hegemann P, Mathes T (2014) Key residues for the light regulation of the blue light-activated adenylyl cyclase from Beggiatoa sp. Biochemistry 53:5121–30. doi: 10.1021/bi500479v

Stierl M, Stumpf P, Udwari D, Gueta R, Hagedorn R, Losi A, Gärtner W, Petereit L, Efetova M, Schwarzel M, Oertner TG, Nagel G, Hegemann P (2011) Light modulation of cellular cAMP by a small bacterial photoactivated adenylyl cyclase, bPAC, of the soil bacterium Beggiatoa. J Biol Chem 286:1181–8. doi: 10.1074/jbc.M110.185496

Stinchcomb DT, Shaw JE, Carr SH, Hirsh D (1985) Extrachromosomal DNA transformation of Caenorhabditis elegans. Mol Cell Biol 5:3484–96.

Stirman JN, Crane MM, Husson SJ, Wabnig S, Schultheis C, Gottschalk A, Lu H (2011) Real-time multimodal optical control of neurons and muscles in freely behaving Caenorhabditis elegans. Nat Methods 8:153–158. doi: 10.1038/nmeth.1555

Stretton AO (1976) Anatomy and development of the somatic musculature of the nematode Ascaris. J Exp Biol 64:773–88.

Sulston JE, Horvitz HR (1977) Post-embryonic cell lineages of the nematode, Caenorhabditis elegans. Dev Biol 56:110–56.

Sulston JE, Schierenberg E, White JG, Thomson JN (1983) The embryonic cell lineage of the nematode Caenorhabditis elegans. Dev Biol 100:64–119.

Swierczek N a, Giles AC, Rankin CH, Kerr R a (2011) High-throughput behavioral analysis in C. elegans. Nat Methods 8:592–598. doi: 10.1038/nmeth.1625

Szobota S, Gorostiza P, Del Bene F, Wyart C, Fortin DL, Kolstad KD, Tulyathan O, Volgraf M, Numano R, Aaron HL, Scott EK, Kramer RH, Flannery J, Baier H, Trauner D, Isacoff EY (2007a) Remote control of neuronal activity with a light-gated glutamate receptor. Neuron 54:535–545. doi: 10.1016/j.neuron.2007.05.010

Szobota S, Gorostiza P, Del Bene F, Wyart C, Fortin DL, Kolstad KD, Tulyathan O, Volgraf M, Numano R, Aaron HL, Scott EK, Kramer RH, Flannery J, Baier H, Trauner D, Isacoff EY (2007b) Remote Control of Neuronal Activity with a Light-Gated Glutamate Receptor. Neuron 54:535–545. doi: 10.1016/j.neuron.2007.05.010

Tochitsky I, Banghart MR, Mourot A, Yao JZ, Gaub B, Kramer RH, Trauner D (2012) Optochemical control of genetically engineered neuronal nicotinic acetylcholine receptors. Nat Chem 4:105–111. doi: 10.1038/nchem.1234

Tonegawa S, Liu X, Ramirez S, Redondo R (2015) Memory Engram Cells Have Come of Age. Neuron 87:918–931. doi: 10.1016/j.neuron.2015.08.002

Touroutine D, Fox RM, Von Stetina SE, Burdina A, Miller DM, Richmond JE (2005) acr-16 encodes an essential subunit of the levamisole-resistant nicotinic receptor at the Caenorhabditis elegans neuromuscular junction. J Biol Chem 280:27013–21. doi: 10.1074/jbc.M502818200

Towers PR, Edwards B, Richmond JE, Sattelle DB (2005) The Caenorhabditis elegans lev-8 gene encodes a novel type of nicotinic acetylcholine receptor alpha subunit. J Neurochem 93:1–9. doi: 10.1111/j.1471-4159.2004.02951.x

Trott O, Olson AJ (2010) AutoDock Vina: improving the speed and accuracy of docking with a new scoring function, efficient optimization, and multithreading. J Comput Chem 31:455–61. doi: 10.1002/jcc.21334

Unwin N (2005) Refined structure of the nicotinic acetylcholine receptor at 4A resolution. J Mol Biol 346:967–89. doi: 10.1016/j.jmb.2004.12.031

Van Der Horst MA, Hellingwerf KJ (2004) Photoreceptor Proteins, “Star Actors of Modern Times”: A Review of the Functional Dynamics in the Structure of Representative Members of Six Different

Photoreceptor Families. Acc Chem Res 37:13–20. doi: 10.1021/ar020219d

Van Voorhies WA, Ward S (2000) Broad oxygen tolerance in the nematode Caenorhabditis elegans. J Exp Biol 203:2467–78.

Vassilatis DK, Arena JP, Plasterk RH, Wilkinson HA, Schaeffer JM, Cully DF, Van der Ploeg LH (1997) Genetic and biochemical evidence for a novel avermectin-sensitive chloride channel in Caenorhabditis elegans. Isolation and characterization. J Biol Chem 272:33167–74.

Velema WA, Szymanski W, Feringa BL (2014) Photopharmacology: beyond proof of principle. J Am Chem Soc 136:2178–91. doi: 10.1021/ja413063e

Vidal-Gadea AG, Davis S, Becker L, Pierce-Shimomura JT (2012) Coordination of behavioral hierarchies during environmental transitions in Caenorhabditis elegans. Worm 1:5–11. doi: 10.4161/worm.19148

Volgraf M, Gorostiza P, Numano R, Kramer RH, Isacoff EY, Trauner D (2006) Allosteric control of an ionotropic glutamate receptor with an optical switch. Nat Chem Biol 2:47–52. doi: 10.1038/nchembio756

Vowels JJ, Thomas JH (1994) Multiple chemosensory defects in daf-11 and daf-21 mutants of Caenorhabditis elegans. Genetics 138:303–16.

Wald G (1968) Molecular basis of visual excitation. Science 162:230–9.

Walker CS, Brockie PJ, Madsen DM, Francis MM, Zheng Y, Koduri S, Mellem JE, Strutz-Seebohm N, Maricq A V (2006a) Reconstitution of invertebrate glutamate receptor function depends on stargazin-like proteins. Proc Natl Acad Sci U S A 103:10781–6. doi: 10.1073/pnas.0604482103

Walker CS, Francis MM, Brockie PJ, Madsen DM, Zheng Y, Maricq A V (2006b) Conserved SOL-1 proteins regulate ionotropic glutamate receptor desensitization. Proc Natl Acad Sci U S A 103:10787–92. doi: 10.1073/pnas.0604520103

Wang Q, Shui B, Kotlikoff MI, Sondermann H (2008) Structural basis for calcium sensing by GCaMP2. Structure 16:1817–27. doi: 10.1016/j.str.2008.10.008

Wang R, Mellem JE, Jensen M, Brockie PJ, Walker CS, Hoerndli FJ, Hauth L, Madsen DM, Maricq A V (2012) The SOL-2/Neto auxiliary protein modulates the function of AMPA-subtype ionotropic glutamate receptors. Neuron 75:838–50. doi: 10.1016/j.neuron.2012.06.038

Wang W, Qin L-W, Wu T-H, Ge C-L, Wu Y-Q, Zhang Q, Song Y-X, Chen Y-H, Ge M-H, Wu J-J, Liu H, Xu Y, Su C-M, Li L-L, Tang J, Li Z-Y, Wu Z-X (2016) cGMP Signalling Mediates Water Sensation (Hydrosensation) and Hydrotaxis in Caenorhabditis elegans. Sci Rep 6:19779. doi: 10.1038/srep19779

Warrier S, Belevych AE, Ruse M, Eckert RL, Zaccolo M, Pozzan T, Harvey RD (2005) Beta-adrenergic- and muscarinic receptor-induced changes in cAMP activity in adult cardiac myocytes detected with FRET-based biosensor. Am J Physiol Cell Physiol 289:C455–61. doi: 10.1152/ajpcell.00058.2005

Watanabe S, Liu Q, Davis MW, Hollopeter G, Thomas N, Jorgensen NB, Jorgensen EM (2013)

Ultrafast endocytosis at Caenorhabditis elegans neuromuscular junctions. Elife. doi: 10.7554/eLife.00723

Waterston RH, Thomson JN, Brenner S (1980) Mutants with altered muscle structure of Caenorhabditis elegans. Dev Biol 77:271–302.

Weissenberger S, Schultheis C, Liewald JF, Erbguth K, Nagel G, Gottschalk A (2011) PACα--an optogenetic tool for in vivo manipulation of cellular cAMP levels, neurotransmitter release, and behavior in Caenorhabditis elegans. J Neurochem 116:616–25. doi: 10.1111/j.1471-4159.2010.07148.x

White JG (2013) Getting into the mind of a worm--a personal view. WormBook 1–10. doi: 10.1895/wormbook.1.158.1

White JG, Southgate E, Thomson JN, Brenner S (1986) The Structure of the Nervous System of the Nematode Caenorhabditis elegans. Philos Trans R Soc B Biol Sci 314:1–340. doi: 10.1098/rstb.1986.0056

Wightman B, Ha I, Ruvkun G (1993) Posttranscriptional regulation of the heterochronic gene lin-14 by lin-4 mediates temporal pattern formation in C. elegans. Cell 75:855–62.

Wolstenholme AJ (2012) Glutamate-gated chloride channels. J Biol Chem 287:40232–8. doi: 10.1074/jbc.R112.406280

Wood KC, Batchelor AM, Bartus K, Harris KL, Garthwaite G, Vernon J, Garthwaite J (2011) Picomolar nitric oxide signals from central neurons recorded using ultrasensitive detector cells. J Biol Chem 286:43172–81. doi: 10.1074/jbc.M111.289777

Wu Q, Gardner KH (2009) Structure and insight into blue light-induced changes in the BlrP1 BLUF domain. Biochemistry 48:2620–9. doi: 10.1021/bi802237r

Wyart C, Del Bene F, Warp E, Scott EK, Trauner D, Baier H, Isacoff EY (2009) Optogenetic dissection of a behavioural module in the vertebrate spinal cord. Nature 461:407–410. doi: 10.1038/nature08323

Yamaguchi R, Nakamura M, Mochizuki N, Kay SA, Nagatani A (1999) Light-dependent translocation of a phytochrome B-GFP fusion protein to the nucleus in transgenic Arabidopsis. J Cell Biol 145:437–45.

Yang HQ, Wu YJ, Tang RH, Liu D, Liu Y, Cashmore AR (2000) The C termini of Arabidopsis cryptochromes mediate a constitutive light response. Cell 103:815–27.

Yates DM, Portillo V, Wolstenholme AJ (2003) The avermectin receptors of Haemonchus contortus and Caenorhabditis elegans. Int J Parasitol 33:1183–93.

Yizhar O, Fenno LE, Prigge M, Schneider F, Davidson TJ, O'Shea DJ, Sohal VS, Goshen I, Finkelstein J, Paz JT, Stehfest K, Fudim R, Ramakrishnan C, Huguenard JR, Hegemann P, Deisseroth K (2011) Neocortical excitation/inhibition balance in information processing and social dysfunction.

Yu H, Olshevskaya E, Duda T, Seno K, Hayashi F, Sharma RK, Dizhoor AM, Yamazaki A (1999)

Activation of retinal guanylyl cyclase-1 by Ca2+-binding proteins involves its dimerization. J Biol Chem 274:15547–55.

Yu S, Avery L, Baude E, Garbers DL (1997) Guanylyl cyclase expression in specific sensory neurons: a new family of chemosensory receptors. Proc Natl Acad Sci U S A 94:3384–7.

Yue L, Pawlowski M, Dellal SS, Xie A, Feng F, Otis TS, Bruzik KS, Qian H, Pepperberg DR (2012) Robust photoregulation of GABA(A) receptors by allosteric modulation with a propofol analogue. Nat Commun 3:1095. doi: 10.1038/ncomms2094

Zaccolo M, De Giorgi F, Cho CY, Feng L, Knapp T, Negulescu PA, Taylor SS, Tsien RY, Pozzan T (2000) A genetically encoded, fluorescent indicator for cyclic AMP in living cells. Nat Cell Biol 2:25–9. doi: 10.1038/71345

Zaccolo M, Pozzan T (2002) Discrete microdomains with high concentration of cAMP in stimulated rat neonatal cardiac myocytes. Science 295:1711–5. doi: 10.1126/science.1069982

Zemelman B V., Lee G a., Ng M, Miesenböck G (2002) Selective photostimulation of genetically chARGed neurons. Neuron 33:15–22. doi: 10.1016/S0896-6273(01)00574-8

Zemelman B V, Nesnas N, Lee G a, Miesenbock G (2003) Photochemical gating of heterologous ion channels: remote control over genetically designated populations of neurons. Proc Natl Acad Sci U S A 100:1352–1357. doi: 10.1073/pnas.242738899

Zhang F, Vierock J, Yizhar O, Fenno LE, Tsunoda S, Kianianmomeni A, Prigge M, Berndt A, Cushman J, Polle J, Magnuson J, Hegemann P, Deisseroth K (2011) The microbial opsin family of optogenetic tools. Cell 147:1446–1457. doi: 10.1016/j.cell.2011.12.004

Zhang F, Wang L-P, Boyden ES, Deisseroth K (2006) Channelrhodopsin-2 and optical control of excitable cells. Nat Methods 3:785–92. doi: 10.1038/nmeth936

Zhang F, Wang L-P, Brauner M, Liewald JF, Kay K, Watzke N, Wood PG, Bamberg E, Nagel G, Gottschalk A, Deisseroth K (2007) Multimodal fast optical interrogation of neural circuitry. Nature 446:633–639. doi: 10.1038/nature05744

Zhang X, Cote RH (2005) cGMP signaling in vertebrate retinal photoreceptor cells. Front Biosci 10:1191–204.

Zhao Y, Araki S, Wu J, Teramoto T, Chang Y-F, Nakano M, Abdelfattah a. S, Fujiwara M, Ishihara T, Nagai T, Campbell RE (2011) An Expanded Palette of Genetically Encoded Ca2+ Indicators. Science (80-) 333:1888–1891. doi: 10.1126/science.1208592

Zheng Y, Brockie PJ, Mellem JE, Madsen DM, Maricq A V (1999) Neuronal control of locomotion in C. elegans is modified by a dominant mutation in the GLR-1 ionotropic glutamate receptor. Neuron 24:347–61.

Zheng Y, Mellem JE, Brockie PJ, Madsen DM, Maricq A V (2004) SOL-1 is a CUB-domain protein required for GLR-1 glutamate receptor function in C. elegans. Nature 427:451–7. doi: 10.1038/nature02244

Zimmer M, Gray JM, Pokala N, Chang AJ, Karow DS, Marletta MA, Hudson ML, Morton DB, Chronis

N, Bargmann CI (2009) Neurons detect increases and decreases in oxygen levels using distinct guanylate cyclases. Neuron 61:865–79. doi: 10.1016/j.neuron.2009.02.013

Zoltowski BD, Gardner KH (2011) Tripping the light fantastic: Blue-light photoreceptors as examples of environmentally modulated protein-protein interactions. Biochemistry 50:4–16. doi: 10.1021/bi101665s

ACKNOWLEDGEMENTS

The last few years in Frankfurt have been a wonderful roller coaster ride laden with ups and downs and now as I seem to end this phase of life, I am glad that the ups have out-numbered the downs by a good margin. And for this fulfilling experience, I have some people to thank:

Alexander: I have learnt to do and think about science in a rigorous, honest and an insightful manner and I am thankful to Alex for this. And he has always lent a patient ear to concerns beyond the science.

Dirk, Georg, Noelle: For being valuable collaborators and Martin: for his consent to be the second reviewer of the thesis.

Lab-mates: I have been fortunate to have been surrounded by some wonderful people in the lab who have contributed in their own special ways to make these PhD years quite rewarding and I am glad to have found valuable friendships that I hope to cherish forever. Some of these fine people whom I am thankful to are: Wagner, Liese, Basi, Florian, Mona, Christian, Negin, Alex, Karen, Jana, Tina, Szi-chieh, Oleg, Steven, Petrus, Arunas, Conny, Anke, Tine, Heike.

Students: Kerstin, Anna, Tim, Tobias, Tanita, Thilo and Martin. I have thoroughly enjoyed teaching them and in return have also got to learn a whole lot from them.

Indian (and now Spanish too) gang in Göttingen and Frankfurt: For making a home away from home.

And finally the Family at home. And Home is where the Heart is. This thesis and possibly every other important thing in my life derives support and blessings from my family: my grandparents, my brother, my father, my mother and now my wife and our coming little bundle of joy.

Eidestattliche Erklärung

Hiermit versichere ich, Jatin Nagpal, dass ich die vorliegende Arbeit selbstständig verfasst und keine anderen als die angegebenen Quellen und Hilfsmittel benutzt habe.

Ort, Datum Jatin Nagpal

CURRICULUM VITAE

Name: Jatin Nagpal

Born on 7th October 1987 in Delhi, India

Citizenship: India

Current residence:

Am Brückengarten 9,

60431 Frankfurt am Main, Germany

Contact number: +4917682115124

E-Mail: jatinagpal@gmail.com

Academic History

August 2010 - June 2016 – **PhD student** in the group of **Prof. Alexander Gottschalk** at the Institute of Biochemistry and Buchmann Institute for Molecular life sciences, **Goethe University, Frankfurt**, Germany, working on the development and implementation of novel optogenetic tools to investigate *Caenorhabditis elegans* nervous system.

September 2010 - June 2010 – **M.Sc. in Neurosciences** from the International Max Planck Research School (**IMPRS**) in Neurosciences**, Georg August University, Göttingen** with scholarship from the **Excellence Foundation** for the Promotion of the **Max Planck Society**. Overall Grade: Very Good

Master thesis – 'Characterization of channelrhodopsin responses to fluctuating and constant light stimuli' with Prof. Walter Stühmer, Molecular Biology of neuronal signals, Max Planck Institute for experimental medicine and Prof. Fred Wolf, Theoretical Neurophysics, Max Planck Institute for dynamics and self-organization.

July 2005 – May 2008 – **B.Sc. (Honours) in Biochemistry** from Sri Venkateswara College, **University of Delhi**, India with an overall aggregate of 87.6 % (Ranked 1st in the university year 2007 and 2nd in 2008).

2004-2005 (Final year of high school)

– All India Senior Secondary Certificate Examination of Central Board of Secondary Education (CBSE), India. Subjects- Physics, Chemistry, Mathematics, Biology. Aggregate 94.25 % (Awarded **Merit scholarship for undergraduates in basic sciences** by CBSE, India from **2005-2008**).

Publications

(# co-first author, * co-corresponding author)

Peer-reviewed papers

1) Photoswitchable diacylglycerols enable optical control of protein kinase C. Frank JA, Yushchenko DA, Hodson DJ, Lipstein N, **Nagpal J**, Rutter GA, Rhee J-S, Gottschalk A, Brose N, Schultz C*, Trauner D*. **Nature Chemical Biology 2016 Jul 25. doi: 10.1038/nchembio.2141**.

2) Optogenetic manipulation of cGMP in cells and animals by the tightly light-regulated guanylyl-cyclase opsin CyclOp. Gao S#, **Nagpal J#**, Schneider M, Kozjak-Pavlovic J, Nagel G*, Gottschalk A*. **Nature Communications 2015 Sep 8;6:8046.**

3) AzoCholine enables optical control of alpha 7 nicotinic acetylcholine receptors in neural networks. Damijonaitis A, Broichhagen J, Urushima T, Hüll K, **Nagpal J**, Laprell L, Schönberger M, Woodmansee DH, Rafiq A, Sumser MP, Kummer W, Gottschalk A, Trauner D. **ACS Chemical Neuroscience 2015 May 20;6(5):701-7.**

4) Synthetic retinal analogues modify the spectral and kinetic characteristics of microbial rhodopsin optogenetic tools. AzimiHashemi N#, Erbguth K#, Vogt A#, Riemensperger T, Rauch E, Woodmansee D, **Nagpal J**, Brauner M, Sheves M, Fiala A, Kattner L, Trauner D, Hegemann P, Gottschalk A*, Liewald JF*. **Nature Communications 2014 Dec 15;5:5810.**

5) In-vivo cGMP imaging in C. elegans using a robust and sensitive cGMP sensor. Sarah Woldemariam#, **Jatin Nagpal#**, Yanxun Yu#, Mary Bethke, Chantal Brueggemann, Joy Li, Michelle Krzyzanowski, Martin W.Schneider, Wagner Steuer Costa, Scott Oldham, Raakhee Shankar, Benjamin Barsi-Rhyne, Alan Tran, Denise Ferkey, Miri VanHoven, Piali Sengupta, Alexander Gottschalk, Noelle L'Etoile ***(In preparation)***.

6) Food sensation modulates locomotion by dopamine and neuropeptide signaling in a distributed neuronal network. Oranth A, Schultheis C, Liewald J, Tolstenkov O, Erbguth K, **Nagpal J**, Hain D, Wabnig S, Steuer Costa W, Brauner M, Beets I, Miller D, Gottschalk A. ***(In preparation).***

7) Identification of SNARE complex associated factors in *Caenorhabditis elegans* reveals a plasma membrane Ca2+ ATPase. Csintalan F, Liewald J, **Nagpal J**, Wabnig S, Heide H, Wittig I, Gottschalk A. ***(In preparation)***.

Book Chapters/ Reviews:

1) Microbial Rhodopsin Optogenetic Tools: Application for Analyses of Synaptic Transmission and of Neuronal Network Activity in Behavior. Glock C[#], **Nagpal J[#]**, Gottschalk A. **Methods Mol Biol. 2015;1327:87-103.**

2) From synapse to behavior- Optogenetic tools for investigation of *C. elegans* nervous system. **Jatin Nagpal.** Optogenetics: From Neuronal Function to Mapping & Disease Biology**, Cambridge University Press,** Ed. K. Appasani (due October **2016**).

Pre-print servers:

1) Continuous Dynamic Photostimulation - inducing in-vivo-like fluctuating conductances with Channelrhodopsins. Andreas Neef[#], Ahmed El Hady[#], **Jatin Nagpal[#],** Kai Bröking, Ghazaleh Afshar, Oliver M Schlüter, Theo Geisel, Ernst Bamberg, Ragnar Fleischmann, Walter Stühmer, Fred Wolf. **arXiv:1305.7125v2** May **2013** [q-bio.NC].

Poster/Abstracts (only first author are included)

1) Optogenetic control of cGMP mediated signal transduction. **Jatin Nagpal**, Shiqiang Gao, Martin Schneider, Sarah Woldemariam, Mary Bethke, Chantal Brueggemann, Wagner Steuer Costa, Noelle L'Etoile, Georg Nagel, Alexander Gottschalk. **European worm meeting, Berlin**. June 1-3**, 2016**.

2) Optogenetic control of cGMP mediated signal transduction. **Jatin Nagpal**, Shiqiang Gao, Martin Schneider, Sarah Woldemariam, Mary Bethke, Chantal Brueggemann, Wagner Steuer Costa, Noelle L'Etoile, Georg Nagel, Alexander Gottschalk. **International worm meeting, Los Angeles**. June 24 - 28, **2015**.

3) Optogenetic control of cGMP mediated sensory transduction pathways in Caenorhabditis elegans. **Jatin Nagpal**, Martin Schneider, Wagner Steuer Costa, Mary Bethke, Chantal Brueggemann, Sarah Woldemariam ,Georg Nagel, Noelle L'Etoile, Alexander Gottschalk. **First BMLS student symposium, Frankfurt**. 8 November **2014**.

4)Optogenetic control of cGMP mediated sensory transduction pathways in Caenorhabditis elegans.**Jatin Nagpal**, Martin Schneider, Wagner Steuer Costa, Mary Bethke, Chantal Brueggemann, Sarah Woldemariam ,Georg Nagel, Noelle L'Etoile, Alexander Gottschalk. **Channelrhodopsin et al. – Optogenetic Tools and Applications meeting in Wuerzburg,** September 28 - October 1, **2014**.

5) Optochemical control of genetically engineered glutamate and acetylcholine receptors in C. elegans. **Jatin Nagpal**, Jana F. Liewald, Tatsuya Urushima, Dirk Trauner, Alexander Gottschalk. **Channelrhodopsin et al. – Optogenetic Tools and Applications meeting in Wuerzburg,** September 28 - October 1, **2014**.

6) Optogenetic control of cGMP mediated sensory transduction pathways in Caenorhabditis elegans. **Jatin Nagpal**, Wagner Steuer-Costa, Georg Nagel, Alexander Gottschalk. **International Symposium of the German Society for Biochemistry and Molecular Biology (GBM) in Frankfurt.** October 03 -October 06, **2013**.

7) Optochemical control of genetically engineered glutamate and acetylcholine receptors in C. elegans **Jatin Nagpal**, Jana F. Liewald, Tatsuya Urushima, Dirk Trauner, Alexander Gottschalk. **10th Göttingen Meeting of the German Neuroscience Society** (34th Göttingen Neurobiology Conference), March 13 - March 16, **2013**.

8) Optochemical control of genetically engineered glutamate and acetylcholine receptors in *C. elegans*. **J Nagpal**, J Liewald, T Urushima, D Trauner, A Gottschalk. **EMBO C. elegans Neurobiology** meeting, Heidelberg, June 14-17, **2012**.

Talks

February 11, 2016 - I delivered a talk titled 'The development and implementation of novel optogenetic tools in *C elegans*' at the **Young Investigators' Colloquium** organized by the Interdisciplinary Center for Neuroscience Frankfurt (ICNF) .

February 26, 2015 - I presented a talk at the **3rd Good Evening Symposium of Biochemistry** organised by the Institute of Biochemistry, Goethe University, Frankfurt titled 'Optogenetic increase of cGMP levels in cells and animals using CyclOp, a tightly light-regulated guanylyl cyclase opsin'.

October 03-October 06, 2013 - I presented a poster for which I was awarded the **best poster prize** and also was selected for a 'pecha kucha' talk at **2013 International Symposium of the German Society for Biochemistry and Molecular Biology (GBM)** : 'Optogenetic control of cGMP mediated sensory transduction pathways in Caenorhabditis elegans' by **Jatin Nagpal**, Wagner Steuer-Costa, Georg Nagel, Alexander Gottschalk.

Research experience

03 - 16 February 2014 – Research visit to the lab of Prof. Dirk Trauner, Department of Chemistry, Ludwig Maximilians University, Munich to perform whole cell patch clamp electrophysiology experiments with synthetic photo-switches.

04 - 08 March 2013 – Visit to Laboratoire de Biochimie Théorique UPR 9080 CNRS Institut de Biologie Physico-Chimique, Paris, France to learn and perform in silico docking studies under the supervision of Dr. Antoine Taly.

May-June 2009 – Worked in the Molecular Neurobiology Lab headed by Dr. Oliver Schlüter in the European Neuroscience Institute, Göttingen on molecular mechanisms underlying synaptic plasticity.

March-April 2009 – Worked in the lab of Prof. Dr. Dr. Detlev Schild in the Department of Neurophysiology and Cellular Biophysics, University of Göttingen performing calcium imaging to investigate dynamics between glomeruli and mitral cells in the olfactory bulb of *Xenopus laevis* tadpole.

January-February 2009 – Computational neuroscience project in the theoretical neurophysics lab headed by Prof. Dr. Fred Wolf at the Max Planck Institute for dynamics and self-organisation.

May-June of 2006-2008 – Selected as a fellow of the undergraduate science outreach program – 'Project Oriented Biological Education' organized by Jawaharlal Nehru Centre for Advanced Scientific Research, Bangalore. The program focuses on broad unifying themes such as genetics, behavior, evolution, biochemistry, molecular biology, development, and ecology. As a part of the program, I spent two summers in the chronobiology lab headed by Prof. V.K. Sharma

doing projects pertaining to the molecular and behavioral study of circadian rhythms in *drosophila melanogaster*.

Courses

July - August, 2015 – Successfully completed and received a passing grade in 'Introduction to **R Programming**' - a course of study offered by Microsoft, an online learning initiative of Microsoft through **edX**.

April 19-June 14, 2013 – Obtained a statement of accomplishment upon successfully completing the **Computational Neuroscience** course offered by Rajesh Rao and Adrienne Fairhall on **Coursera** (Grade achieved: 91.3/100). It was an advanced online undergraduate course introducing a broad range of computational techniques for analyzing, modeling, and understanding the behavior of neurons and networks of neurons in the brain.

October 11-16, 2009 – Selected to participate in the course, 'Analysis and Models in **Neurophysiology**' organized by the **Bernstein Center for Computational Neuroscience**, Freiburg, Germany and the German Neuroscience Society. The course provided advanced approaches for the analysis of electrophysiological data and the theoretical concepts behind them.

Teaching/ Other services

I **guided** five master's students – Ms. Kerstin Schott, Mr. Tim Philip Waldow, Mr. Tobias Leva, Mr. Thilo Henβ (Goethe University, Frankfurt), and Ms. Anna Kramer (Technical University, Munich) for their **rotation projects** in the Gottschalk lab and supervised Mr. Martin Schneider's and Ms. Tanita Lang's **bachelor thesis**.

I have been a **teaching assistant** for the 'Cell Biology' practical course for the Biochemistry students of the Goethe University, Frankfurt and 'Basics of Optogenetics' course for the students of the International Max Planck Research School for Neural Circuits, Goethe University, Frankfurt.

I was the **PhD student representative (2014-2015)** in the research assembly of Buchmann Institute for Molecular Life Sciences (BMLS) and **co-organized of 1st BMLS student symposium 2014**.

I participated in the **Tag der Offenen Tür (Open day)** on 01.06.2014, Campus Riedberg, Goethe University Frankfurt giving demonstrations on the application of optogenetics in worms to general public.

I was a **co-organizer of Neurizons 2011**, an international neuroscience conference of the IMPRS for neuroscience, Goettingen.

As the **president** of 'Catalysis' - the **Biochemistry Society** of Sri Venkateswara College, I helped organize its inter-college festival and contributed to the annual magazine – 'Expressions' with an article on evolution of cooperation in nature.

Other Achievements

November 7-8, 2010 - I was awarded full scholarship to attend '**Falling walls 2010**' – Berlin Conference on Future breakthroughs in Science and Society.

2008: 1st place in the merit list for admission to Integrated PhD (biological sciences) in Indian Institute of Science, Bangalore, India.

2008: 1st place in All India entrance for M.Sc. life sciences by Jawaharlal Nehru University, Delhi.

2008: 3rd place in Joint Admission Test for M.Sc. (biotechnology) by Indian Institute of Technology (IITs).

2008: One among the four students selected for admission to Integrated PhD in National Centre for Biological Sciences, Tata Institute for Fundamental Research, Bangalore.

2008: Awarded a medal for being 1st in University B.Sc. Biochemistry (Honors) examinations.

2007: Member of the winning team of the 'Quest 2006-2007', which is a competition consisting of tests on science awareness, conceptual understanding, problem solving and expositions on scientific topics and their defense, organized by Center for Science Education and Communication, University of Delhi.

2007: Awarded the third prize for paper presentation event in the National symposium on Molecular Biology – Current Innovations and Trends held at Shivaji College, University Of Delhi.

2005: Awarded a certificate of merit for being among the top 0.1% of the successful candidates in physics in senior secondary school exams by CBSE.

2004: Awarded merit certificate by Delhi Association of Mathematics Teachers for clearing the National Mathematics Olympiad.